UNIVERSITY OF GLOUCESTERSHIRE

A Method for Determining the Flow Front Position and Velocity of a Polymer Melt in an Injection Moulding Process

Holger Mensler

A thesis submitted to

The University of Gloucestershire

In accordance with the requirements of the degree of

Doctor of Philosophy in the

School of Computing and Engineering

August 2021

Word Count: 63,164

Abstract

During the filling phase of an injection moulding process, the flow front velocity of the plastic melt decisively influences the form part quality. It has been believed that a constant flow front velocity of the melt leads to form parts that are free of distortion and residual stress. A process control strategy based on a constant flow front velocity of the melt, however, requires the full understanding of the flow front position as a function of the screw position of the injection moulding machine. With current methods, this can only be achieved by direct measurements using a number of sensors inside the mould, which leads to a complicated structure, great effort, and a high cost for tooling equipment. **This study proposes, designs, and develops an innovative method for determining the flow front velocity of a plastic melt in an injection moulding machine using only one pressure sensor at the front of the screw, which is based on the idea of mapping a simulated filling process to a real injection moulding process.** The mapping ensures that the characteristic event points are identified and matched for both the simulated and real filling processes.

The results of the simulation analysis and experimental evaluation demonstrate that the proposed method is effective for determining the flow front position and resulting flow front velocity of the melt on the entire flow path. No specific measuring devices (sensors) were used within the mould cavity to locate the melt front position during the filling phase in any of the experimental studies. Only one single pressure sensor, located outside the mould, was required to determine the flow front velocity of the melt. **The two case studies have provided the necessary evidence that the new method offers great potential for rule-based setting of the injection moulding machine and advanced process control strategies based on machine-independent parameters, such as constant melt front velocity or constant melt viscosity during the filling phase.**

With the new method, it is conceivable that transferring a single form part-specific event pattern (determined at the time of part development), in combination with its filling pattern, to the proposed process parameter determination unit assigned

to the mould is possible. With its methods and functions for determining the real and form part-specific event patterns and for matching these patterns, the flow front position of the melt can be reliably determined from shot to shot. **The results from the analysis and evaluation for pattern matching show that a comparatively simple matching algorithm with linear transformation would be sufficient** for this purpose. Depending on the amount of available data and the complexity of the control unit, machine-independent parameters can be determined in real time on the entire flow path and used to closed-loop control the machine setup.

Because the method dispenses with any sensor technology within the mould, it can be used for any existing application without complex and expensive retrofits of existing moulds. With the obtained parameters, the new method could be an essential component in the search for advanced process control strategies and thus for autonomous injection moulding.

Author’s Declaration

I declare that the work in this thesis was carried out in accordance with the regulations of the University of Gloucestershire and is original except where indicated by specific reference in the text. No part of the thesis has been submitted as part of any other academic award. The thesis has not been presented to any other education institution in the United Kingdom or overseas. Any views expressed in the thesis are those of the author and in no way represent those of the University.

Date 12th August 2021

Doi: 10.46289/PO17BF22

Acknowledgements

I would like to thank Professor Shujun Zhang for his guidance throughout this project. He has been an ideal teacher, mentor, and thesis supervisor, offering me advice, encouragement, and a tremendous amount of support.

And I would like to thank my wife Carmen for her patience. Giving up was not an option.

Table of Contents

List of Figures

List of Tables

Nomenclature

A_b	Cross-sectional area of screw
A_m	Area of melt front
A_1	First Rivlin-Ericksen tensor
A_2	Second Rivlin-Ericksen tensor
a_T	Time – temperature shift factor
b	Flow channel width
D	Diameter of screw
E_a	Activation energy
E_i	Singular event
E_{mach}	Real singular event
E_{sim}	Virtual singular event
f_k	Scaling factor
$f_{k\,lin}$	Linear component of scaling factor
$f_{k\,nlin}$	Non-linear component of Scaling factor
f_{max}	Maximum scaling factor
f_{min}	Minimum scaling factor
Δf	Scaling increment
h	Flow channel height
$h_{sim\,i}$	Information on form part geometry at virtual event time
j	Number of displacements
j_{min}	Displacement at the smallest pattern deviation
k	Number of transformations
k_{min}	Transformation at the smallest pattern deviation
L	Length of the flow channel
F_i	Event point
m	Number of real events
M_k	Transformed event pattern
M_m	Real event pattern
M_s	Form part-specific event pattern
n	Number of virtual events

Δp	Pressure loss
p_e	Melt pressure
p_{mach}	Measured (real) melt pressure
p_{mk}	Time-corrected melt pressure
p_{sim}	Form part-specific (virtual) melt pressure
R_g	Gas constant
$S_{k,i}$	Deviation between events
S_k	Deviation between patterns
$S_{min\ k}$	Smallest pattern deviation of all transformations
S_{min}	Smallest pattern deviation of all transformations and displacements
$s_{mach\ i}$	Position of screw at real event time
t	Time for injection
t_{mach}	Machine time
$t_{mach\ i}$	Real event time
t_{sim}	Virtual injection time
$t_{sim\ i}$	Virtual event time
T_m	Melt temperature
T_{wz}	Mould temperature
v	Velocity of screw
V	Volume form part
$\dot{V}$	Volumetric flow rate
v_b	Injection velocity
$v_b\ SP$	Injection velocity profile (set points)
v_m	Melt front velocity
x_b	Position of screw
x_m	Position of melt front
$x_{simi}, y_{simi}, z_{simi}$	Position of melt front at virtual event time
$\dot{\gamma}$	Shear rate
τ	Wall shear stress
Ψ	Specific error bound
η	Melt viscosity
$\mathcal{F}_{\mathrm{m}}$	Magnitude of relative deviation of melt temperature

$\mathcal{F}_{\dot{V}}$ Magnitude of relative deviation of volume flow

$\mathcal{F}_{\mathrm{wz}}$ Magnitude of relative deviation of mould surface temperature

1 INTRODUCTION

1.1 Background

Due to their special properties, plastic materials are developing rapidly and conquering many new areas of implementation. This wide spectrum of applications, achieved through the suitable combination of different types of polymers and manufacturing processes, distinguishes polymers from all other construction materials.

By examining what plastic materials contribute to today's 'megatrends', the versatility of these applications becomes clear. Examples include the following:

- Lightweight polymer structures play a major role in all vehicle components, from the interior to supporting structural parts. This enables lower emissions mobility and thus contributes to sustainability.
- In the construction industry, plastic materials are used for the thermal insulation of pipes, facades, and windows. Plastic is also the material of choice for low-energy buildings.
- Current applications in electronics such as printed sensors (RFID), organic diodes in displays (OLED), and power generation.
- Forty-five percent of all medical products manufactured worldwide consist of plastics, including prostheses, artificial blood vessels, and capsules that release drugs in the body after ingestion (Plastverarbeiter, 2016).
- In the case of renewable energies, plastic materials contribute to efficient and environmentally friendly energy generation as, for example, heat exchangers and pipes in geothermal energy or as rotor blades in wind turbines.
- Efficient processes in polymer processing, as well as in reuse (recycling), enable a simultaneously sustainable and economic production.

For more than 50 years, plastics processing has experienced nearly continuous growth. In 1989, the volume of plastics produced worldwide exceeded that of pig iron for the first time. Statistics (Hohmann, 2021) show that the plastics industry (manufacturing, processing, and mechanical engineering) is critical for Germany; in 2019, the industry comprised 1,729 companies with 291,354 employees. With a 7% share of global production, Germany is one of the largest polymer producers; and with a consumption of approximately 13.6 million tonnes, Germany is also one of the world's largest plastics processors in terms of production.

About 60% of all plastics processing units are injection moulding machines (Hohmann, 2021). An injection moulding system produces complex plastic parts fully automatically; in addition to the injection moulding machine, the system includes a mould and peripheral (up- and downstream) equipment. Injection moulding is a cyclic process in which molten plastic material is injected into a mould cavity and solidifies under pressure into usable form parts of various geometries (Osswald, Turng, & Gramann, 2008). The filling phase of the process is characterised by the high flow rates and hence high shear rates of the polymer (Michaeli & Schreiber, 2009; Stitz & Keller, 2001). Due to the rapid filling, heat is generated by viscous dissipation. However, dissipation depends on both the viscosity and shear rate of the resin. As such, molecular orientation is not homogeneously distributed over the flow front cross section, and the distribution of orientation depends on flow front velocity. Orientation, however, leads to anisotropy and residual stress (Belofsky, 1995); the relationship between process variables and form part quality is thus complicated. In practice, fully understanding the relationship between pre-set parameters and form part quality is difficult without knowledge of the melt's flow pattern within the mould cavity (Kennedy & Zheng, 2013).

Many researchers in injection moulding have shown that for high quality form part production, it is important to have a full knowledge of the flow behaviour of the melt within the cavity (Chen, Zhang, Kong, Lu, & Gao, 2010; Chiu, Shih, & Wei, 1991; Kennedy & Zheng, 2013; Zhou, Yao, Chen, & Gao, 2009). Chen (2002), for example, believes that an approximately constant flow front velocity of the entire

melt flow path leads to optimised residual stress and homogenous form parts. Bader, König, and Schmidt (2013) have found that to continuously achieve a high surface quality, it is critical to keep melt viscosity constant during injection.

In other words, form part quality is significantly affected by both the flow pattern and injection rate (Boldizar, Kubat, & Rigdahl, 1990, Yang, 2004;), the latter is related to the forward speed of the injection piston of the screw and can vary during the filling phase. Injection rate is a fundamental process parameter in the setting (setup) of the injection moulding machine and thus the optimisation of the moulding process.

During machine setup, the injection rate profile is entered into the machine control unit by operators (Osswald et al., 2008; Stitz & Keller, 2001). The problem lies in identifying a suitable injection velocity profile to meet the above-mentioned requirements, such as a constant flow front velocity or melt viscosity during the filling phase (Ouyang et al., 2004; Yang, 2004). In practice, the setting of the injection moulder is still largely empirical and follows a similar pattern; the machine operator 'performs a basic setting' and then optimises the moulded part 'on the basis of experience'. Such an approach is not only time consuming and cost intensive but also characterised by the fact that 'success' depends largely on the 'knowledge and experience' of the operator. When asked to describe their 'experience', operators regularly come up to limits. Only in the rarest cases does an optimisation follow a 'rule-based strategy'. However, since the quality of the moulded part is largely determined by rheological conditions during the filling phase (above all), a rule-based procedure for profiling the injection velocity would be desirable to achieve constant and predictable form part quality. In the past, repeated attempts have been made to develop general guidelines for profiling injection velocity (Boldizar et al., 1990; Chiu et al. 1991, Hunkar, 1975). Although some methods can roughly outline an ideal injection velocity profile qualitatively, its quantitative determination remains empirical.

This deficiency occurs because optimisation strategies require a full understanding of the flow front velocity in relation to the screw position along the entire flow

path of the cavity. Zhou (2013), for example, believes that even though injection speed can be accurately closed-loop controlled with good robustness, setting the injection speed profile remains difficult. He raises the question of how injection speed should be profiled to produce parts with evenly distributed quality. He further argues that limited methods exist for practically and effectively measuring melt flow front position and velocity.

According to current state-of-the-art technology, for any given injection moulding process, it is not possible to make any statement about the flow front position or velocity of the melt in relation to the screw position of the injection moulding machine with reasonable effort. This makes it nearly impossible to optimise the injection process according to objective criteria.

Fig. 1-1 illustrates the problem, showing the relationships between injection speed, v_b (with screw cross-sectional area A_b, and screw position x_b), and melt flow front velocity, v_m (with the cross-sectional area of the flow channel A_m, at position x_m). Melt front velocity v_m, differs from injection velocity v_b, and is influenced by mould geometry A_m. Due to the non-linear nature of the filling process, the melt front flow path is not predetermined and depends on location and time. For constant flow front velocity, an injection speed profile must compensate for geometric changes in flow channel cross sections, but profiling the injection speed is only possible with knowledge about melt front velocity.

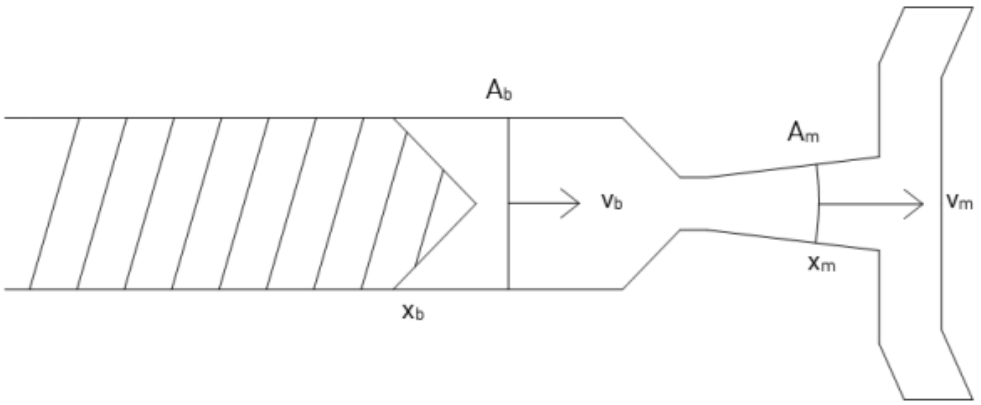

Fig. 1-1: Relationship of screw position and flow front velocity

To date, for the setting of the injection moulding machine, the problem of profiling the injection velocity remains unsolved, and the profiling of the injection velocity is done by the operator, primarily empirically. However, in the field of advanced control techniques, efforts have been made that have led to the realisation that the problem of 'profiling the injection rate for a constant melt front velocity' can only be solved if it can be transformed into a much simpler 'control problem', in which the flow front velocity can be directly determined during the filling process.

With the controller developed by various researchers (Bader & Zeller, 2011; Zhou et al., 2009), nearly all conceivable advanced control strategies, such as constant flow front velocity or constant melt viscosity, can be achieved. However, despite the good performance of the controller, the injection moulding industry is hesitant to switch to advanced control strategies based on machine-independent parameters. The limitations do not lie in the concept of the controller itself but rather in its input. The controller relies upon (among other data for machine-independent parameters) the determination of the relationship between screw position and melt front location. This requires methods for direct measurement of the flow front velocity along the flow path. For this purpose, researchers in injection moulding have developed various techniques to determine melt flow front pattern during the filling phase (Bader & Zeller, 2010; Bress & Dowling, 1998; Chen, Chen, & Gao, 2004; Yokoi, Hayashi, Tado, & Morikita, 1988; Yokoi & Inagaki, 1992; Wang, Fung, & Gao, 2008).

From a kinematics point of view, flow front velocity can be determined using flow front position (Bader, 2013; Bader & Zeller, 2010). If the relationship between flow front position and screw position can be determined, the relationship between flow front velocity and screw position can also be established, and thus the problem of identifying a suitable injection rate profile can be solved. For simple form part geometries in which the cavity fills along a single flow path (one dimensionally), Chen et al. (2004) have developed a capacitive transducer to measure melt front position directly. Despite some good performance, capacitive

measurement is more scientific in nature. In practice, it is difficult to implement; only in the rarest cases do form parts have simple geometries, and not all moulds are (or can be) equipped with capacitive sensors.

At present, and for real production conditions with complex part geometries, the relationship between screw position and melt front velocity can only be determined using at least two sensors installed along the flow path to measure melt front positions in relation to injection time and/or screw position (Bader, 2013; Bader & Zeller, 2010). Although such systems for the direct measurement of the melt front position by two or more sensors inside the mould have been studied and occasionally adopted for real production with some levels of success, they have not been widely applied in injection plastic moulding. The most significant problem associated with the direct measurement method is that flow front position and all derived parameters, such as flow front velocity and melt viscosity, can only be determined in the limited spaces between the two successive sensor positions; continuous measurement over the entire flow path is nearly impossible. In addition, other problems are associated with system design and form part quality. For example, it is often too complicated to place more sensors in the limited space along the flow path, and the installation of the sensors significantly reduces the stiffness of the mould and the ability of the part surface to cool uniformly. Furthermore, equipping and retrofitting the mould is quite time consuming and expensive, so the direct measurement method is suitable only for limited practical applications.

If a new innovative method needs to not employ complex sensor methods inside the mould, it could be used or adapted to any new or existing application in practice. Machine-independent parameters, such as flow front velocity or melt viscosity, could serve advanced process monitoring and control strategies. A variety of fully automatic, algorithm-based adjustment or optimisation strategies is conceivable. Such an innovative method would make a major contribution to the prevention of defective form parts and thus to sustainability and profitability in the injection moulding industry.

It is difficult to accurately quantify the average waste rate of injection moulded parts caused solely by poor control strategies, as rejection depends on many factors, such as application and specification. However, due to the high overall throughput volume in injection moulding, even small percentage improvements resulting from advanced control strategies would have large tonnage effects in avoiding plastic waste. Depending on source, the average scrap rate for injection moulding ranges from 1.5 to 2.5 % (Franchetti & Kress, 2017; Vijayakumar & Gajendran, 2014). With an annual global processing volume of approximately 55 million metric tonnes (Kutsch, 2021), an injection moulding process with a rejection rate improved by just 1 % due to optimised advanced control strategies would mean a potential savings of 11,000 metric tonnes annually.

To address this problem, a new method is proposed, designed, and developed in this thesis to determine flow front velocity in relation to screw position via the comparative analysis of event patterns. The method is based on the idea of mapping a simulated filling process to a real injection moulding process. The mapping occurs at event points. The theory behind the thesis predicts particular events at the so-called event locations. In this definition, a relationship is established between the time when a singular event happens and the associated position within the cavity. The mapping thus occurs at the event points when the melt front has a particular characteristic at a position within the cavity.

A singular event is defined as an individual event when the melt front has a particular characteristic at a certain position within the cavity. Part geometry typically changes along the flow path of the melt; these geometrical changes occur at tapering, enlargement, edges, corners, and flow obstacles. It is widely accepted that these changes result in a significant alteration of melt pressure during the flow through of the melt. These positions are defined as event points, or *F*. A singular event, denoted by *E,* correspondingly occurs. Singular events can occur in the form of event groups. The sequence of all events can be analysed to identify a pattern of the form part. This pattern is the form part-specific event pattern, or M_s, and can be considered the ‘fingerprint’ of the form part.

Two kinds of singular events are used: those identified through simulation analysis and those identified through experimental measurements. The former are called virtual singular events, or E_{sim}, and can be determined from a melt pressure curve generated from simulation analysis. Similarly, events identified through experimental measurement are called real singular events, or E_{mach}, and can be determined from a pressure curve measured at a specific location, such as in the nozzle of the injection unit. A number of virtual singular events form a virtual form part-specific event pattern, M_s, and a number of real singular events form a real event pattern, M_m.

To determine flow front velocity in relation to screw position, a new method via comparative analysis of the two event patterns described above is proposed. The matching of the form part-specific pattern to the real event pattern of the filling process represents the actual mapping process. Through assignment of the events, the relationship between the flow front position and the screw position is established. This could lead to a completely new approach to and understanding of setting up injection moulding machines and controlling injection moulding processes (advanced control strategies). Because it would not employ complex sensor methods, it could be used or adopted to any new or existing application in practice.

1.2 Overall Aim and Research Objectives

The overall aim of this project is to propose, design, and develop a method for determining the flow front position and velocity of a plastic melt by establishing a relationship between simulated and measured injection pressures. The proposed method is verified and validated by experimental studies under various boundary conditions to design and develop a control strategy for practical injection moulding.

The research objectives are as follows:

1. To critically review the existing methods for determining the flow front position and velocity of the melt as a function of screw position and injection time to identify research gaps and to investigate methods for directly determining the melt front in injection moulding for advanced control strategies.

2. To establish the relationship between simulated and practically measured pressure signals by matching event patterns and their application to process monitoring and control injection moulding.

3. To verify the functional requirements for the matching algorithm and to analyse the conditions under which the matching of the patterns can be conducted, even with 'large' deviations between the boundary conditions of the simulation and the setting values of the machine.

4. To propose and develop a generic matching method for a robust matching process.

5. To propose, design, and develop a new method for determining the flow front position and velocity of a plastic melt by using the concept of matching (and thus dispensing with complex sensors) for an advanced process control strategy.

1.3 Contributions to New Knowledge Generation

The significance of this project is that the new method can be used or adopted to any new or existing application in practice and can lead to a completely new approach and understanding in setting up injection moulding machines and controlling injection moulding processes.

Contributions to new knowledge are anticipated in both theoretical advancement and practical applications. From a theoretical advancement perspective, the thesis will make the following contributions in generating new knowledge:

1. The thesis will critically review current research activities in the areas of measurement and control of the melt front velocity to identify research gaps and will investigate methods for directly determining the melt front in injection moulding to create a framework for advanced control strategies.

2. The thesis will demonstrate that by matching, a quantity of virtual events can be assigned to a quantity of real events and the relationship between the flow front position and the screw position can be established.

3. The thesis will analyse and evaluate the particular conditions under which the mapping of the simulated injection moulding process to the real injection moulding process can be conducted with the aid of a matching algorithm proposed in this thesis with linear transformation, even with 'large' deviations between the boundary conditions of the simulation and the setting parameters of the machine.

4. The thesis will examine matching methods and will identify and analyse which functional requirements the matching algorithm must meet so that the event locations of the simulated filling process can be reliably assigned to the event locations of the real injection moulding process.

5. The thesis will advance the theoretical study in injection moulding with a new method for determining the flow front position and velocity of a plastic melt with only a single sensor and a generic (non-linear) matching method for the robust matching of moulded parts with a large deviation between machine settings and boundary conditions.

From a practical application perspective, the thesis will make the following contributions:

1. A new method for determining the flow front position and velocity of a plastic melt with only a single sensor will be developed to design practical injection moulding control strategies in industry.

2. A generic (non-linear) matching method will be developed for the robust matching of moulded parts with a large deviation between machine settings and boundary conditions.

1.4 Publications

Partial results of the thesis have been published.
Mensler, H., Zhang, S., & Win, T. (2019). A method for determining the flow front velocity of a plastic melt in an injection moulding process. *Polymer Engineering and Science, 59*(6), 1132–1145. doi: 10.1002/pen.25092

1.5 Thesis Structure

This thesis consists of eight chapters. Chapter 1 introduces the background of this research. It begins with a general introduction to plastic materials, injection moulding, and the process sequence, explaining the problem of profiling the injection velocity. This chapter also gives the motivations and objectives of this research as well as the structure view of this thesis.

Chapter 2 provides a review of literature relevant to this thesis. It starts with an overview of the material properties of plastics and describes the rheological relationships in the shear flow of plastic melts. Common methods for process monitoring and control in injection moulding are presented, and their suitability is critically questioned. Existing methods for determining the flow front position and velocity of the melt are critically reviewed to create a framework for an advanced injection moulding control strategy.

In Chapter 3, working hypotheses are derived and methods for their validation are presented on the basis of theoretical considerations, for the purpose of proposing a new method for determining flow front position.

In Chapter 4, an innovative method for determining the flow front velocity in relation to the screw position is presented. The function of the method and all

procedures and process steps are described, and important basic terms are defined and explained. In this chapter the application of the proposed method in an injection moulding process is discussed, a process parameter determination unit is developed, and an interactive injection moulding terminal is introduced.

The verification and validation of the proposed method is performed via comparative simulative and real experiments. Two case studies serve this purpose. In Chapter 5 the one-dimensional filling process is used to demonstrate and validate the method proposed. In Chapter 6 the case of multidimensional filling is validated.

In Chapter 7 different methods for matching event patterns and assigning the events are examined and their suitability tested, and a generic matching method with non-linear transformation algorithm is presented.

Chapter 8 summarises the results of the investigations. In this final chapter, conclusions are reached, original contributions are claimed, and the outlook for future investigations—both theoretical and practical—are charted.

2 LITERATURE REVIEW

2.1 Introduction

In this chapter, the critical literature review is carried out with a focus on the areas of polymer processing, the non-linear viscous flow of polymer melts, their viscous-elastic behaviour during processing and the mathematical approaches required to model flow problems, as well as process control methods and control strategies in injection moulding. The literature review provides an overview of current knowledge in these areas with the goal of identifying the gap in the existing research on advanced process control methods in injection moulding, based on machine-independent parameters, such as flow front location and velocity.

2.2 Polymer Processing

2.2.1 Polymeric Materials and their Macromolecular Structures

Polymers consist of long molecular chains of covalently bonded atoms with functional chemical groups and branches along the chains. In thermoplastic polymers, individual molecule chains are not connected. Thus, thermoplastic plastics can change between different aggregation states (solid and liquid) by heating and cooling.

Like many other scientists, Osswald (2011) and Domininghaus (1992) believe that the physical properties of thermoplastic polymers and their behaviour under the impact of stresses or in melts essentially depend on their macromolecular structure. This macromolecular structure, however, determines the morphology of the material.

Kennedy and Zheng (2013) distinguish amorphous from semi-crystalline plastics and investigate the varying degrees of freedom of molecular chain segments at certain transition temperatures. In the melt state, molecules have increased mobility and tend to adopt an entangled, disordered configuration. While molecular configuration for amorphous polymers is preserved as the melt

solidifies, semi-crystalline polymer molecules align in some regions in a regular lattice shape.

In plastics technology, it is widely accepted that to understand the influence of processing parameters on the mechanical properties of an injection moulded part, the orientation of the macro molecules must be considered (Brinkmann, 2010; Domininghaus, 1992; Kennedy & Zheng, 2013; Osswald et al., 2008). Orientation, however, depends on 'processing history', including the cooling rate and relaxation characteristics of the material, both of which are temperature- and time-dependent factors that are, in turn, determined by the morphological structure of the polymer.

The literature review has found that to incorporate these temperature- and time-related factors, efforts have been made to predict the mechanical properties of amorphous injection moulded parts (Engels, 2008; Govaert, Engels, Klompen, Peters, & Meijer, 2005). Models originating in the research of Engels allow reliable predictions of shear stress (and thus orientation), according to the temperature- and time-related processing history of the material.

In contrast, the possibility of incorporating time- and temperature-related factors to predict mechanical properties for semi-crystalline materials has not been demonstrated. Engels attributes this to the dependency of the mechanical properties on the degree of crystallinity. This degree, however, is affected by the cooling rate. In general, very rapid cooling (such as near the wall surface of the mould) leads to lower amounts of crystallin content, while slow cooling rates favour higher degrees of aligned lattice structures. Another well-known effect is that flow enhances crystallinity (Kennedy & Zheng, 2013). The moulding process itself affects degree of crystallisation and thus material properties. These complex self-reinforcing relationships explain the difficulty of predicting the mechanical properties of injection moulded semi-crystalline parts. To the best of the author's knowledge, no valid model exists for this prediction. However, if it is not possible to incorporate time-, temperature- and other flow-related factors to predict the mechanical properties of injection moulded parts, the question regarding the

optimisability of the form part properties arises. This question is reviewed in the following sections to identify optimisation methods for the moulding process with respect to molecular orientation.

2.2.2 Flow Properties of Polymeric Materials in the Melt

In an injection moulding process, flow forces generate stresses and deformations. Due to their macro molecularity, plastic melts always flow laminarly and adhere to surfaces at sufficiently low speeds (Menges, Haberstroh, Michaeli, & Schmachtenberg, 2011). Applied shear stress τ deforms the melt particle at the shear rate $\dot{\gamma}$. For some liquids, such as water (Newtonian liquids), shear stress and shear rate are proportional. The coefficient η describes the 'flowability' and thus viscosity of the liquid.

According to Menges et al. (2011), plastic melts show Newtonian behaviour only (if at all) in the range of low shear rates. However, injection moulding usually occurs in a range of shear rates between 10^4–$10^6\ s^{-1}$ (Stitz & Keller, 2001). In this relatively high range, the melt behaves as shear thinning, so the shear stress increases less than proportionally with the increase of the shear rate. The logarithmic plot in Fig. 2-1 shows the exponential dependence of viscosity on shear rate in shear thinning melts.

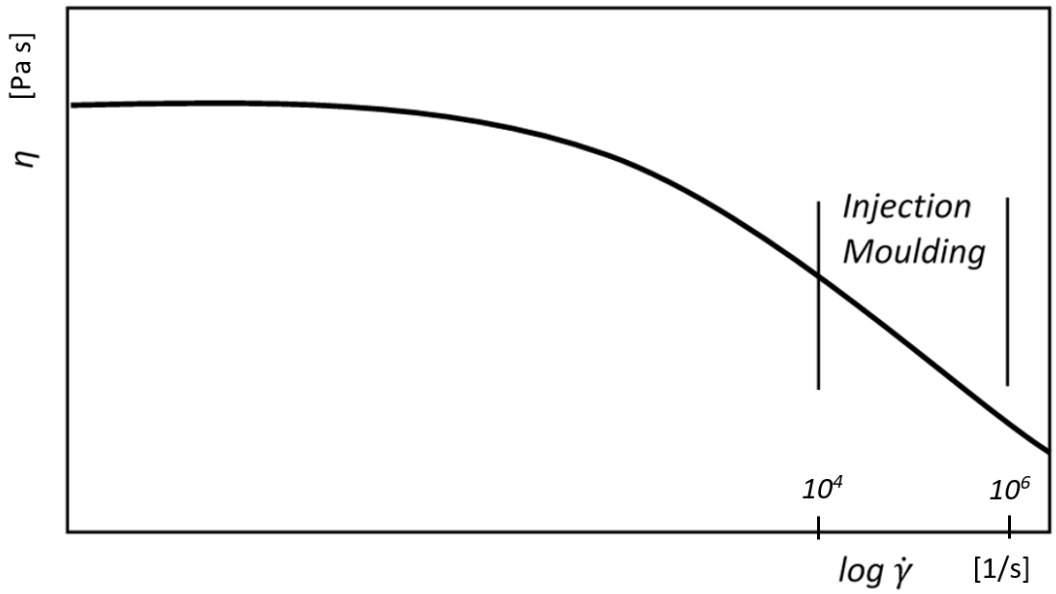

Fig. 2-1: Viscosity of a shear thinning polymer melt

Menges et al. (2011) explain structural viscosity, or shear thinning, by the formation of entanglements. Due to fast flow (at high shear rates), the molecular chains slide better next to each other. The molecular structure, the molecular mass, and the molecular mass distribution exert influence on the absolute level of viscosity, as well as that of the Newtonian range. A polymer with a high molecular mass has a higher viscosity due to the larger clusters. Osswald (2011) and others have shown that in addition to molecular structure and shear rate, temperature and pressure also exert a strong influence on viscosity as chain mobility changes.

A number of different models have been proposed to analyse the determination of plastic melt viscosity (Agassant, Avenas, Carreau, Vergnes, & Vincent, 2017; Menges et al., 2011). These models can provide good predictions of melt viscosity over a wide range of shear rates; they essentially differ only in their abilities to represent viscosity in different processing ranges and in their manner of including variable factors, such as temperature and compressibility, which change continuously during processing (Section 2.3.1.1).

A prerequisite for accurate predictions is that suitable material parameters are available as input variables for viscosity models. Their determination is not trivial

and is critically discussed in the literature. For Stitz, Keller and Osswald, the greatest challenge in predicting melt viscosity is not the lack of suitable models but rather the fact that the laboratory tests to measure the input variables are frequently performed under conditions different than those encountered during the moulding process (Osswald, 2011; Stitz & Keller, 2001). Furthermore, Kennedy and Zheng (2013) find that these data in simulation can lead to intrinsic errors if an incorrect approach is applied in modelling the viscoelasticity.

The exponential dependence of the viscosity on the shear rate complicates calculations in connection with shear thinning melts. The analytical calculations were greatly simplified by the considerations of Schümer et al. that in a real shear flow of a cylindrical pipe, in at least two positions, the results of a Newtonian observation are identical to the shear thinning flow of a molten polymer (Menges et al., 2011). Schümer's method for cylindrical pipe geometry has been widely adopted and can be analogously transferred to the geometry of a flow channel with a rectangular cross section. If a shear thinning plastic melt flows through a flow channel cross section of width *b* and height *h*, at the shear rate

$$\dot{\gamma} = \frac{\pi \cdot \dot{V}}{\sqrt{\frac{2}{3} \cdot b \cdot h^3}} \tag{2-1}$$

the pressure loss *Δp* to overcome the flow path section *l* is

$$\Delta p = \frac{12 \cdot \dot{V} \cdot \eta}{b \cdot h^3} \cdot l \text{ (Hagen-Poiseuille)} \tag{2-2}$$

with the melt viscosity $\eta = f(\dot{\gamma})$.

Thus, Schümer has created a set of equations which, starting from individual processing parameters such as volume flow and temperature, allows predictions of the conditions, such as shear rate and shear stress, that prevail when a shear thinning melt flows through a mould cavity.

This knowledge of shear stress allows predictions about the molecular orientation from which mechanical properties can in turn be derived, as shown in Section 2.2.1. However, the disadvantage of the equations does not lie in the

simplification for analytical derivation, which leads to the determination of the parameters being averaged only over the cross section, but rather in that the system of equations must be applied locally to the individual flow path sections. This is difficult, if not impossible, in a multidimensional application because the preferential direction of the melt and its flow rate depends on time and place. The flow rate affects the preferred direction of the melt, and vice versa. As such, the prediction of shear rate, shear stress and orientation in multidimensional flow paths is usually performed by numerical methods such as simulation.

2.2.3 Viscoelastic Behaviour

During the flow of polymer melts, phenomena are observed that cannot be explained by viscous behaviour alone. Viscoelastic effects cause these phenomena; for their analytical or numerical description, models are required which far exceed approaches of structure-viscous behaviour.

The best-known viscoelastic effects are (a) die swell, which describes the increase in diameter of an extrudate as it exits a die, and (b) the Weissenberg effect, which explains the rise of the free surface of a polymeric liquid near a rotating cylinder due to extra pressure (normal stress) generated by shear flow (Agassant et al., 2017). Both effects make the occurrence of finite normal stress differences in shear flow visible.

Viscoelastic effects are measured in so-called ‘shear recovery’ and ‘stress retardation and relaxation’ experiments. In stress relaxation experiments, a deformation γ_0 is suddenly imposed on a sample, as shown then held constant. Stress is measured as a function of time.

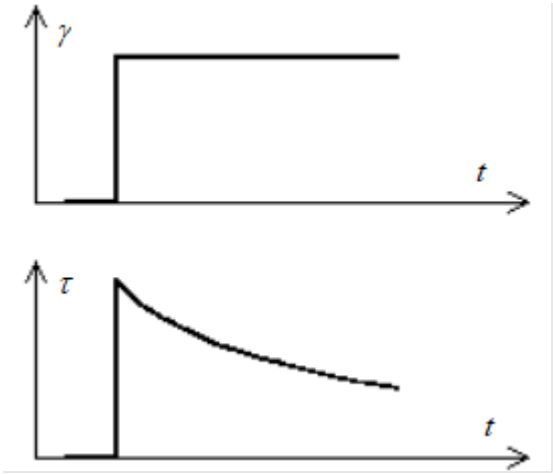

Fig. 2-2: Stress retardation and relaxation

The relaxation time of a liquid is of the order of the time required for a configuration change of the molecules. In simple Newtonian liquids consisting of short molecules, relaxation time is noticeably short. The time for a configurational change in macromolecular liquids, however, is much longer. Domininghaus (1992) states that this time varies between 10^{-2} and 10^{2} s for polymer melts. Such durations are measurable, as they are of the order of the shear rate used in conventional rheometers.

In shear flow, macromolecular chains are oriented in the direction of the flow (Section 2.2.2). To describe the stress, a material particle in shear flow is exposed to the most general form for the total stress tensor σ. The sum of all microscopic tensions (from each of the molecules) is represented in the macroscopic tension in the one-direction flow. The difference in the two- and three-direction flows is small in contrast.

However, according to Agassant et al. (2017) and other researchers, in a polymeric liquid flow in simple shear, one can measure a shear stress and a first normal stress difference, which is positive. On the other hand, Agassant et al. state that the second normal stress difference is one order of magnitude smaller than the first (and is usually negative). This observation can explain the rising of the free surface of the polymeric melt and thus effects such as the Weissenger effect.

Similar to how it is for viscosity, several models exist for the analytical and numerical determination of the viscoelasticity of plastic melts (Böhme, 1981; Cha, Kim, & Park D., 2019). Material properties, such as relaxation time and normal stress differences, can be fed into these models to allow predictions regarding viscoelastic effects in shear flow, such as the vertebrae observed at an inlet in a viscoelastic flow through a rotational hyperboloid. However, unlike with viscosity, for which there is a single model that accurately predicts the shear thinning behaviour of molten plastic in a shear rate range relevant to injection moulding, no such single model exists for viscoelasticity. Rather, a number of models exist, all having strengths and weaknesses. As critically examined in Section 2.3.1.2, this might be the reason why most commercial simulations in injection moulding do not consider viscoelastic effects.

2.2.4 Flow in the Cavity

Many authors agree that since the frozen layers on the wall of the cavity begin to subsequently develop after injection, the flow of the melt can be described as neither a simple pressure flow nor a simple shear flow (Agassant et al., 2017, Zhou, 2013). According to Zhou, it is rather a non-isothermal, non-Newtonian, transient and laminate flow in which the melt still moves in layers. Because melt velocity is highest at the centre of the cross-sectional area of the flow channel and decreases from the centre to the wall, the melt does not reach the wall or surface of the frozen wall layer by simple forward advance; instead, it tends to flow down the centre of the cavity to the melt front and then out towards the wall.

Zhou's figure (Fig. 2-3) demonstrates that this 'fountain flow' can exert important effects on the direction of the flow and orientation of the polymer molecules. It keeps the bulk of the melt from freezing to the walls, but the outer layers freeze as soon as they make contact. These outer layers are completely unoriented. The centre of flow, in turn, has a lower orientation because it is thermally insulated from the wall by the layer that has frozen. Instead, the layers between the centre of the flow channel and the (already frozen) wall layers experience the highest

shear stress in the flow and thus become highly oriented. This occurs because the temperature change has already been initiated at relatively high shear rates.

Zhou's qualitative consideration provides the crucial understanding that (a) molecular orientation is not homogeneously distributed over the flow front cross section and (b) distribution of orientation depends on flow front velocity. This must be considered in the context of Belofsky's (1995) work. In his research, Belofsky shows that orientation leads to anisotropy and residual stress.

However, the fact that the molecular orientation both leads to residual stresses and can never be uniformly distributed over the flow channel cross section suggests that in a filling process, in which the flow front velocity of the melt can be controlled, the molecular orientation of the form part can also be controlled. This explains the findings of Chen (2002). In his research, Chen demonstrates that a constant melt flow front velocity during the filling phase leads to distorted and residual stress-optimised homogeneous form parts.

In summary, these important findings lead to the conclusion that even if, in the absence of a valid model, the prediction of mechanical form part properties based on process parameters is not possible, by controlling certain process parameters, such as a constant flow front velocity, an optimised homogeneous molecular orientation in various flow sections of the injection moulded part can be achieved.

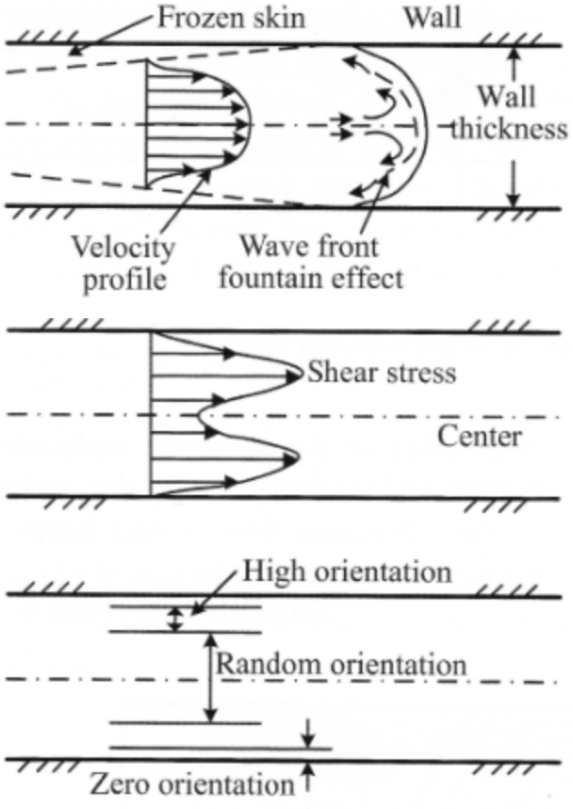

Fig. 2-3: Effects of velocity, freezing, and fountain flow, shear stresses resulting from flow pattern and orientation pattern across the section (Zhou, 2013)

2.2.5 Injection Moulding

Injection moulding is not a continuous process but rather a series of repetitive operations processed by the moulding machine in the specified time and sequence (Stitz & Keller, 2001). As a typical batch process, the actual (injection moulding) procedure is the stringing together of the technical-physical action sequences of the injection moulding system. It comprises several sub-processes: the plasticising (melting) of the polymer resin, the injection and compression of the molten plastic into the mould, the cooling of the moulding compound, and the ejection of the solidified form part from the mould.

These individual operations must all be conducted by the injection moulding machine within the specified time and in a specific (process-oriented) sequence—partially in parallel. The control of the cycle operation as well as of the key process

parameters in injection moulding, occurs regularly by a computer-based control of the moulding machine (MC; Fig. 2-4). The sequence control must realise the logical sequence of all machine functions, such as mould opening, closing, and clamping, as well as monitoring and controlling the moulding cycle so that it runs automatically. The parameter control monitors and controls the process variables.

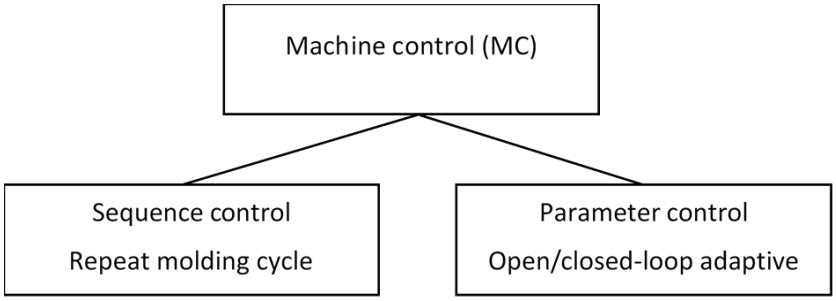

Fig. 2-4: Simplified overview of injection machine control (Stitz & Keller, 2001)

In Fig. 2-5, Yang (2004) illustrates the overall process control for injection moulding as a hierarchical structure with three layers. An advanced process parameter control system constitutes the first layer and provides accurate and robust control of key process variables. The second layer is divided into a parameter setting system, which determines the necessary set points of the key process parameter to achieve the required form part quality, and a process fault detection system for monitoring the operation of the injection moulding process. The third layer consists of a quality controller with functions for closed-loop (direct) control of certain form part quality.

Yang's detailed model clearly explains the complexity of an overall process control system; through its hierarchical structure, the model neatly separates the control of the machine parameter and process variables from the mechanism for closed-loop quality control. However, Yang (2004) misses the opportunity to specifically address the demands that the qualities of the injection moulding process place on the process control.

In his research, Zhou (2013) bridges the gap between the qualities of the injection moulding process and process control. He emphasises that the strongly varying time characteristics of the process are caused by the wide range of materials to be processed. Zhou shows that the non-linear rheological flow properties of polymer melts and their viscoelastic behaviour cause the batch process to function in a wide operation range, which thus places high demand on the process control of the injection moulder. In addition, he emphasises the hybrid system nature of the process, in which individual process subphases are not executed in a rigid sequence and length; rather, the transition from one subphase to another may be decided based on various criteria, for example, checks for certain conditions in the previous subphase. Finally, he underlines the repetitive nature of the operation, because each moulding cycle produces a finite number of products. To reach a certain number of parts, the cycle must be repeated and reproduced stably, despite the complicated dynamics and non-linear characteristics of the process.

As such, overall process control must be considered in the context of the complex and unique characteristics of the injection moulding process, its hybrid nature, and the non-linear behaviour of polymeric materials. The literature review has found that these considerations necessitate the development of new approaches in the field of process control (Section 2.4).

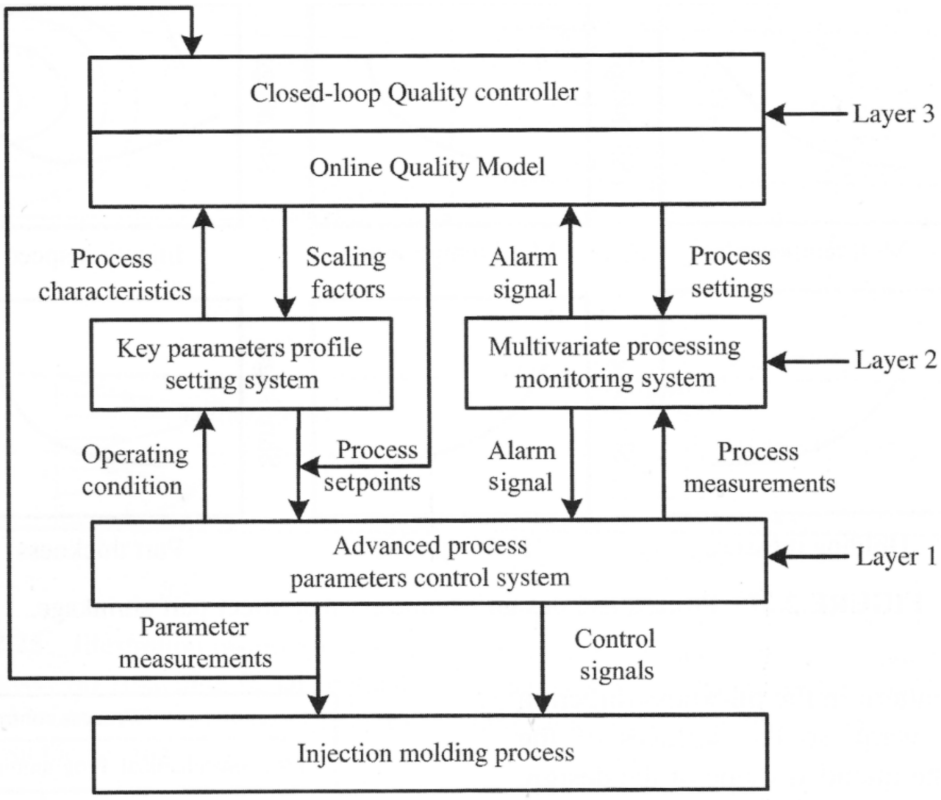

Fig. 2-5: Injection moulding process control system architecture (Yang, 2004)

2.2.6 Injection Moulding Key Process Variables

Due to the complex, non-linear, and repetitive nature of the moulding process, the form part quality is strongly related to processing conditions. It is thus necessary to precisely control the key process variables. It is widely accepted in the plastics industry that injection moulding process variables can be classified as follows:

1. The input parameters of the injection moulding process consist of set parameters and disturbance parameters. The input parameters form the independent variables of the process.

2. The output parameters are the dependent variables of the process and result from the process characteristics and all influencing variables. They provide information about the quality of the resulting product.

3. The target parameters evaluate the production process from an economic point of view and thus form the basis of any optimisation.

Several sets of injection moulding key process variables have been proposed (Menges, Michaeli, & Mohren, 1999; Stitz & Keller, 2001; Yang, Chen, Ningyun, & Furong, 2016). Sitz and Keller define typical setting parameters, such as injection speed, injection pressure, injection time, holding pressure and holding time, cooling time, melt and mould temperature; however, they omit their classification and derivation. As Fig. 2-6 shows, Yang et al. (2016) go further, providing an overview of their basic key process variables scheme, in which they distinguish between stage-dependent and stage-independent process variables. In a stage-based batch process, they emphasise that every operation must have its key process variables (closed-loop) controlled. They define the dominant process variable for each individual subphase of the injection moulding cycle. For the filling phase, a proper setting and control of the flow rate is necessary—one approximated by injection velocity, which can be directly measured. For the holding pressure phase, they recommend packing or holding pressure as the key process variable; for the plasticising stage, they suggest that it is important to closed-loop control screw rotation and back pressure. Stage-independent key variables that must be controlled (throughout the cycle) are typically melt and mould temperatures. Yang et al.'s set of key process variables is sufficiently complete and logically structured. However, it does not do justice to the complexity of injection moulding. Injection velocity, for example, cannot be considered a constant input parameter. Rather, it should be seen as a range of various individual velocities over the screw stroke or the injection time, which form an injection velocity profile. This injection velocity profile is the actual key process variable during the filling process.

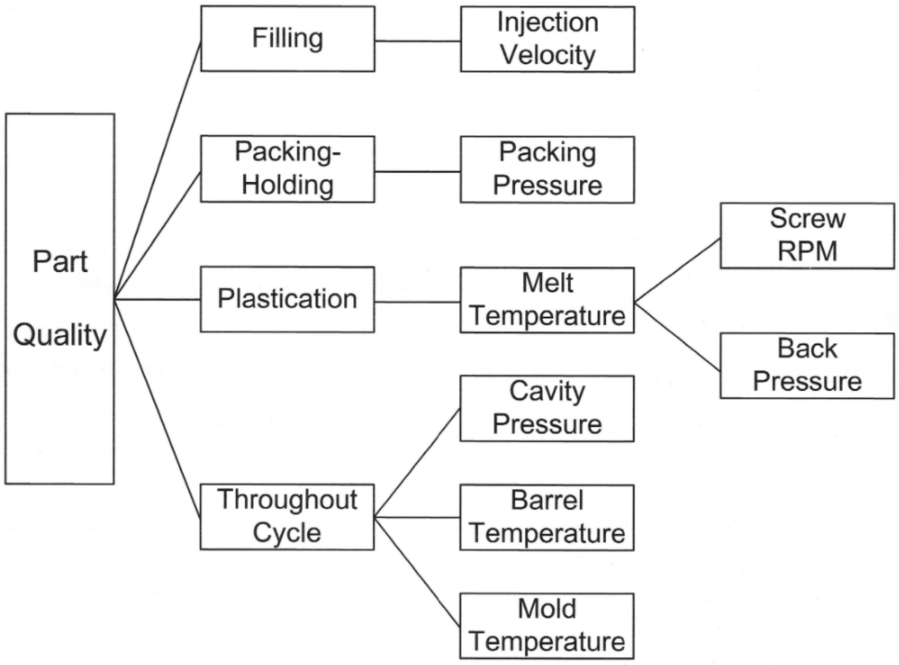

Fig. 2-6: Key process variables in the injection moulding process (Yang et al., 2016)

2.2.7 Statistical Based Approaches in Injection Moulding

According to Kulkarni, the identification of robust process settings in injection moulding is best achieved with design of experiments (DoE) approaches (Kulkarni, 2010). DoE is a structured, efficient method that examines multiple process factors simultaneously with a minimal number of experiments. In contrast to the 'one-variable-at-a-time investigation', the use of DoE can drastically reduce the size of the experimental matrices while maintaining the number of effects tested. This balance allows valid statistical analyses of the results and determination of the main effects of the process parameters.

The study of MKS evaluates different design approaches for minimum runs and shows how the effective use of experimental designs can facilitate the development of models using robust approaches such as multivariate analysis ([MKS], 2012). In the evaluation, a set of conditions for a stable injection moulding process that produces acceptable moulded parts with repeatable part weights and thicknesses for 10 different process factors such as injection velocity, barrel temperature, and holding pressure time is first defined. Then, ranges are specified

around these process settings to capture the expected long-term variations in the process factors. These factors are the independent variables in the process model.

The results of the study demonstrate the need for extensive experimental designs for the estimation of main effects when using multiple regression techniques; moreover, the results demonstrate how the effective use of DoE can facilitate the development of models using robust approaches such as Multivariate Analyses (MA), Principal Components Analysis (PCA), and Projection to Latent Structures (PLS) methods. These methods can employ data from DoEs to effectively predict process faults and to characterise the variational effect of many process factors simultaneously. While such DoEs are inadequate for effective multivariate regression analysis, PCA models provide reasonable fidelity to set up the process and evaluate its robustness. The comprehensive case study shows how neglecting the interaction affects results in poor identification of the process boundaries and gross over-estimations of the process robustness.

2.3 Simulation of the Injection Moulding Process

Exponentially increasing computing power has greatly improved the accuracy of simulation results in recent years. At the same time, intelligent user interfaces—expert systems that support the 'right' selection of processing parameters and improved interfaces in computer-based part development and design platforms—have minimised the effort and thus the cost of simulations. As a result, a growing trend uses the information obtained by simulation for more than the optimisation of moulded parts and subsequent mould design. Instead, simulation is finding its way into the actual production process (Kennedy & Zheng, 2013).

Injection moulding is characterised by the fact that it is often impossible to eliminate part defects in production by simply varying process conditions. In many cases, time-consuming and costly changes to the mould must occur. In contrast, it is much more economical to identify and avoid production-related part defects by simulation in an early phase of the design of the form part and mould by adopting constructive measures.

Among other researchers, Kennedy et al. (2013) and Zhou (2013) show that in combination with a suitable DoE, the simulation of certain process parameters can provide the effects of quality-relevant form part characteristics, such as the variation of shrinkage. They suggest that the information obtained can be used for pre-setting the injection moulding machine and propose that during production, machine set-up can be further optimised by simulation.

However, such considerations on the use of simulation results for pre-setting and control (process control) of the injection moulding machine should be evaluated with caution. As Sections 2.3.1 and 2.3.2 show, suitable models to describe the viscous and viscoelastic behaviour of polymer melts and corresponding numerical methods exist. This allows the flow of a polymer melt within a cavity (Section 2.2.4) to be simulated sufficiently accurately and the quality-determining characteristics to be analysed. However, the literature review has shown that flow enhances crystallinity (Section 2.2.1). Hence, the moulding process itself affects the degree of crystallisation and thus molecular orientation. This complex, self-reinforcing relationship is the reason for the total lack of suitable models for predicting mechanical part properties based on machine setting parameters. Simulation, even in combination with suitable DoE, can therefore not replace an advanced process control strategy for optimising form part properties with respect to their molecular orientation.

2.3.1 Material Properties and Governing Equations Required for Injection Moulding Process Simulation

The material properties required to simulate injection moulding depend on the simulation to be undertaken. For flow and filling analysis, viscosity, thermal properties and viscous-elastic properties are required. As Section 2.2.2 outlines, a prerequisite for accurate predictions is that suitable material parameters are available as input variables for the viscosity and viscoelasticity models.

2.3.1.1 Modelling Viscosity

In contrast to the Newtonian case, viscosity in shear thinning melts is a function of the shear rate:

$$\tau = \eta(\dot{\gamma}) \cdot \dot{\gamma} \tag{2-3}$$

A number of models exist for the analytical description of the viscosity function, $\eta(\dot{\gamma})$. In the 'simplest' model, the power law model, viscosity is set to the power of the shear rate. Because in this relationship $\log \eta$ is proportional to $\log \dot{\gamma}$, the power law model can represent the behaviour of polymer melts only in regions of high shear rates, where injection moulding often occurs. However, in injection moulding it is possible to have lower shear rates in the filling phase (especially when the filling pattern is unbalanced). Thus, a better approach than the power law model is the Carreau model (Agassant et al., 2017):

$$\frac{\eta-\eta_\infty}{\eta_0-\eta_\infty} = [1 + (\lambda \cdot \dot{\gamma})^2]^{\frac{n-1}{2}} \tag{2-4}$$

This model, with its time constant λ and power law index *n*, better incorporates experimental viscosity data for lower shear rates. Khalili et al. (2011) show that the Carreau model generally provides accurate predictions of viscosity, but when the upper limiting Newtonian viscosity is $\eta_\infty = 0$ and at high shear rates, the model reduces to the power law model.

Hieber and Chiang (1992) propose the cross model for the analytical description of the shear thinning viscosity (Equation (2-5)). They prove that the cross model has a better fit for the dependence of the shear rate compared to the Carreau model. When $\dot{\gamma}$ *-> 0*, the cross model predicts the zero-rate viscosity η_0, while at higher shear rates, it predicts power law behaviour.

$$\eta = \frac{\eta_0}{1+(\eta_0 \cdot \frac{\dot{\gamma}}{\tau^*})^{n-1}} \tag{2-5}$$

The incorporation of temperature effects into the cross model is achieved by a time-temperature shift factor. For many polymers, the logarithmic plot of viscosity

at temperature T can be obtained from that at temperature T_0 by shifting the viscosity along the logarithmic time axis by the amount of a shift factor a_T. The time-temperature shift factor has been fitted by Ferry, Williams and Landel (1980). In their WLF equation,

$$\log a_T = \frac{-C_1 \cdot (T - T_0)}{C_2 + T - T_0} \tag{2-6}$$

C_1 and C_2 are constants. The WLF equation is widely applicable to amorphous polymers and is commonly used together with Equation (2-5) as the cross-WLF model with

$$\eta_0 = D_1 \cdot \exp\left(\frac{-C_1 \cdot (T - T_0)}{C_2 + T - T_0}\right) \tag{2-7}$$

and D_1 as a constant to model viscosity in simulation.

For semi-crystalline polymers, Tanner (2000) suggests that the Arrhenius equation,

$$\log (a_t) = \frac{E_a}{R_g} \tag{2-8}$$

with activation energy E_a and the gas constant R_g, is more appropriate for the determination of the time-temperature shift factor of semi-crystalline plastics.

Thus, models exist which describe the shear-thinning behaviour of polymers sufficiently accurately when temperature effects are considered. The cross model is the most commonly used; nearly all commercial simulations incorporate this model. However, Kennedy and Zheng (2013) show that for an accurate determination of the flow pattern of the melt by simulation, the temperature shift effects described above are insufficient because they are in the relatively high temperature range of molten plastic. Kennedy and Zhen argue that for the simulation of the filling process, it is also necessary to consider the viscosity during the cooling and solidification of the melt. Thus, the determination of the temperature balance of the melt is required at any time of the filling process. The determination of the temperature balance is well described in the literature (Agassant et al., 2017; Kennedy & Zheng, 2013; Zhou, 2013) and is essentially

based on three factors: (a) convection due to the incoming melt, (b) conduction out of the melt (through the mould), and (c) shear heating caused by the deformation of the melt in the shear flow.

In the simulation, specific heat capacity is a measure of how much energy is required to raise the temperature of a certain polymer; this is the property governing the convection of heat into the mould. Thermal conductivity is the measure of how conductive a material is to heat, and shearing heat is a function of the polymer's viscosity and rate of deformation. According to Kennedy and Zheng, in addition to these key properties, several other thermodynamic properties are required for flow and filling simulation, which are mainly obtained from the 'equation of state' of the material. For thermoplastic polymers, the equation of state is provided by the PVT diagram, a commonly used three-dimensional representation of a thermodynamic system which provides the specific volume as a function of pressure and temperature (Domininghaus, 1992; van Krevelen & Nijenhuis, 2009; Zoller, Bolli, Pahud, & Ackermann, 1976).

In summary, in the field of filling simulation in the plastics industry, models and methods such as the cross-WLF model exist and are widely adopted, which can accurately describe the shear thinning behaviour of plastic melts and consider temperature effects. Thus, in a multidimensional application, in which the flow rate affects the preferred direction of the melt, and vice versa, the prediction of shear rate and shear stress can be performed by numerical methods such as simulation.

2.3.1.2 Modelling Viscoelasticity

For the determination of the viscoelastic behaviour of non-Newtonian fluids, the literature review has found that a number of models exist, including (a) models for second-order fluids, (b) differential models, and (c) integral models.

a) Second-Order Fluids

In a second-order fluid, the stress tensor σ is described by the following equation:

$$[\sigma] = -p\underline{E} + \mu\underline{A_1} + \alpha_1\underline{A_2} + \alpha_2\underline{A_2}^2 \qquad (2\text{-}9)$$

with Rivlin-Ericksen tensors A_1 and A_2, viscosity μ and normal stress coefficients α_1 and α_2. Böhme's (1981) Equation (2-9) of a second-order fluid provides the first and second normal stress differences. The two normal stress coefficients can be determined experimentally and, like viscosity, depend on shear rate. However, the model does not incorporate viscoelastic time effects.

b) Differential Models

In essence, all differential models are derived from the Maxwell model and are characterised by the fact that the stress tensor is described by the means of a differential equation.

The Maxwell model consists of a spring with constant modulus G in series with a dashpot with constant viscosity μ (Fig. 2-7).

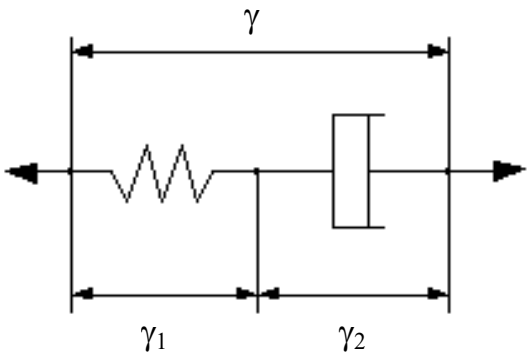

Fig. 2-7: Maxwell model

The deformation in total γ is the sum of the individual deformation of the spring γ_1 and dashpot γ_2. The following equation applies to the spring:

$$\tau = G \cdot \gamma_1 \qquad (2\text{-}10)$$

The dashpot is described as

$$\tau = \mu \cdot \frac{d\gamma_2}{dt}. \tag{2-11}$$

The series connection leads to the simplest form of the Maxwell model,

$$\tau + \lambda \frac{d\tau}{dt} = \mu \frac{d\gamma}{dt} \tag{2-12}$$

with the relaxation time λ.

Equation (2-12) qualitatively describes one-dimensional viscoelastic time effects. However, the equation does not provide a normal stress difference, which is required even for the simulation of a simple shear flow. Better results are obtained with other (more complex) types of differential models, such as the Oldroyd 8-parameter model (Oldroyd, 1958). For shear flow, this model provides first and second normal stress differences other than zero; thus, all essential viscoelastic effects can be determined. In practice, however, only a few of the material properties that the Oldroyd 8-parameter model requires can be measured directly from rheological experiments. The missing ones are usually obtained by simply adjusting predictions to experimentally determined values (trial and error method). This often leads to situations in which viscoelastic flows cannot be simulated. Becker and Schümmer (2000), for example, show that in a viscoelastic flow through a rotational hyperboloid, which has been analysed using an Oldroyd 8-parameter model, the vertebrae observed at the inlet could not be simulated. In contrast, they show that with a second-order fluid model, the vertebrae appeared in the simulation, at least qualitatively.

c) Integral Models

Characteristic for all integral models is that they contain a ‘memory function’ (Crochet, Davies, & Walter, 1984; Dupont, Marchal & Crochet, 1985). In such a model, the stress tensor is represented by the following equation:

$$[\sigma] = \int_{-\infty}^{t} m(t,t') \cdot H(t,t')\, dt' \text{ with } t' \leq t \tag{2-13}$$

in which

$$m(t,t') = \frac{\mu}{\lambda} e^{\left(-\frac{t-t'}{\lambda}\right)} \tag{2-14}$$

is the memory function, and *H* is the deformation tensor.

The K-BKZ model—named after Kaye, Bernstein, Kearsley, and Zapas—is currently the most advanced integral model for describing viscoelastic behaviour (Bernstein, Kearsley, & Zapas, 1963; Kaye, 1962). Cha et al. (2019) show that also including the structural viscosity of polymer melts leads to realistic predictions. In addition to the relaxation spectrum, the model contains only two further material parameters that can be obtained from three independent rheological experiments. From a molecular perspective, the K-BKZ model maps the survival probability of the entanglement network of a polymer melt as a function of its age. At the same time, the survival probability of the entanglement network, depending on the amount of deformation and magnitude of the deformation rate, is considered.

The main problem in solving integral models is so-called particle tracking—the tracking of the streamlines (locations of a material particle) at the integration points. Based on this information, the stress tensor can be calculated. Particle tracking, together with the time integration along the streamlines of a particle, is thus the essential part of the strategy of solving flow problems aided by integral models.

To summarise, no viscoelastic fluid model exists that is equally suited for all flow types while being simple to administer in practice. Although second-order fluids have been used to qualitatively simulate effects such as vertebrae at an inlet, they are less suitable for predicting viscoelastic time effects. The most realistic differential model currently available, the Oldroyd 8-parameter model, considers both first and second normal stress differences and time effects, but few of its material parameters can be determined from rheological experiments. In contrast, for the most promising integral model currently available, the K-BKZ model, material parameters can be determined relatively easily. The difficulty with integral models lies rather in the determination of the deformation history

(particle tracking). Thus, in none of the reviewed studies could a multidimensional flow problem for injection moulding be found that has been solved using a K-BKZ model. This suggests that complex particle tracking is time consuming and probably not practicable at present.

Kennedy and Zheng (2013) observe that in injection moulding, most commercial simulations do not explicitly consider viscoelastic effects. An explanation for this could be the difficulties in using appropriate viscoelastic models. This is an important finding; in view of the overall aim of the thesis to propose a new method for determining the flow front velocity of a plastic melt by establishing a relationship between simulated and measured injection pressures, it is important to examine the non-consideration of viscoelastic effects in the simulation. In the unfavourable case, this could lead to larger deviations between model and reality, especially in simulations employing the variation of boundary conditions.

2.3.2 Numerical Methods

The motion of any fluid is described by Cauchy's equation (2-15) of motion (Flügge, 1960). According to the equation, specific momentum change is initialised by the specific gravity and the drive by the stresses. All variables in the equation are dependent on both place and time. By considering the stress tensor, as well as the material parameter μ, as constant viscosity, one obtains the Navier Stokes system, consisting of a total of four equations, three of which are equations of motion (with the partial derivatives of the velocity field $\underline{u}$), as well as the equation of continuity and the initial and boundary conditions (2-15).

$$\rho\left(\left(\frac{\partial \underline{u}}{\partial t} + (\underline{u} \cdot \nabla)\underline{u}\right)\right) = \underline{f} - \nabla p + \mu\, \Delta\, \underline{u} \quad \text{'equation of motion'} \tag{2-15}$$

where $\nabla \cdot \underline{u} = 0$ is the 'equation of continuity', and $\underline{u}_{\Gamma\Omega} = \underline{g}$ and $\underline{u}_{t=0} = \underline{u}_0$ are boundary and initial conditions.

Because not every fluid is Newtonian, non-linear polymeric behaviour can be considered by incorporating approaches such as the cross-WLF model (Section

2.3.1). The constitutive relationship is the mathematical expression of the rheological behaviour of the fluid, determined for experiments conducted in simple flows with instruments, including viscometers and rheometers.

In addition to incorporating the non-linear behaviour of molten plastics, flow and filling analysis by simulation requires injection moulding-specific boundary conditions (Kennedy & Zheng, 2013). These boundary conditions must be described upon several surfaces: (a) the surface through which the melt enters the cavity (gate surface); (b) the top, bottom, and edge of the mould surfaces; (c) surfaces defining any inserts or pockets of the mould; and finally, (d) the (free) surface defining the melt front of the injected polymer. On all cavity and insert surfaces, the pressure gradient in the normal direction to the boundary is zero (impermeable boundary). This also applies to the velocity vector in the normal direction to the boundary due to the adhesion of the melt to the wall in shear flow. At the melt front surface, the pressure condition is zero. Since the mould is vented to allow air to escape the cavity, this condition is acceptable. In advanced simulations, however, some counter pressure conditions are described on the melt front surface. In addition to pressure and flow rate, temperature conditions are required; individual temperatures are usually predetermined on all mould surfaces. The temperature profile through the cavity cross section is prescribed for the surface through which the melt is injected into the cavity.

In injection moulding, it is widely accepted that the actual solution of the systems of equations upon which the flow problems are based is usually obtained numerically, with the aid of the finite element method (Kennedy & Zheng, 2013; Rannacher, 2000; Zhou, 2013).

Different approaches thus exist (Agassant et al., 2017; Kennedy & Zheng, 2013). These methods can be based either on primary variables—and consist of solving a set of equations with respect to the unknown—or on solving stream or penalty terms. By introducing a stream function, for example, it is possible to define the velocity field in such a way that the continuity equation is fulfilled identically. If the continuity equation applies, a stream function also regularly exists; for every

incompressible flow, there is also a stream function. This makes the system of equations uniquely solvable.

Chorin-Temam suggests a solution of velocity and pressure via decoupling the equations of continuity and of motion (Quartapelle, 1993). In a diffusion step, freedom from divergence (i.e., fulfilment of the continuity equation) is waived by removing the pressure gradient from the equation of motion. In an incompressible fluid, density is spatially constant, and the flow field is free of divergence. In a second step, the continuity step, the velocity from the diffusion step is projected onto its divergence-free component. The system of equations is thus solved down to the boundary condition. This is attenuated to the impermeability condition and is therefore only an approximate solution. A given error bound can approximate to any desired accuracy. Chorin-Temam sees the advantage of the method in the fact that it converges more quickly than methods with stream functions.

Another method has been proposed by Heinrich and Vionnet (1995). The penalty term method uses a 'slightly' compressible fluid instead of an incompressible one. Instead of the continuity equation, the artificial equation of state is used,

$$\varepsilon' p + \nabla \cdot \underline{u} = 0 \tag{2-16}$$

with ε', the so-called penalty parameter. By inserting Equation (2-16) into the Stokes equations (2-15), the pressure is eliminated. In the formulation of the Stokes equations, the secondary condition, freedom of divergence, is extended by the penalty term. The 'punishment' becomes greater the further one moves from the fulfilment of the continuity equation, which can cause this method to converge more quickly than methods with stream functions.

Numerical solution methods are often referred to as explicit or implicit. If a direct calculation of the dependent variables can be performed in terms of known quantities, the calculation is called explicit. If the dependent variables are defined by coupled sets of equations as described above and either a matrix or an iterative technique is required to obtain the solution, the numerical method is called implicit. In fluid dynamics, the governing equations are non-linear and the number

of unknown variables is usually quite large (Flow Science, 2021). Under these conditions, implicitly formulated equations are almost always solved using iterative methods.

Iterations are used to bring a solution from an initial state to a final, converged state through a sequence of steps. This is true whether the solution sought is a step in a transient problem or a final result in steady state. In both cases, the iteration steps resemble a time-like process. Of course, the iteration steps do not normally correspond to realistic time-dependent behaviour. In fact, it is this aspect of an implicit method that makes it attractive for steady-state computations, since the number of iterations required for a solution is often much smaller than the number of time steps required for an accurate transient process that asymptotically approaches steady-state conditions.

In summary, the numerical solution of a flow problem, using the finite element method, even with non-linear polymeric behaviour, is not a real challenge in the simulation of polymer flow. The methods existing for solving the differential equations are all widely adopted in commercial simulation and show good results in the ability to converge quickly. Thus, more important than the numerical approach remains the selection of the rheological model to describe the viscous and viscoelastic behaviour of molten plastic. As such, the literature review has found that this choice depends significantly on the following criteria:

1. The ability to describe the underlying rheological behaviour of the flow problem in such a way that it includes as many viscous and viscoelastic effects as possible, so that the numerically determined behaviour comes as close as possible to the real behaviour; and

2. The possibility of obtaining the material parameters required by the model in question by means of rheological tests that are as simple as possible, and not, if possible, by extrapolation.

2.4 Control Strategies for Injection Moulding

2.4.1 Feedback Control for Injection Velocity

In addition to controlling parallel and successive mechanical movements and processes, the control of an injection moulding machine comprises the monitoring and control of key process variables—temperatures, pressures, velocities, and strokes—which either serve as setting parameters for the injection moulding process or are obtained during the process by appropriate sensors for the purpose of process monitoring.

Hunker (1975) finds that at the beginning of the development of injection moulding, the control components were more of an open-loop nature. However, other more recent researchers believe that the increasing complexity of the moulded parts, as well as rising demands on tolerances and precision, necessitates increasing compensation for disturbances during the moulding process with closed-loop controls (Menges et al., 1999; Menges et al., 2011; Stitz & Keller, 2001).

In classical feedback control, the controller regulates the parameters based on real-time measurements during the process. The previously analogously modelled—and today in injection moulding, mostly *digitally* modelled—proportional-integral-derivative (PID) controllers form the main group of the classical feedback control. In the plastics industry, it is widely accepted that PID feedback control can eliminate steady state errors through integral action and predict future dynamics through derivative action (Yang et al., 2016; Zhou, 2013). However, the review has found that process control in injection moulding must be considered in the context of the complex and unique characteristics of the injection process, its hybrid nature, and the non-linear behaviour of polymeric materials (Section 2.2.5). These considerations necessitate the development of new approaches in the field of closed-loop controlling injection velocity.

To summarise, since the filling process in injection moulding usually occurs at high pressures and rates, the injection units of the moulding machines have mostly

been designed on a hydraulic basis. For a long time (until well into the 1980s), the control of such hydraulic injection units during the filling phase was limited to melt temperature and injection pressure. According to Equation (2-2), this caused injection velocity to become the dependent variable and become adjusted to the respective set injection pressure, depending on external conditions. The injection velocity that self-adjusted to injection pressure became neither foreseeable nor reproducible for the operator. Only with the availability of servo valves has the injection velocity (and later, with the advent of microprocessor-controlled machines—the injection velocity profile) become a set variable and thus now be able to be closed-loop controlled. In such a closed-loop injection velocity control, screw position and velocity are measured during filling by a transducer connected to the screw. The input variable injection velocity is 'translated' by the controller into a voltage output, which controls the opening amount of the servo valve and thus leads to a controlled forward movement of the screw proportional to the melt flow rate inside the barrel of the injection unit and independent from the injection pressure. In today's state-of-the-art electro-mechanically designed injection moulding machines (at least for smaller and medium injection rates), injection velocity is controlled directly and proportionally by the electric servo drive.

For the purpose of closed-loop controlling injection velocity, Tsoi and Gao (1999) have developed a PID controller. Fig. 2-8 shows the response of the controller to a two-stage injection velocity profile (set point). In the initial range, the controller works satisfactorily, but it begins to oscillate strongly at the change-over point from 50 to 10 mm/s injection speed due to the non-linearity of the filling process. Tsoi and Gao show that the oscillation can be reduced by adjusting the controller parameters (response time), but they also demonstrate that due to the variability of process conditions during injection moulding, a PID-based feedback control strategy is not sufficient for controlling injection velocity because the control of the injection velocity involves a large degree of uncertainty. Different moulds and materials are used for the same moulding machines, which causes strong variations in process dynamics. Non-linearity and time variations seriously affect

velocity response and are difficult to quantify. Therefore, traditional PID feedback controllers, with fixed parameter settings, fail to achieve performance to control injection velocity over a wide range of operation conditions. To solve this problem, various advanced feedback control strategies have been adopted in injection moulding (Ouyang et al., 2004, Yang & Gao, 1999): adaptive control, model predictive control, and intelligent control strategies.

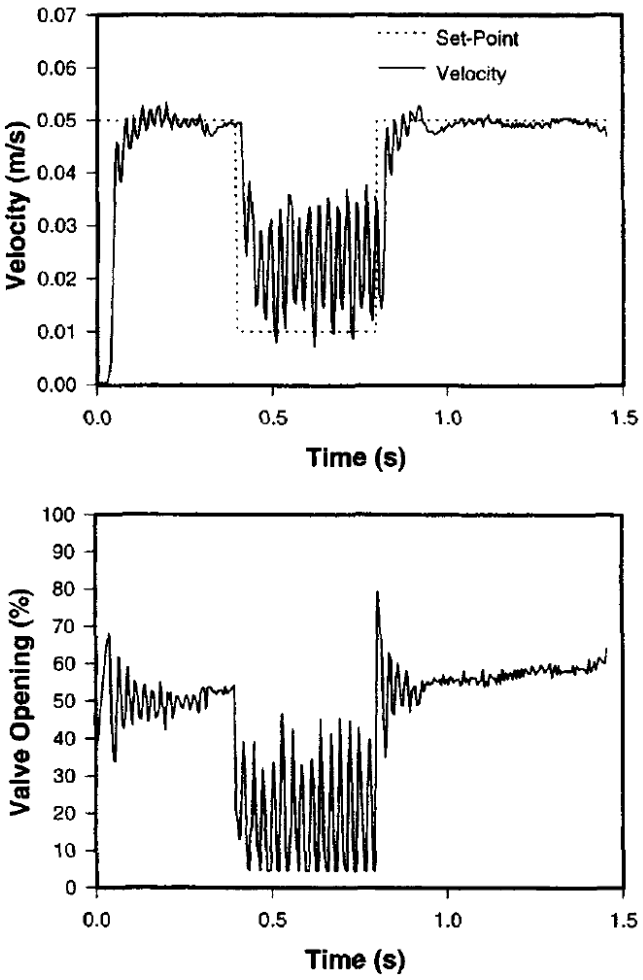

Fig. 2-8: Velocity response of proportional-integral-derivative control (Tsoi & Gao, 1999)

In adaptive control, controller parameters are adjusted to compensate for changes in process dynamics. In research by Yang et al. (2016), the adaptive controller comprises two loops: an inner (ordinary) feedback loop and an outer, parameter-adjusting loop. Process model parameters are updated during each sampling period with a specified model structure. Yang and Gao (2000) have applied

adaptive feedback control for testing an injection velocity set point profile and find that the controller can provide good control. Compared to the PID controller, the injection velocity follows the set point well, but the response time is still too slow to fulfil the requirements.

In contrast to adaptive control, model predictive control explicitly utilises a prediction model to obtain the control signal by optimising future behaviour. Various model predictive algorithms have been proposed (Camacho & Bordons, 1995; Clark, Mohtadi, & Tuffs, 1987; Wang, Zhou, & Gao, 2008). According to Zhou (2013), in injection moulding, intelligent control refers to control strategies based on fuzzy logic systems. These strategies attempt to use fuzzy logic, constructed on human knowledge in the form of 'fuzzy if-then rules', as a universal approximator to describe the non-linearity of the injection process. The key to fuzzy system design and implementation is the accumulation and formulation of knowledge. It performs non-linear mapping from fuzzy input sets to an output set using fuzzy logic principles.

In an advanced control concept in which an injection velocity profile must compensate for geometric changes in the flow channel cross-sections, a constant flow front velocity places high demand on the control of the injection speed over a wide set point range. Tsoi and Gao (1999) show that a fuzzy logic-based feedback control is capable of fulfilling this demand. Their research demonstrates the velocity response (and corresponding servo valve opening) for feedback fuzzy logic control, as shown in Fig. 2-9. Compared to the PID controller response (Fig. 2-8), the injection velocity closely follows the set point at 50 to 10 mm/s, indicating good system performance. This demonstrates that, despite non-linearity and time variation, in an injection moulding process with a feedback controller based on fuzzy logic, closed-loop control of the injection velocity is possible for a wide range of applications.

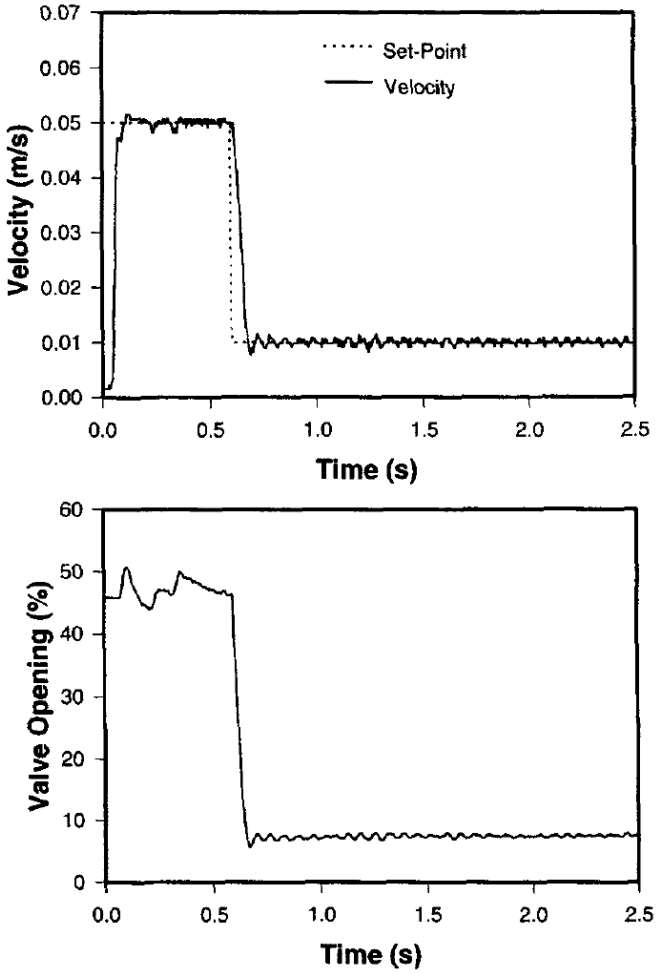

Fig. 2-9: Velocity response of feedback fuzzy logic control (Tsoi & Gao, 1999)

2.4.2 Learning Control

As the Section 2.2.5 demonstrates, the injection moulding process is a typical batch process with a repetitive character. In such a process, it is common practice to use information from previous process cycles to optimise current or future process cycles. This type of cycle-to-cycle optimisation is similar to human learning and is thus referred to as iterative learning control (ILC).

In his study, Zhou (2013) defines an ILC system for injection moulding comprising two feedback loops: one is a timewise feedback control strategy maintaining control performance within the cycle, and the other is a batchwise controller adjustment system that updates controller parameters from cycle to cycle. The ILC control algorithm can be described as follows:

$$u(t) = u_{k-1}(t) + F_{ilc}(U_{k-1}, Y_{k-1}, Y_r) \quad (2\text{-}17)$$

where *u(t)* is the output at the t^{th} sample in the k^{th} cycle, Y_r is the desired output trajectory, and U_{k-1} and Y_{k-1} are the controller output (and process response) from the $(k-1)^{th}$ cycle.

Among other researchers, Yang et al. (2016) propose learning control strategy to exploit the repetitive nature of injection moulding processes, as with any other batch process. They see the advantage of learning control in injection moulding in the fact that the control can converge well along the cycle direction when the process dynamic is exactly repeatable and the design of the control law requires little process knowledge, but with relatively good robustness. An ILC system is the right choice as a controller since, in an advanced control concept based on machine-independent parameters such as a constant flow front velocity, the determination of the set points for the injection velocity control occurs exclusively between injection cycles. This is further discussed in Sections 2.5 and 2.6.

2.4.3 Direct Quality Control

To date, less attention has been paid in injection moulding to the direct control of final part quality. Yang (2004) attributes this to the difficulty of measuring part quality online. Another reason why direct quality control is still rarely seen in the context of an overall process control concept in injection moulding might be the complex thermal and rheological properties of the polymeric material, which makes it difficult to analyse the relationship between quality characteristics and process condition. Another difficulty is that changes in the machine and the mould cause shifts in process dynamics. The same process setting in the moulding machine could result in different form part quality on different machines.

One of the few studies that has incorporated direct quality control in an overall concept for process control comes from Karbasi and Reiser (2006). In their detailed concept, injection moulding control can be regarded as three nested process loops, as shown in Fig. 2-10. The first loop controls machine parameters

such as velocities, pressures, and temperatures, while the middle loop controls key process variables. The third layer that Karbasi and Reiser describe provides a mechanism for closed-loop quality control of certain part quality (direct quality control).

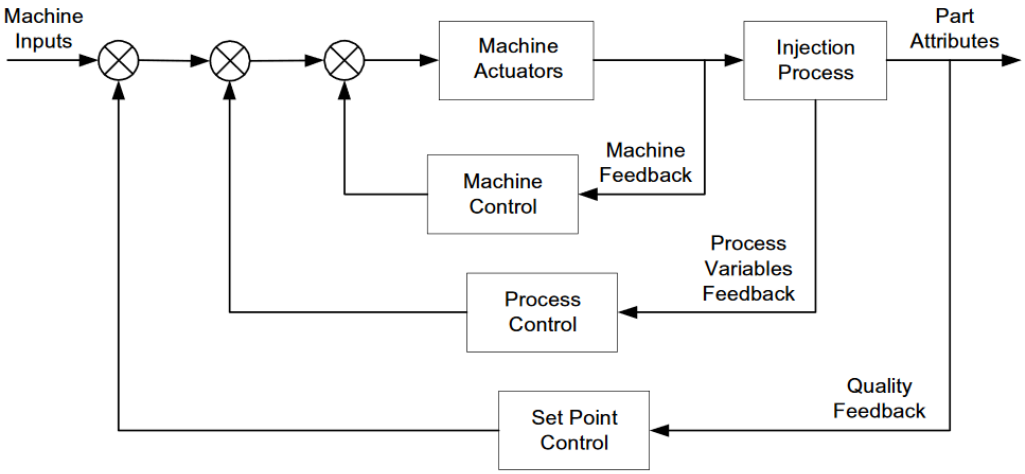

Fig. 2-10: Injection moulding control loops (Karbasi & Reiser, 2006)

Applied to an advanced machine control concept based on flow front velocity, the inner loop of Karbasis and Reiser's concept describes the control of the injection speed during the filling phase via a fuzzy logic-based feedback control (Section 2.4.1). Flow front velocity, or any other machine-independent parameter, is controlled between machine cycles by an ILC controller (Section 2.4.2) and is expressed by the middle loop of Karbasis and Reiser's scheme. In an advanced control concept, the third layer that Karbasi and Reiser describe provides a mechanism for closed-loop quality control of certain technical or mechanical part properties such as distortion; residual stress-optimised, homogeneous form part structure; and high surface quality. As described in Section 2.2.4, the direct quality control of these characteristics can only be achieved by advanced controlling machine-independent process parameters, such as constant flow front velocity or constant melt viscosity.

Against the background of increasing quality requirements in the plastics industry, the approach of Karbasi and Reiser is logical and consistent and will thus be crucial in the future. Such a concept can also be applied to an advanced machine control based on machine-independent parameters. A general prerequisite for direct quality control is the development of methods that better relate the relationship between quality characteristics and process conditions.

2.5 Measurement and Control of Polymer Melt Status

2.5.1 Measurement Inside the Injection Mould

The review has found that most measurements inside the mould are related to pressure and temperature (Bader, 2013, Karbasi & Reiser, 2006; Kulkarni, 2010; Michaeli & Schreiber, 2009). A pressure sensor located along the flow path provides information about the melt pressure during the filling, holding pressure, and cooling phases. A temperature sensor can provide the temperature of either the polymer or the mould. In combination with a pressure sensor, a temperature sensor can also obtain information about flow front velocity. This is further discussed in Section 2.6.1.

Research by Zhao et al. (2020) finds that the information obtained from the pressure graph is important for several reasons; the pressure graph provides information gained from the melt pressure inside the mould and therefore on the specific volume-temperature relationship, which relates directly to form part quality. Karbasi and Reiser (2006) propose a model comprising five phases through which the melt passes when injected into the mould (Fig. 2-11). Their model is important because it is used to define the classification of the various subphases during the mould filling and holding pressure processes. In the transition from filling to the holding pressure phase, the injection machine switches from a closed loop-controlled injection velocity mode to a closed loop-controlled holding pressure mode. However, the model does not provide any information about the quality of the information of the melt pressure in relation to the location where the melt pressure is determined. This relationship is well known in injection

moulding and has been studied by various researchers.

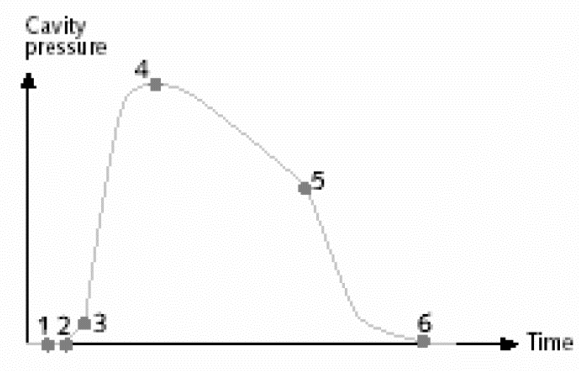

Fig. 2-11: Phases in the cavity pressure profile (Karbasi & Reiser, 2006)

Kulkarni (2010), for example, compares the characteristics of the hydraulic pressure and cavity pressure graphs at these transition points and shows that the control of cavity pressure is the better choice. Because cavity pressure relates directly to the status of the melt inside the mould where the forming process occurs, the measured cavity pressure provides information, such as about the sealing of the gate, which can be used to determine the switchover time (set-point tracking) between the injection and holding pressure phases. Several references to this are found in the literature (Bader et al., 2013; Gao, Patterson, & Kamal, 1994; RWTH Aachen University, 2017; Stitz & Keller, 2001). However, if cavity pressure provides sufficiently good information to execute between individual process subphases, adaptive process control of the cavity pressure might be a good option to process control the filling phase of the injection cycle.

2.5.2 Adaptive Control of Cavity Pressure

Process-relevant control parameters have long been related solely to the injection moulding machine. Process optimisation has comprised the optimisation of machine set-up parameters, such as injection speed or holding pressure. The actual forming process, however, occurs inside the injection mould. Thus, the measurement and monitoring of polymer melt status along its flow path is, to a

high degree, important to the online quality control of the injection moulding process, as well as to repeatability from cycle to cycle. If each cycle occurs under exactly the same conditions that are measured inside the cavity, all of the form parts produced will be identical. Sitz and Keller (2001) examine whether deviations between cycles can be determined with the cavity pressure process. With information from the sensor fed back to the injection machine, the filling pressure within the cavity can be monitored, and deviations between cycles can be minimised by an appropriate control concept (Kulkarni, 2010; RWTH Aachen University, 2017). Some efforts have been made in self-reliant control systems, which can adjust the cavity pressure successfully during the filling and holding pressure phase with excellent ability for set point tracking (Gao et al., 1994).

The literature review has shown that despite the good performance of cavity pressure adaptive control, the injection moulding industry is still reluctant to move to closed-loop controlled cavity pressure (Kulkarni, 2010). On the one hand, this occurs because the mould must be equipped with the necessary measuring technology; undesirable marks on the surface of the moulded part appear due to the installation of the sensor, and the additional tooling costs for using an in-mould sensor for each mould are high. On the other hand, this occurs because of the lack of a direct relationship between the cavity pressure and the rate of filling (Tsoi & Gao, 1999). As such, instead of cavity pressure, injection velocity should be used as a preferred control parameter for the filling phase of the injection moulding process. The problem is that for the set-up of the injection speed profile, a rule-based strategy is required. This is further discussed in the next section.

2.5.3 Profile Setting of Injection Velocity

The filling phase in injection moulding begins with the start of the injection process and ends with the switch to holding pressure. The filling phase takes place at a controlled injection velocity. The pressure loss resulting from injection can easily exceed 100 MPa and often occurs due to the economic efficiency of the

manufacturing process. The trend towards material savings leads to thinner walls, thus causing high injection pressures (Menges et al., 1999).

Injection speed depends strongly on the geometry and material properties of the moulded part and can be optimised based on pressure losses and temperature changes (Stitz & Keller, 2001). In general (and described in a highly simplified way), a high injection speed (i.e., a high flow rate) leads to high pressure losses when filling the cavity. However, even extremely low injection speeds can lead to high pressure losses due to decreasing flow channel heights, caused by frozen wall layers. To address this problem, Stitz suggests that optimised injection velocity should be in the range of minimum injection pressure and should consider the temperature changes of the melt on its way from the injection piston to the end of the flow path. The aim is to prevent the flow front from freezing by providing approximately the same amount of heat (the dissipation energy) through the appropriate flow rate as is being withdrawn from the melt by heat transport to the mould wall (Fernandes, Pontes, Viana, & Gaspar-Cunha, 2016; Schröder, 2018).

Gao et al. (2018) believe that most setting parameters in an injection moulding process are traditionally determined ‘empirically’ by ‘trial and error’. The operator takes random samples during the set-up phase and then uses their experience to optimise the process from cycle to cycle to improve part quality. Such an approach is not only time consuming and cost intensive but also characterised by the fact that ‘success’ depends largely on the ‘knowledge and experience’ of the operator. According to Gau, the operator regularly reaches limits when trying to ‘describe experience’, and there is often no justification for the setting. Only in the rarest cases does an optimisation follow a ‘rule-based strategy’.

However, since the quality of the moulded part is largely determined by rheological conditions during the filling phase, a rule-based procedure for profiling the injection velocity would be desirable above all to achieve constant and predictable form part quality. In the past, repeated attempts have been made to develop general guidelines for profiling injection velocity. One of the first was by Hunkar (1975), who proposed a multistep injection velocity profile for form parts

with different cross-sectional flow paths, as shown in Fig. 2-12. Hunkar suggests setting injection velocity height while filling the runner (Section I). To avoid jetting, the velocity needs to be reduced when passing the gate (Section II). In the region of increasing melt-front-area, the injection velocity is ramped up proportionally (Section III) until it is maintained in the area where the melt-front-area is constant (Section IV). At the end of the filling (Section V), the injection velocity is reduced to avoid flashing.

Although Hunkar's method roughly describes how an injection velocity profile should look qualitatively, the quantitative determination of injection velocity remains empirical because of the non-existence of calculation methods in his model.

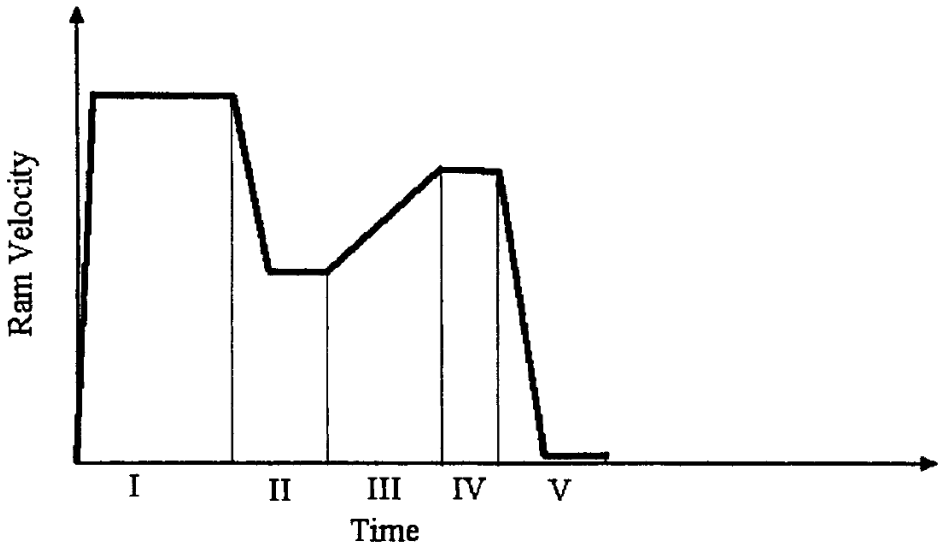

Fig. 2-12: Injection velocity profile (Hunkar, 1975)

Various studies have shown the effects of injection velocity on orientation, residual stress, and the surface properties of the moulded part (Boldizar et al., 1990; Chiu et al., 1991; Tan & Tang, 2002). A real milestone for a rule-based strategy occurred when it was realised that a constant flow front velocity of the melt during the filling phase (from gating to mould filling) leads to distortion and residual stress-optimised, homogeneous form parts (Chen, 2002; Zhou, 2013). However, as far as the author is aware, limited previous research exists on the

modelling and analysis of the flow front of the melt inside the mould in relation to the position of the injection moulding machine screw.

Fig. 1-1 illustrates this problem. Melt front velocity v_m differs from injection velocity v_b and is influenced by mould geometry A_m. Due to the non-linear nature of the filling process, the flow path of the melt front is not predetermined and depends on location and time. For constant flow front velocity, an injection speed profile must compensate for geometric changes in flow channel cross-sections, but profiling the injection speed is only possible with knowledge about the melt front velocity.

To date, for the setting of the moulder, this problem remains unsolved, and the profiling of the injection velocity is done by the operator primarily empirically. However, the literature review has found that efforts have been made in the field of advanced control techniques, such as 'control for a constant melt front velocity through average flow path length' (Section 2.5.4 and 2.5.5).

2.5.4 Control of Melt Front Velocity through Average Flow Length

Since no knowledge of flow front velocity v_m exists, Chen and Gao (2000) propose determining the appropriate injection velocity profile $v_b\ SP$, for a given constant flow front velocity v_m, by measuring the area of the melt front A_m using a soft sensor model. Because the cross-sectional area of injection barrel A_b is constant, melt front velocity v_m can be held constant if the injection velocity v_b is profiled and closed-loop controlled proportionally to melt front area A_m.

Fig. 2-13 shows the block diagram of the soft sensor-based controller Chen and Gao propose. The inner loop describes the classic feedback controller for set injection velocity. The outer loop has a controller which determines injection speed profile $v_b\ SP$ for a constant melt front velocity v_m based on the measured melt front area A_m, provided by the soft sensor.

The key function is therefore the measurement of the melt front area A_m. For this purpose, Chen and Gao suggest a soft sensor algorithm based on average flow

path length, which can be derived as a time integral of melt front velocity. To simplify, Chen and Gao use a discrete form to express the equation proposed by Yang et al. (2016) and assume that the melt and mould temperature would remain constant during the filling process. They determine the average flow path length for the n^{th} sample by

$$x_{m\,n} = f(x_{m\,n-1}, p_n, \Delta p_n, x_{b\,n}, \Delta x_{b\,n}, v_{b\,n}) \tag{2-18}$$

as a function, among other variables, of the length of the flow path of the previous sample, injection pressure, screw position, and injection velocity.

The problem is that even with simplifications, the function (2-18) is too complex to solve since it represents a combination of mass, momentum, and (if temperature is not considered to be constant) energy conservation. The algorithm is not able to feed the soft sensor model with the average flow length.

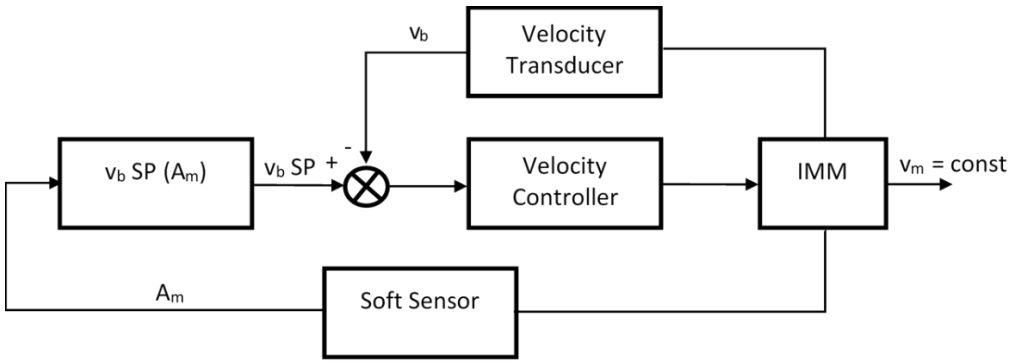

Fig. 2-13: Velocity profile setting based on melt front area (Chen & Gao, 2000)

2.5.5 Neuronal Network Model on Average Flow Length

To overcome this problem, Chen and Gao (2000) propose replacing their soft sensor algorithm by a 'black box model' in which input and output relationships are represented by a 'neuronal network'. In the absence of real flow front data, they train and test the neuronal network on different part geometries using filling studies obtained by simulation. With their 'neuronal network model' feeding the soft sensor, Chen and Gao (2000) demonstrate that predicting average flow front

length and thus determining a suitable injection set-up profile for a constant melt front velocity is possible under certain circumstances, within a certain error tolerance.

Fig. 2-14 shows melt front area A_m predicted with the aid of the soft sensor, fed by the neuronal network, in comparison to the predicted results from the simulation for two different, simple form part geometries that both have one-dimensional flow paths. The diagram proves that the determination of melt front area, and thus of a suitable injection speed profile for a 'constant melt front velocity' strategy, is possible in principle.

However, such a 'soft sensor model' requires simulation to teach the neuronal network and cannot be verified under real conditions because the melt front area cannot be measured directly. In practical applications, the soft sensor model does not play a role due to the underlying simplifications (i.e., isothermal model with simplified, one-dimensional part geometries) and high inaccuracy. However, despite this unsuitability for practical applications, the literature review has found that the considerations of Chen, Goa and other researchers have greatly impacted further developments of advanced control systems and led to the realisation that the problem of 'profiling the injection rate for a constant melt front velocity' can only be solved if it can be transformed into a much simpler 'control problem', in which the flow front velocity can be directly determined during the filling process (see Section 2.6.1).

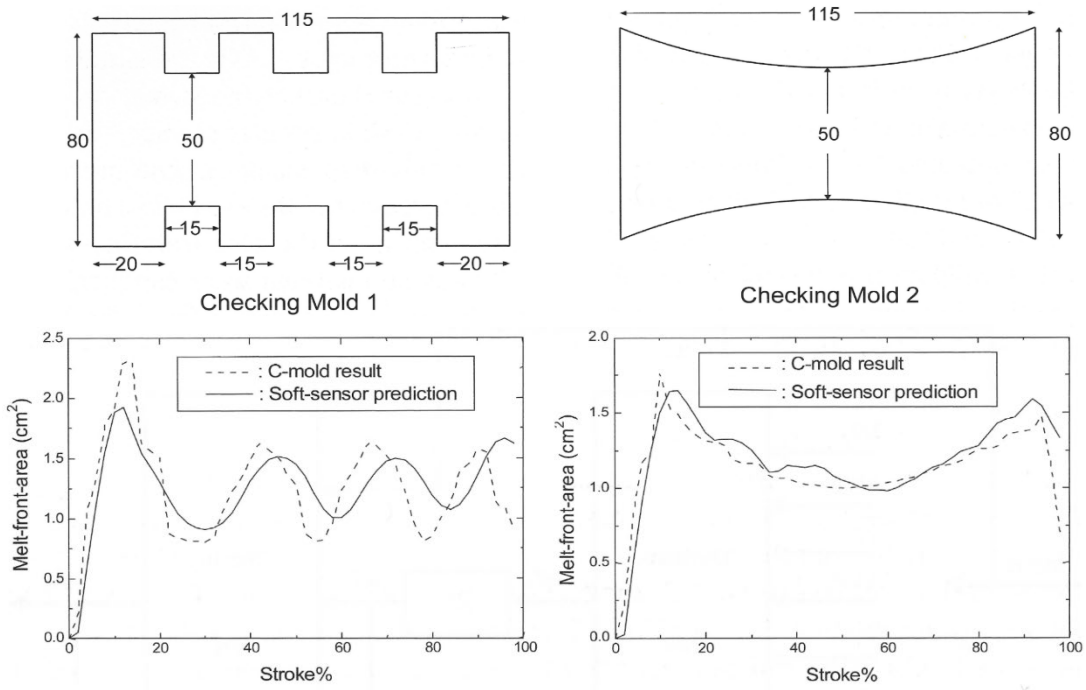

Fig. 2-14: Soft sensor-predicted melt front areas (Chen & Gao, 2000)

2.6 Other Related Methods

2.6.1 Direct Determination of Melt Front Position and Velocity

The first attempts to obtain information on melt front spreading during the filling phase were made in the late 1980s; Yokoi and others employed glass inserts and high-speed cameras (Yokoi et al. 1988; Yokoi & Inagaki, 1992). Over time, this method has been continuously improved—for example, by Bress and Dowling (1998)—to observe the melt front in 'larger' cavities and moulds. This relatively simple technique facilitated, for the first time, visual impressions of the flow and spread of the melt along its flow path. However, such methods are not suitable for real measurements in practice. Glass inserts do not resist real conditions during injection moulding (high pressures) and have different properties (thermal conductivity, etc.) than steel surfaces.

To monitor the filling, holding pressure and the cooling phases, Wong, Fung, and Gao (2007) have developed a capacitive transducer. Fig. 2-15 shows the schematic structure of the test mould equipped with a capacitive sensor inside the cavity. By

measuring change in the dielectric constant (CT signal) during the transition from air to plastic, the status of the polymer melt (flow path length) inside the cavity during filling can be determined. Various test measurements on one-dimensional form part geometries show good proportionality between the CT signal and various constant injection rates (Fig. 2-16). Despite some promising performance in simple form part geometries, capacitive measurement is more scientific in nature. In practice, it is difficult to implement such online monitoring because not all moulds are, or can be, equipped with capacitive sensors. Thus, for an advanced control strategy that can be applied in practice, methods other than capacitive measurement are necessary.

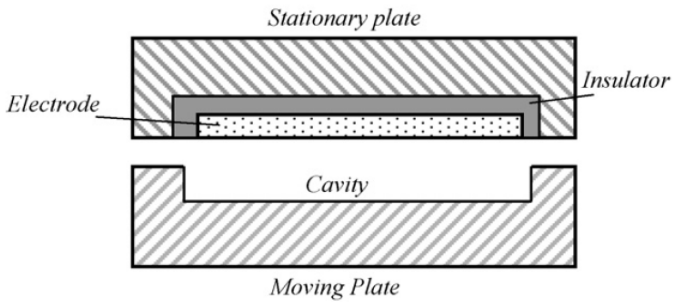

Fig. 2-15: Schematic illustration of mould design with capacitive transducer (Wang et al., 2008)

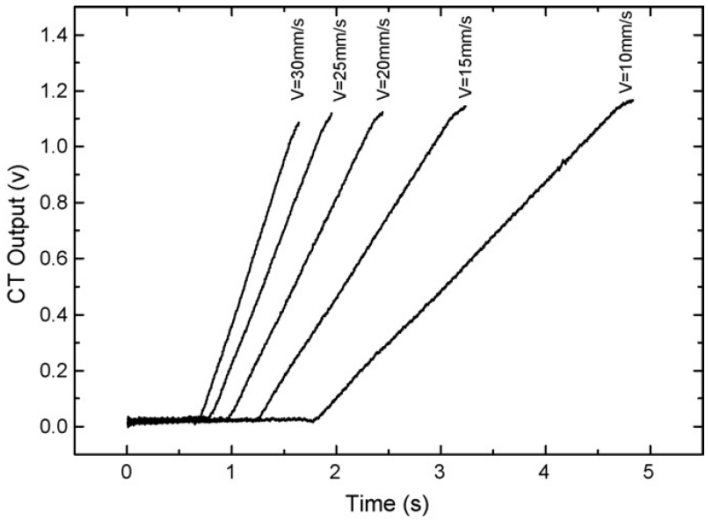

Fig. 2-16: Capacitive transducer output of different constant injection velocity settings (Wang et al., 2008)

Bader and Zeller (2010) have taken a different approach to direct measuring the flow front; they have developed a method in which the flow front position is directly measured through sensors inside the mould. In their method, the melt front first passes a pressure sensor and then, towards the direction of the flow path, a temperature sensor. Fig. 2-17 shows the measured signals of such a two-sensor configuration. When the melt front reaches the location of the pressure sensor *P1*, melt pressure begins to rise. If the melt front then arrives at the temperature sensor *T1*, a temperature rise is measured. Melt front velocity can be directly determined from the time difference between the two sensors. Because the first sensor passing the melt front gains a pressure signal, the differential pressure between the two sensor positions can be obtained. Due to the installation situation of the sensors (i.e., fixed position within the cavity), information about flow channel geometry between the sensor positions is available. From the height of the flow channel cross section, together with the measured flow front velocity and the obtained pressure increment, machine-independent parameters can be determined, such as shear rate, shear stress, and viscosity.

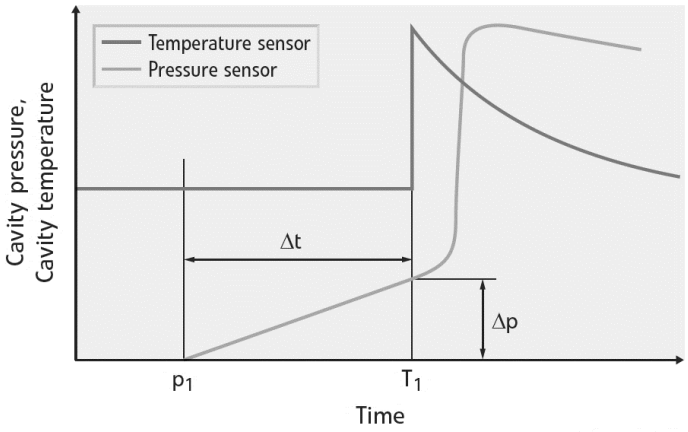

Fig. 2-17: Pressure and temperature signals for detecting melt front velocity (Bader & Zeller, 2010)

Gordon et al. (2013) have developed a similar method by measuring flow front velocity using a multifunctional sensor. This sensor uses an infrared thermopile for temperature measurement and a piezoelectric ring for pressure measurement. The melt front velocity is estimated by the rise of the pressure signal, and viscosity can be estimated using pressure and velocity based on constitutive rheological models. These rheological models are used to correct the height of the flow channel cross section by the amount of the frozen boundary layers. Due to this correction, the derivation of the viscosity of the melt from the measured data is comparable to the viscosity calculation of common simulation programs.

Fig. 2-18 shows characteristic machine-independent parameters determined through direct measurement of the melt front in a two-sensor configuration of a test mould developed by Bader and Zeller, each for different injection rates and melt and mould temperatures. Despite good performance, the most significant problem associated with the 'sensors in mould' method is that the flow front position and all derived parameters, such as velocity and viscosity, can only be determined in the spaces between the two sensor positions, which makes continuous measurement over the entire flow path practically impossible. Furthermore, placing sensors in the limited space along the flow path is often extremely difficult, and the installation of the sensors significantly reduces the stiffness of the mould and the ability of the part surface to cool uniformly. This method has little practical application, primarily because equipping and

retrofitting moulds is time consuming and expensive.

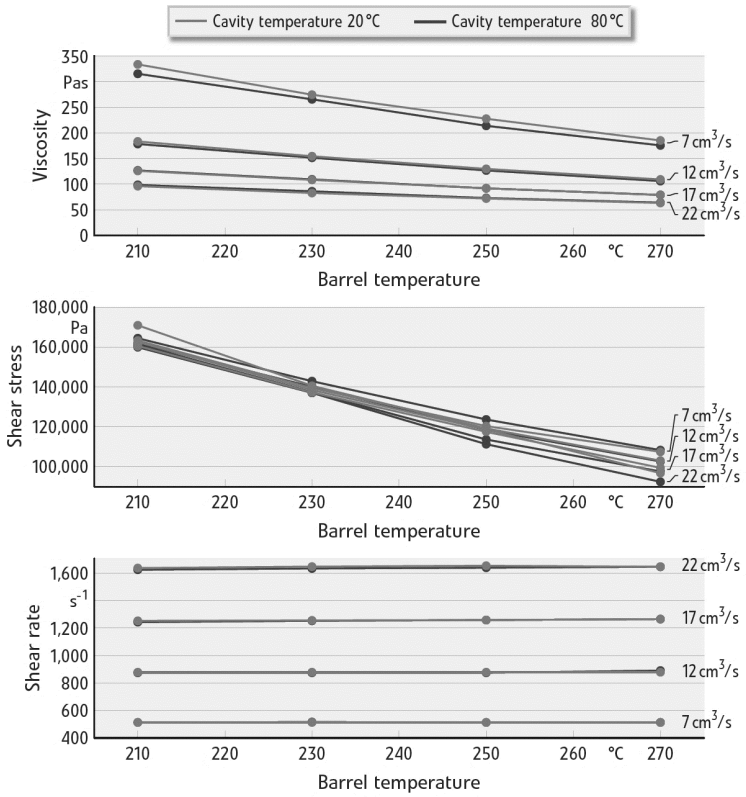

Fig. 2-18: Viscosity, shear stress, and shear rate for different injection rates and melt temperatures (Bader & Zeller, 2010)

2.6.2 Control of Melt Front Velocity through Capacitive Sensors

With a capacitive in-mould sensor, it was possible for Zhou et al. (2009) to develop for the first time a controller for a constant melt front velocity strategy based on the direct determination of the flow path length. For this purpose, they add a new module to their controller: the melt front position (MFP) controller. The melt front position is an integral part of a control system, which dynamically determines and adjusts injection velocity v_b for $v_m = const.$ from the flow path length x_m, provided by the capacitive sensor. Because injection moulding is a batch process, Zhou et al. (2009) consider a learning control model using the information from the previous cycle to improve the parameters of the new cycle.

Fig. 2-19 shows the block diagram of the learning control algorithm-based controller that Zhou, Yao, Chen, and Gao have developed. Their two-dimensional feedback control system, with one dimension along the cycle axis and the other along the time axis, consists of two loops: an inner loop for traditional feedback control of the injection velocity profile and an outer loop with the melt front position controller, which relates injection velocity to measured flow length between cycles based on learning control algorithms.

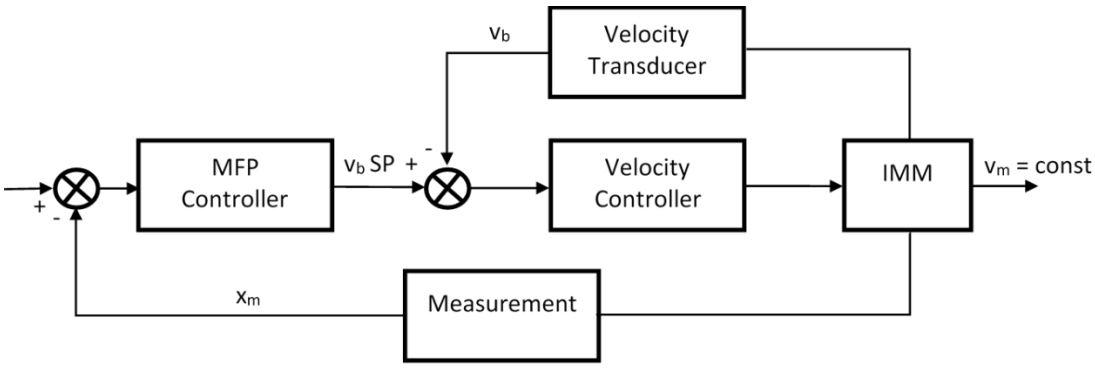

Fig. 2-19: Block diagram of melt front position controller system (Zhou et al., 2009)

Over the past two decades, much research and development has applied this two-dimensional velocity control concept in injection moulding, primarily in the research group headed by Gau. Related works include two-dimensional learning control-based feedback and output feedback robust designs (Shi, Gao, & Wu, 2005), robust fault-tolerant control (Wang, Liaw, & Chen , 2006), predictive iterative learning control (Shi & Gao, 2007), and even two-dimensional control algorithms for batch processes of key process parameters other than injection velocity (Shi, Gao, & Wu, 2006). This research has contributed significantly to the understanding and improvement of 'advanced control strategies based on learning control principles' in injection moulding, for the goal of 'intelligent setting and adjustment of the key process parameters', especially for the 'profiling of the injection rate'. Zhou (2013) demonstrates how quickly a melt front position controller for a constant melt front velocity can adjust an injection speed profile. Fig. 2-20 (a) shows a capacitively measured melt front position in a test mould for

the first iterations of the advanced learning control. The part geometry (Fig. 2-14, Mould 2) requires an adapted injection speed profile (fast-slow-fast) for a constant flow front velocity. In the first cycle, the pre-set injection speed is a constant 25 mm/s. As Fig. 2-20 (b) demonstrates, after only three iterations, the melt front position controller provides an injection speed profile which nearly leads to a constant flow front velocity (Fig. 2-20 [a]).

Although Zhou uses only simple (one-dimensional) form part geometries to demonstrate the performance of the controller, he has shown that it is possible, in principle, to control the injection profile for a constant melt front velocity. The limitations of Zhou's melt front position controller lie not in the concept of the controller itself but rather in the input of the controller. Fed by a capacitive sensor, which is not capable of being used beyond laboratory standards, an industrial application in real moulded parts with non-one-dimensional flow front courses is unlikely.

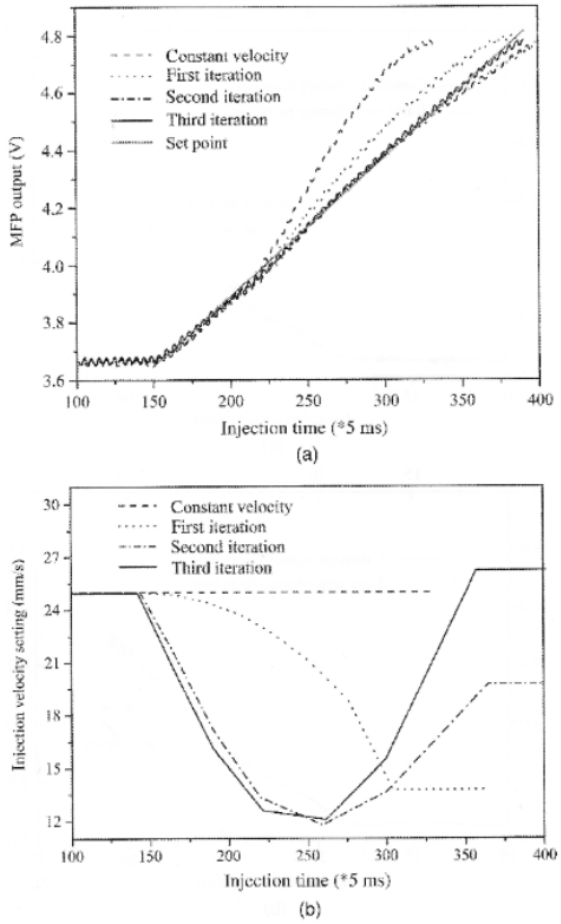

Fig. 2-20: (a) Melt front position response and (b) corresponding velocity setting (Zhou, 2013)

2.6.3 Advanced Control Strategies based on Machine-Independent Parameters

Bader and Zeller (2011) describe an advanced control strategy that far exceeds the determination and control of the injection speed profile for a constant flow front velocity, described above. By employing two sensors—for pressure and temperature, respectively—they directly measure flow front velocity inside the mould and determine other process parameters, such as the melt viscosity, shear rate, and shear stress of the melt. Based on these machine-independent parameters, Bader and Zeller developed a multifunctional control concept. Their controller not only determines and adjusts the injection speed profile of the moulding machine but also controls other key process variables, such as melt and mould temperature. In addition, this controller monitors the switchover point

between the filling and holding pressure phases (when the melt front reaches the end of the flow path) and controls holding pressure.

Fig. 2-21 shows how efficiently the multifunctional controller developed by Bader and Zellner functions. Starting from a constant injection speed (volume flow rate) of 10 cm^3/s, a melt temperature of 280°C, and a mould temperature of 50°C, the specified target values of (a) shear stress of 65,700 Pa and (b) shear rate of 510 s^{-1} are simultaneously achieved and held stable within a few cycles by the automatic adjustment of the injection speed profile. The viscosity in shear thinning melts is a function of shear rate and shear stress. If both can be controlled, melt viscosity can be controlled and held constant.

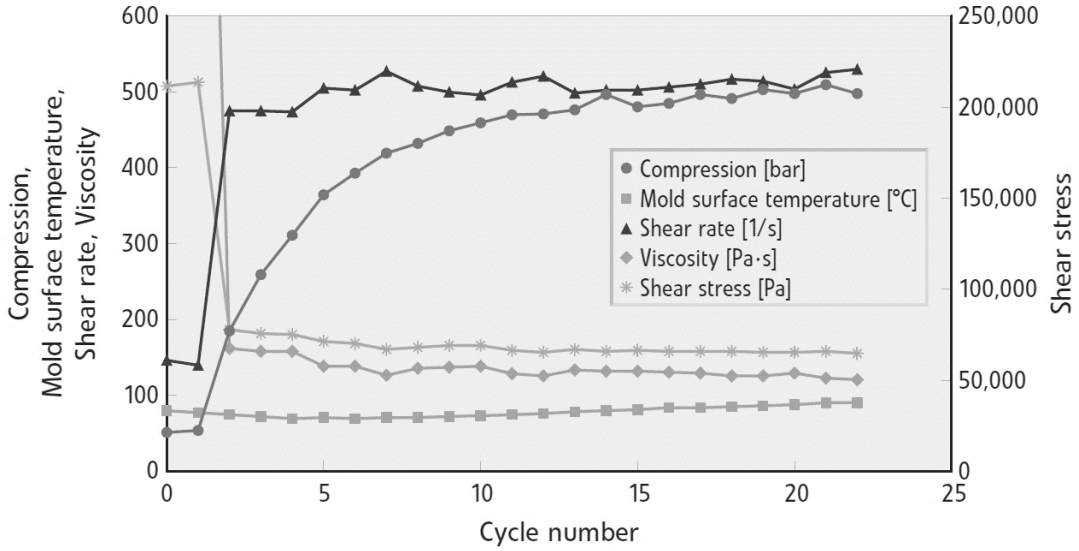

Fig. 2-21: Simultaneous shear stress, shear rate, and mould temperature control (Bader & Zeller, 2011)

With the controller developed by Bader and Zeller, nearly all conceivable advanced control strategies can be achieved. This is a desirable result; it proves the existence of a functioning and—in contrast to the controller concept of Zhou, Yao and Zheng—industrially suited controller which can control not only the flow front velocity but also machine-independent parameters such as viscosity and shear rate. But, as with the adaptive control of cavity pressure (Section 2.5.1), the injection moulding industry is hesitant to switch to advanced control strategies

based on machine-independent parameters due to issues in the determination of flow front velocity. The controller developed by Bader and Zeller relies upon (among other data for machine-independent parameters) the determination of the flow front velocity, done by direct measurement along the flow path. With at least two sensors in the mould (Section 2.6.1), the method has little practical application, primarily because (a) equipping and retrofitting the mould is time consuming and expensive, (b) the sensors may cause surface defects or reduce the stiffness of the mould, or (c) it is simply too complicated to place sensors in the limited space along the flow path.

In other words, advanced control strategies for injection moulding processes based on machine-independent parameters do not fail to produce practical applications due the non-existence of suitable controller concepts. The problem lies rather in how the controllers are fed with flow front information. According to the findings from the literature review, if the input signal for an advanced controller concept comes from a method that determines information about the front position and its velocity with sensors outside the mould, this will enable a wider distribution of advanced control strategies in injection moulding.

2.7 Chapter Summary

The overall aim of this thesis is to research, design, and develop a method for determining the flow front position and velocity of a polymer melt in an injection moulding process by mapping a simulated filling process to a real injection moulding process for an advanced process control. As such, this chapter has first reviewed definitions and provided an overview of the non-linear behaviour of polymers, the qualities of the injection moulding process, the simulation of mould filling, and the process control of the injection velocity, before considering existing methods for the measurement and control of the flow front in particular.

With regards to polymeric materials, this chapter has presented a literature review in the following areas: morphological structure, viscosity, shear thinning, and

viscous-elastic behaviour, as well as the flow of molten polymer. The following key issues have been identified:

- It is widely accepted that the behaviour of polymers can be considered non-linear.
- The flow of polymeric melt inside a cavity can be described as a non-isothermal, non-Newtonian, transient, laminate flow, in which the melt flows in layers.
- Complex, non-linear model approaches are necessary to describe melt flow. Hence, predicting the flow front position is exceedingly difficult.
- The flow of molten polymer in the cavity causes orientation. Orientation, however, leads to anisotropy and residual stress.
- The prediction of mechanical form part properties based on process parameters is not possible.
- Producing homogeneous, distortion-free, high quality form parts necessitates keeping flow front velocity constant during the filling phase.

For the area of injection moulding and process control, this chapter has identified the following key issues:

- Injection moulding is a repetitive batch process, with strong time-variant and non-linear characteristics and a hybrid system nature.
- In an advanced control concept, in which an injection velocity profile must compensate for geometric changes in flow channel cross-sections, a constant flow front velocity places high demand on the control of the injection speed over a wide set-point range.
- A fuzzy logic-based feedback control is capable of fulfilling this demand.
- To exploit the repetitive nature of injection moulding, learning control strategies are required.
- In an advanced control concept based on machine-independent parameters, the control of the flow front velocity can be conducted via an ILC controller, with one dimension along the cycle axis and the other along the time axis.

- Due to increasing quality requirements, an overall concept for process control that incorporates direct quality control will be crucial in the future. Such a concept could also be applied to an advanced machine control based on machine-independent parameters.

With regards to simulation, governing equations and numerical methods for simulation, the following key issues have been identified:

- Provided the 'right' mathematical model and 'right' material properties are used in the simulation to be undertaken, the analysis of simulation results can provide quality-determining characteristics, such as homogeneity or the variance of shrinkage.
- The information obtained from the analysis of simulation results can be used to pre-set the key process parameters of the injection machine.
- Simulation, even in combination with suitable DoE cannot replace an advanced process control strategy for optimising form part properties with respect to their molecular orientation.

In the area of the measurement and control of the cavity pressure inside the injection mould, the following key issues have been identified:

- Common process monitoring and control strategies of the polymer melt status inside the mould are limited to the injection pressure measured during the filling process.
- The adaptive control of cavity pressure is preferable to the control of the melt pressure in front of the screw.
- The adaptive control of the cavity pressure can lead to a high degree of repeatability between cycles.
- Despite the good performance of cavity pressure adaptive control, the injection moulding industry is still reluctant to move to closed-loop controlled cavity pressure, for several reasons: (a) undesirable marks on the surface of the moulded part due to the installation of the sensor, (b) additional tooling costs for using an in-mould sensor for each mould, and (c) the lack of a direct relationship between cavity pressure and filling rate.

- Instead of cavity pressure, injection velocity should be used as a preferred control parameter for the filling phase of the injection moulding process.

Reviewing the profile setting of injection velocity has provided the following findings:

- The profile setting of the injection velocity requires a valid rule-based strategy.
- The realisation that a constant flow front velocity leads to homogeneous, distortion-free moulded parts has led to the development of a valid rule-based strategy.
- For constant flow front velocity, the injection speed profile compensates for geometric changes in flow channel cross-sections.
- The problem with profiling the injection speed is the lack of knowledge about the flow front of the melt inside the mould in relation to the screw position of the injection moulding machine.
- To date, knowledge about the flow front remains lacking, and the profiling of injection velocity is mainly done empirically by the operator.
- Efforts have been made in the area of advanced control techniques based on rule-based strategies.

The investigation of existing methods for the control of the melt front velocity has provided the following results:

- Several attempts have been made to control flow front velocity through soft sensor technologies.
- It has hence been possible to show that the control of a constant flow front velocity is possible in principle.
- In practical applications, existing soft sensor models are not relevant due to the underlying simplifications and high inaccuracy.
- These models have significantly contributed to the realisation that the problem of ‘profiling the injection rate for a constant melt front velocity’ can only be solved if it can be transformed into a much simpler ‘control

problem', in which flow front velocity can be directly determined during the filling process.

With regards to the direct determination of melt front velocity, this chapter has presented a literature review of the following areas: a history and overview of methods for directly determining the melt front in injection moulding and associated methods for advanced control strategies. The following key issues have been identified:

- For the direct determination of the melt front, several approaches have been implemented, such as using a capacitive sensor for measuring the length of the average flow path and a method in which the flow front position is directly obtained through at least two different sensors inside the mould.
- With input from the sensors, advanced two-dimensional learning control algorithm-based controllers to close loop control flow front velocity can be developed.
- With an advanced controller fed by a method that uses a pressure and a temperature sensor inside the mould, in addition to flow front velocity, machine-independent key process parameters such as melt viscosity can be determined and controlled.
- As with the adaptive control of cavity pressure, the injection moulding industry is hesitant to switch to advanced control strategies because of the determination of the flow front velocity. Not all moulds can be equipped with capacitive sensors, and equipping or retrofitting moulds with multiple pressure and temperature sensors is time consuming, expensive, and can cause marks and significantly reduce the stiffness of the mould and the ability for the part surface to cool uniformly.

To solve the above problems, it is both theoretically important and practically necessary to propose, design, and develop a new method for determining the flow front velocity and other machine-independent parameters for the purpose of profile setting the injection velocity, as well as for an advanced control strategy. In

the proposed method, only a single pressure sensor is employed outside the mould, rather than two or more sensors located along the flow path and inside the cavity. The melt velocity can thus be determined in any form part geometry and for any application, without prior modification of the mould. Provided that the method works—and due to the lack of restrictions such as surface marks or expensive modifications of the tooling equipment—melt front velocity can be used as an input for any pre-existing advanced controller concepts, thus enabling a wider distribution of advanced control strategies in the plastics industry.

3 RESEARCH DESIGN AND METHODS

3.1 Introduction

As discussed in Section 1.1, to determine flow front velocity in relation to screw position, a new method is proposed via the comparative analysis of event patterns. This method is based on the idea of mapping a simulated filling process to a real injection moulding process. The theory of the thesis predicts particular events at the so-called event locations. In this definition, a relationship is established between the time when a singular event happens and the associated position within the cavity. The mapping thus occurs at the event points when the melt front has a particular characteristic at a position within the cavity.

Events can occur in the form of event groups, and the sequences of all events can be analysed to identify patterns. The events determined through simulation analysis are called virtual singular events, or E_{sim}, and the events identified through experimental measurement are called real singular events E_{mach}. A number of virtual singular events form a virtual form part-specific event pattern, M_s, and a number of real singular events form a real event pattern, M_m. The matching of the form part-specific pattern to the real event pattern of the filling process represents the actual mapping process.

To verify the proposed new method for determining the flow front position of molten polymer, comparative real and simulative experimental results using multiple cases (i.e., models, boundary conditions) are defined and conducted using the concept of mapping and matching. The experiments analyse whether the particular filling patterns show the flow front at the expected event locations, for two distinct models: (a) one-dimensional flow (because some components can be classified as one dimensional, the findings from this relatively simple case can be used for more complicated cases); and (b) multidimensional flow.

3.2 Research Methodology

This research comprises a positivistic epistemology focused on measurable and observable phenomena. The chosen methodology relates to this realist ontology in the choices of experimental and quantitative strategies. The experiments are implemented for two models: one-dimensional flow and multidimensional flow. A number of considerations apply, as described below.

3.2.1 Simulation and the Concept of Matching

The ability to simulate real processes, for example, to simulate the flow front pattern of a plastic melt during mould filling using simulation software (computer aided engineering, or CAE) is accepted as a given and has previously been investigated in numerous studies (Kennedy & Zheng, 2013; Zhou, 2013). As the new proposed method uses a simulation software-computed flow front associated with a measured event, the following considerations apply:

1. A measured event occurs in reality and with the accuracy with which the measuring sensor detects the event.

2. Through the matching of the pattern, virtual and real events can be assigned to each other. Both the virtual and real events are superimposed in a singularity (the event location). By this superimposition, the real and simulated flow front meet the event site at the time of the real event. The accuracy (the position of the flow front) at the singularity depends on the accuracy of the assignment of the method (the matching).

3. If, in addition, the simulation software describes a multidimensional flow front profile (the flow front course) starting from the event location, the accuracy of the simulated flow front outside the singularity (the event location), compared to the real flow front course, depends on the following:

a. The ability of the simulation software to predict real processes within a certain accuracy. In other words, because the method uses a simulated model to calculate the moulding-specific event pattern, the deviation (inaccuracy) between the real and simulated models must always be considered. However, the investigation of this deviation is beyond the scope of this work.

b. The boundary conditions with which the simulated model is calculated are crucial. Through different boundary conditions (e.g., viscosity, volume flow, melt temperature, etc.), the simulated melt front can embellish differently outside the singularity. As part of the work, the deviation of the melt front outside the singularity *X,* at different event sites, is investigated by varying the boundary conditions.

3.2.2 One-Dimensional Mould Filling

To satisfy the continuity equation, the flow front of the melt—in its idealised simplest case, the 'one-dimensional flow front course'—passes proportionally to the volume flow ahead, regardless of boundary conditions. The following considerations thus apply:

1. If the generation of the form part-specific event pattern M_s take place under idealised boundary conditions similar to those described in the real case, the pattern can be directly matched without transformation to the real event pattern or to parts thereof. The stretching factor f_k is 1 (no stretching); the smallest total deviation S_{min} is 0 (full coverage without stretching). Since the simulated and real flow fronts within the singularities (event positions) are united in the one-dimensional case, the deviation of the simulated melt front to the real one is 0.

2. If the generation of the form part-specific event pattern occurs while varying the flow rate $\dot{V}$, the pattern can be matched by transformation.

For the stretching factor f_k at the iteration $k = k_{min}$, the smallest total deviation would be $S_{min} = 0$. The flow rate exerts linear influence on f_k.

3. If the generation of the form part-specific event pattern takes place while varying boundary conditions other than flow rate (denoted as η), for example, material specifications (viscosity), melt temperature, or mould surface temperature, then the pattern can be directly assigned without transformation to the measurement event pattern or to parts thereof. The stretching factor f_k is 1; the smallest total deviation S_{min} is 0.

4. In summary, the following relationship can be derived:

$$\begin{aligned} &f_k = f(\dot{V}), \text{ linear dependence} \\ &S_{min},\ X \neq f(\dot{V}) \\ &f_k,\ S_{min},\ X \neq f(\eta) \end{aligned} \tag{3-1}$$

3.2.3 Multidimensional Mould Filling

If the form part fills multidimensionally, the preferential direction of the melt and its flow rate depend on time and place. As described above regarding the one-dimensional case, the flow rate impacts the stretching factor. In the multidimensional case, the flow rate also affects the preferred direction of the melt, and vice versa. The following considerations thus apply:

1. If the generation of the form part-specific event pattern takes place under idealised boundary conditions similar to those described in the real case, the pattern can be directly assigned without transformation to the measurement event pattern or to parts thereof. The stretching factor f_k is 1; the smallest total deviation S_{min} is 0. The simulated and real flow fronts unite within the singularities (event points). At these locations, there is no deviation of the melt front. Even outside the singularities, the calculated melt front coincides with the real one.

2. If the generation of the form part-specific event pattern occurs while varying the flow rate, the pattern can be assigned by transformation within a specified error bound. For the stretching factor f_k at the iteration $k = k_{min}$, the smallest total deviation has the value S_{min}. The total deviation increases with the strength of the variation of the volumetric flow rate. The simulated and real flow fronts unite within the singularities (event points). At these locations, there is no deviation of the melt front. Outside the singularities, the deviation of the melt front course X varies with the strength of the variation of the flow rate.

3. If the generation of the form part-specific event pattern takes place while varying boundary conditions other than flow rate—for example, material specifications (viscosity), melt temperature, or mould surface temperature—the impact of boundary conditions on the (a) stretching factor f_k, (b) smallest total deviation S_{min}, and (c) deviation of the melt front course X will follow the same assumptions as described in Paragraph 2 above.

4. In summary, the following relationship can be derived:

$$f_k,\ S_{min},\ X = f(\dot{V})$$
$$f_k,\ S,\ X = f\ (\eta) \tag{3-2}$$

3.3 Assumptions

The proposed method for determining flow front position as a function of screw position is based on the following assumptions:

1. In both the real injection moulding process (measured pressure signal) and the simulated model of the injection process (simulated pressure signal), singular events exist.

2. These singular events can be clearly determined and isolated from a measured or simulated pressure curve and described mathematically.

3. A relationship exists between the real and virtual events.

4. A quantity of virtual events (form part-specific event pattern) can be assigned to a quantity of real events (real event pattern) with sufficient accuracy (and vice versa). Therefore, appropriate procedures exist.

5. The accuracy of the matching, as well as its influence due to different boundary conditions in the simulated and real models, can be measured using mathematical key figures.

6. The accuracy of the matching describes the accuracy of the proposed method at the event points.

7. By assigning virtual and real events, a relationship between the flow front position of the melt and the screw position of the injection moulder can be determined within a specified error bound.

8. The relationship between assigned events can be proven by visualising the filling pattern at the event sites, where simulated virtual events and measured real events are superimposed. The proof is provided if, at these superimposed event sites, the filling pattern regularly shows flow front locations where events can be expected (at tapering, enlargements, edges, corners, flow obstacles, etc.).

9. From a kinematic point of view, flow front velocity can be determined using flow front position. If the relationship between flow front position and screw position can be established, the relationship between flow front velocity and screw position can also be established.

3.4 Methods for Data Collection and Analysis

To verify and validate the new method, real and simulated experiments are defined and conducted. The flow front velocity in relation to screw position is determined via the comparative analysis of the event pattern. Only the mould

filling phase is examined; the pressure holding phase subsequent to mould filling is not relevant for the process and is thus not subject to observation.

All sources and methods of this research focus on measurable and observable phenomena. This research comprises a structure that has identifiable causes; the following experiments and quantitative methods are used for validation:

1. Two different form part geometries (models) and associated injection moulds with different characteristics in terms of flow path.

    a. A step plate with a sprue bar, lateral dovetail gate, and three-step varying wall thickness over the flow path. The step plate represents an idealised one-dimensional flow front course.

    b. A symmetrical stack box, front-centrally injected with one recessed side and near-constant wall thickness over the flow path. The stack box represents the multidimensional flow course.

2. Pressure signals measured in an injection moulding process, using an injection moulding machine and an injection mould for each of the form part geometries described under Paragraph 1 above. The measured pressure curve defines the melt pressure on a time referenced to the injection moulder (e.g., real injection time). The signal is generated by a pressure sensor fitted in the nozzle in front of the screw with a resolution of 2 ms.

3. For the form part geometries, a numerical simulation is conducted to determine the melt flow pattern, as well as a simulated pressure curve, simulated under identical boundary conditions (properties of the polymer, flow rate, melt temperature, mould temperature) as the real injection moulding process described in Paragraph 2 above. The simulated pressure curve defines the simulated injection pressure over a virtual (injection) time and should match at least the resolution of the measured pressure signal. For example, 500 finite elements flown through per second virtual

injection time correspond to a resolution of 2 ms of the simulated pressure curve.

4. Software (Origin Pro) for the analysis and processing of signals to isolate events by performing a differentiation and peak or flank analysis of both the measured and the simulated pressure curve.

5. An algorithm for mapping a simulated filling process to a real injection moulding process by allocating and matching virtual or form part-specific event patterns to the measurement or real event pattern, which adds an iterative process to the pattern within a predetermined error bound to overlap, while determining (a) the deviation of individual events of the pattern $S_{,ki}$, (b) the smallest total deviation of the matching S_{min}, and (c) the scaling or stretching factor f_k at the smallest deviation.

6. A full factorial DoE for characterising the influence of different boundary conditions (flow rate, melt temperature, mould surface temperature) of the simulation on (a) the smallest total deviation S_{min} and (b) the scaling or stretching factor f_k, when matching and assigning form part-specific event pattern to measured event patterns. To do so, simulated pressure curves are generated by numerical calculation (simulation) under varied boundary conditions, according to the simulation described in Paragraph 3 above, for the form part geometries described in Paragraph 1, and further processed and analysed, as described in Paragraphs 4 and 5.

7. Mould filling studies for multidimensionally visualising the flow front filling pattern for the form part geometries, as described in Paragraph 1 above, to prove the relationship between the assigned virtual and real events and determine the largest deviation between varying the boundary conditions and under real boundary conditions of the simulated melt front at characteristic event times outside the singularities.

8. A DoE (for non-linear correlations) to study the relationship between flow rate and scaling or stretching factor for the non-linear transformations. To

investigate non-linear influences, the volume flow at otherwise constant boundary conditions is gradually altered.

3.5 Possible Sources of Error in the Methods and Accuracy Assessment

1. When measuring the real pressure melt curve, the set volume flow rate may vary through (a) leakage at the check ring valve, (b) control inaccuracy of the injection unit, or (c) the compressibility of the melt.

2. The accuracy of the measurement of the real measured pressure signal, and thus the accuracy of the determination of the real event pattern, is essentially determined by the range and resolution of the pressure sensor.

3. In the simulation, and thus in the determination of the simulated pressure curve, an appropriate meshing model (in 3D) is used. Therefore, after the meshing of the part geometry, all elements with unsuitable aspect ratios for the simulation are adjusted. The simulation comprises only the stage of mould filling (i.e., the injection phase). Boundary conditions for the mould filling simulation are the properties of the polymer, flow rate, melt temperature, and mould surface temperature. The crystallinity and orientation (anisotropic behaviour) of the molten polymer are not essential for the process.

4. The resolution of the simulated pressure curve depends on the discretisation density of the nodes in the 3D mesh. The goal in the numerical simulation is to choose a number of meshed elements sufficient to achieving a resolution of the simulated pressure curve, at least upon the resolution of the measured pressure curve. If, for some reason, this is not possible (e.g., due to computing time in a real-time model), it may be necessary to estimate the influence of the element size on the accuracy and resolution of the simulated curve using a full factorial DoE (with the number of nodes or density of the mesh as factors).

3.6 Ethical Issues

This self-funded research in the context of injection moulding is conducted under the guidance of the handbook of research ethics. The researcher generates and uses data from two different models (geometric data: step plate and stack box) by the Süddeutsches Kunststoffzentrum (SKZ), which has agreed to provide the models.

3.7 Chapter Summary

All of the sources and methods of the research support a positivistic epistemology focused on measurable and observable phenomena. From a realist viewpoint, the research comprises a structure that has identifiable causes and effects that can be proven due to relationships.

The chosen methodology relates or subscribes to this realist ontology by using a choice of experimental and quantitative strategies. The principle of data generation is hypothesis testing by observation, simulation, and measurement. To understand the causal relationships, the hypothesis in the research shows the links between the independent and dependent variables (‘x causes y’). To validate the assumptions, or hypothesis, in addition to the experimental methods, a range of quantitative strategies, or research methods, are employed:

1. To validate the new method for determining the flow front position of molten polymer, comparative real and simulated experiments using multiple cases (dimensions, boundary conditions) are defined and conducted using the concept of matching. The theory of the thesis predicts particular events at the so-called event locations. Based on the experiments, whether the particular filling patterns show the flow front at the expected event locations is analysed. The experiments are conducted on two different models: one-dimensional flow and multidimensional flow.

2. For the analysis and evaluation of the pattern matching methods, the variation of the independent variables occurs via the variation of the models and boundary conditions (e.g., melt temperature, mould temperature, and volumetric flow rate). The analysis of the dependent variables by a suitable DoE may or may not show an effect due to a particular cause on (a) the smallest total deviation S_{min} of the patterns and (b) the scaling factor f_k and final tests of the hypothesis.

4 A NEW METHOD FOR DETERMINING FLOW FRONT VELOCITY

4.1 Introduction

With current methods, an advanced controlling strategy based on machine-independent parameters, such as a constant flow front velocity of the melt, can only be achieved by direct measurement using a number of sensors inside the mould, which leads to complicated structures, great effort, and high costs for tooling equipment.

In this chapter, a new method is proposed, designed, and developed for determining flow front velocity as a function of the screw position over the entire part geometry using only one sensor. Based on part geometry, methods for the analytical and numerical determination of the pressure change required to fill the cavity are described. This chapter describes how, by analysing both the calculated and measured pressure curves, events can be identified and isolated and their sequence analysed to identify two event patterns. Via the comparative analysis of real and simulated moulding processes, the concept of matching the two event patterns and thus assigning virtual and real events is presented.

The proposed method comprises three stages consisting of 14 total steps (Mensler, Zhang, & Win, 2019). In the first stage, the form part-specific event pattern is determined by analysing the numerically calculated pressure curve. In the second stage, the real event pattern is derived from a measured pressure signal. In the third stage, by comparative analysis, the two patterns are matched, singular events assigned, and the relationship between melt front position and screw position is established.

For the purpose of matching, a matching algorithm with linear transformation and four iteration loops are developed and presented. The matching process is explained in detail, and a method is outlined for determining machine-independent parameters, such as flow front velocity, melt viscosity, shear rate, and shear stress, from the obtained relationship between melt front location and

injection time.

4.2 Analysis of Pressure Losses

In the idealised case of one-dimensional mould filling, the plastic melt flow during injection moulding comprises a straight path from the injection point (gate) to the end where the cavity is volumetrically filled. In such simple cases, it is possible to determine the pressure loss required to fill the cavity through analytical methods.

Along this flow path, part geometry normally changes geometrically at tapering, enlargement, edges, corners, and flow obstacles. To determine pressure loss, dividing the flow path into calculable sections at points where the part geometry changes is useful. Although the exponential dependence of viscosity on shear rate complicates calculations for shear thinning melts, using appropriate models, such as the Cross-BKS model (Bernstein et al., 1963; Ferry, 1980; Hieber & Chiang, 1992) in Equation (2-5), and a thermally homogeneous melt at a constant volume flow, allows the approximation of the pressure loss Δp, for flow through a flow channel section of length ΔL and a cross-sectional area with width b and height h at shear rate $\dot{\gamma}$ and melt viscosity $\eta(\dot{\gamma})$.

By aggregating the pressure losses on the individual flow path sections, the total pressure loss required to fully fill the cavity is determined. According to Equation (2-2), changes in flow channel geometry lead to disproportionately high or low changes in the pressure gradient, Δp. If the plastic melt flows through such a geometric change, a singular event E occurs at event location L and time t. In this definition, a relationship is established between the time when a singular event happens and the associated position within the cavity.

The upper section of Fig. 4-1 demonstrates schematically a one-dimensional form part model (step plate) that is filled along a straight flow path (arrow) from the largest to the smallest cross section.

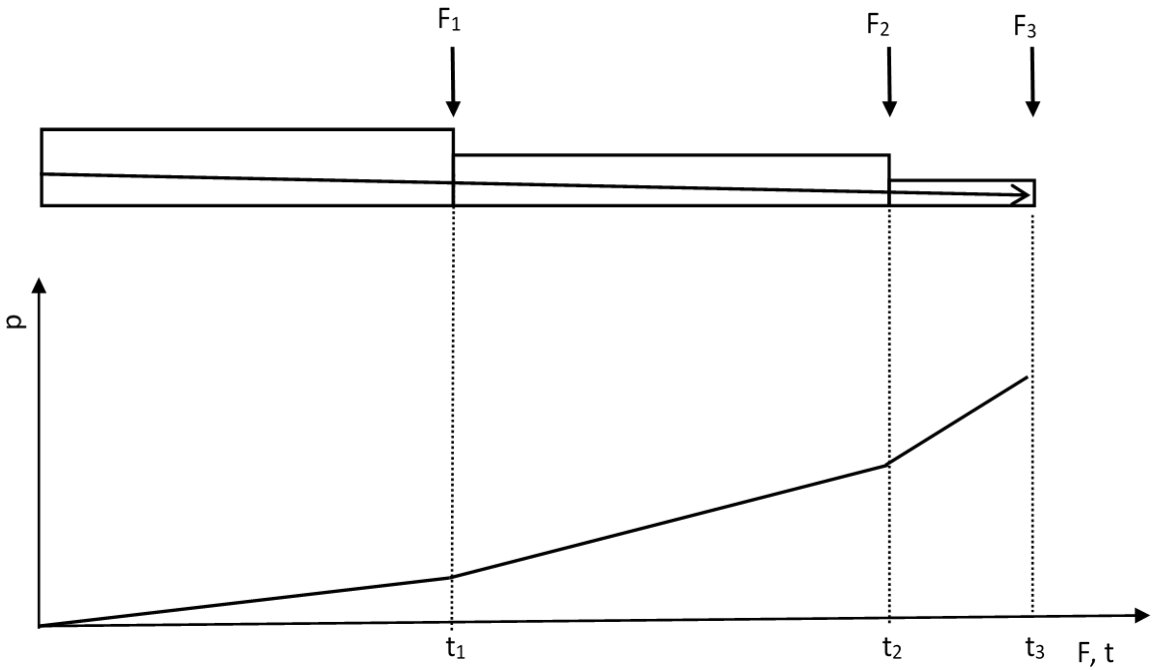

Fig. 4-1: Analytically determined pressure loss with three event locations

By joining the pressure losses in the individual sections, the total pressure loss curve over the flow path and filling time is generated. The lower section of the figure presents the analytically determined pressure loss for the one-dimensional step plate. In the example shown, the pressure gradient changes three times: at the two transitions from the larger cross section to a smaller one and at the end of the flow path. In general, on the entire flow path of a one-dimensional form part, n events E_i, with i = 1 ... n at event times t_i, occur at those event locations, F_i, where the pressure gradient, Δp, changes.

To fulfil the continuity equation under the assumption that the molten polymer is largely incompressible, the events on the one-dimensional flow path are expected to occur inversely proportionally to the change of the volume flow. The prerequisite for this assumption is a constant flow rate, and thus a constant injection speed, during the filling phase. However, the injection speed in modern injection moulding machines is usually set as a multistep velocity profile (Section 2.5.3). Thus, depending on machine settings, the volume flow can vary during injection. As the flow rate changes, the occurrence of the events also changes. As explained in more detail in Section 4.7.2, for the purpose of matching a form part-

specific event pattern determined by simulation with constant volume flow to a real event pattern determined with changing volume flow during injection, it can be helpful to determine corrected event times t_i', for a fictitious constant volume flow by means of a simple conversion: if, in a filling process with *n* events, the volume flow rate $\dot{V}$ changes by a factor *f* to

$$\dot{V}' = f \cdot \dot{V} \tag{4-1}$$

then the event E_i at event location L_i instead occurs at event time

$$t_i' = \frac{1}{f} t_i \tag{4-2}$$

4.3 Pressure Loss Determined by Simulation

If the moulded part is, for example, injected at a centrally located gate, it will fill multidimensionally. The determination of the injection pressure curve in multidimensional form parts with complex geometries can be conducted not analytically but from a simulation of the filling process (Section 2.2.2). Before the simulation, the part geometry (model) is meshed to the finite element (FE) mesh with nodes at the connections. The simulation software has solvers which, with the aid of the Navier Stokes equation system and suitable terms for heat transport (convection and conduction), viscosity (for shear thinning and viscous-elastic fluids) and other governing equations (Sections 2.3.1 and 2.3.2), for example, can generate a two- or three-dimensional filling pattern. This pattern represents the simulated flow front course, from the injection point (gate) through the entire filling phase.

At each node, the simulation software calculates parameters—such as injection pressure, pressure gradient, and melt temperature—as a function of filling time. The discretisation density and thus the resolution of each respective calculated parameter over the filling time is determined by the element size of the FE mesh. Fig. 4-2 shows the form part-specific pressure curve p_{sim} determined by a numerical analysis (simulation) of the filling process at the location (node) of the

gate. This form part-specific pressure curve defines the melt pressure over simulated injection time t_{sim}, which represents the injection time in relation to a specific start time (1). This start time, for example, can be defined as the moment when the melt front enters the sprue or passes through the gate of the cavity. The simulated injection time ends with the volumetric filling (2) of the form part. After reaching the volumetric filling, the melt is further compressed by the holding pressure to compensate for shrinkage effects. For the analysis of the form part-specific pressure curve, only the mould filling phase is examined; the pressure holding phase subsequent to mould filling is irrelevant for the filling process and is thus excluded from observation.

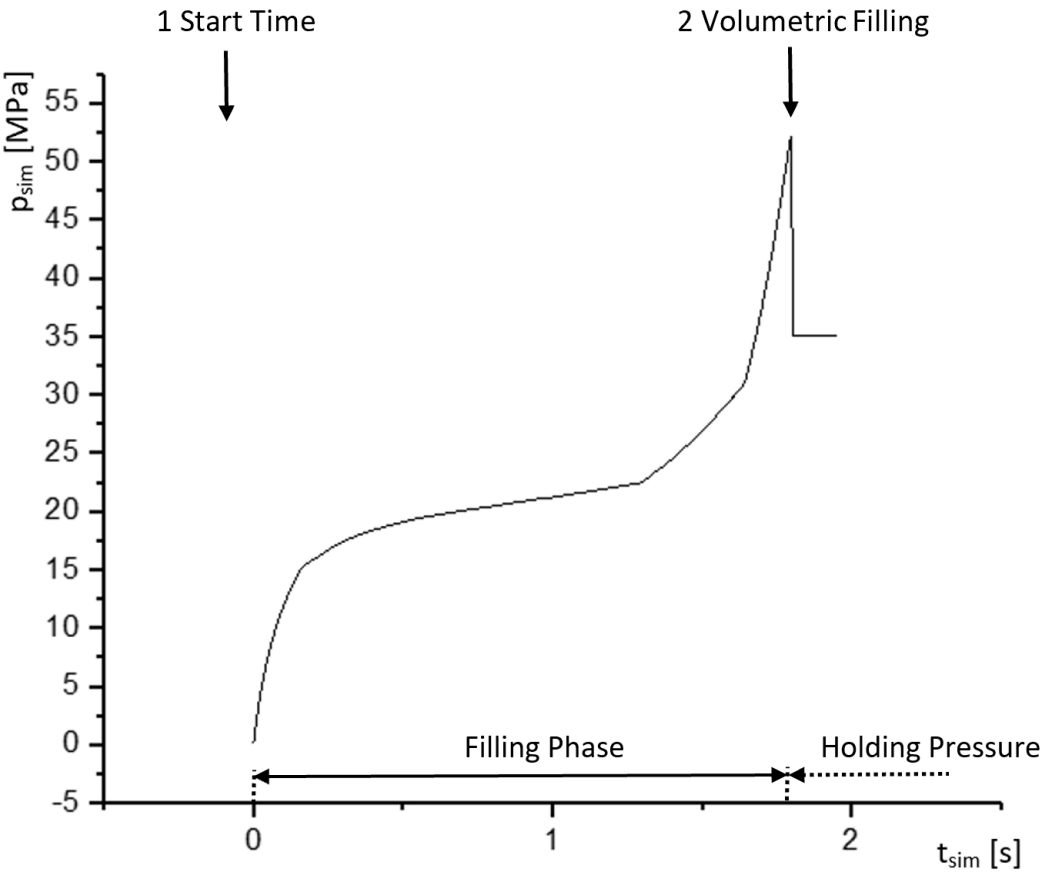

Fig. 4-2: Form part-specific pressure curve

The filling phase is characterised by the steady rise of the simulation-determined form part-specific pressure until the switchover point to holding pressure is

reached. In contrast to identifying events from the analytically determined pressure loss (Section 4.2), form part-specific events from a pressure curve determined by simulation cannot be identified without further analysis of the pressure graph.

4.4 Form Part-Specific Event Patterns

As demonstrated in Section 4.2, in the one-dimensional flow course, the form part-specific pressure curve can be determined analytically. In this case, the singular events occur between the basic geometry sections. If, conversely, the form part fills multidimensionally, the form part-specific pressure curve is calculated numerically by simulation (Section 4.3). In this case, virtual events can be identified by analysing the form part-specific pressure curve (Fig. 4-2). As shown above, the characteristic changes in the flow part geometries result in significant changes in melt pressure during the flow through of the melt. These characteristic positions are defined as event points, and a singular virtual event, $E_{sim\ i}$, correspondingly occurs. The analysis of the differentiated pressure curves determines the virtual events. Singular virtual events can occur in the form of event groups, and the sequence of all virtual events can be analysed to identify a pattern of the form part.

Fig. 4-3 presents a special example in which three individual event locations are identified and isolated from the differentiated pressure curve. For this purpose, the differentiated graph is examined for significant sections where the pressure gradient changes from a relatively less steeply sloped section to a deeply sloped one. Two tangent lines can be determined, and the intersection of the vertical line from the cross points of the tangents to the horizontal axis (time) defines the time of each respective event.

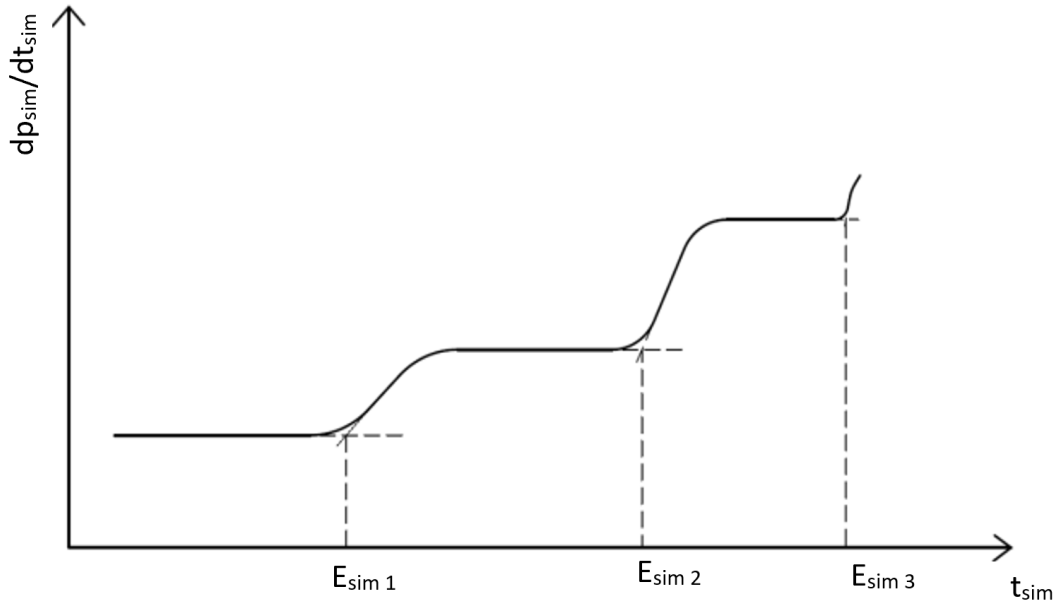

Fig. 4-3: Three events identified from a numerically calculated pressure in accordance with virtual time

The sequence of all virtual events can be analysed to identify a pattern of the form part. This pattern is called the form part-specific event pattern, or M_s, and can be considered the 'fingerprint' of the form part. Such a pattern comprises a number *n* of singular, virtual events $E_{sim\,i}$, which are linked to the characteristic event locations of the part geometry.

The form part-specific event pattern M_s can be represented as

$$M_s(E_{sim\,1}, \dots, E_{sim\,n}).$$

This event pattern consists of *n* virtual events $E_{sim\,i}$, which are associated with the characteristic event points of the part geometry. Each virtual event is assigned to a relative time when the event happens and the associated position. This can be simple information on the position if only a one-dimensional flow path is

considered. In an FE network, these are the positions of all nodes, along which the melt front lies at the time of the event.

$E_{sim\,i}$ is thus a vector:

$$E_{sim\,i}(t_{sim\,i}, x_{sim\,i}, y_{sim\,i}, z_{sim\,i}, p_{sim\,i}, h_{sim\,i})$$

In addition to event time $t_{sim\,i}$, this vector also includes other components: position data represent the positions of the melt front $X_{sim\,i}$, $Y_{sim\,i}$, $Z_{sim\,i}$, respectively, and the simulated melt pressure $p_{sim\,i}$, as well as information on the form part geometry $h_{sim\,i}$, at the event location. Plotted against time, all events form an individual and unique form part-specific event pattern, M_s. Fig. 4-4 demonstrates a form part-specific event pattern with four virtual events. The pattern describes the relative assignment of all events occurring during a simulated filling phase and is considered the fingerprint of the form part.

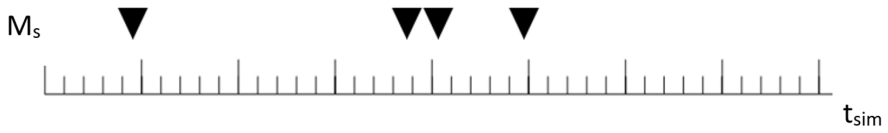

Fig. 4-4: Form part-specific event pattern M_s

4.5 Pressure Signal of the Melt

The injection unit illustrated in Fig. 4-5 consists of a barrel (1) in which a screw (2) is situated as an actor. The screw itself is connected to an injection piston (4), which, for example, can be moved hydraulically or electrically. During plasticising, plastic granulate is transported via the rotating screw flights along the barrel walls to the front of the screw tip. A smaller portion of the energy required for melting the resin is provided by heat transfer from the heated barrel wall, while a larger portion of the energy reaches the melt through shear (frictional heat) on the screw flanks. The melt cushion in front of the screw tip pushes the screw in the opposite direction of the conveying direction of the melt. This backward

movement of the screw (and thus the amount of energy introduced by friction) can be actively controlled by the back pressure. The plasticising volume (amount of molten mass) is limited by the screw stroke and can be adjusted to the weight of the moulded part.

For injection, the plasticising unit moves to the closed mould, and injection is then affected by a controlled forward movement of the screw, in which a non-return valve prevents the melt from flowing back into the screw flights. To compensate for contraction (shrinkage) due to the cooling of the melt after the volumetric filling of the mould, the injected melt is further compressed by holding pressure. The holding pressure phase ends with the sealing of the cavity (freezing of the gate) when no additional melt can be fed into the mould. To ensure that the moulded part has sufficient stiffness for ejection from the mould, the holding pressure phase is followed by residual cooling time. The length of the cooling phase depends on the moulded part's required demoulding temperature.

For the direct acquisition of the signal, measurement is accomplished using pressure sensors inside the melt, for example, in the injection unit's nozzle (6). For indirect measurement, the melt pressure signal is derived from the hydraulic pressure (5) of the injection piston or the torque of the electrically driven injection unit.

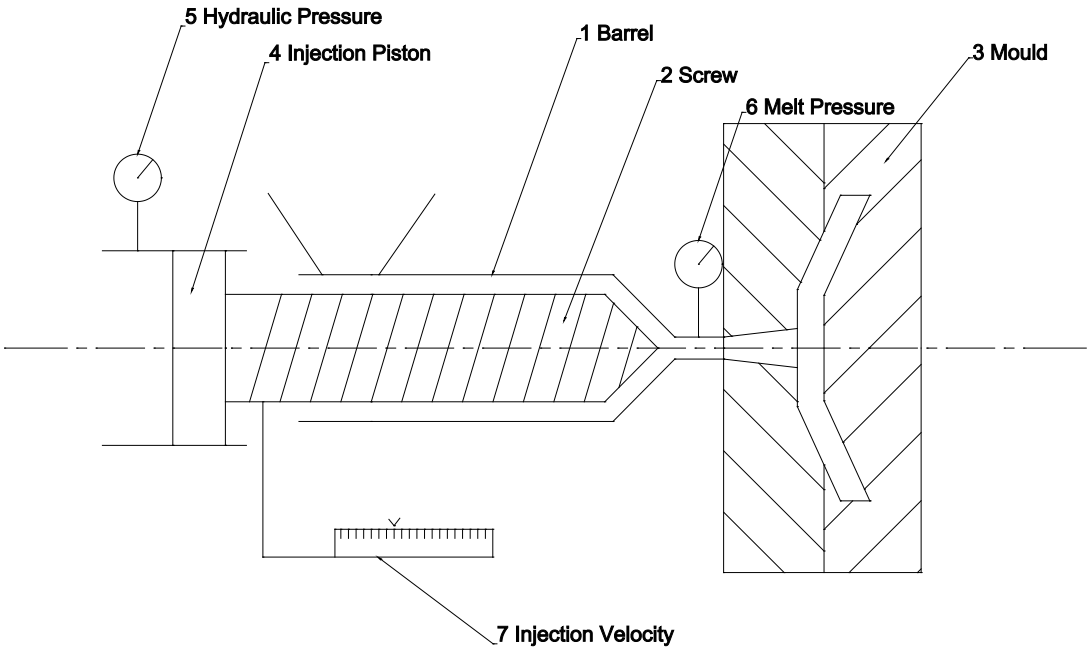

Fig. 4-5: Injection Unit

Modern injection moulding machines can control parameters such as temperature, pressure, and velocity within narrow ranges of values (Stitz & Keller, 2001). The machine controller (MC) compares a set of parameters with the measured data and subsequently acts on built-in or external actuators (Yang, 2004). As outlined in Section 2.2.5, with closed loop-controlled injection, melt pressure, p_{mach}, is a function of the injection rate and thus the volume flow of the melt:

$$p_{mach} = f(\dot{V}) = f(v) \tag{4-3}$$

For each cycle, the counting of the machine time, t_{mach}, starts with the beginning of the injection process. For a given injection rate or volume flow, the position of the screw (with screw diameter D), s_{mach}, can be determined using the following relationship:

$$\dot{V} \cdot t_{mach} = \frac{D^2 \cdot \pi}{4} \cdot s_{mach} \tag{4-4}$$

When the plastics melt passes through the cavity, the resulting pressure to overcome the filling resistance can be directly or indirectly measured as a function of machine time and screw position.

Fig. 4-6 shows the measured pressure curve p_{mach} in front of the screw at constant volume flow during the filling phase. The pressure sensor provides information about the melt pressure during the filling (3), holding pressure (4), and cooling (5) phases. The pressure curve defines the melt pressure over a referenced machine time t_{mach}, which begins with 'the start of the injection' or 'the start of the cycle' (1). When the melt is injected, the pressure signal starts to rise. After reaching volumetric filling (2), the melt is further compressed by the holding pressure to compensate for shrinkage effects. The holding pressure phase begins when the maximum cavity pressure is reached, and the cooling phase follows, in which the pressure inside the cavity drops to atmospheric pressure after gate freezing. As with the form part-specific pressure, only the mould filling phase is examined for the analysis of the measured pressure curve; the pressure holding phase subsequent to mould filling is irrelevant for the filling process and is thus excluded from observation.

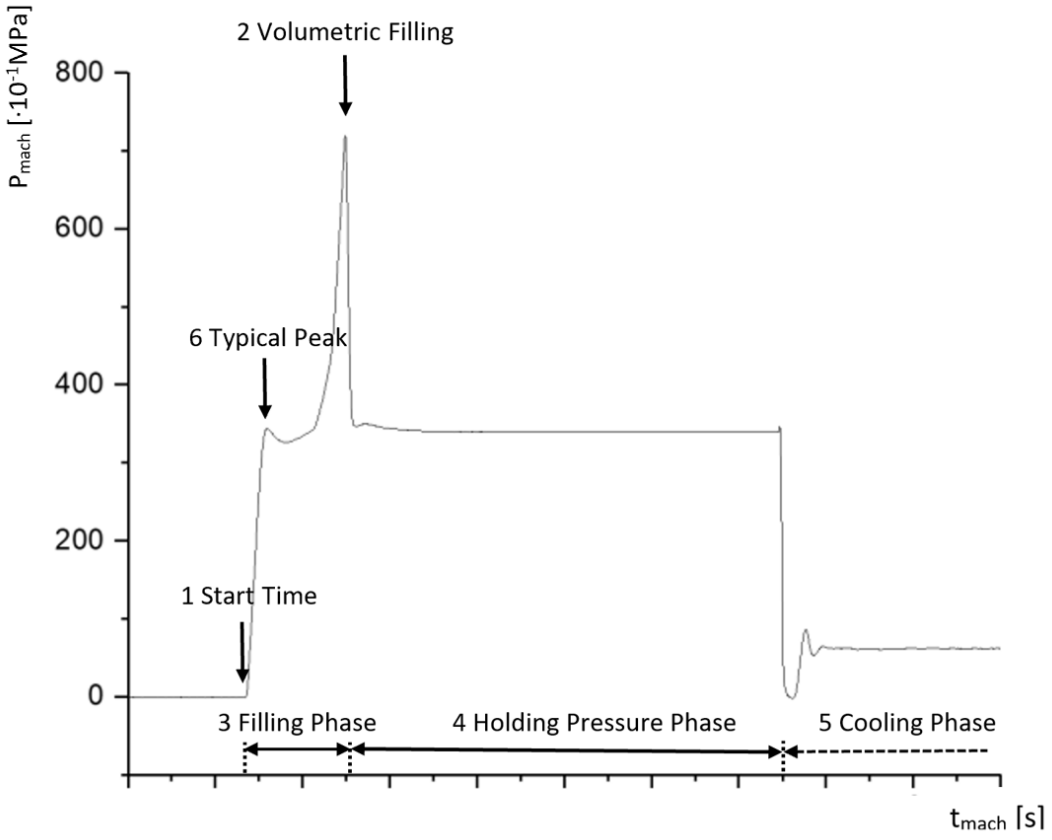

Fig. 4-6: Measured real injection pressure curve

Although the filling phase is also characterised by a steady rise in measured pressure, the measured pressure graph (Fig. 4-6) bears little resemblance to the form part-specific pressure curve determined by simulation (Fig. 4-2). This is expected to occur, even if the form part-specific pressure graph has been determined with the same boundary conditions as the setting of the injection moulding machine. This may occur due to deviations between simulation and reality. In addition, various influencing factors ensure that the two pressure graphs will deviate and can never exactly align. A good example of this is the typical overshooting of the measured pressure curve (6), which occurs immediately after the start of the injection phase. This is due to friction and flow resistances as well as the compressibility of hydraulic oil and melt (Johannaber & Michaeli, 2004). Because deviation in the pressure curves also results in deviation in the event patterns, a matching algorithm with certain basic functionalities, as explained in Section 4.8, is required for the matching of the event patterns. Chapter 7 provides a detailed evaluation of the factors influencing the deviation of the patterns and assesses the suitability of the proposed matching algorithm.

As described in Section 2.5.3 the injection speed in modern injection moulding machines is usually set as a multistep velocity profile. Depending on machine settings, the volume flow can vary during injection. As the flow rate changes, the occurrence of the events also changes. As explained in more detail in Section 4.7.2, if the volume flow is not held constant during the injection process, for the purpose of matching, it can be helpful to covert the measured pressure signal into a fictitious pressure signal, in which the occurrence of the events changes to a fictitious machine time t'_{mach}, corresponding to a constant volume flow. As shown in Section 4.2, this can be achieved by simple transformation, using the relationship in Equations (4-1) and (4-2) at any constant volume flow (e.g., initial volume flow $\dot{V}_0$).

4.6 Real Event Patterns

As with the form part-specific pressure curve, one or more ‘real events’ can be identified by analysing the measured real pressure curve (Fig. 4-6). Singular real events $E_{mach\,i}$ can occur in the form of event groups, and the sequence of all real events can be analysed to identify patterns in the measured injection pressure. This is called the real event pattern. A real event pattern M_m comprises a number of m singular, real events, $E_{mach\,i}$, which are linked to characteristic event locations of the mould geometry.

For the case shown in Fig. 4-6, for example five individual event locations can be identified and isolated from the differentiated pressure curve, as shown in Fig. 4-7. For this purpose, the differentiated graph is examined for significant sections where the pressure gradient changes from a relatively less steeply sloped section to a deeply sloped section. Two tangent lines can be determined, and the intersection of the vertical line from the cross points of the tangents to the horizontal axis (time) defines the time of each respective event. In the example, $E_{mach\,1}$ and $E_{mach\,5}$ indicate the beginning and end, respectively, of the filling phase, whereas $E_{mach\,2}$ represents the end of the typical overshoot at the beginning of the injection phase (Section 4.5), and the events $E_{mach\,3}$ and $E_{mach\,4}$ are related to geometrical changes in flow channel geometry.

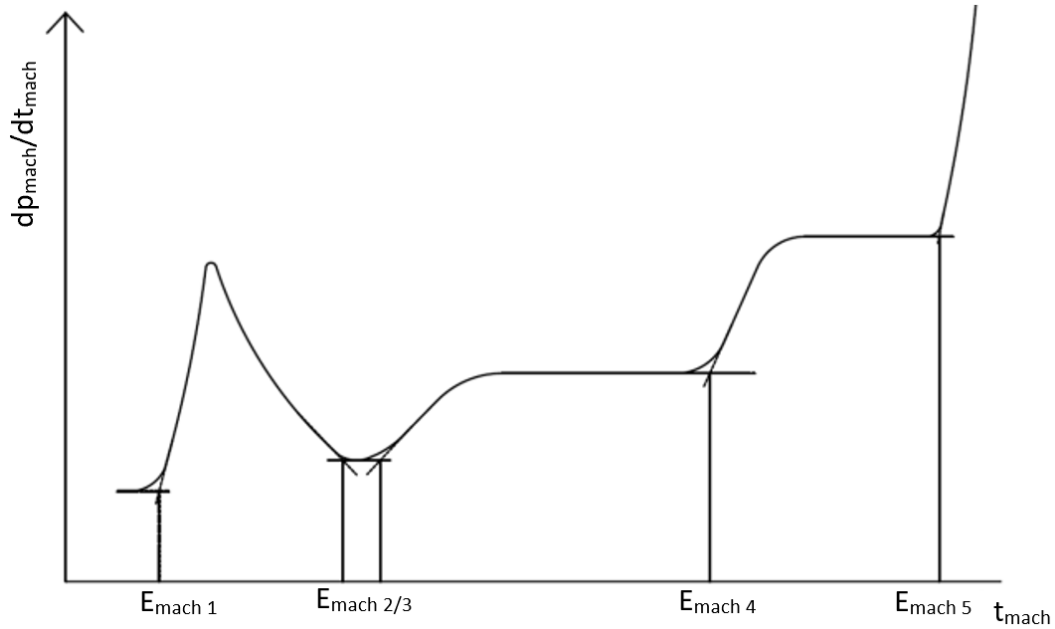

Fig. 4-7: Five events identified from a measured melt pressure in accordance with machine time

To create the real event pattern M_m, the sequence of all real events can be analysed. Such a pattern comprises a number *m* of singular, real events $E_{mach\ I}$, which can be represented as

$$M_m(E_{mach\ 1}, \dots, E_{mach\ m}).$$

A typical pattern consists of *m* real events $E_{mach\ i}$, which are associated with the characteristic event points of the part geometry. Each real event is assigned to a machine time and a screw position.

$E_{mach\ i}$ is a vector, described as

$$E_{mach\ i}(t_{mach\ i}, p_{mach\ i}, s_{mach\ i})$$

with three components: machine time $t_{mach\ i}$, screw position $s_{mach\ i}$ and measured melt pressure $p_{mach\ i,}$ at the time when the event occurs. Plotted against time, all events form an individual and unique real event pattern. Fig. 4-8 demonstrates a real event pattern with six event locations. The pattern describes the relative assignment of all measured events occurring during the filling phase.

Fig. 4-8: Real event pattern M_m

4.7 Functions of the New Method

To determine flow front velocity in relation to screw position, a new method is proposed via the comparative analysis of the two event patterns described above. Two types of singular events are used: one for the events identified through simulation analysis and the other for those identified through experimental measurements. The former are called form part-specific (or virtual) singular events E_{sim} and can be determined from a melt pressure curve generated from simulation analysis. Similarly, events identified through experimental measurement are called real singular events E_{mach}, and can be determined from a pressure curve measured at a specific location, such as in the nozzle of the injection unit. A number of virtual singular events comprise a form part-specific event pattern M_s, and a number of real singular events form a real event pattern M_m.

The proposed method comprises three stages consisting of a total of 14 steps, as shown in Fig. 4-9.

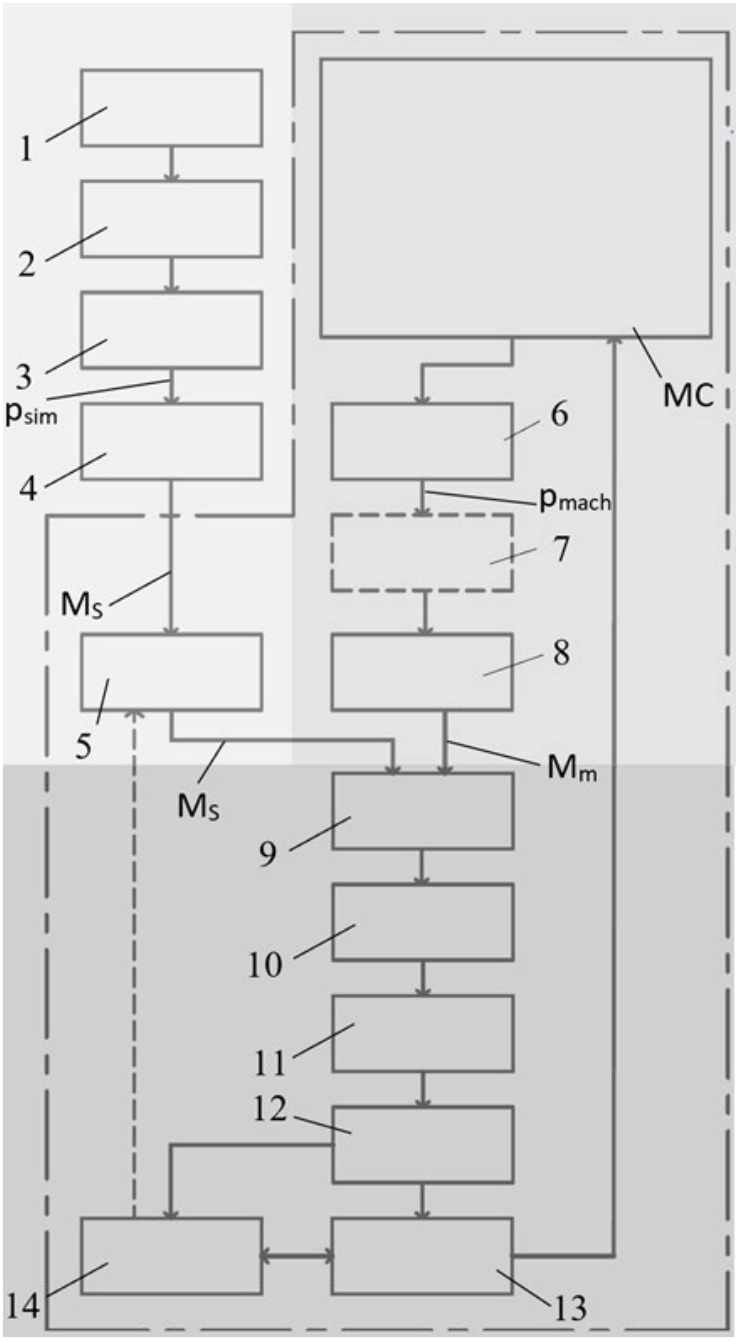

Fig. 4-9: Flow chart of the proposed method

4.7.1 Stage 1: Analysis of the Form Part-Specific Event Pattern

In this stage, the form part-specific event pattern is determined in five steps.

In Step 1, all required geometric data of the form part are fully captured. They usually exist as machine-readable data, for example, in a step file (.stp).

In Step 2, the data of the gating system are obtained in the same manner.

In Step 3, using the geometric data, a simulation of the filling process can be performed to determine the form part-specific pressure curve p_{sim}. This curve (Fig. 4-2) defines the melt pressure during the filling phase over time t_{sim}, which represents injection time in relation to a specific start time. This start time can, for example, be defined as the moment when the melt front enters the sprue channel or passes the gate of the cavity.

The time when virtual events $E_{sim\,1}$, $E_{sim\,2}$, …. and $E_{sim\,n}$ occur can be determined by the analysis of the differentiated form part-specific pressure curve (Step 4). Fig. 4-3 shows a special case with three virtual events. Here, the pressure gradient changes from a relatively less steeply sloped section to a deeply sloped one. Two tangent lines can be determined for each section, after which the cross point of these two tangent lines can be determined and a vertical line drawn through this cross point. The intersection of this vertical line with the horizontal axis (time) can be defined as the time of each respective event. In Fig. 4-3, for example, three events can be identified.

In Step 5, the form part-specific pattern M_s is generated and, together with the geometric and other data, such as the filling pattern obtained through the simulation analysis, uploaded into the control unit of the injection moulding machine.

4.7.2 Stage 2: Identification of Real Event Pattern

Stage 2 consists of three steps (6–8) for identifying the real event pattern. In Step 6, the pressure measurement is conducted to obtain the melt pressure curve p_{mach}. Fig. 4-6 shows a typical measured curve, which can optionally be adjusted into a time-corrected pressure curve in Step 7. This may be necessary if the volumetric flow rate $\dot{V}$ is not held constant during injection, as in the simulation. As shown in Section 4.2, for the purpose of matching a form part-specific event pattern determined by simulation with constant volume flow to a real event

pattern determined with changing volume flow during injection, it can be helpful to determine corrected event times t_i', for a fictitious constant volume flow by means of a simple conversion using data on the change in flow rate. For the virtual events, the real events $E_{mach\,1}$, $E_{mach\,2}$, … and $E_{mach\,m}$ can be determined by differentiating the measured pressure signals. For example, for the case shown in Fig. 4-6, five events can be identified, as shown in Fig. 4-7. In Step 8, the real event pattern M_m is generated and uploaded into the control unit of the injection moulding machine.

4.7.3 Stage 3: Mapping a Simulated Filling Process to a Real Injection Moulding Process

Stage 3 consists of six steps (9−14). In this stage, the simulated and real injection processes are mapped, the form part-specific and real event patterns are matched, and virtual events are assigned to real events. The method for determining the flow front position is based on the idea of mapping a simulated filling process to a real injection moulding process. This mapping occurs at the event points. The matching of the form part-specific pattern to the real event pattern of the filling process represents the actual mapping process. The patterns cannot be assumed to be identical after identification since they differ due to, for example, deviations between real machine settings and simulation boundary conditions. Similarly, the patterns cannot be assumed to be the same size. Depending on the location of the pressure sensor or the scope of the simulation, the patterns might have different numbers of events. The extent to which the individual patterns deviate from one another (and which factors influence deviation) can be assessed only after analysing the event patterns; this is the subject of further investigation in Chapter 7. However, the existence of deviation between the patterns—due to the fact that the simulated process from which the form part-specific event pattern originates will never exactly match the real injection process from which the real event pattern originates—leads to the realisation that for the proposed method, an algorithm for matching patterns is needed which can compensate for the deviation of the patterns. The matching

algorithm must comprise certain basic functionalities; in addition to the possibility of transforming event patterns (for example, by linear scaling), functionalities to adjust pattern sizes and allow certain criteria for the elimination of events must be present. A new matching algorithm with linear transformation is thus proposed, designed, and described in Section 4.8. Chapter 7 is dedicated to a detailed evaluation of the factors influencing the deviation of the patterns and the assessment of the suitability of the proposed matching algorithm.

In Step 9, the new matching algorithm is performed. For this purpose, both the form part-specific event pattern M_s and the real event pattern M_m are transferred to an allocation unit, the purpose of which is to match whole event patterns, or at least parts of them. By matching patterns, the virtual events can be assigned to the real events.

In Step 10, after the process matching, individual virtual events are assigned to real events. Based on this assignment, the melt front position (a component from the virtual event vector E_{sim}) can be determined against the respective screw position (a component from the real event vector E_{mach}).

In Step 11, the flow front velocity can then be determined on the basis of the times when these events occur. In Step 12, machine-independent parameters such as melt viscosity and shear rate can finally be determined. In Step 13, a set of machine-independent parameters can be saved for delivering the best form part quality. In the event of a machine change, these parameters can be used in Step 14 to recalculate machine parameter settings (such as injection velocity profile) for the new injection moulding machine in order to deliver the best form part quality.

4.8 A New Algorithm for Matching the Form Part-Specific Event Pattern with the Real Event Pattern

As shown in Section 4.6, the simulated pressure graph from which the form part-specific event pattern originates will never exactly match the measured pressure graph from which the real event pattern originates. Thus, as presented in Section 4.7.3, an algorithm with certain basic functionalities, such as the possibility to

transform event patterns, adjust pattern sizes, and allow the elimination of events by certain criteria, is required for matching the form part-specific event pattern with the real event pattern. In the matching process, both patterns are aligned by transformation and then matched. A detailed analysis of the requirements and functionalities of an algorithm for a robust matching can be found in Chapter 7.

The proposed algorithm is shown in Fig. 4-10. There are four iteration loops; the inner two loops (1) perform the transformation of the patterns. In the outer two loops, the displacement of the patterns (2), as well as the elimination of individual events (3), occurs.

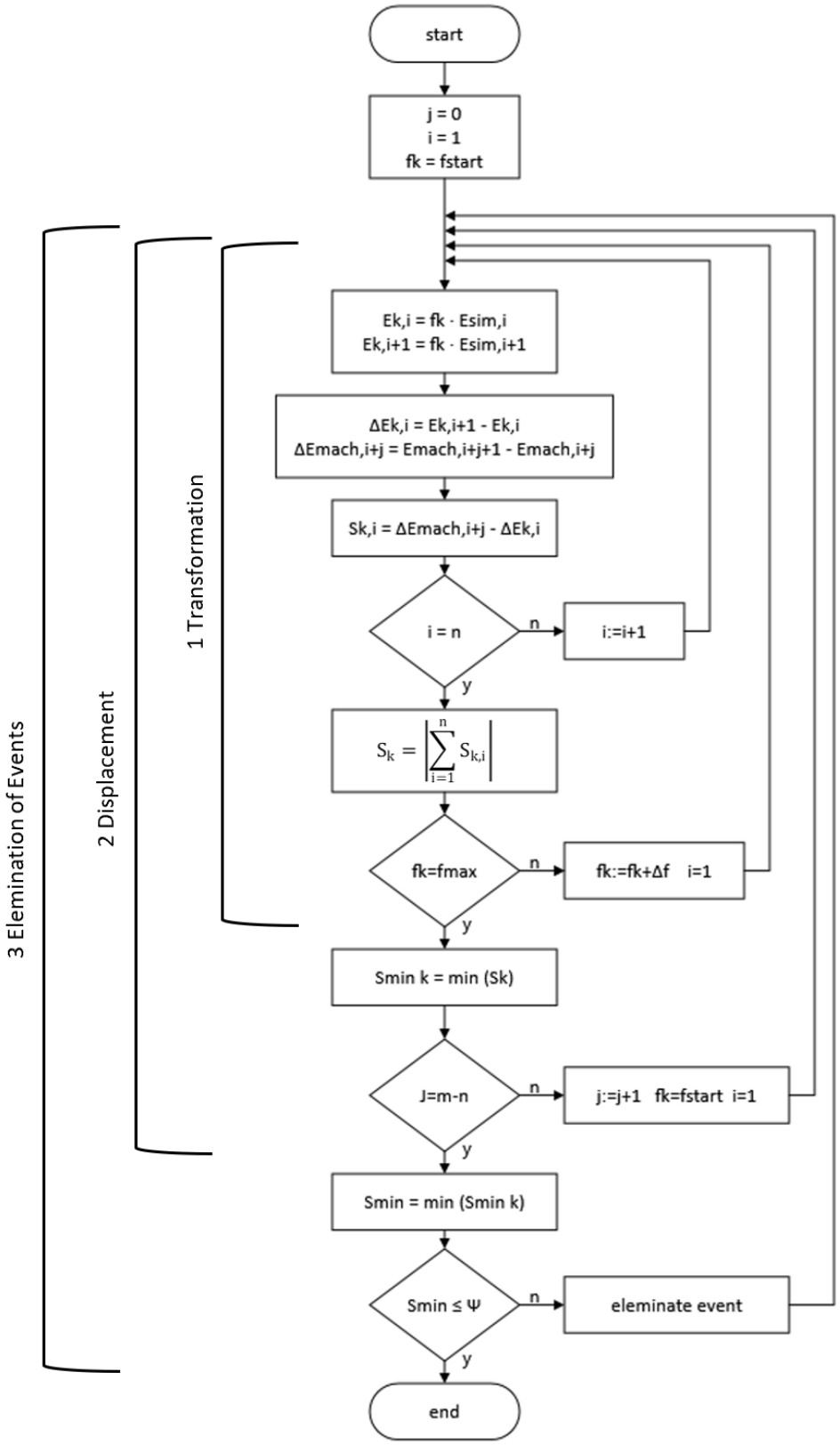

Fig. 4-10: A new algorithm for matching event patterns

In the inner two loops of the algorithm (1), the form part-specific event pattern M_s is transformed. The scaling factor f_k passes through a total of k transformations between f_{start} and f_{max}, with a scaling increment of Δf. Equation (4-5) shows how the scaling increment is determined.

$$\Delta f = \frac{f_{max} - f_{start}}{k} \tag{4-5}$$

Fig. 4-11 illustrates the transformation of the form part-specific event pattern, M_s. The transformation has the effect of pulling (or pushing) the pattern in the direction of the arrow (2) while simultaneously fixing the pattern at the first event location (1).

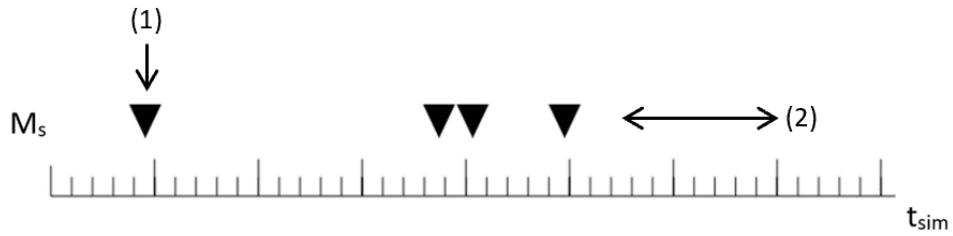

Fig. 4-11: Transformation of form part-specific event pattern M_s

As a result of the transformation, a proportionally stretched (or shrunk) event pattern M_k is obtained, which is illustrated in Fig. 4-12.

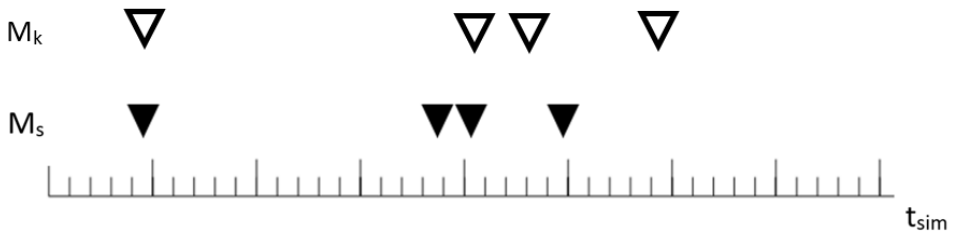

Fig. 4-12: Transformed form part-specific event pattern M_k

For each transformation, a new pattern, M_k, is calculated from the pattern M_s, after which aligning M_k with the real event pattern M_m is attempted. For this

purpose, two adjacent virtual events of the form part-specific event pattern $E_{sim\ i}$ and $E_{sim\ i+1}$, are multiplied by the scaling factor f_k, and the difference in time of the scaled virtual events is then calculated. The deviation $S_{k,i}$ is subsequently determined between the previously calculated time intervals in the form part-specific and real event patterns. From the absolute value of the sum of all individual deviations of the scaled pattern with the measured events, the total deviation for the respective scaling iteration is calculated. The inner loop is repeated k times, with the scaling factor f_k incremented by Δf each time. As further discussed in Chapter 7, even after transformation, a matching of the patterns with a deviation of 0 (identical pattern) cannot be expected. Thus, the smallest (pattern) deviation of all transformations $S_{min\ k}$ is searched and recorded at the iteration k_{min}.

Fig. 4-13 depicts a form part-specific event pattern M_s (triangle symbol) and a real event pattern M_m (circle symbol) plotted against machine time t_m before M_s undergoes k transformations. As shown in Fig. 4-12, through the linear transformation the relative time relations of the patterns change. The form part-specific event pattern is scaled, which means its size is stretched or shrunk against the real event pattern.

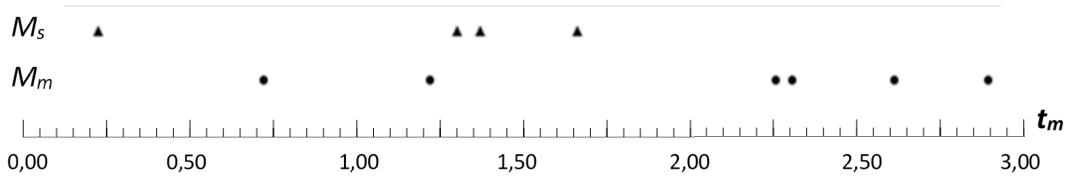

Fig. 4-13: Real event pattern and form part-specific pattern before scaling

In practice, the virtual injection time and machine time have no absolute time reference. The start time for the form part-specific event pattern, for example, can be defined as the time when the melt flow front enters the sprue channel or passes the gate of the cavity, depending on the scope of the simulation. The count of the machine time, for example, could begin for each cycle with the start of the injection phase. For example, as demonstrated in Fig. 4-13, the form part-specific

event pattern has an absolute time deviation from the real event pattern. In addition, both patterns have different sizes (i.e., different numbers of events). The real event pattern is obtained via pressure sensor from the measured pressure curve of the injection moulding (filling) process, while the form part-specific event pattern is obtained via simulation from the calculated pressure curve of a simulated filling process. Depending on the location and placement of the pressure sensor and the scope of the simulation (for example, with or without the runner system), both pressure curves might see a different part or section of the total filling pressure and thus a different number of events. Furthermore, in the real injection moulding process, the existence of 'interference' in the measured pressure curve is conceivable. Such interferences can have 'external causes', such as damage to the cavity along the flow path. In the worst case, interferences can generate events in the real pressure curve that have no equivalent in the simulated one. Therefore, in practice, both patterns can be assumed to have a different number of events (different size). Matching in the sense of the new method does not necessarily mean the assignment of patterns consisting of all identified real and virtual events; it is much more likely that a subset of events (parts or fragments of the patterns) will be matched. Chapter 7 is dedicated to a detailed evaluation of the factors influencing the deviation of the patterns and the assessment of the suitability of the proposed matching algorithm. So, if the number of events of the virtual event pattern n is not equal to the number of events of the real event pattern m (as demonstrated in Fig. 4-13), each virtual event $E_{sim\ i}$ is displaced by the index, $j = 0 \ldots j_{max}$, into a real event $E_{mach\ i+j}$ in a further (higher level) iteration loop (2). All transformations are then performed to determine at which displacement j_{min} the best matching (at the smallest pattern deviation) is achieved. This higher iteration loop is repeated j times until all possible displacements, $j_{max} = m - n$, have been performed. S_{min} at displacement, $j = j_{min}$, is searched and recorded.

If interferences generate events in the real pressure curve that have no equivalent in the simulated pressure curve, the algorithm must have a functionality to filter and eliminate these events. Since the algorithm does not search for the pattern

deviation 0 but for the smallest deviation S_{min} at the displacement j_{min}, the filtering and elimination of events generated by interference can occur most simply by specifying an error bound Ψ. Therefore, in a further step of the algorithm (3), a condition is tested to verify whether the smallest total deviation over all displacements S_{min} lies within this specified error bound Ψ. If the test condition is not met, single events can be eliminated and the entire process in the outer loop must be repeated to meet this condition.

For example, for the case shown in Fig. 4-13, the transformed form part-specific event pattern $M_{s,j}$, is presented in Fig. 4-14 after it has undergone *three* higher level iterations, with displacements $j = 0 \ldots 2$. For each displacement, an absolute time reference is established by shifting the first event of the form part-specific event pattern into each of the first three events of the real event pattern. In Fig. 4-14, in each displacement, the form part-specific event pattern has undergone the transformation $k = k_{min}$ with the smallest (pattern) deviation. For pattern $M_{s,j=1}$ (rectangle symbol), the best alignment to M_m (circle symbol) with the smallest deviation S_{min} is achieved.

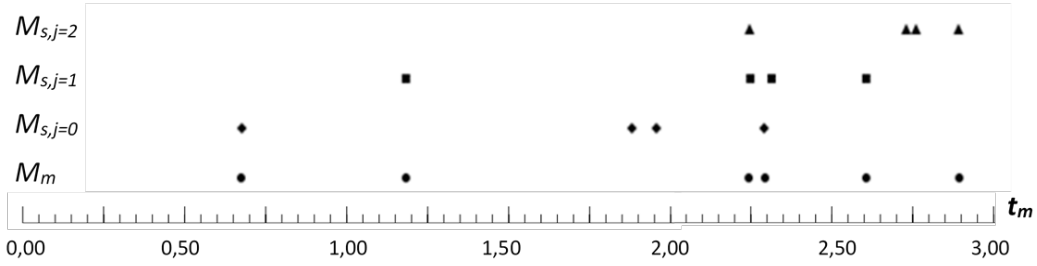

Fig. 4-14: Real event pattern and form part-specific pattern after scaling and displacing

4.9 Assigning Virtual Singular Events to Real Singular Events and Determining the Flow Front Position

Fig. 4-15 shows the assignment of the virtual and real events (Step 10) from the matched pattern. The assignment allows the real event vectors $E_{machi+j}$ at transformation $k = k_{min}$ and displacement $j = j_{min}$ to be expanded by the

components $x_{sim\ i}$, $y_{sim\ i}$ *and* $z_{sim\ i}$ (positions of all nodes along the melt front lines) of the assigned virtual event vectors $E_{sim\ i}$. Thus, the melt front position is consequently associated with machine time $t_{mach\ i+j}$ and screw position $s_{machi+j}$:

$$E_{sim\ i} \rightarrow E_{mach\ i+j}\ for\ \ k = k_{min}, j = j_{min}\ and\ S_{min} \leq \Psi \tag{4-6}$$

The real event vectors $E_{mach\ i+j}$, expanded by the components of the virtual event vectors assigned, are expressed as

$E_{mach\ i+j}$ ($t_{mach\ i+j}$, $p_{mach\ i+j}$, $s_{machi+j}$, $x_{sim\ i}$, $y_{sim\ i}$, $z_{sim\ i}$, $h_{sim\ i}$).

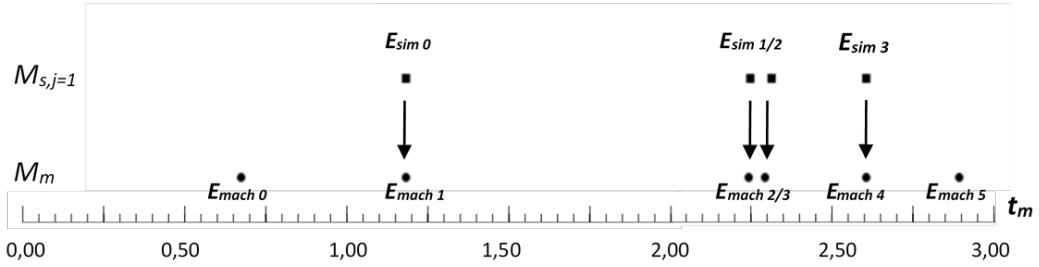

Fig. 4-15: Assigning virtual and real events

Fig. 4-15 demonstrates a case for pattern $M_{s,j=1}$ (rectangle symbol) when the best alignment to M_m (circle symbol) is achieved. According to Equation (4-6) and with j_{min} = 1, four virtual events, $E_{sim\ i}$, can be assigned to four real events $E_{mach\ i+j}$ ($E_{sim\ 0}$ to $E_{mach\ 1}$, $E_{sim\ 1}$ to $E_{mach\ 2}$, …). The two real events $E_{mach\ 0}$ and $E_{mach\ 6}$ have no corresponding virtual events and are thus excluded from further consideration.

4.10 Determining Machine-Independent Parameters

By considering two successive and assigned event vectors, $E_{mach\ i+j}$ and $E_{mach\ i+j+1}$, the mean flow front velocity of melt v_i, and the increase in melt pressure Δp_i can be expressed as Equations (4-7) and (4-8), respectively, and the computation can be conducted between these events (Step 11).

$$v_i = \frac{x_{sim\,i+1} - x_{sim\,i}}{t_{mach\,i+j+1} - t_{mach\,i+j}} \tag{4-7}$$

$$\Delta p_i = p_{mach\,i+j+1} - p_{mach\,i+j} \tag{4-8}$$

From the calculated flow front velocity and the increase in melt pressure (together with information on the flow channel geometry $h_{sim\,l}$), based on the Hagen-Poiseuille Equation (2-2), machine-independent parameters, such as wall shear stress τ_i, shear rate $\dot{\gamma}_i$ and melt viscosity η_i, can be derived between the event points (Step 12), as expressed in Equations (4-9), (4-10) and (4-11), respectively (Schröder, 2018). To further increase the accuracy, the machine-independent parameters can be approximated between the event locations. By means of analytical or numerical methods, the components of two successive event vectors can serve as boundary conditions. With this method, a continuous determination of the respective machine-independent parameters over the entire flow path can be achieved.

$$\tau_i = \frac{\Delta p_i \cdot h_{sim\,i}}{2 \cdot (x_{sim\,i+1} - x_{sim\,i})} \tag{4-9}$$

$$\dot{\gamma}_i = 0.772 \cdot \frac{6 \cdot v_i}{h_{sim\,i}} \tag{4-10}$$

$$\eta_i = \frac{\Delta p_i \cdot h_{sim\,i}^2}{12 \cdot (x_{sim\,i+1} - x_{sim\,i}) \cdot v_i} \tag{4-11}$$

4.11 Discussion of the Application of the Proposed Method in an Injection Moulding Process

For the purpose of implementing the new method into an injection moulding process, the software and hardware development of a process parameter determination unit (PPDU) comprising an interactive injection moulding terminal for the following two applications, is proposed and discussed:

- The application of injection velocity profiling by the operator through visualisation of machine-independent parameters on an interactive machine control terminal.

- The application of an algorithm-based, advanced learning control strategy for injection velocity profiling and closed-loop controlling the filling process on machine-independent parameters such as melt front velocity, melt viscosity, and melt shear rate.

4.11.1 Process Parameter Determination Unit

The PPDU is to be understood as a device that consists of the required hardware and software components, based on the proposed new method, for determining process parameters such as the flow front position and velocity of the polymer melt front, as well as machine-independent process parameters, such as melt viscosity, shear rate, and shear stress. In this definition, the PPDU is a device for detecting the melt front position and determining the melt front velocity and other machine-independent parameters.

In the injection unit for a moulding machine illustrated in Fig. 4-16, the essential parts are drawn schematically. The injection unit has a barrel (13), in which the screw (14) is situated as an actuator. The screw itself is connected to the injection piston (12), which for example can be moved hydraulically. At the sensor position (11), the hydraulic pressure can be measured. By increasing the hydraulic pressure, the injection piston is extended forward and thus moves the screw inside the barrel forward and injects the molten polymer from the nozzle (16) into the cavity of the mould (1F). The screw position x_b and its velocity v_b are determined by another measuring device (17). The injection pressure of the plastic melt p_{mach} may also be measured directly in front of the nozzle (15).

The various components and actuators are controlled by the control unit (MC), which, in addition to other conventional components, such as a graphical user interface with screen and control panel, consists of the PPDU (20) for determining the flow front position and other process parameters based on the proposed

method.

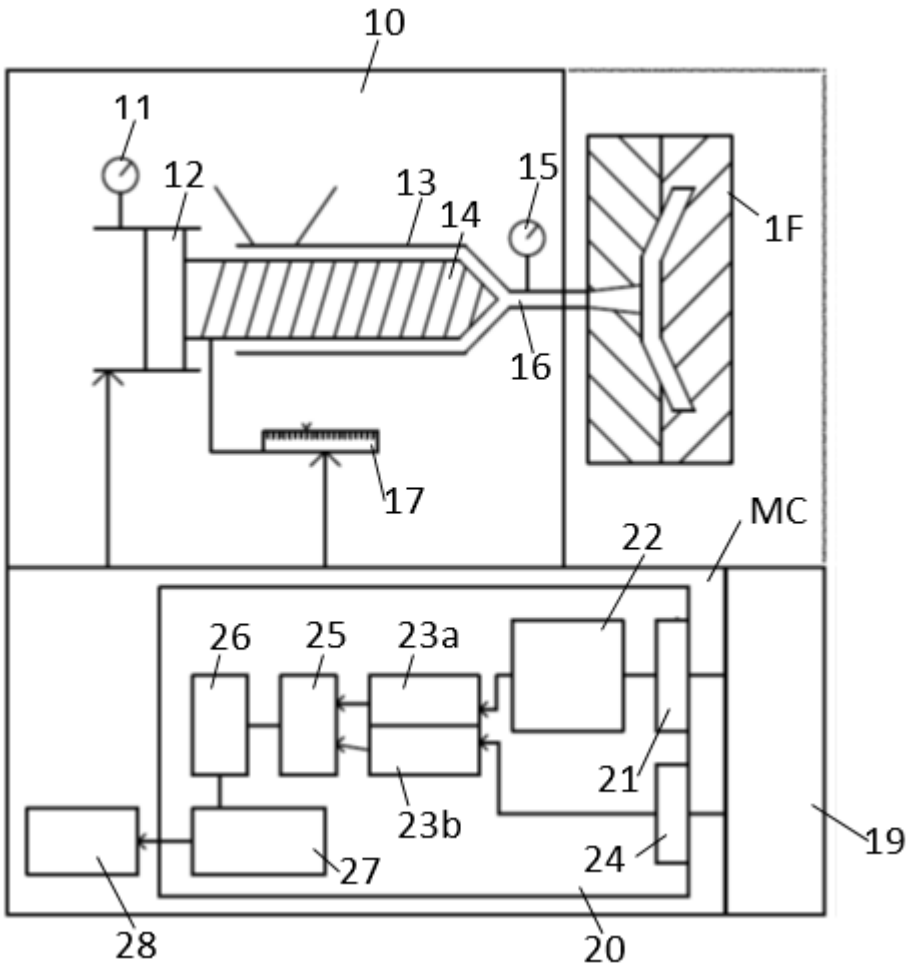

Fig. 4-16: Injection moulding machine with a process parameter determination unit

The PPDU (20) consists of various subcomponents. It comprises a first interface (21) through which the geometry data of the form part can be adopted. These data are passed to a pressure curve determination unit (22), which performs the simulation of the filling and determines the form part-specific pressure curve p_{sim}. By analysing the p_{sim}, the unit (23a) determines the form part-specific event pattern M_s.

Over the interface (24), the melt pressure p_{mach} can be measured either indirectly or directly by the pressure sensor for the hydraulic pressure (11) or the sensor

inside the melt channel (15). During the measurement, if the volumetric flow rate (injection velocity) is not constant but changes according to a certain parameter setting, the thus obtained pressure curve p_{mach} can be optionally adjusted into a time-corrected pressure curve p_{mk} with a constant volumetric flow rate as described in Section 4.7.2 (Step 7). The measured pressure signal p_{mach} (or its time-corrected counterpart p_{mk}) can be passed to the pattern detection unit (23b), which determines the real event pattern M_m from the measured pressure curve for each cycle. In addition to reading data from the injection moulding machine's sensors, the interfaces (21 and 24) can also receive the data through a common interface (19) of the controller (MC), which allows external data exchange to other units or memories.

Both the form part-specific event pattern M_s and the real event pattern M_m are then transferred to the matching unit (25) to match the patterns and assign individual events. After assigning the events, the relationship between flow front location and injection time in relation to the screw position is established, and the flow front velocity and other machine-independent parameters are determined. These steps are performed in the evaluation unit (26).

All determined data, particularly the process parameter values as a function of the injection time and screw position, can be forwarded from the evaluation unit (26) to an output unit (27) that controls the display device of the graphical user interface (28). The aim of the output unit is to plot the process parameter values, particularly the location of the flow front and its velocity, in relation to the injection time and screw position.

For the particular setting parameters of the injection moulding machine that provide the best form part quality, it might be prudent to store the determined information, such as flow front velocity or melt viscosity, in a dataset which serves as reference. If the moulding machine changes, for example, the new setup can be determined by recalculating the injection velocity profile from these reference data.

4.11.2 Interactive Injection Moulding Terminal

To visualise the machine-independent parameters, the device to be developed consists of an interactive machine control terminal (28) with a high-resolution display and associated hardware. The functions can be controlled by a user interface with touch screen functionality. The interactive injection moulding terminal provides intuitive handling and animated data visualisation, including for the filling pattern of the form part or other machine-independent parameters related to the injection time and screw position of the moulder.

Fig. 4-17 demonstrates how the location of the melt front (MF) in the form part or the cavity of the form part can be visualised on a device with a high-resolution display and user interface, preferably with touch screen functionality. The visualisation is readily possible because the location of the melt front is known by the method proposed in Chapter 4 and determined by the PPDU.

Therefore, the form part (1) is plotted simply in a suitable, three-dimensional representation, and therein the filling pattern is visualised. Fig. 4-17 presents an example of an interactive terminal and a user interface of the injection moulding machine as part of the PPDU shown in Fig. 4-16 (28). In addition to a screen or display device in the form of a touch panel (2), the terminal consists of a control panel (3) with mechanical control elements. On the touch panel, in the two upper adjacent display areas with different view angles (4 and 5), the location of the flow front inside the form part or its cavity (1) is visualised. The display areas (4) and (5) show the form part with the flow front location in a perspective view and in a plan view from above.

The operator can, by touching the screen in the respective area, twist and turn the view. As explained below, the display areas (4 and 5) also serve to represent the distribution of the molten polymer inside the form part under different conditions.

Below the simulated representation of the form part are more display areas (6 and 7). As an example, a diagram of the setting parameter ‘injection velocity’ is presented. The diagram depicts the set velocity profile of the actuator v_b (injection

velocity) on its position x_b (injection stroke). In the example, the screw itself is visualised together with the injection barrel on the overlying display area (6).

The virtual controls are located below the display and diagram area. A control panel (8) sets the dynamic visualisation of the filling of the mould. A preferred appearance of the mould filling could be done dynamically as an animation in the form of a film sequence that animates the flow front course (Display Areas 4 and 5) together with the location of the screw (Display Area 6). The corresponding controls to stop, start, run slowly back and forth or fast forward and run back the animation are located on the control panel. Next to this is a virtual slider (9), which allows the operator to quickly jump to the specific location of the melt front that she or he requests.

With the aid of the diagram in the display area (7), it is possible for the operator to change the injection speed v_b as a function of the actuator or screw position s_b. For this reason, the operator simply varies the curve by moving it up and down using the touch facilities. Alternatively, additional adjusting controllers, particularly virtual ones, could be provided to facilitate a more precise adjustment to the respective actuator position. In this case, the altered parameter setting (injection velocity profile) would no longer correspond to the setup used in the previous injection moulding process or the simulated injection moulding process being visualised; it would instead represent a ‘desired curve’ which can be stored as a process control parameter function for a subsequent injection moulding process. This is explained below in reference to Fig. 4-18 and Fig. 4-19.

An alternative way to track and adjust the position of the flow front (and then to vary a process control parameter at a specific point) is provided by the mechanical controls of the control panel. This includes a turning button (10) in the form of a wheel. By turning the wheel, the operator can accurately move the melt front forward and backward image-wise. In addition to the above-mentioned control elements, a keyboard (11) is used to, for example, enter a set of process control parameters.

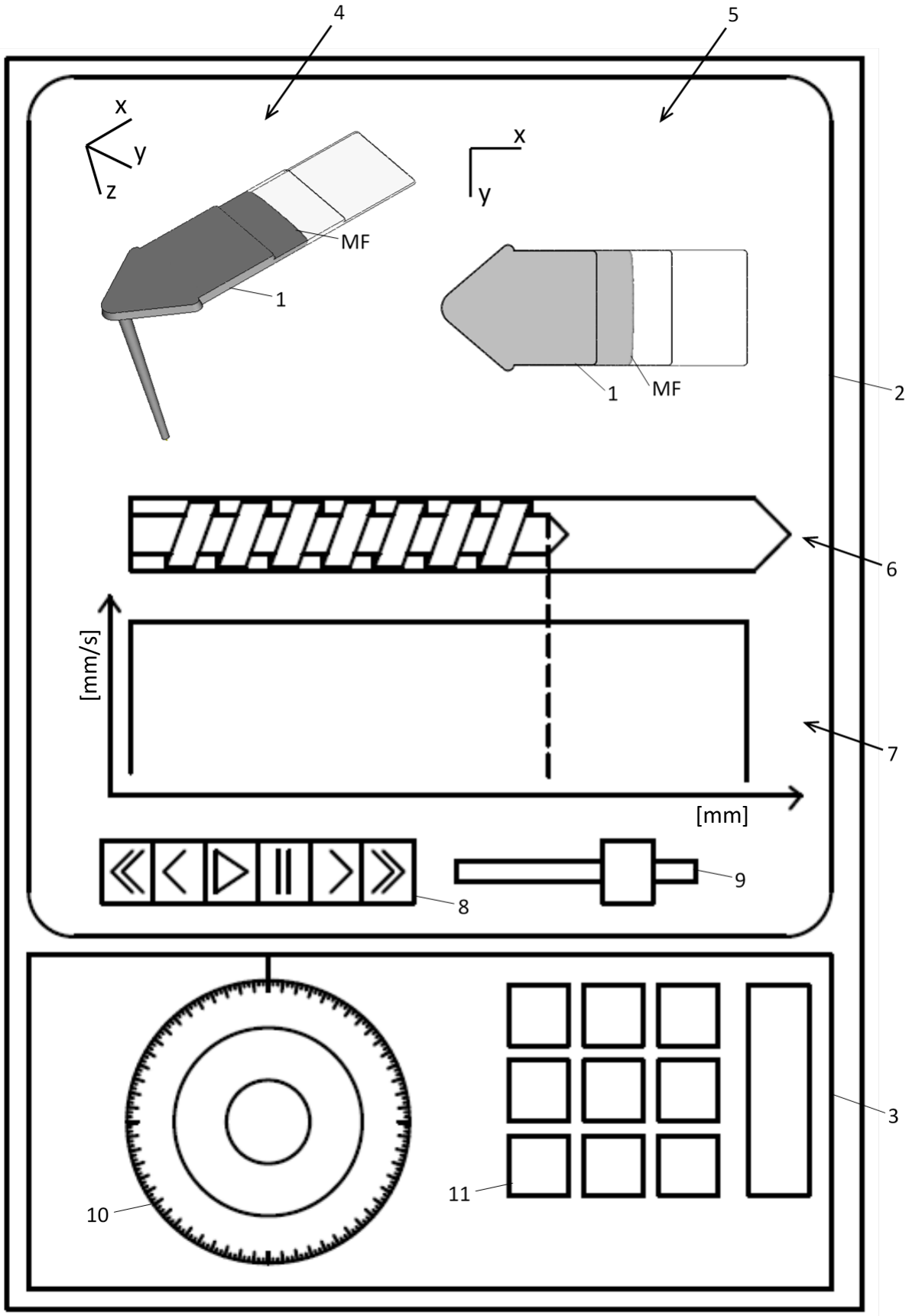

Fig. 4-17: Interactive injection moulding terminal

4.11.3 Application of Injection Velocity Profiling Through Visualisation

With the interactive injection moulding terminal providing intuitive handling and animated data visualisation, including for the filling pattern of the form part or other machine-independent parameters related to the injection time and screw position of the moulder, the operator can have the course of the flow front displayed over the entire flow channel and assigned to the respective screw position. To compensate for surface defects of the moulded parts, for example, the front course animation can be stopped at particular melt front locations, such as characteristic event points, where machine parameters could be entered or adjusted. This provides the operator with the opportunity to optimise the injection moulding process quickly. Fig. 4-18 and Fig. 4-19 demonstrate how the quick optimisation of the injection moulding process is possible by means of visualisation. As in Fig. 4-17, these figures depict the interactive terminal with a visualisation of the form part or form part cavity. The display areas are arranged in a similar manner as in Fig. 4-17. Furthermore, the control elements are similarly located on the screen.

In Fig. 4-18, however, the operator has set the display area (4) with the simulated representation of the form part in a 'plan view from above', similar to the display area next to it (5). In addition, different melt front velocities are shown or marked by different grey levels (scales) within the form part. The form part model step plate, described in the experimental evaluation in Chapter 5, with its three cross-sectional heights, is used to illustrate the example of an interactive injection moulding terminal. As can clearly be seen, with three different wall thicknesses of the form part, the flow front velocity changes (increases). In other words, whenever the melt front passes through a lower wall thickness in the moulded part, the injection velocity v_b of the screw is set constant over the injection stroke x_b; thus, the flow rate is constant, as shown in the diagram in the display area (7). However, this particular setup may not be desirable. A possible optimisation

strategy in the setting process could be to hold the flow front velocity constant over the entire flow path.

To achieve this, the operator may, by means of the diagram in the display region (7, presented in red) and the controls of the control panel (3), reduce the velocity of the screw v_b at precisely defined actuator positions that correspond exactly to the positions where the flow front in each case reaches a new section within the mould cavity (at the event points). Then, with the predetermined velocity function, as shown in the display area (7) in Fig. 4-19, a simulation of the injection moulding process is first conducted. The result of this simulation or numerical calculation can be displayed in the screen part (5). This allows an accurate comparison of the previously visualised injection moulding process and the outcome of the expected new injection moulding process.

The operator can immediately recognise that the flow front velocity over the entire flow path will be constant, as indicated by the uniform grey display. The operator can subsequently set up the optimised function of the screw velocity v_b (as a function of the screw position x_b) and thus conduct the next injection moulding cycle.

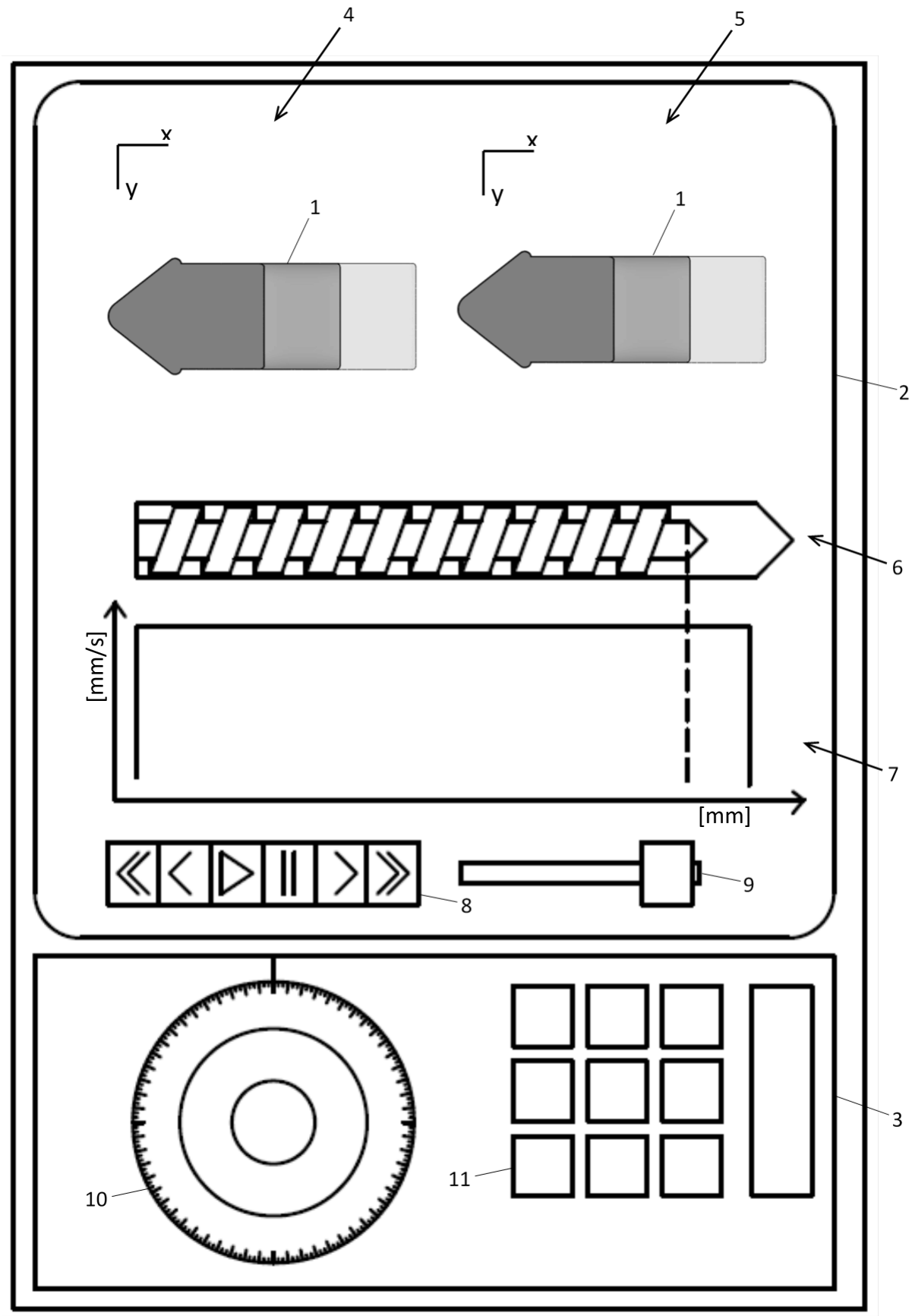

Fig. 4-18: Optimisation of the moulding process – constant injection velocity

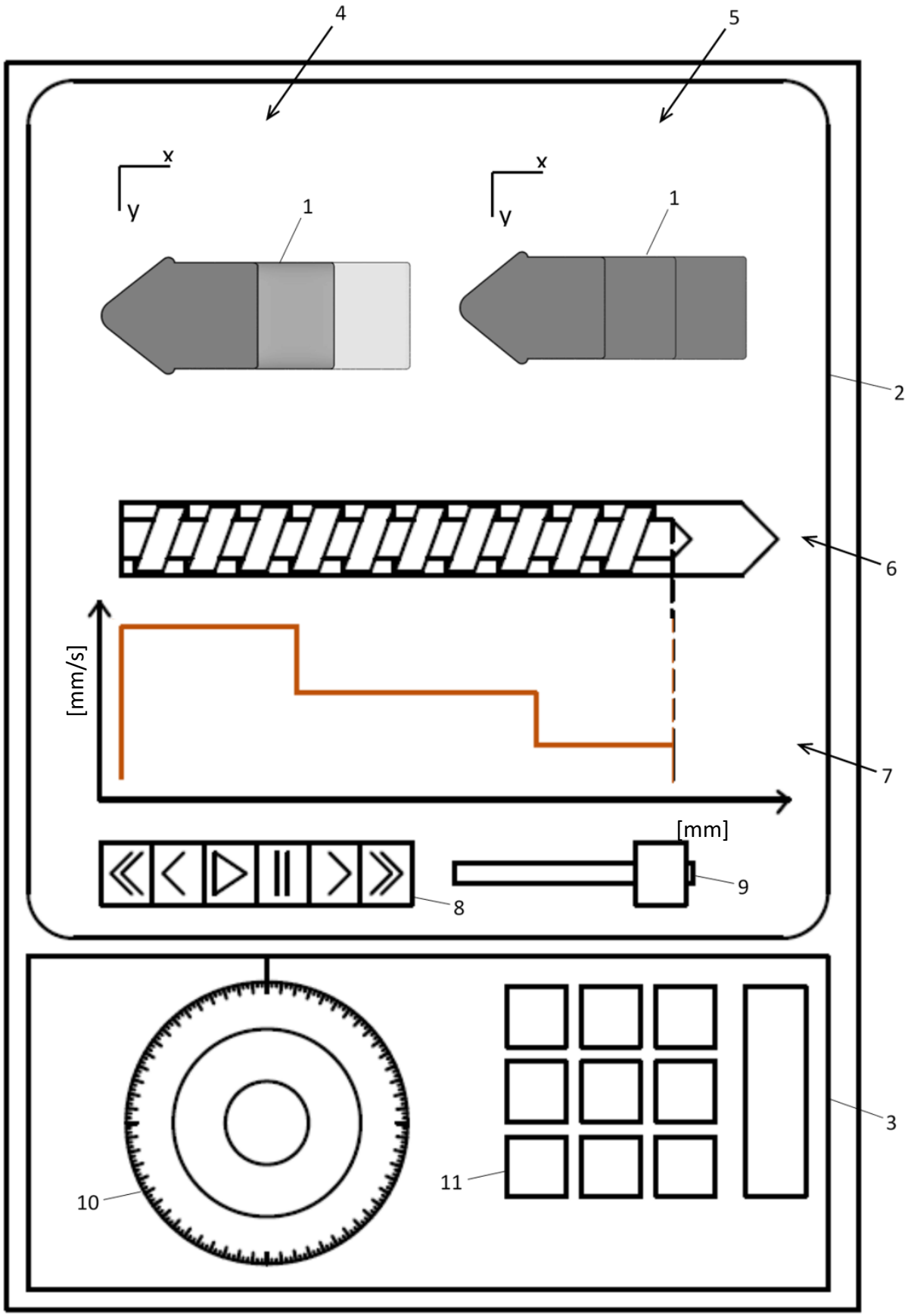

Fig. 4-19: Optimisation of the moulding process – adjusted injection velocity

4.11.4 Application of Advanced Control for Injection Velocity Profiling

As demonstrated in Section 4.11.3, the PPDU can be used to set and optimise the injection velocity profile by visualising the melt front velocity and machine-independent parameters, such as melt viscosity. For this purpose, the PPDU detects the melt front and determines the melt front velocity and other machine-independent parameters. Fig. 4-20 presents the corresponding block diagram. In the outer loop, parameters determined by the PPDU, such as flow front velocity v_m, are transferred to the operator by a graphical user interface (GUI). As Section 4.11.3 describes, the optimisation (e.g., according to the criterion of 'constant melt front velocity') is conducted offline at the terminal by the operator and provides a setting v_b *SP* (injection velocity profile). The set points serve as input variables for the inner loop of the feedback controller to closed-loop control the injection speed of the injection moulding machine (IMM).

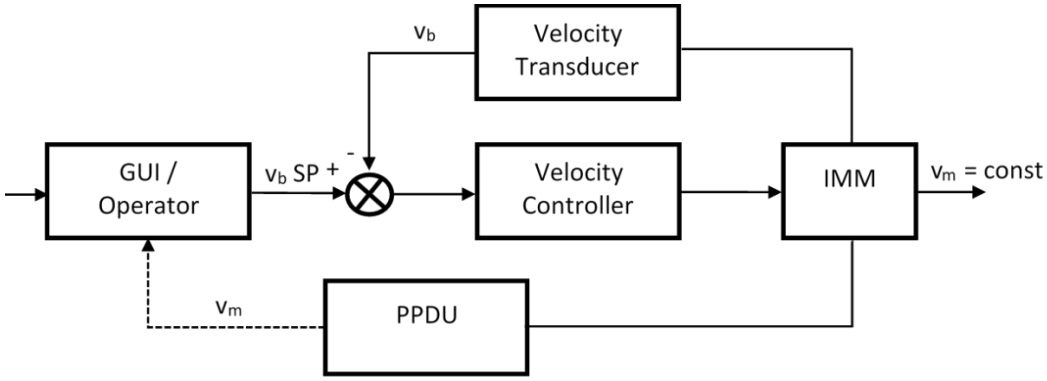

Fig. 4-20: Offline velocity profile setting through visualisation

For the application of an algorithm-based, advanced control strategy for injection velocity profiling and closed-loop control of the filling process on machine-independent parameters such as melt front velocity, melt viscosity, and melt shear rate, the PPDU can be used as an input for any pre-existing advanced controller concepts. As the literature review has revealed, an advanced control strategy of the filling process based on machine-independent parameters can be performed with the aid of a two-dimensional controller: (a) an inner feedback controller for closed-loop control of the injection speed within the injection moulding cycle

(during filling) and (b) an outer melt front velocity controller based on learning control algorithms between the cycles. In addition to the melt front velocity, all other machine-independent parameters determined by the PPDU such as melt viscosity, melt shear rate, and shear stress can be closed-loop controlled.

In such a configuration, all of the advanced control strategies based on machine-independent parameters that are reviewed in Section 2.6.3—such as constant melt front velocity (or minimisation of variance on all flow paths)—can be performed. If operating conditions shift during operation, for example, due to disturbances such as outside temperature or changes in material viscosity, the reference parameters stored in the PPDU (Section 4.11.1) can also serve as input variables for controlling the injection moulding process.

Fig. 4-21 presents the corresponding block diagram of the advanced controller. Through feedback control, the inner loop of the controller closed-loop controls the injection velocity during the filling process. In the outer loop, the input parameters (control variables) for the melt front velocity controller—such as the flow front velocity, melt viscosity, shear rate, or shear stress of the melt—are determined by the PPDU. For each injection cycle, the melt front velocity controller determines the injection velocity profile set points v_b *SP* based on learning control algorithms and the desired optimisation strategy. These set points serve as input variables (dependent variables) for the inner closed-loop injection velocity control of the moulder.

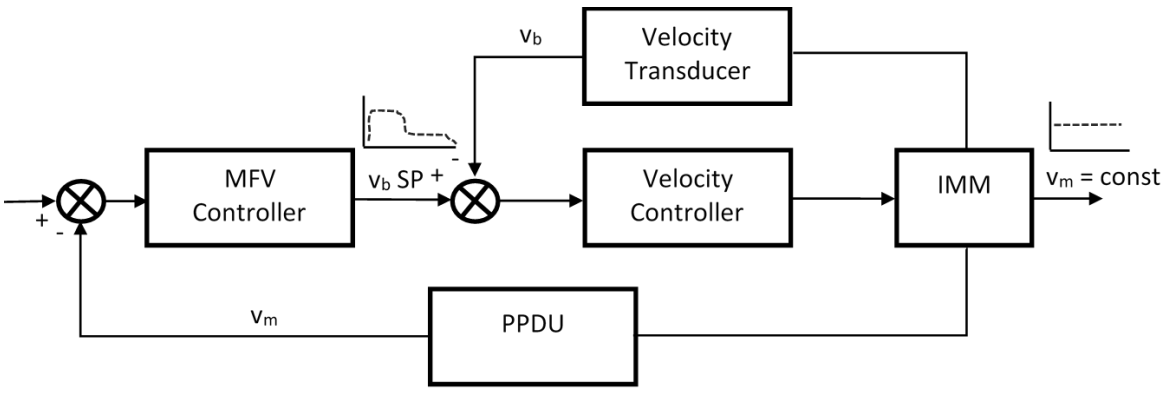

Fig. 4-21: Learning control with process parameter determination unit and melt front velocity controller

4.12 Chapter Summary

In this chapter, a new and innovative method for determining flow front location and velocity as a function of screw position and injection time over the entire part geometry using only one sensor has been proposed, designed, and developed.

The new method comprises three stages consisting of 14 total steps and is characterised as follows:

- The method is based on the idea of mapping a simulated filling process to a real injection moulding process.
- The mapping occurs at the event points when the melt front has a particular characteristic at a position within the cavity.
- Two kinds of singular events are used: those identified through simulation analysis and those identified through experimental measurements.
- Singular events can occur in the form of event groups, and the sequence of all events can be analysed to identify a pattern of the form part.
- To determine flow front location in relation to screw position, the form part-specific pattern is matched to the real event pattern of the filling process.
- For the purpose of matching, a new linear matching algorithm is proposed, designed, and developed.
- By matching patterns, the virtual events can be assigned to the real events, and the melt front position can be determined against the respective screw position.
- By considering two successive and assigned events the flow front velocity of the melt can be determined.

- From the calculated flow front velocity, machine-independent parameters, such as wall shear stress τ_i, shear rate $\dot{\gamma}_i$ and melt viscosity η_i, can be derived.

For the implementation of the new method into an injection moulding process, the development of a PPDU has been proposed, and, for the applications (a) velocity profiling by the operator and (b) advanced injection moulding machine control, the functional requirements of the PPDU have be assessed and discussed.

The results from the assessment suggest that the development and use of the PPDU for the application profiling injection velocity can solve the problem of the lack of knowledge regarding the flow front of the melt and the associated problem of mainly empirical profiling by the operator. This can lead to the desired rule-based strategy in the setting of the injection-moulding machine. The functional requirements of the PPDU for the application injection velocity profiling suggest the following:

- The device to be developed consists of an interactive machine control terminal with high-resolution display and associated hardware.
- The functions of the machine control terminal can be controlled by a user interface with touch screen functionality.
- The PPDU provides intuitive handling and animated data visualisation, including for the filling pattern of the form part related to the injection time and screw position of the moulder.
- The operator can have the course of the flow front displayed over the entire flow channel and assigned to the respective screw position.
- To compensate for surface defects of the moulded parts, the front course animation can be stopped at particular melt front locations, such as characteristic event points, where machine parameters such as injection velocity could be entered or adjusted.

For the application of an algorithm-based advanced control strategy, the following implications arise:

- For the closed-loop control of the filling process on machine-independent parameters such as melt front velocity, melt viscosity, and melt shear rate, the PPDU can be used as an input for any pre-existing advanced controller concept.

- In such a configuration, all of the advanced control strategies based on machine-independent parameters (reviewed in Section 2.6.3), such as constant melt front velocity (or minimisation of variance on all flow paths), can be performed.

- An advanced control strategy of the filling process based on machine-independent parameters can be performed with the aid of a two-dimensional controller: an inner feedback controller for closed-loop control of the injection speed within the injection moulding cycle during filling and an outer melt front velocity controller, based on learning control algorithms between the cycles.

- In the advanced control strategy, the melt front velocity determined by the PPDU acts as control variable and can be closed-loop controlled. The required setting parameters, such as the velocity profile of the screw, are determined by the melt front velocity controller and become dependent variables.

- In addition to the melt front velocity, all other machine-independent parameters determined by the PPDU such as melt viscosity, melt shear rate, and shear stress can be closed-loop controlled.

- If operating conditions shift during operation, for example, due to disturbances such as outside temperature or changes in material viscosity, the reference parameters stored in the PPDU (Section 4.11.1) can also serve as input variables for controlling the injection moulding process.

For the validation of the new method, comparative real and simulated experiments using multiple cases (dimensions, boundary conditions) are conducted, as described in Chapters 5 and 6.

- If the assumptions made are correct, it will be possible, for different geometrical cases (one-dimensional and multidimensional filling) to determine both virtual and real events at the event locations.
- In this case, event patterns can be analysed from the form part-specific and measured pressure curves.
- The proposed matching algorithm will be able to match form part-specific event patterns to real event patterns.
- Through the matching of form part-specific event patterns to real event patterns, virtual and real events can be assigned.
- Through assigning virtual and real events, a relationship between the flow front position of the melt and the screw position of the injection moulding machine can be established.
- The relationship between assigned events can be proven by visualising the filling pattern at the event sites, where simulated virtual events and measured real events are superimposed.
- The proof that the relationship between the flow front position and the screw position has been established is provided if, at these superimposed event sites, the filling pattern regularly shows flow front locations where events can be expected (at tapering, enlargements, edges, corners, flow obstacles, etc.).
- If the relationship between flow front position and screw position can be established, the relationship between flow front velocity and screw position can also be established.

- If the relationship between flow front velocity and screw position can be established, other machine independent parameters such as wall shear stress, shear rate, and melt viscosity can be determined.

5 APPLICATION OF ONE-DIMENSIONAL FILLING

5.1 Introduction

In this chapter, one-dimensional filling process is used to demonstrate and validate the method proposed in Chapter 4. For this validation, the process steps presented in Section 4.7 are applied to the step plate, a form part model with a sprue bar, lateral dovetail gate, and three-step varying wall thickness over the flow path. The step plate represents an idealised one-dimensional flow front course.

In the experimental validation, pressure signals are measured in an injection moulding process to identify real events and determine real event patterns. A numerical calculation (simulation) with boundary conditions identical to the parameter setting of the moulding machine is performed to determine the simulated pressure curve. If the assumptions made in Section 3.2.2 are correct, virtual and real events exist and form part-specific and real event patterns can be identified and matched from the analysis of the pressure curves. According to theory, individual events can be assigned by matching the patterns. If the relationship between the assigned events can be proven, it can also be proven that for the one-dimensional case, the new proposed method can be used to establish the relationship between the flow front position of the melt and the screw position of the injection moulder.

The proof is achieved if, at the superimposed event sides, the filling patterns show flow front locations where events can be expected. In this case, the flow front velocity and other machine-independent parameters, such as shear rate, shear stress, and melt viscosity, can be obtained over the entire flow path.

5.2 Models of One-Dimensional Filling

The step plate, as shown in Fig. 5-1, comprises a sprue bar, lateral dove tail gate, and three-step varying wall thickness over the flow path; injection occurs via a sprue bar, and the melt is distributed over a dovetail gate located on the largest

cross section of the step plate (Fig. 5-4). Due to its rheologically balanced runner system, the flow front develops uniformly at the gate and runs almost perpendicularly to its main axis direction.

Due to the predetermined flow path, this relatively simple form part has been chosen for the first case study of the experimental validation. The step plate represents the one-dimensional flow front course and allows the expectation of event locations L_i at the transitions between the different cross-section heights and at the end of the flow path.

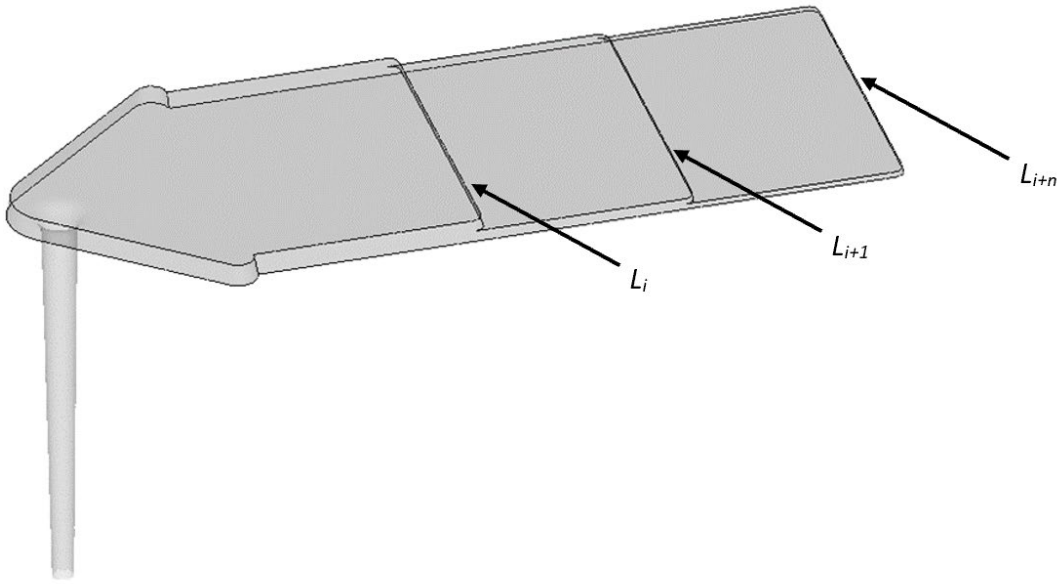

Fig. 5-1: Step plate

5.3 Experimental Validation

5.3.1 Numerical Model

For the form part geometry, Moldflow 2016 was used to perform the simulation to determine melt flow pattern, as well as a simulated pressure curve. Moldflow is a developer of simulation software for high-end plastic injection moulding computer-aided engineering (Reference for Business, n.d.). The company was founded in Melbourne, Australia in 1978 and is owned by Autodesk.

To perform the simulation, the part geometry is imported as a step file into the simulation software. Thereafter, the mesh is generated as a solid 3D model. To obtain high quality simulation, mesh elements with unsuitable aspect ratios have been manually adjusted. The aspect ratio of an element is the ratio of the longest edge of a triangle to its shortest edge. By definition, the aspect ratio of a perfect triangle element is 1 (Dassault Systems, 2021). A higher aspect ratio indicates poorer element quality. Elements with an aspect ratio between 8 and 20 (and even above) are characterised as 'bad elements' and must be manually adjusted to lower aspect ratios.

To attain precise results, it is necessary to use a small element size in the 3D mesh. In this definition, precise results are associated with a high resolution of the simulated pressure curve. Since this resolution depends on the density of the mesh, the element size of 1 mm was chosen, which results in a total number of 677,859 elements (3D mesh with eight layers) for the step plate. Thus, the calculated flow through time per element, at a total injection time of 1.8 s (corresponding to a volume flow of 15 cm^3/s with which the real injection moulding test has been conducted), falls below the signal resolution of the pressure sensor of 2 ms.

The mould filling is simulated with a mould surface temperature of T_{wz} = 33°C, a melt temperature of T_m = 248°C, and a flow rate of $\dot{V}$ = 15 cm^3/s. Under these boundary conditions, the real injection moulding tests were conducted. As further described in Section 5.3.2, these chosen parameter settings led to high quality moulded parts free of surface defects. The switchover from filling phase to holding pressure phase is performed at 98% of the volumetric filling (the default setting of the Moldflow solver). The selected resin for the simulation, an Acrylnitril Butadien Stryrol (ABS) polymer, type Terluran GP-22 from the Badische Anilin- und Soda Fabrik ([BASF], 2007), is identical with the resin used for the real injection moulding test. The material specification is shown in Fig. 5-2. Viscosity dependence is expressed through the Williams-Landel-Ferry (Agassant et al., 2017) cross model in Equation (2-5), and the required resin properties are obtained using

the simulation software's database.

BASF
Terluran® GP-22 (ABS)

05/2007 Page 1

Easy-flow, general purpose injection moulding grade with high resistance to impact and heat distortion; intended for a wide range of applications, particularly in the housings sector.

Typical values at 23 °C		Test method	Unit	Values
1. Properties				
Polymer abbreviation			-	ABS
Density		ISO 1183	g/cm³	1.04
Melt volume-flow rate MVR 220 °C / 10kg		ISO 1133	cm³/10min	19
Water absorption, equilibrium in water at 23 °C		similar to ISO 62	%	1
Moisture absorption, equilibrium 23 °C/50% r. h.		similar to ISO 62	%	0.22
Moulding shrinkage, free, longitudinal		-	%	0.4 – 0.7
2. Flammability				
UL94 rating at 1.6mm thickness	**(E41871)**	UL 94	class	HB
Automotive materials (thickness d≥1mm)		FMVSS 302	-	+
3. Mechanical properties				
Tensile modulus		ISO 527-1/-2	MPa	2300
Yield stress (50 mm/min)		ISO 527-1/-2	MPa	45
Yield strain (50 mm/min)		ISO 527-1/-2	%	2.6
Nominal strain at break (50 mm/min)		ISO 527-1/-2	%	10
Flexural strength		ISO 178	MPa	65
Charpy impact strength	(+ 23 °C)	ISO 179/1eU	kJ/m²	180
Charpy impact strength	(- 30 °C)	ISO 179/1eU	kJ/m²	100
Izod notched impact strength	(+ 23 °C)	ISO 180/A	kJ/m²	26
Izod notched impact strength	(- 30 °C)	ISO 180/A	kJ/m²	8
Charpy notched impact strength	(+ 23 °C)	ISO 179/1eA	kJ/m²	22
Charpy notched impact strength	(-30 °C)	ISO 179/1eA	kJ/m²	8
Izod notched impact strength, method A	(+23 °C)	ASTM D 256	J/m	300
Ball indentation hardness at 358 N/30 s		ISO 2039-1	MPa	97
4. Thermal properties				
HDT A (1.80 MPa) / HDT B (0.45 MPa)		ISO 75-1/-2	°C	80 / 92
Vicat softening temperature VST/A/50 / VST/B/50		ISO 306	°C	105 / 96
Max. service temperature (short cycle operation)		-	°C	80
Coefficient of linear therm. expansion, longit. (23-80) °C		ISO 11359-1/-2	10^{-4}/°C	0.8 – 1.1
Thermal conductivity		DIN 52612-1	W/(m•K)	0.17
5. Electrical properties				
Relative permittivity at 100 Hz / 1 MHz		IEC 60250	-	2.9 / 2.8
Dissipation factor at 100 Hz / 1 MHz		IEC 60250	10^{-4}	48 / 79
Volume resistivity		IEC 60093	Ω • m	10^{13}
Surface resistivity		IEC 60093	Ω	10^{13}
Electric strength K20/P50, d = 0.6 - 0.8 mm		IEC 60243-1	kV/mm	37
CTI, test liquid A		IEC 60112	-	600
CTIM, test liquid B		IEC 60112	-	225

Fig. 5-2: Material specification (BASF, 2007)

Fig. 5-3 shows the meshed part geometry of the step plate with its thrice-varying wall thickness,

$$h_1 = 2 \cdot h_2 = 4 \cdot h_3 = 4\ mm \tag{5-1}$$

over the flow course. The base area of the step plate is 120 x 60 mm^2.

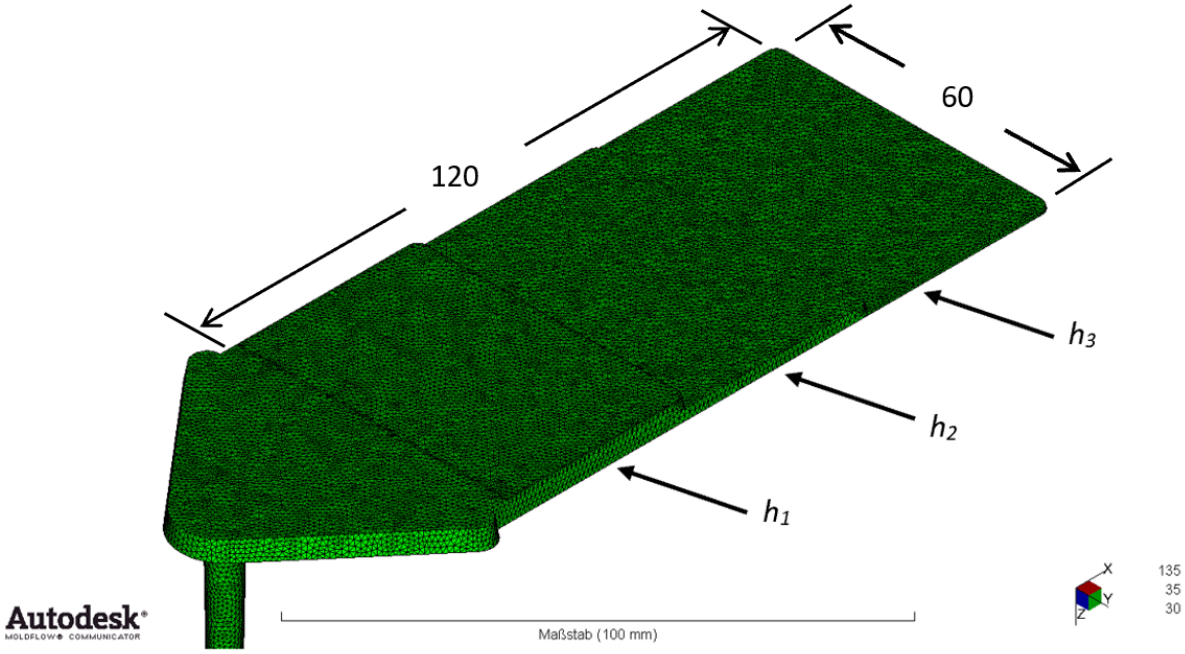

Fig. 5-3: Meshed part geometry of the step plate

The runner system—a cold runner—is part of the filling analysis (simulation) and is meshed with the same element size, 1 mm, as shown Fig. 5-4.

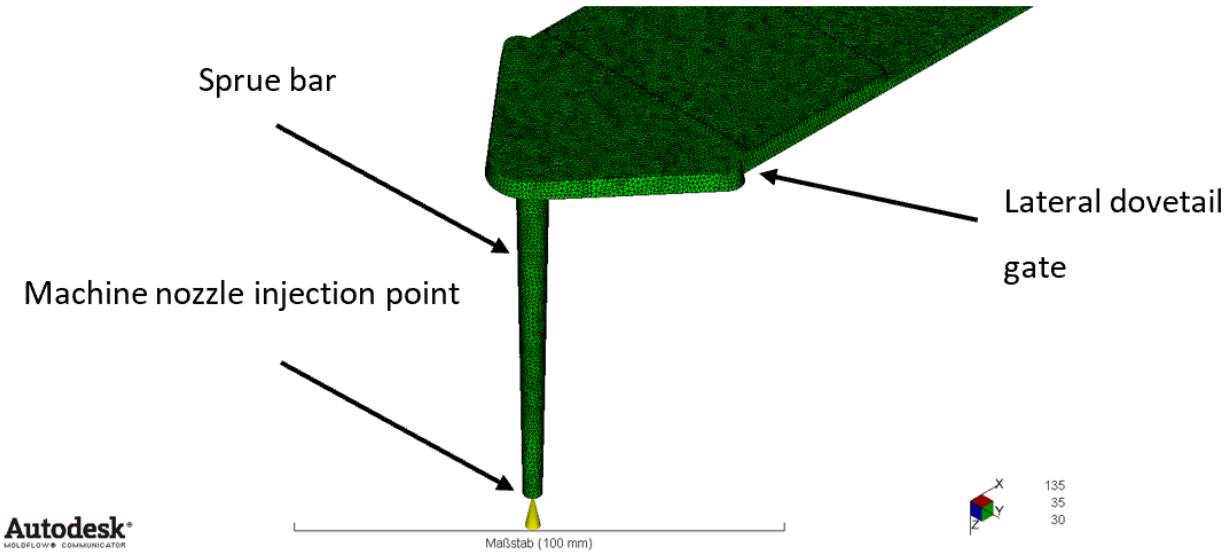

Fig. 5-4: Meshed cold runner system of the step plate

Fig. 5-5 shows the form part-specific pressure curve determined by the simulation. Because the step plate runner system is part of the simulation, the curve shows the simulated pressure loss p_{sim} of the molten plastic at the position of the machine nozzle injection point. The simulated injection time t_{sim} begins with the injection time of the moulding machine (1) and ends by switching to simulated holding pressure at 98% volumetric filling of the form part (2).

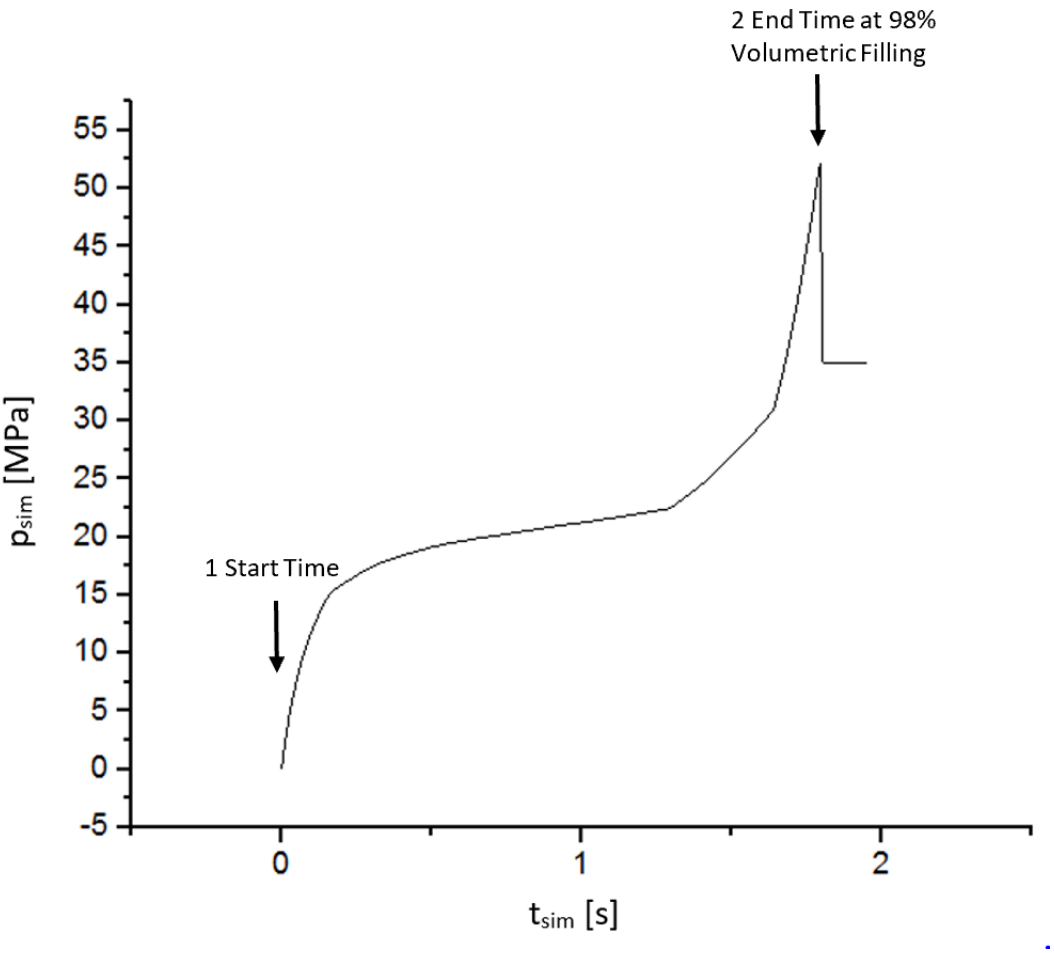

Fig. 5-5: Step plate form part-specific pressure curve

5.3.1.1 Model Validation

All numerical calculations converge; however, despite the high mesh density of 677,859 elements, the resolutions of the calculated pressure curves in the first attempts were insufficient for further analysis. Since it was initially assumed that the resolution of the simulated pressure curve would depend only on the density of the mesh, the element size (and thus number of elements) in the simulation was chosen so the flow through time per element would fall significantly below the signal resolution of the pressure sensor of 2 ms. However, during the experimental work it was found that in the default setting, the Moldflow solver computes pressure curves with a maximum resolution of only 110 data points over the virtual injection time, independent of the element size of the mesh and length of the filling phase. This can be remedied by changing the default setting of the

simulation software. By increasing the number of iteration steps to a filling volume per time step of 0.1% (the smallest possible input value) and an iteration limit value of 2,000 (the largest possible input value), the Moldflow solver determines the pressure curve as a function of the virtual injection time with a maximum resolution of 1,050 points. Through these changes in the solver setting, the computing time of the simulated mould filling increased from less than 20 minutes to approximately three hours.

Table 5-1 and Fig. 5-6 show the dependency of volume flow and injection time and the resulting resolution of the simulated pressure curve for a range of injection times between 0.4 and 2.7 s. For the step plate with 677,859 elements (eight layers), the calculated resolution of the simulated pressure curve at an injection time of 2.7 s (corresponding to a volume flow of 10 cm^3/s with 98% filling) is $3 \cdot 10^{-3}$ s. The resolution reaches and surpasses the signal resolution of the pressure sensor of $2 \cdot 10^{-3}$ s at or above a volume flow of 15 cm^3/s (shown in red type).

Table 5-1: Step plate resolution of the form part-specific pressure curve

$\dot{V}$ $[cm^3/s]$	10	**15**	20	25	30	40	50	75
t_{sim} **[s]**	2.7	**1.8**	1.4	1.1	0.9	0.7	0.5	0.4
Resolution [s]	0.003	**0.002**	0.001	0.001	0.001	0.001	<0.001	<0.001

Section 5.3.3 shows that with the improved resolution through the changed default setting of the Moldflow solver, the analysis of the differentiated form part-specific pressure curves becomes reliably possible. However, against the initial assumption that the resolution of computed pressure curve would depend only on element size, with the existing solver, the maximum resolution of 1,050 points cannot be exceeded. In other words, the upper limit of 1,050 points specified by the Moldflow solver leads to a fixed dependency of resolution of the computed pressure curve and injection time such that the longer the injection time, the lower the resolution. Once this limit is reached, no higher resolution can be achieved by reducing the element size of the mesh. For larger form parts with long

injection times in particular, this could be a limiting factor in the application of the new method.

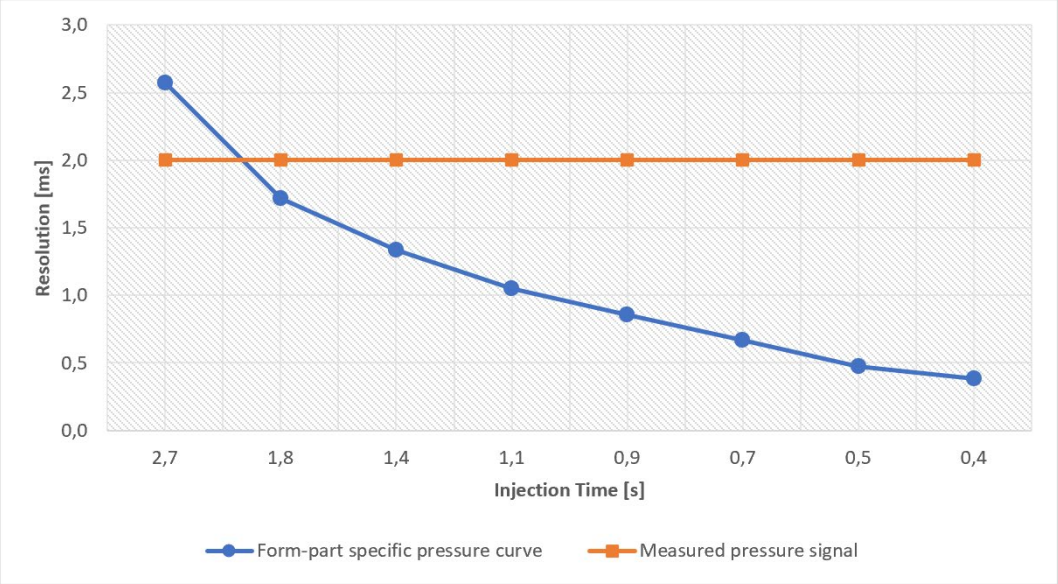

Fig. 5-6: Step plate comparison of the resolution of the form part-specific and the measured pressure curve as a function of the injection time

5.3.2 Experimental Setup

The injection moulding tests were conducted on a Battenfeld HM 800 machine with a closed loop-controlled injection unit and 30 cm screw diameter. An ABS Terluran GP-22 was used as the material. The specifications can be found in Fig. 5-2. Fig. 5-7 shows the injection moulded test part of the step plate. As Table 5-2 demonstrates, three distinct test cases with increasing volume flows were conducted and recorded. The number of 100 specimens per case ensures that the process parameters can be stabilised.

Test case (1.2) was selected for further analysis. In this case, the volume flow is 15 cm^3/s, the melt temperature is 248°C, and the mould surface temperature is 33°C. At these conditions, the parameter setting led to high quality moulded parts, free of surface defects. Compared with the other two test cases, the surface quality of the parts was rated as subjectively better.

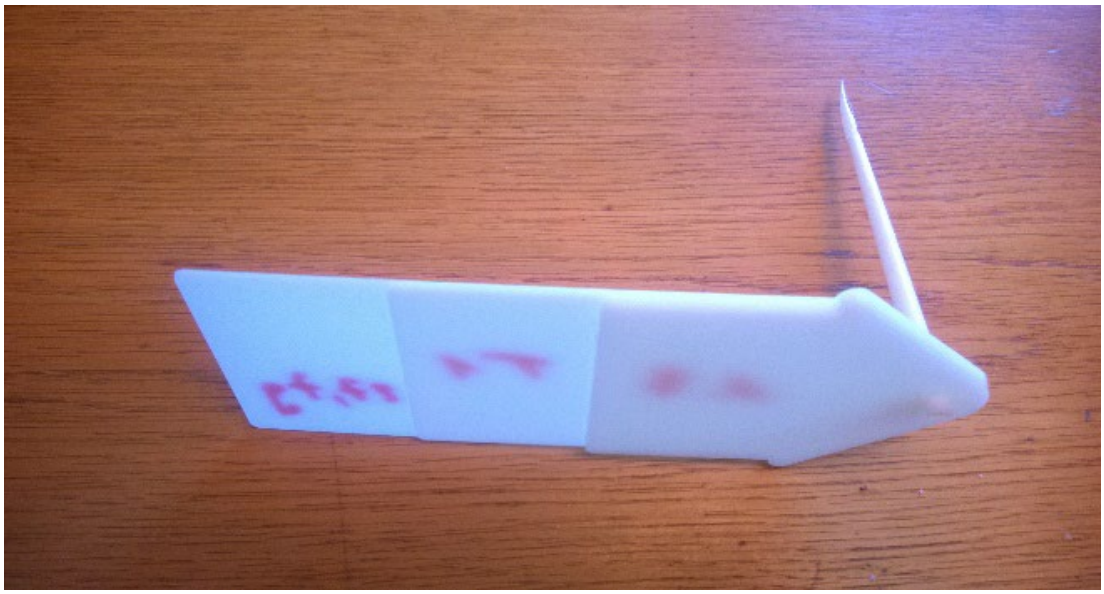

Fig. 5-7: Injection moulded test sample of the step plate

Table 5-2: Test conditions of step plate injection moulding

	Test sample production		**Sample**	**Step plate, polished**	
			Resin	ABS, BASF – Terluran GP 22	
	Test cases		1.1	1.2	1.3
	Sample number		100	100	100
Velocity	Peripheral speed	[mm/s]	200	200	200
	Volume flow	[cm^3/s]	10	15	20
Stroke	Switching point	[cm^3]	14.0	14.0	14.0
	Dosing stroke	[cm^3]	45	45	45
	Melt cushion	[cm^3]	13.7	13.5	13.2
Time	Cycle time	[s]	39.6	38.4	37.9
	Injection time	[s]	3.75	2.58	2.03
	Holding pressure time	[s]	10	10	10
	Cooling time	[s]	20	20	20
	Plasticising time	[s]	5.6	5.6	5.6
Pressure	Injection pressure	[MPa]	77.7	80.5	83.9
	Holding pressure	[MPa]	35.0	35.0	35.0
	Back pressure	[MPa]	6.0	6.0	6.0
Temperature	Feeding zone	[°C]	40	40	40
	Barrel zone 3	[°C]	220	220	220
	Barrel zone 2	[°C]	230	230	230
	Barrel zone 1	[°C]	240	240	240
	Melt sensor	[°C]	247	248	248
	Nozzle	[°C]	230	230	230
	Mould surface moving side	[°C]	33	33	33
	Mould surface fixed side	[°C]	33	33	34
Force	Clamping pressure	[kN]	800	800	800
Drying	Drying time	[h]	4	4	4
	Drying temperature	[°C]	80	80	80
	Remaining moisture	[%]	0.015	0.015	0.015

The test setup and the mould of the step plate are shown in Fig. 5-8 and Fig. 5-9, respectively.

Fig. 5-8: Test setup with moulder

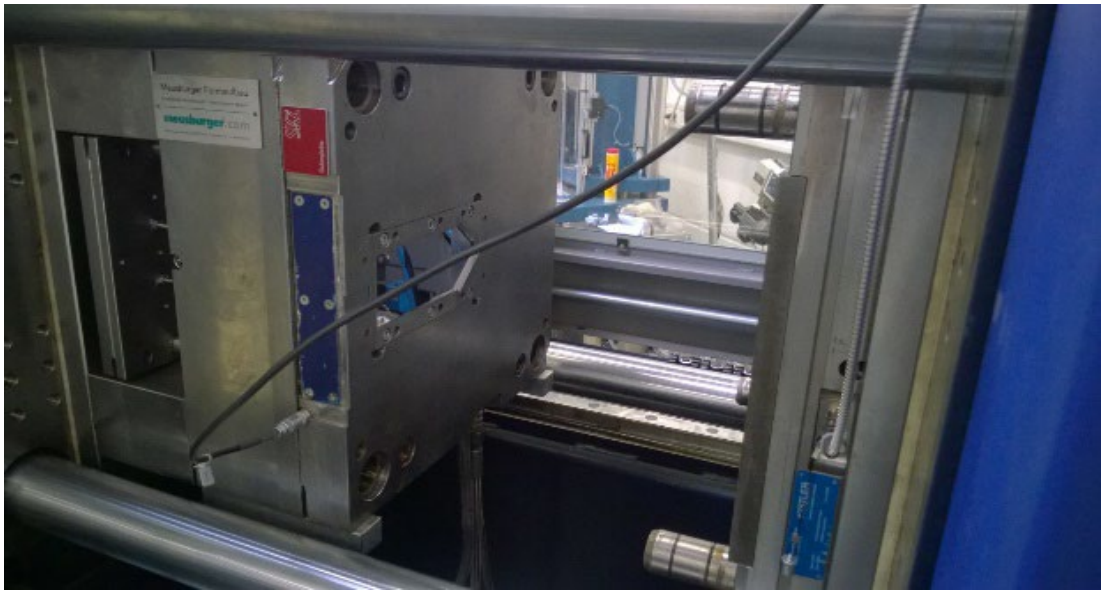

Fig. 5-9: Mould for the step plate

Fig. 5-10 illustrates the test setup, consisting of the injection moulding machine with clamping unit and injection unit, together with the data acquisition unit.

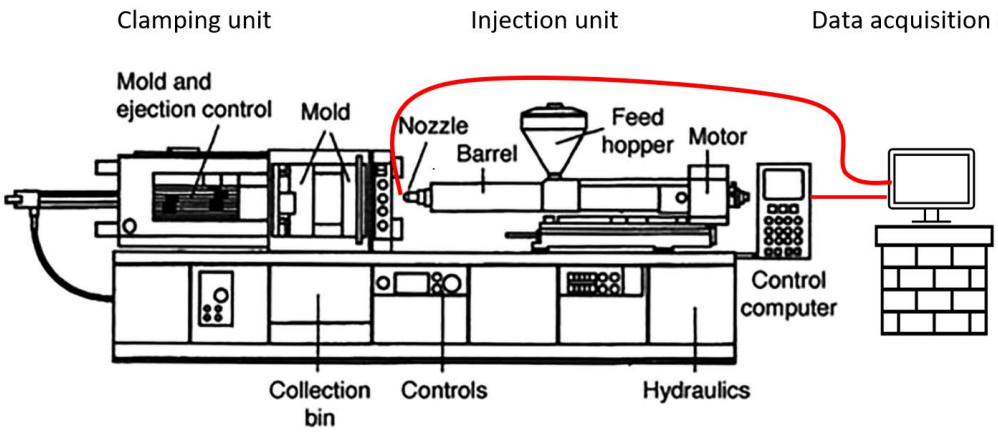

Fig. 5-10: Diagram of test setup

The acquisition of the data is conducted via a PC connected to both the machine control (MC) and a pressure sensor located in the machine nozzle (shown in red). The interface to the machine control system is used to record process parameters that are responsible for process stability. These parameters include melt and mould temperature, injection and holding pressure time, and hydraulic pressure at the injection cylinder for each cycle. The actual measurement of the injection pressure curve is conducted via the pressure sensor fitted in the machine nozzle.

The exact mounting location of the pressure sensor is presented in Fig. 5-11. The Dynisco sensor, type MDT465FXL, is placed in a mounting ring located between the machine nozzle and injection unit, so melt pressure is acquired directly in front of the screw of the injection unit.

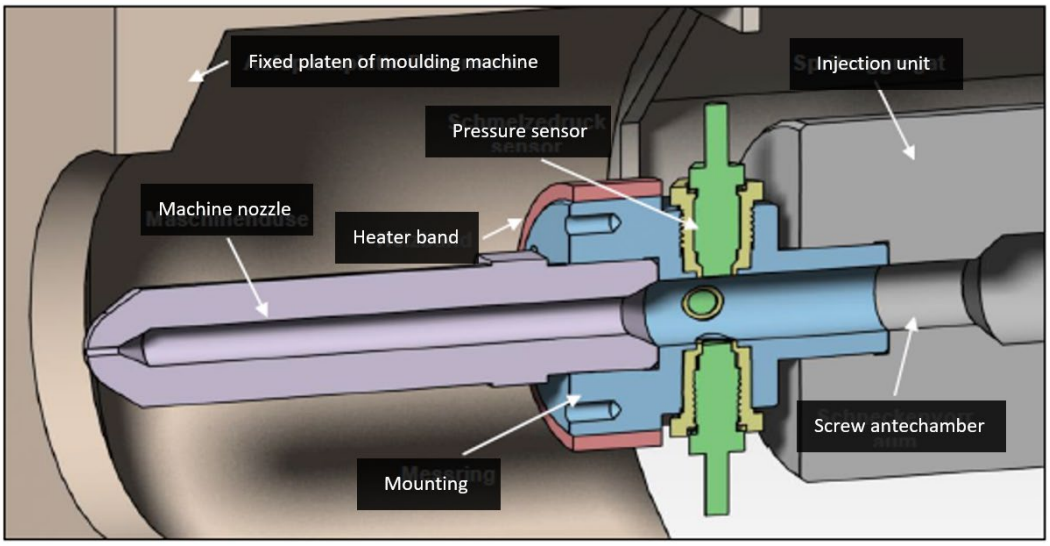

Fig. 5-11: Mounting location of the pressure sensor

The Dynisco sensor has a measuring range of 0–200 MPa, with an accuracy of +- 1% and a repeatability of +- 0.2% over the entire measurement range (Table 5-3). Since the sensor is not capable of automatic temperature compensation, it is necessary to wait until the sensor has heated fully to the set processing temperature and a manual zeroing has been conducted before sample production begins.

Table 5-3: Dynisco MDT465FXL specifications (Dynisco, 2021)

Pressure rage	0–200 MPa
Max. overload	245 MPa
Accuracy	+- 1 % of full scale
Repeatability	+- 0.2 % of full scale
Output signal	4–20 mA
Max. temp. (at diaphragm)	400 °C
Zero shift due to temp. change	< 0.04 MPa / 10 °C

Fig. 5-12 demonstrates the functional principle of the pressure sensor (Dynisco, 2021). Through a closed, liquid-filled pressure transmission system, the sensor

furnishes an electrical signal that is proportional to the pressure of the melt. The pressure applied by the medium is forwarded to the measuring diaphragm via the separating diaphragm and the transmission medium (mercury) in the capillary. The deflection of the measuring diaphragm changes the resistance of the strain gauge bonded to the measuring diaphragm. The integrated amplifier generates an electrical signal (mA) proportional to the pressure acquired by the data acquisition unit.

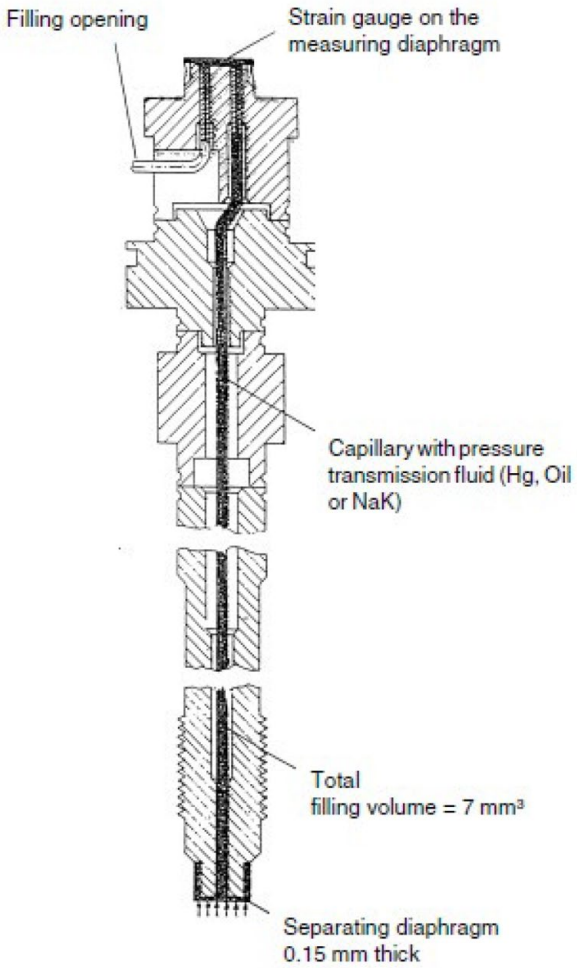

Fig. 5-12: Functioning principle of the Dynisco pressure sensor (Dynisco, 2021)

The Dynisco sensor has an internal calibration signal. By connecting ports ‘E’ and ‘F’ of the sensor, the calibration signal is applied to the signal output. The signal must correspond to 80% of the nominal pressure. The calibration is carried out in a depressurised state and at room temperature. For this purpose, two

potentiometer adjustment screws in the cover part of the electronics housing are used ('N' for zero point adjustment, 'B' for range adjustment). After connecting the pressure sensor to the indicator, the zero point is set with the potentiometer adjusting screw 'N'. The calibration signal at the signal output is set to the calibration value (80% of the nominal pressure) with the potentiometer adjusting screw 'B' and checked on the indicator.

Fig. 5-13 demonstrates the setup of the data acquisition unit. During the filling phase of each cycle, the melt pressure signal is acquired from the Dynisco sensor. For further analysis, the data gained from the sensor are formatted as an ASCII file and transferred to Origin Pro software.

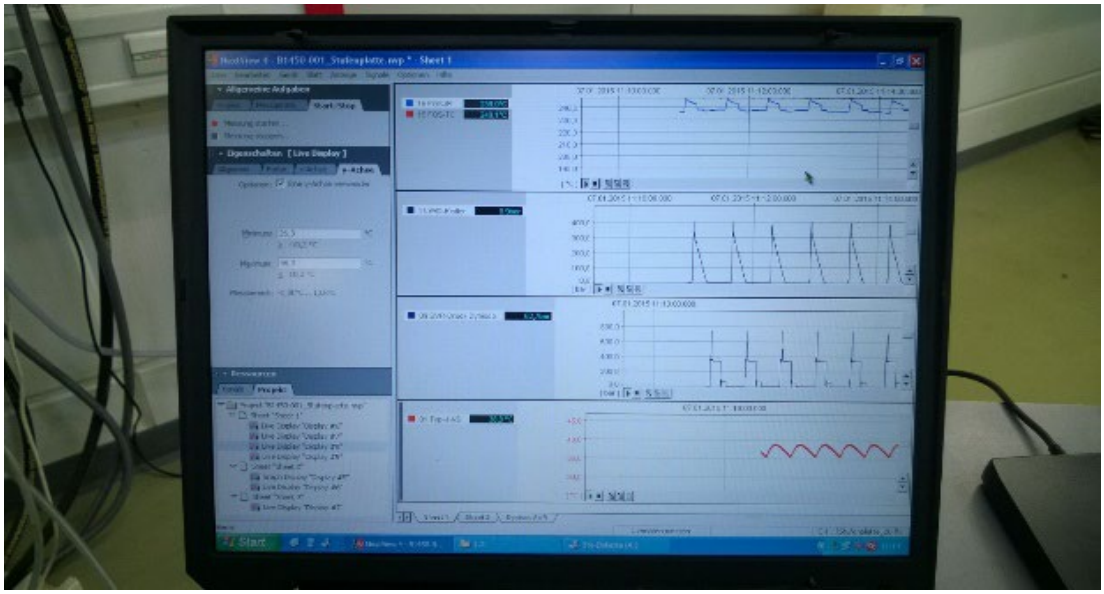

Fig. 5-13: Melt pressure data acquisition setup

The results of the injection moulding test are shown in the graph in Fig. 5-14. The curve represents the measured pressure loss p_{mach} at the location of the machine nozzle during filling phase of the moulding cycle. The resolution of the graph is 2 ms. As stated in Section 5.3.3, for further analysis of the measured pressure curve, only the yellow highlighted mould filling phase is examined. The pressure holding phase subsequent to mould filling is irrelevant for the filling process and is

thus excluded from observation.

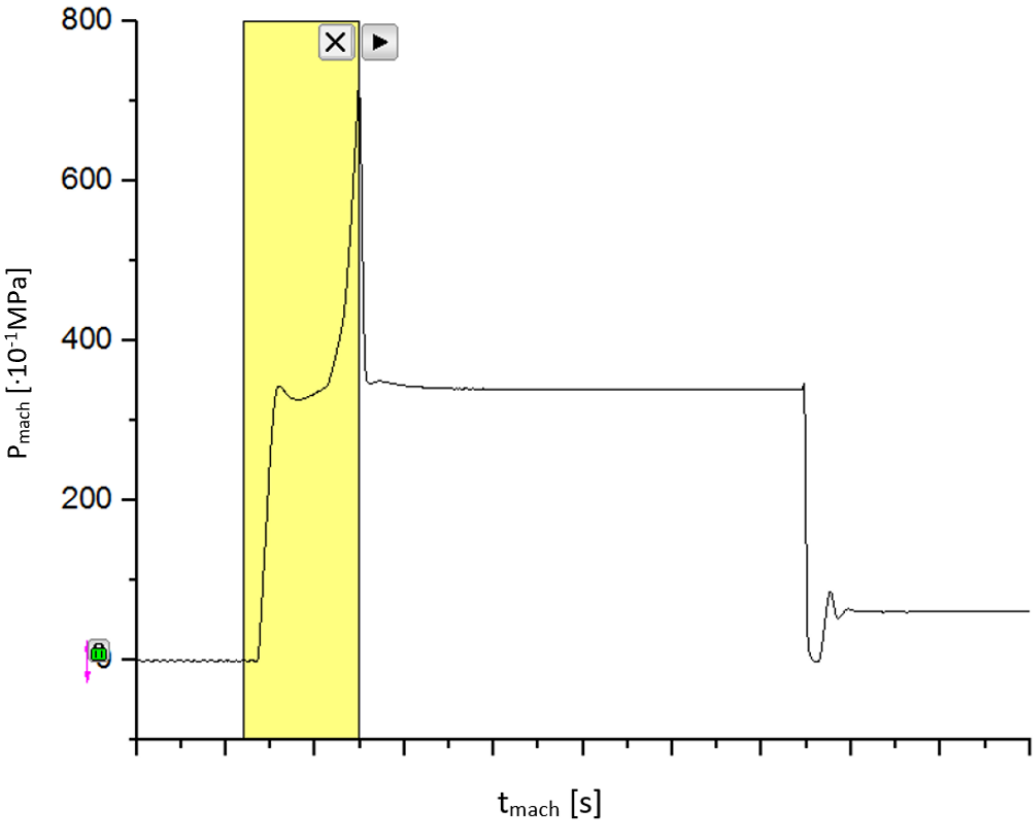

Fig. 5-14: Step plate melt pressure curve

5.3.3 Identification of Events and Determination of Patterns

The analysis of the differentiated pressure curves determines the event patterns. To create the patterns, individual event locations are isolated from the differentiated pressure curve. For this purpose, the pressure graph, obtained either by simulation or measurement, is initially differentiated using Origin Pro, and the differentiated graph is then examined for significant sections where the pressure gradient changes from a relatively less steeply sloped section to a deeply sloped one. This can be done by manually evaluating the graph. In this case, two tangent lines can be determined, and the intersection of the vertical line from the cross points of the tangents to the horizontal axis (time) defines the time of each respective event. However, to gain consistent results for the validation, the

examination of the differentiated pressure graphs is performed using the standardised function peak/flank analysis tool in Origin Pro, rather than manually.

This peak/flank analysis tool analyses the differentiated pressure graph for peaks, slopes (positive or negative slopes), or both, depending on pre-set parameters. For this purpose, the tool defines the 'rise time' as the time required for a signal to change from a specified low value to a specified high value, or vice versa (OriginLab, n.d.). These values typically represent 10% and 90% of step height. The function allows the user to select an area on the graph using a rectangle added to the graph and calculate the rise or fall time within that area. Low and high state levels are calculated, and the step height can then be determined by subtracting the low state level from the high one. A low reference level and a high reference level are then calculated with two specified percentages of the step height. Finally, the start of the rise (or fall) time is determined, which defines the time of each respective event. In the default setting of the function (linear search for slopes, 10% rise time), the rise time of the pressure is determined from the difference between the lowest and highest state levels (local minimum and maximum values). The sensitivity of the analysis can be pre-set. The relationships between these parameters are shown in Fig. 5-15.

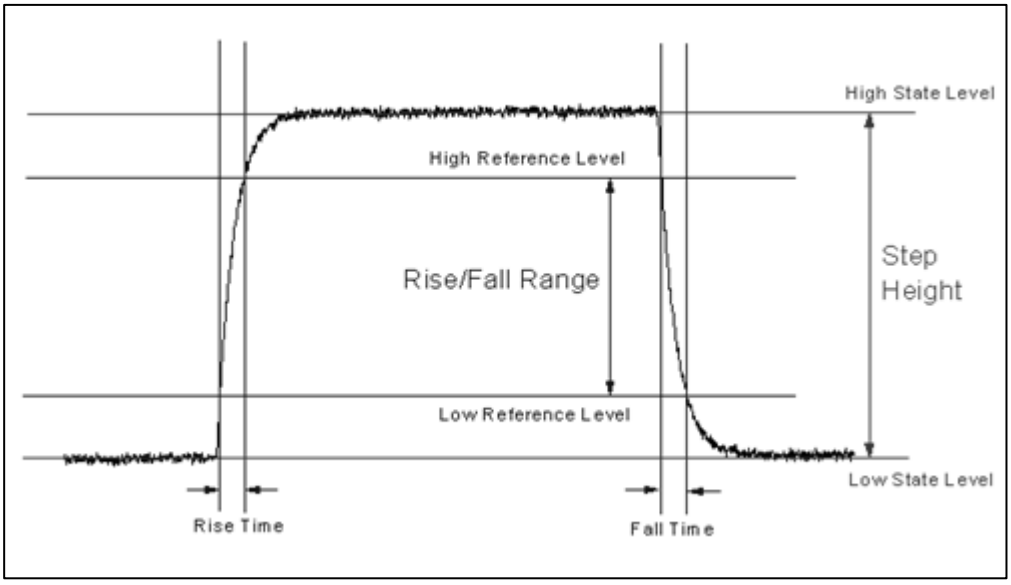

Fig. 5-15: Peak/flank analysis tool (OriginLab, n.d.)

5.3.3.1 Form Part-Specific Event Pattern

The upper section of Fig. 5-16 shows the form part-specific pressure curve in the range relevant for the analysis between the start of the injection time and the switchover to holding pressure. The graph is obtained from the simulation software (Fig. 5-5) and transferred to the analysis tool. The lower section of the figure shows the differentiated graph, which is examined for virtual events by locating the rise (or fall) time for peaks or flanks.

As described in Section 5.3.3, the evaluation is done by the peak/flank analysis tool in Origin Pro. In the evaluation, the default setting is used (linear search for slopes, 10% rise time), and virtual event times are determined at 10% of the rise time of the pressure slopes.

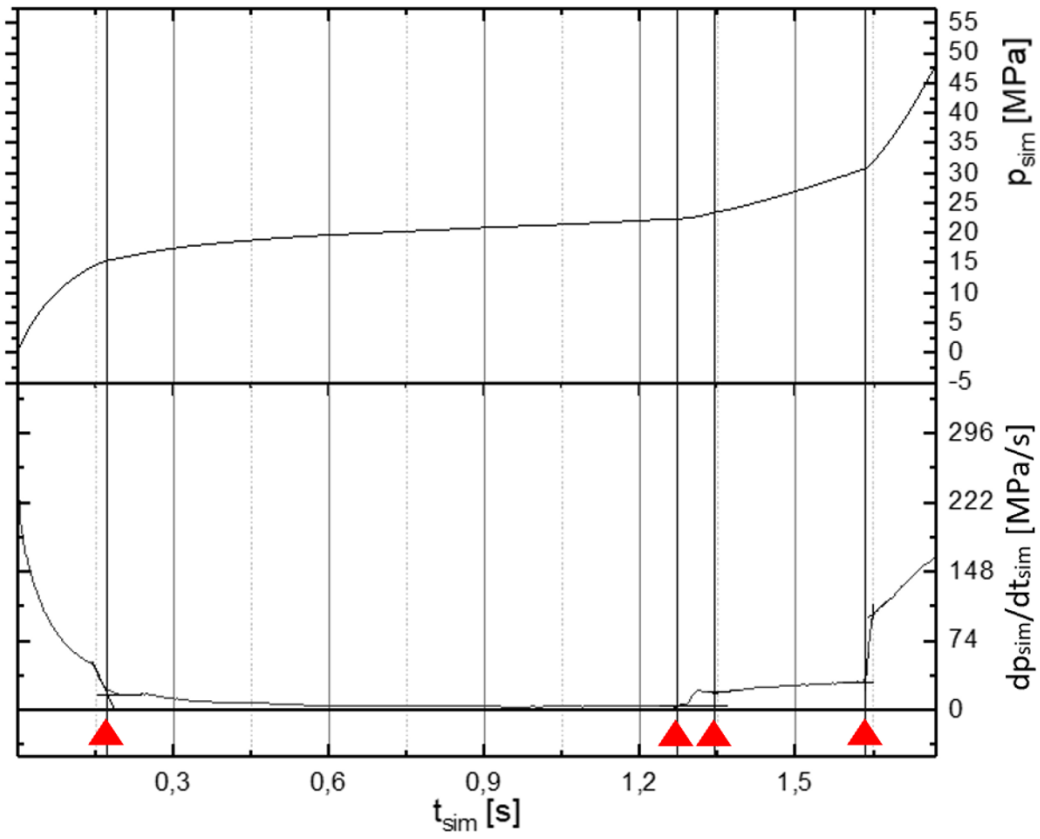

Fig. 5-16: Step plate determination of virtual events

The analysis of the differentiated form part-specific pressure curve determines the form part-specific event pattern consisting of four virtual event vectors, as shown in Fig. 5-16 (presented in red). The virtual event vectors have the following components: virtual event time t_{sim}, melt front position x_{sim}, and melt channel geometry h_{sim}. The entire form part-specific event pattern M_s, comprising four virtual event vectors and their components, is shown in Table 5-4.

Table 5-4: Step plate form part-specific event pattern

	t_{sim} [s]	x_{sim} [mm]	h_{sim} [mm]
$E_{sim\ 0}$	0.173	0	4.0
$E_{sim\ 1}$	1.270	72.5	4.0
$E_{sim\ 2}$	1.340	75.8	2.0
$E_{sim\ 3}$	1.640	112.5	1.0

5.3.3.2 Real Event Pattern

The analysis of the real event pattern is done in a similar way as for the form part-specific one. The pressure graph obtained by measurement is transferred from the data acquisition unit to the analysis tool and initially differentiated. By examining the differentiated pressure curve for rise (or fall) time for peaks or flanks, real events are determined. In the evaluation, the default setting is used (linear search for slopes, 10% rise time), and real event times are determined at 10% of the rise time of the pressure slopes.

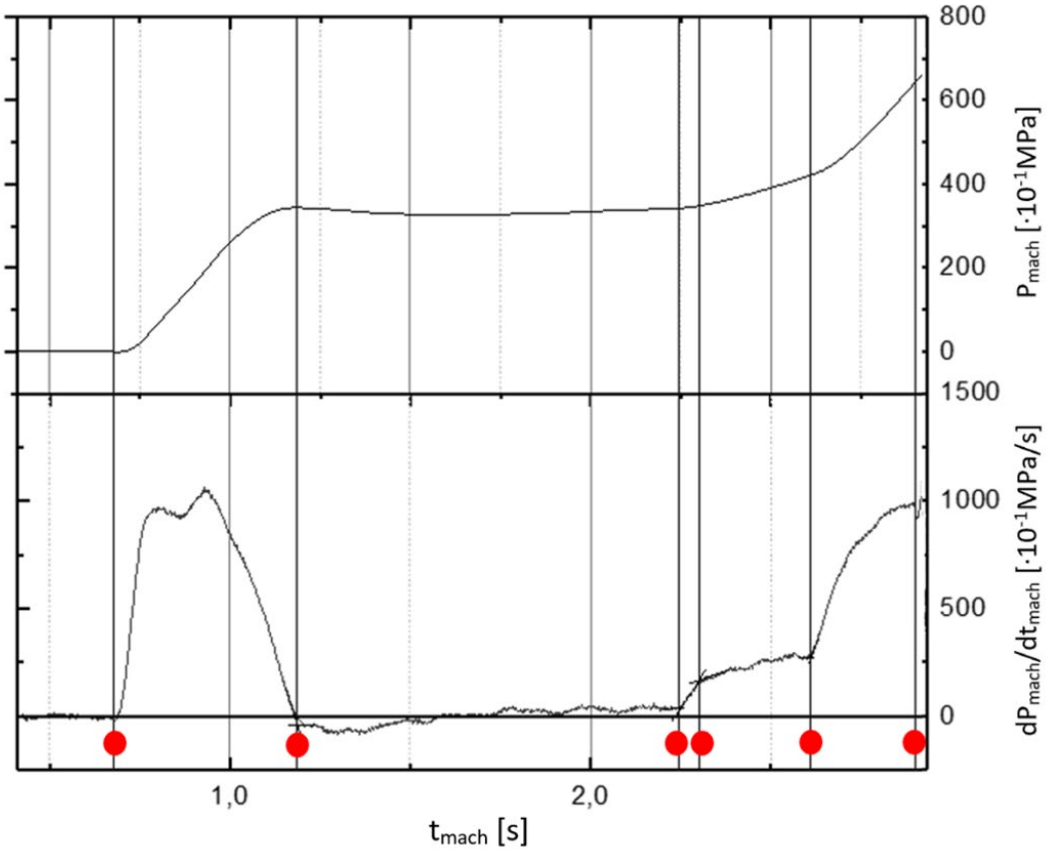

Fig. 5-17: Step plate determination of real events

The analysis of the differentiated measured pressure signal (Fig. 5-17) provides the real event pattern, consisting of six event vectors, for the step plate. Table 5-5 shows the entire real event pattern M_m comprising six real event vectors with the following components: machine time t_{mach}, melt pressure $p_{mach,}$ and screw position s_{mach}.

Table 5-5: Step plate real event pattern

	t_{mach} [s]	P_{mach} [MPa]	S_{mach} [mm]
$E_{mach\ 0}$	0.680	0.0	14.4
$E_{mach\ 1}$	1.190	32.6	25.3
$E_{mach\ 2}$	2.250	34.3	47.8
$E_{mach\ 3}$	2.300	34.8	48.8
$E_{mach\ 4}$	2.610	42.1	55.4
$E_{mach\ 5}$	2.900	64.4	61.6

5.3.4 Pattern Matching and Assigning of Events

In Fig. 5-18, both the real event pattern M_m (circle symbol), and the form part-specific event pattern M_s (triangle symbol), are plotted against machine time t_m. Pattern matching and event assignment are performed using the matching algorithm described in Section 4.8, by means of transformation as well as the displacement of the events.

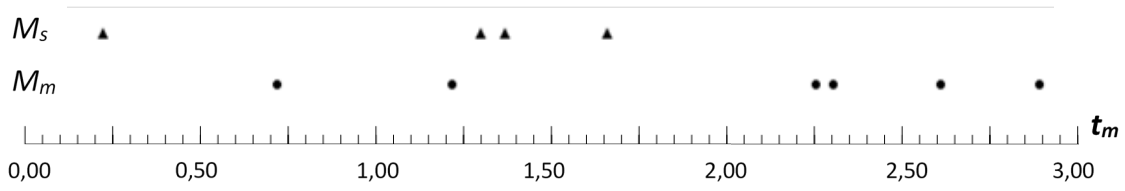

Fig. 5-18: Step plate real and form part-specific event patterns

The matching algorithm passes three levels of iterations, with $j_{max} = m - n$ displacements and transformations, with an interval of $f_{min} = 0.1$ to $f_{max} = 10$, for a scaling increment of $\Delta f = 0.01$.

For the step plate, the algorithm determines the best matching of the patterns at a stretching factor $f_k = 0.97$ and a displacement $j_{min} = 1$, with a total pattern

deviation of S_{min} = 0.00299 s. The transformed form part-specific event pattern $M_{s,j}$ is shown in Fig. 5-19 after having undergone three higher level iterations, with displacements for j = 0 … 2, each at the transformation $k = k_{min}$ with the smallest pattern deviation. For pattern $M_{s,j=1}$, the best alignment to M_m is made (with the smallest deviation S_{min}).

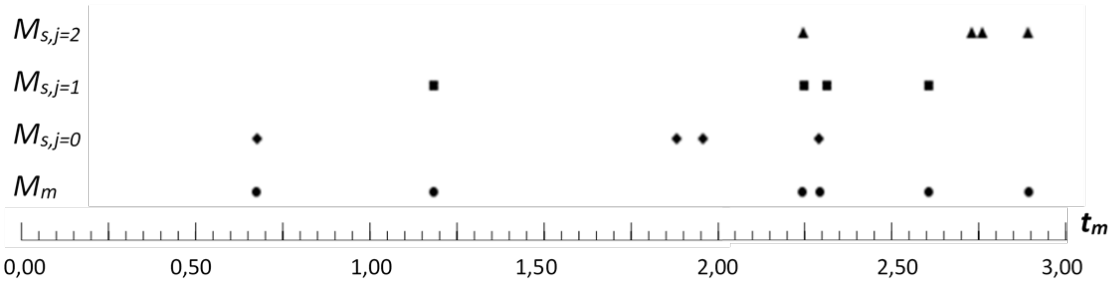

Fig. 5-19: Step plate real and form part-specific event patterns after scaling and displacing

Fig. 5-20 shows the assignment of the virtual and real events from the matched pattern. According to Equation (4-6) and with j_{min} = 1, four virtual events $E_{sim\ i}$ can be assigned to four real events $E_{mach\ i+j}$ ($E_{sim\ 0}$ to $E_{mach\ 1}$, $E_{sim\ 1}$ to $E_{mach\ 2}$, …). The two real events $E_{mach\ 0}$ and $E_{mach\ 5}$ have no correspondent virtual events and are thus excluded from further consideration.

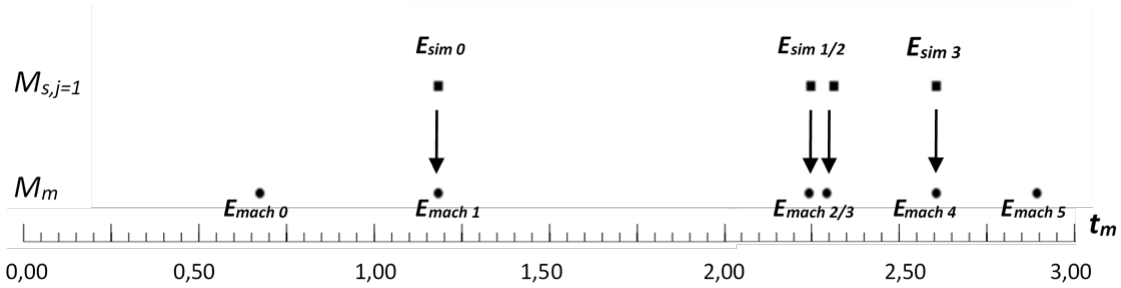

Fig. 5-20: Step plate assignment of virtual and real events

The assignment allows the real event vectors $E_{mach\ i+j}$ to be expanded by the components $x_{sim\ i}$, $y_{sim\ i}$ and $z_{sim\ i}$ (positions of all nodes along the melt front lines)

of the assigned virtual event vectors $E_{sim\ i}$. Thus, the melt front position is consequently associated with machine time $t_{mach\ i+j}$ and screw position $s_{mach\ i+j}$, according to Equation (4-4). Table 5-6 shows the four real event vectors $E_{mach\ i+j}$, of the step plate, with j = 1 expanded by the component of the assigned virtual event vectors $E_{sim\ i}$.

Table 5-6: Step plate real event vectors expanded by assigned virtual event vector components

$E_{mach\ i+j}$	$t_{mach\ i+j}$ [s]	$P_{mach\ i+j}$ [MPa]	$S_{mach\ i+j}$ [mm]	$x_{sim\ i}$ [mm]	$h_{sim\ i}$ [mm]
$E_{mach\ 1}$	1.190	32.6	25.3	0	4.0
$E_{mach\ 2}$	2.250	34.3	47.8	72.5	4.0
$E_{mach\ 3}$	2.300	34.8	48.8	75.8	2.0
$E_{mach\ 4}$	2.610	42.1	55.4	112.5	1.0

5.3.5 Determining Machine-Independent Parameters

Flow front velocity can be determined using flow front position. By considering two successive and assigned event vectors $E_{mach\ i+j}$ and $E_{mach\ i+j+1}$, the mean flow front velocity of the melt from Equation (4-7) v_i as well as the increase in melt pressure from Equation (4-8) Δp_i are calculated between these events. From the calculated flow front velocity and increase in melt pressure (together with information on flow channel geometry $h_{sim\ i}$), and based on the Hagen-Poiseuille equation, machine-independent parameters, such as wall shear stress τ_i, shear rate $\dot{\gamma}_i$, and melt viscosity η_i,, expressed in Equations (4-9), (4-10), and (4-11), can be derived between the event points.

The determined flow front velocity, shear rate, shear stress, and melt viscosity for the step plate are shown in Table 5-7.

Table 5-7: Step plate machine-independent event vector component

	v_i [mm/s]	ΔP_i [MPa]	τ_i [kPa]	$\dot{\gamma}_i$ [1/s]	η_i [Pas]
$E_{mach\ 1/2}$	68.4	1.7	47	79.2	457
$E_{mach\ 2/3}$	66.0	0.5	303	76.4	3061
$E_{mach\ 3/4}$	118.4	7.3	199	274.2	560

5.4 Discussion and Evaluation

For the visualisation of the melt front, the filling pattern that is originated through the CAE simulation software is successively set to the event points assigned to each other. Fig. 5-21 shows the precise melt front position at which the form part-specific event $E_{sim\ 0}$, is assigned to the real (measured) event $E_{mach\ 1}$. The visualisation is achieved by setting the filling pattern to the virtual event time $t_{sim\ 0}$ = 0.173 s (a component of the virtual event vector). Through the assignment of the events, the virtual event time corresponds to the machine time $t_{mach\ 1}$ = 1.190 s (a component of the real event vector). As Fig. 5-21 shows, the melt front at this particular event has already passed through the sprue bar, hit the upper front plate of the step plate cavity, and been deflected by 90°, while the screw of the injection moulder is at the position of $s_{mach\ 1}$ = 25.3 mm.

The next event $E_{mach\ 2}$ occurs at machine time $t_{mach\ 2}$ = 2.250 s when the melt front 'experiences' the first change in the cross-sectional area of the flow channel. This can be visualised by setting the filling pattern to the virtual event time $t_{sim\ 1}$ = 1.270 s, as Fig. 5-22 shows. At this event, the screw is at position $s_{mach\ 2}$ = 47.8 mm.

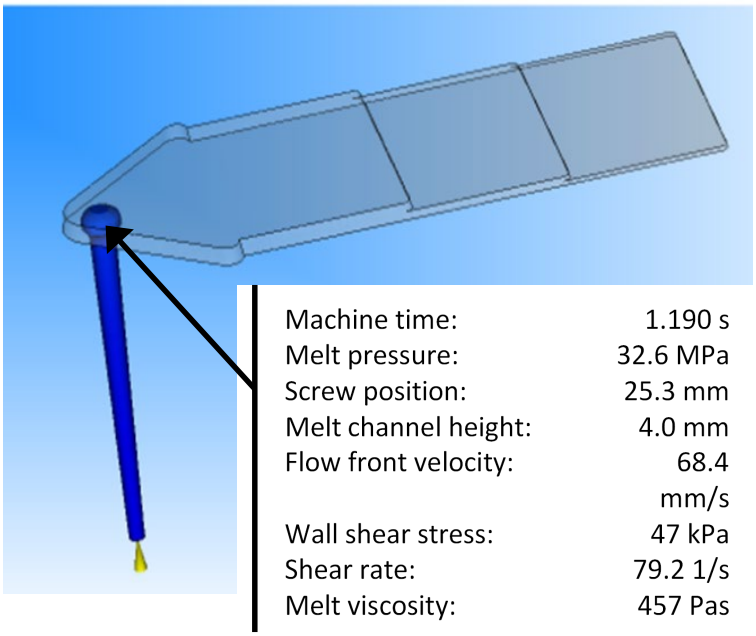

Fig. 5-21: Simulation result of the flow pattern of the step plate at event $E_{mach\ 1}$

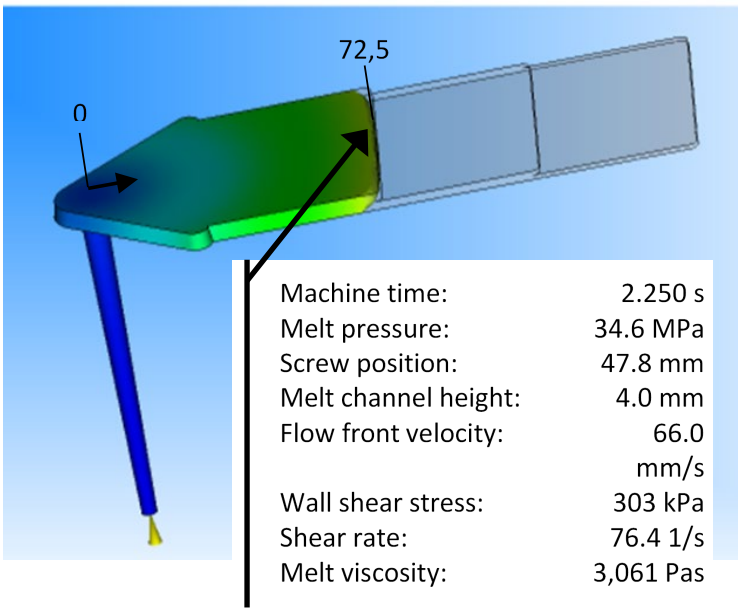

Fig. 5-22: Simulation result of the flow pattern of the step plate at event $E_{mach\ 2}$

After passing through the cross-sectional change, the melt front is fully re-developed. This situation is shown in Fig. 5-23 and occurs at machine time of 2.300 s and a screw position of 48.8 mm. A final event occurs at 2.610 s, when the melt front passes the second change in the cross section towards the flow

direction. In this case, the screw of the injection unit is at position 55.4 mm, as shown in Fig. 5-24.

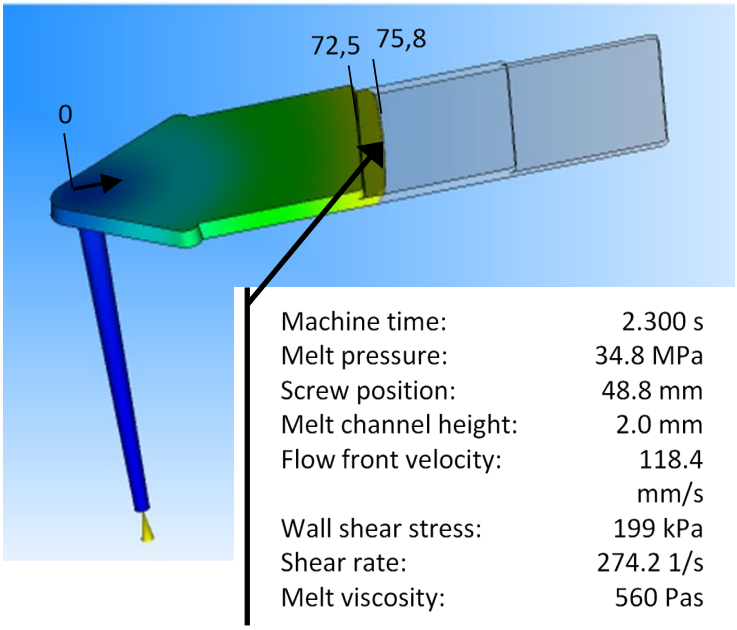

Fig. 5-23: Simulation result of the flow pattern of the step plate at event $E_{mach\ 3}$

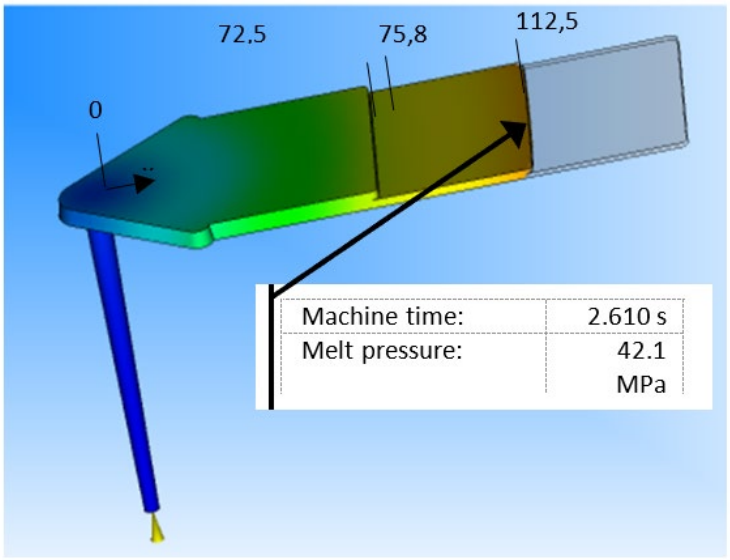

Fig. 5-24: Simulation result of the flow pattern of the step plate at event $E_{mach\ 4}$

Even though in the idealised one-dimensional case, the flow of the melt front progresses proportionally to the injected volume and is therefore easy to predict, the experiments of the one-dimensional case provide important information for

the theory upon which the new proposed method is based. The visualisation of the filling pattern at the event sites where simulated virtual events and measured real events are superimposed clearly shows how precisely the new method works in the one-dimensional case. At all event sites where events are superimposed, the filling patterns regularly show flow front locations where events are expected. The first event identified by the visualisation of the flow pattern is the 90° deflection of the melt front, which occurs after flowing through the sprue bar and hitting the upper front plate of the cavity. The subsequent three events are clearly related to the cross-sectional changes in the geometry of the flow channel. In other words, at all four event locations where virtual and real events are assigned, typical geometry changes occur in the flow channel. According to the theory on which the new method is based, this is predicted. The fact that the filling patterns show situations at all four event sites that plausibly undergo a change in pressure gradient due to changes in the geometry of the flow channel proves the relationship between virtual and real events; thus, the relationship between screw position and flow front location has been successfully established. However, if the relationship between screw position and flow front location is successfully established, evidence is provided that machine-independent parameters, such as flow front velocity, wall shear stress, shear rate, and melt viscosity, can be determined from the components of the virtual and real event vectors, as demonstrated in Section 5.3.5.

5.5 Chapter Summary

In this chapter, the method proposed in Chapter 4 has been validated for the one-dimensional filling process. For this purpose, comparative real and simulated experiments have been applied to the step plate, a form part model that represents an idealised one-dimensional flow front course. For the validation, pressure signals have been measured in an injection moulding process, numerical calculations (simulations) performed, and pressure graphs further analysed to identify event sites, match event patterns, and assign events.

The results from the experimental validation of the one-dimensional case demonstrate the following:

1. In both the real injection moulding process and the simulated models of the injection process, singular events exist. These events can reliably be identified by analysing the differentiated pressure graphs and applying the peak/flank analysis.

2. Singular events occur in the form of event groups. The sequence of all events from both the real injection moulding process and the simulated models of the injection process can be analysed to identify patterns.

3. The results from the experiments for the one-dimensional form part model show that the form part-specific event pattern comprises four virtual events, and the real event pattern comprises six real events.

4. The matching of the patterns and the assignment of the events ensues by means of a transformation as well as a displacement of the events.

5. For one-dimensional form part model, the algorithm determines the best matching of the patterns at a stretching factor of f_k = 0.97 and a displacement of j_{min} = 1.

6. Through matching the patterns, four virtual events can be assigned to four real events.

7. The assignment allows the real event vectors to be expanded by components of the assigned virtual event vectors (i.e., the positions of all nodes along the melt front lines).

8. Through assigning virtual and real events, a relationship between the flow front position of the melt and the screw position of the injection moulding machine can be established.

9. The relationship of flow front position and screw position can be proven by visualising the filling pattern at the event sites where simulated virtual

events and measured events are superimposed. At these particular event sites, the filling patterns of the one-dimensional form part model show flow front locations where events can be expected.

10. Through knowledge of the relationships between the melt front locations, injection time, and geometry of the form part, machine-independent parameters, such as melt front velocity, wall stress, shear rate, and melt viscosity, can be determined.

From the experimental validation, evidence is provided that the assumptions in Chapter 3 for the one-dimensional case are correct and the new method proposed in Chapter 4 successfully establishes a relationship between the flow front location of the melt and the screw position of the injection moulding machine. For the one-dimensional case, the method is effective for determining flow front position and the resulting velocity on the entire flow path. The results provide understanding and knowledge that can be used for the determination of the multidimensional flow front course. If the proposed method proves successful in the general case of multidimensional mould filling (Chapter 6), this will show that the new method is suitable for real practical applications in injection moulding and that it thus holds great potential for future machine control strategies based on machine-independent parameters.

6 APPLICATION OF MULTIDIMENSIONAL FILLING

6.1 Introduction

In the previous chapter, the results of the simulation analysis and experimental evaluation show that for the application of one-dimensional filling, the proposed method is effective for determining flow front position and the resulting velocity on the entire flow path. To further demonstrate and validate the new method proposed in Chapter 4, the case of multidimensional filling is selected. For this validation, the process steps presented in Section 4.7 are applied to stack box: a symmetrical box that is front-centrally injected with one recessed side and nearly constant wall thickness over the flow path. The stack box represents the multidimensional flow course in which the preferential direction of the melt depends on time and place.

In contrast to the one-dimensional case, the application of multidimensional filling places much higher demands on the new proposed method, and thus the results from experimental validation can provide important information about its suitability for applications under realistic real conditions. As in the one-dimensional case, for validation, comparative real and simulated experiments are performed to understand whether it is possible to map the simulated moulding process to the real one.

If the assumptions made for the multidimensional case (Sections 3.2.3 and 3.3) are correct, the form part-specific and real event patterns can be identified and matched by transformation within a specified error bound. If the pattern can be matched and the relationship between the assigned events proven, it can further be proven that the new proposed method is valid and can be used to establish a relationship between the flow front position of the melt and the screw position of the injection moulder for cases other than the one-dimensional one.

6.2 Multidimensional Filling Models

The stack box is a symmetrical form part with one recessed side and an almost constant wall thickness of

$$h = 1.5\ mm \tag{6-1}$$

over the flow path, as shown in Fig. 6-1. The base area of the stack box is 160 x 75 mm^2.

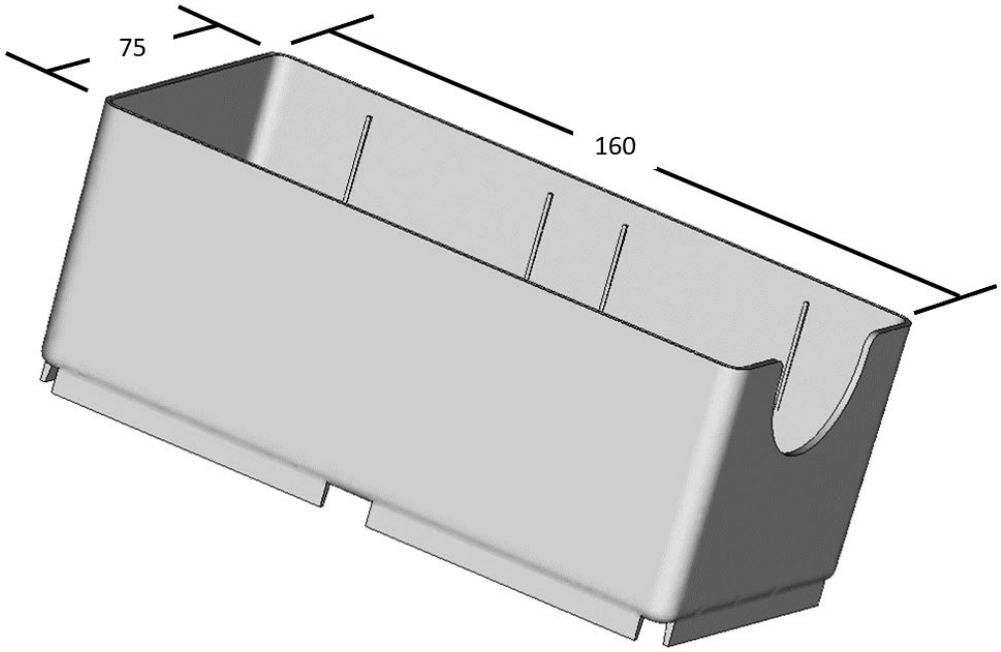

Fig. 6-1: Stack box

The stack box represents the multidimensional flow course. Due to its symmetrical structure and uniform wall thickness, it poses a challenge in analysing patterns and assigning events to the method proposed in Chapter 4. Unlike the step plate, where the flow channel cross section changes several times, no apparent event sites can be observed. After injecting the molten plastic from the machine nozzle into the sprue bar, the plastic melt front passes the centrally located gate and subsequently spreads in its preferential direction. Due to the almost uniform wall thickness, the molten plastic undergoes only small pressure changes along the

entire flow path. Only at the recess placed on one side of the form part is the melt front prevented from travelling freely on its flow path. Overall, a relatively small number of significant events are expected due to the stack box geometry.

An additional challenge is that the cold runner system of the front-centrally injected form part is deliberately excluded from the filling simulation. As a result, the pressure signal determined by simulation does not start to rise until the flow front has passed the centrally located gate (Fig. 6-2). In contrast, the measured pressure signal of the sensor located between the injection unit and the nozzle rises with the start of injection. Thus, the simulated pressure loss occurs in a smaller time range than the measured pressure loss during real injection. However, due to functionalities such as transformation and displacement, the matching algorithm presented in Section 4.8 should compensate for the varying time ranges in the pressure graphs and match event patterns (even patterns of different sizes) reliably.

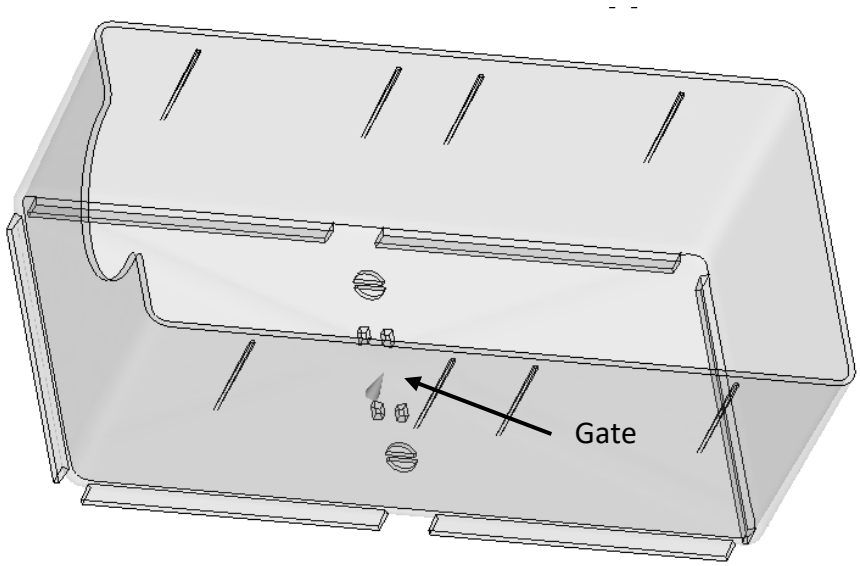

Fig. 6-2: Front-centrally located stack box gate

6.3 Experimental Validation

6.3.1 Numerical Model

As in the one-dimensional case study, Moldflow was used to perform the simulation to determine melt flow pattern, as well as a simulated pressure curve. To execute the simulation, part geometry was imported as a step file into the simulation software. Thereafter, the mesh was generated as a solid 3D model, and mesh elements with unsuitable aspect ratios were manually adjusted.

To attain precise results, the element size of 1.5 mm was chosen, which generates a solid 3D mesh with four layers, resulting in a total number of 662,399 elements. Thus, for the stack box, the calculated flow through time per element at an injection time of 3.2 s (corresponding to a volume flow of 25 cm^3/s, with which the real injection moulding test was conducted), with 98% filling, falls below the signal resolution of the pressure sensor of 2 ms.

The mould filling is simulated with a mould surface temperature of T_{wz} = 45°C, a melt temperature of T_m = 248°C, and a volumetric flow rate of $\dot{V}$ = 25 cm^3/s. Under these boundary conditions, the real injection moulding tests were conducted, and (as further described in Section 6.3.2) the chosen parameter settings led to high quality moulded parts free of surface defects. The switchover from the filling to holding pressure phase was performed at 98% of the volumetric filling. The selected resin for the simulation—an ABS polymer, type Terluran GP-22 from BASF—is identical with the resin used for the real injection moulding test. The material specification is shown in Fig. 5-2. Viscosity dependence is expressed through the Williams-Landel-Ferry (Agassant et al., 2017) cross model in Equation (2-5), and the required resin properties are obtained using the simulation software's database.

The form part-specific pressure curve determined by the simulation is shown in Fig. 6-3. Without the runner system included in the simulation, the curve shows the simulated pressure loss p_{sim}, of the molten plastic at the gate location. The simulated injection time, t_{sim}, starts when the melt passes the gate and ends with

the volumetric filling of the form part at 98% volumetric filling.

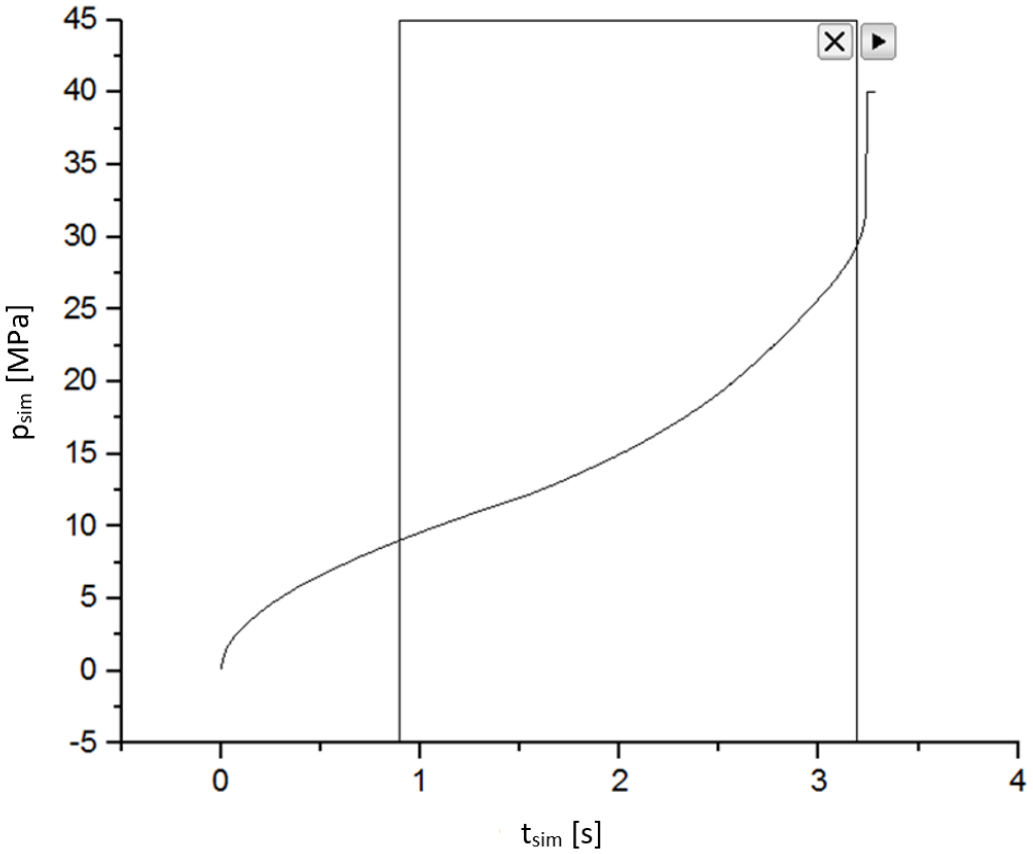

Fig. 6-3: Stack box form part-specific pressure curve

6.3.1.1 Model Validation

All numerical calculations converge; through changing the default setting of the simulation software (as described in Section 6.3.1.1) to a filling volume per time step of 0.1% and to an iteration limit value of 2,000, the Moldflow solver determines the pressure curve with a resolution of 1,050 points. With this resolution, the analysis of the differentiated form part-specific pressure curves is reliably possible; however, against the initial assumption that the resolution of the computed pressure curve depends only on element size and volume flow, the maximum resolution of 1,050 points cannot be exceeded with the existing solver.

Table 6-1 shows the dependency of volume flow and injection time and the resulting resolution of the simulated pressure curve for a range of injection times between 1.1 and 8.5 s. In the case of the stack box, the resolution reaches and surpasses the signal resolution of the pressure sensor of 2 10^{-3} s at and above a volume flow of 40 cm^3/s, which corresponds to a simulated injection time of 2.0 s (presented in red type).

Table 6-1: Stack box resolution of form part-specific pressure curve

$\dot{V}$ $[cm^3/s]$	10	15	**25**	30	**40**	50	75
t_{sim} *[s]*	8.5	5.5	**3.2**	2.7	**2.0**	1.6	1.1
Resolution [s]	0.008	0.005	**0.003**	0.003	**0.002**	0.002	0.001

Since the maximum resolution of 1,050 data points cannot be exceeded, the resolution of the simulated pressure curve at an injection speed of 3.2 s (volume flow of 25 cm^3/s), which corresponds to the volume flow at which the real injection moulding tests occurred, is 3 ms and is thus below the resolution of the measured pressure curve, as shown in Table 6.1 (presented in green). However, even with the lower resolution of 3 ms, Section 6.3.3 shows that the analysis of the differentiated form part-specific pressure curves is reliably possible.

6.3.2 Experimental Setup

The injection moulding tests were conducted on a Battenfeld HM 800 machine with a closed loop-controlled injection unit and a 30 cm screw diameter. Fig. 6-4 shows the injection moulded test part of the step plate. As Table 6-2 demonstrates, three distinct test cases with different volume flows were conducted and recorded. The number of 100 specimens per case ensures that process parameters can be stabilised.

Test case (2.1) was selected for further analysis. In this case, the volume flow is 25 cm^3/s, melt temperature is 248°C, and mould surface temperature is 45°C. At these conditions, the parameter setting led to high quality moulded parts free of surface defects. Compared with the other two test cases, the surface quality of the parts were rated as subjectively better.

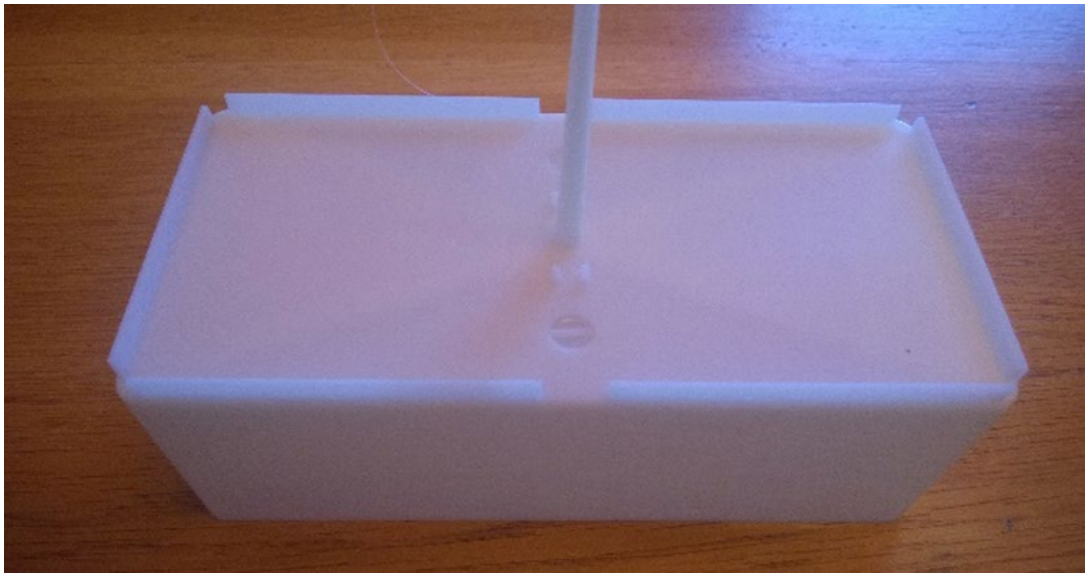

Fig. 6-4: Injection moulded test sample of the stack box

The test setup is shown in Fig. 5-8. As illustrated in Fig. 5-10, the data acquisition was conducted via a PC connected to both the machine control (MC) and a pressure sensor located in the machine nozzle. As in the one-dimensional case study, the melt pressure during the filling phase was measured using a single pressure sensor with a resolution of 2 ms per reading. The Dynisco MDT465FXL pressure sensor has a measuring range of 0–200 MPa and is placed in a mounting ring that is located between the machine nozzle and injection unit (Fig. 5-11). Thus, the melt pressure is acquired directly in front of the screw of the injection unit. The sensor specifications can be found in Table 5-3. The acquired data are formatted as an ASCII file and transferred to Origin Pro for further analysis.

The results of the injection moulding test are shown in the graph in Fig. 6-5. The curve represents the measured pressure loss, p_{mach}, at the location of the machine

nozzle during filling phase of the moulding cycle. The resolution of the graph is 2 ms. The yellow highlighted area marks the actual filling process. Only this section of the measured signal is used in further analysis.

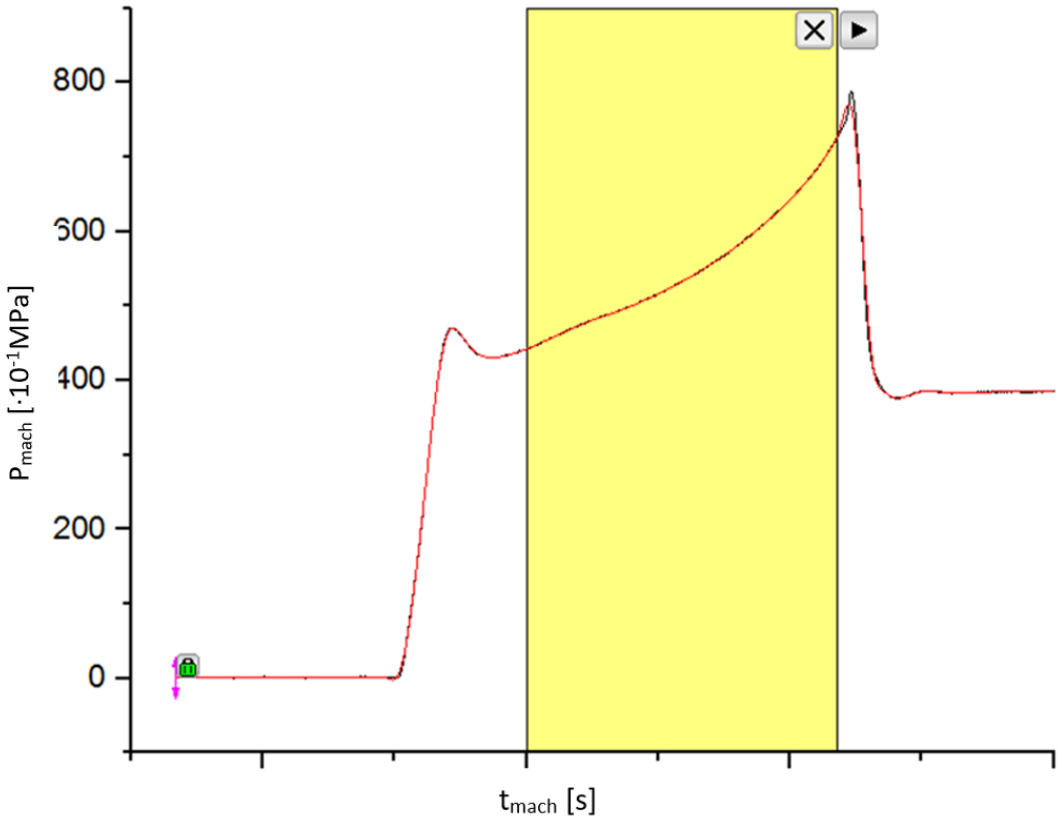

Fig. 6-5: Stack box melt pressure curve

Table 6-2: Test report for stack box injection moulding

	Test sample production		**Sample**	**Stack box**	
			Resin	ABS, BASF – Terluran GP 22	
	Test cases		2.1	2.2	2.3
	Sample number		100	100	100
Velocity	Peripheral speed	[mm/s]	200	200	200
	Screw advance speed	[cm^3/s]	25	10	50
Stroke	Switching point	[cm^3]	10.5	4.5	14.5
	Dosing stroke	[cm^3]	90	90	90
	Melt cushion	[cm^3]	8.5	4.2	8.8
Time	Cycle time	[s]	36.1	41.8	34.3
	Injection time	[s]	3.65	9.24	1.83
	Holding pressure time	[s]	6	6	6
	Cooling time	[s]	20	20	20
	Plasticising time	[s]	15.6	16.0	15.7
Pressure	Injection pressure	[MPa]	88.4	132.6	84.2
	Holding pressure	[MPa]	40.0	40.0	40.0
	Back pressure	[MPa]	6.0	6.0	6.0
Temperature	Feeding zone	[°C]	40	40	40
	Barrel zone 3	[°C]	220	220	220
	Barrel zone 2	[°C]	230	230	230
	Barrel zone 1	[°C]	240	240	240
	Melt sensor	[°C]	248	248	248
	Nozzle	[°C]	230	230	230
	Mould surface moving side	[°C]	45	45	45
	Mould surface fixed side	[°C]	45	45	45
Force	Clamping pressure	[kN]	800	800	800
Drying	Drying time	[h]	4	4	4
	Drying temperature	[°C]	80	80	80
	Remaining moisture	[%]	0.015	0.015	0.015

6.3.3 Identification of Events and Determination of Patterns

The analysis of the differentiated pressure curves determines the event patterns. To create the patterns, individual event locations are isolated from the differentiated pressure curve. For this purpose, the pressure graph, obtained either by simulation or measurement, is initially differentiated using Origin Pro. The differentiated graph is then examined for significant sections where the pressure gradient changes from a relatively less steeply sloped section to a deeply sloped one. As in the one-dimensional case, to obtain consistent results for validation, the examination of the differentiated pressure graphs is performed using the standardised function peak/flank analysis tool in Origin Pro.

6.3.3.1 Form Part-Specific Event Pattern

In the upper section, Fig. 6-6 shows the form part-specific pressure curve in the range relevant for the analysis between the start of the injection time and the switchover to holding pressure. The graph is obtained from the simulation software (Fig. 6-3) and is transferred to the analysis tool. The lower section of the figure shows the differentiated graph, which is examined for virtual events by locating the rise (or fall) time for peaks or flanks.

As described in Section 6.3.3, the evaluation is done by the peak/flank analysis tool in Origin Pro. In the evaluation, the default setting (linear search for slopes, 10% rise time) is used, and virtual event times are determined at 10% of the rise time of the pressure slopes.

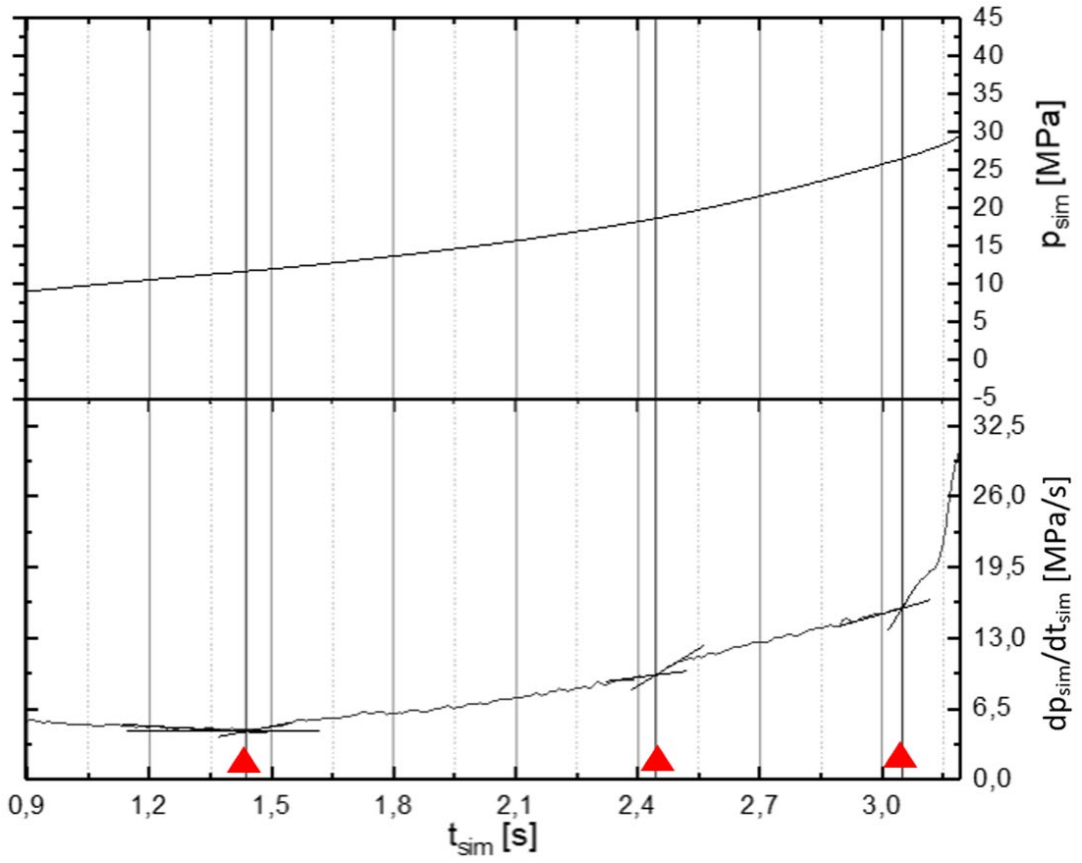

Fig. 6-6: Stack box determination of virtual events

The analysis of the differentiated form part-specific pressure curve determines the form part-specific event pattern (presented in red), consisting of three virtual event vectors. The virtual event vectors have the following components: virtual event time t_{sim}, melt front position x_{sim}, and melt channel geometry h_{sim}. The entire form part-specific event pattern M_s, comprising three virtual event vectors and their components, is shown in Table 6-3.

Table 6-3: Stack box form part-specific event pattern

	t_{sim} [s]	x_{sim} [mm]	h_{sim} [mm]
$E_{sim\ 0}$	1.440	84.0	1.5
$E_{sim\ 1}$	2.440	114.0	1.5
$E_{sim\ 2}$	3.050	145.0	1.5

6.3.3.2 Real Event Pattern

The analysis of the real event pattern is done in a similar way as for the form part-specific event pattern. The pressure graph obtained by measurement is transferred from the data acquisition unit to the analysis tool and is initially differentiated. Real events are determined by examining the differentiated pressure curve for rise (or fall) time for peaks or flanks. In the evaluation, the default setting is used (linear search for slopes, 10% rise time), and real event times are determined at 10% of the rise time of the pressure slopes.

The analysis of the differentiated measured pressure signal (Fig. 6-7) provides the real event pattern consisting of three real event vectors for the step plate. Table 6-4 shows the entire real event pattern M_m comprising three real event vectors with the following components: machine time t_{mach}, melt pressure p_{mach}, and screw position s_{mach}.

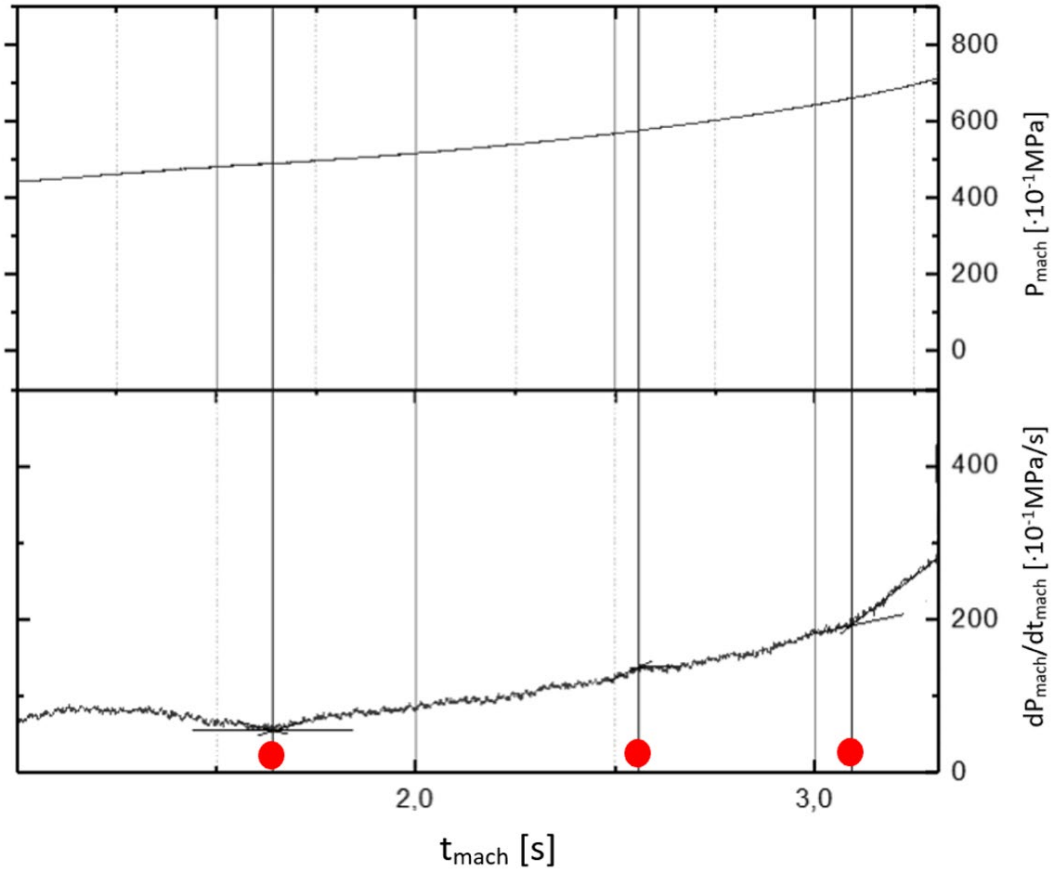

Fig. 6-7: Stack box determination of real events

Table 6-4: Stack box real event pattern

	t_{mach} [s]	P_{mach} [MPa]	S_{mach} [mm]
$E_{mach\ 0}$	1.640	49.0	58.0
$E_{mach\ 1}$	2.560	57.6	90.6
$E_{mach\ 2}$	3.090	66.1	109.3

6.3.4 Pattern Matching and Assignment of Events

In Fig. 6-8, both the real event pattern, M_m (circle symbol), and the form part-specific event pattern, M_s (triangle symbol), are plotted against machine time t_m. Pattern matching and event assignment are performed using the matching algorithm described in Section 4.8, by means of transformation, as well as the displacement of the events.

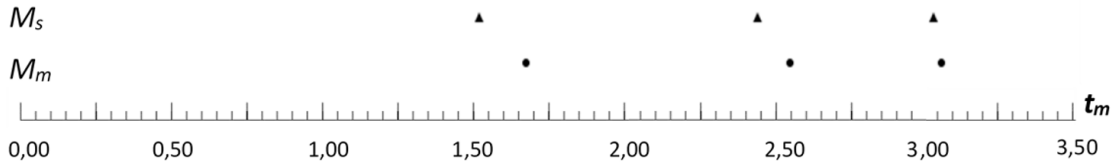

Fig. 6-8: Stack box: Real and form part-specific event pattern

The matching of the patterns and the assignment of the events ensues by means of a transformation as well as a displacement of the events. Because the number of virtual events n corresponds to the number of real events m, the matching algorithm passes one level of iterations with zero displacements and transformations, with an interval of f_{min} = 0.1 to f_{max} = 10, for a scaling increment of Δf = 0.01.

For the stack box, the best matching is obtained with a stretching factor of f_k = 0.90 and a displacement of j_{min} = 0. At this transformation, the patterns deviate a total of S_{min} = 0.001 s.

The transformed form part-specific event pattern, $M_{s,j}$, is shown in Fig. 6-9 after having undergone one higher level iteration at the transformation, k = k_{min}, with the smallest pattern deviation. For pattern $M_{s,j=0}$, the alignment is made to M_m, with the smallest deviation S_{min}.

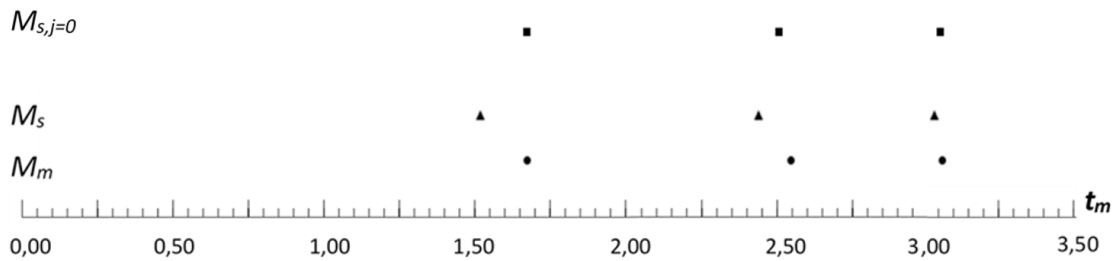

Fig. 6-9: Stack box real and form part-specific event patterns after scaling and displacing

Fig. 6-10 shows the assignment of the virtual and real events from the matched pattern. According to Equation (4-6), and with j_{min} = 0, all three virtual events $E_{sim\ i}$ can be assigned to the three real events $E_{mach\ i+j}$ ($E_{sim\ 0}$ to $E_{mach\ 0}$, $E_{sim\ 1}$ to $E_{mach\ 1}$, $E_{sim\ 2}$ to $E_{mach\ 2}$).

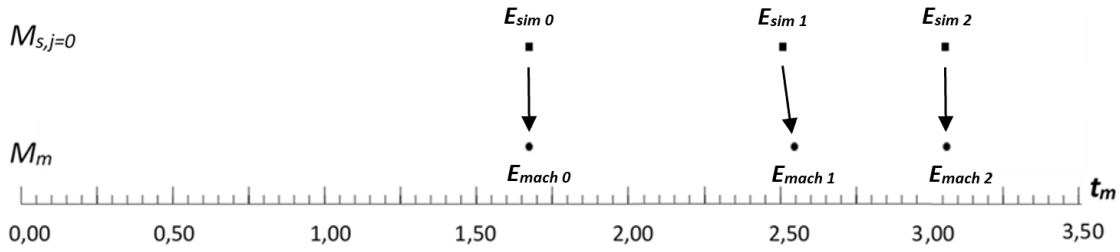

Fig. 6-10: Stack box assigning virtual events and real events

The assignment allows the real event vectors $E_{mach\ i+j}$ to be expanded by the components $x_{sim\ i}$, $y_{sim\ i}$, and $z_{sim\ i}$ (i.e., positions of all nodes along the melt front

lines) of the assigned virtual event vectors $E_{sim\ i}$. Thus, the melt front position is consequently associated with machine time $t_{mach\ i+j}$ and screw position $s_{mach\ i+j}$, according to Equation (4-4).

Table 6-5 shows the three real event vectors $E_{mach\ i+j}$ of the step plate, with $j = 0$, expanded by the component of the assigned virtual event vectors $E_{sim\ i}$.

Table 6-5: Stack box real event vectors expanded by components of the assigned virtual event vector

$E_{mach\ i+j}$	$t_{mach\ i+j}$ [s]	$P_{mach\ i+j}$ [MPa]	$S_{mach\ i+j}$ [mm]	$x_{sim\ i}$ [mm]	$h_{sim\ i}$ [mm]
$E_{mach\ 0}$	1.640	49.0	58.0	84.0	1.5
$E_{mach\ 1}$	2.560	57.6	90.6	114.0	1.5
$E_{mach\ 2}$	3.090	66.1	109.3	145.0	1.5

6.3.5 Determining Machine-Independent Parameters

Flow front velocity can be determined using flow front position. By considering two successive and assigned event vectors $E_{mach\ i+j}$ and $E_{mach\ i+j+1}$, the mean flow front velocity of the melt v_i shown in Equation (4-7), as well as the increase in melt pressure Δp_i shown in Equation (4-8), are calculated between these events. From the calculated flow front velocity and the increase in melt pressure (together with information on the flow channel geometry $h_{sim\ i}$), based on the Hagen-Poiseuille equation, machine-independent parameters such as wall shear stress τ_i, shear rate $\dot{\gamma}_i$, and melt viscosity η_i, expressed in Equations (4-9), (4-10) and (4-11), can be derived between the event points. For the stack box, the determined flow front velocity, shear rate, shear stress, and melt viscosity are shown in Table 6-6.

Table 6-6: Stack box machine-independent components of event vectors

	v_i [mm/s]	ΔP_i [MPa]	τ_i [kPa]	$\dot{\gamma}_i$ [1/s]	η_i [Pas]
$E_{mach\ 0/1}$	32.6	8.6	215	100.7	1,648
$E_{mach\ 1/2}$	58.5	8.5	206	180.6	879

6.4 Discussion and Evaluation

For the visualisation of the melt front, the filling pattern of the stack box is successively set to the assigned event points. Fig. 6-11 shows the arrival of the melt front at event point $E_{mach\ 0}$. Once the base plate of the stack box cavity has been filled through the central gate (located at the middle of the front side), the melt front reaches the base of the downward-pointing bottom rim, at a machine time of 1.640 s. At this time, the screw is at position 58.0 mm, the pressure measured is 49.0 MPa, and flow front velocity is calculated as 32.6 mm/s. The wall shear stress at this section is 215 kPa, the melt viscosity is 1,648 Pas, and the shear rate is 100.7 s^{-1}.

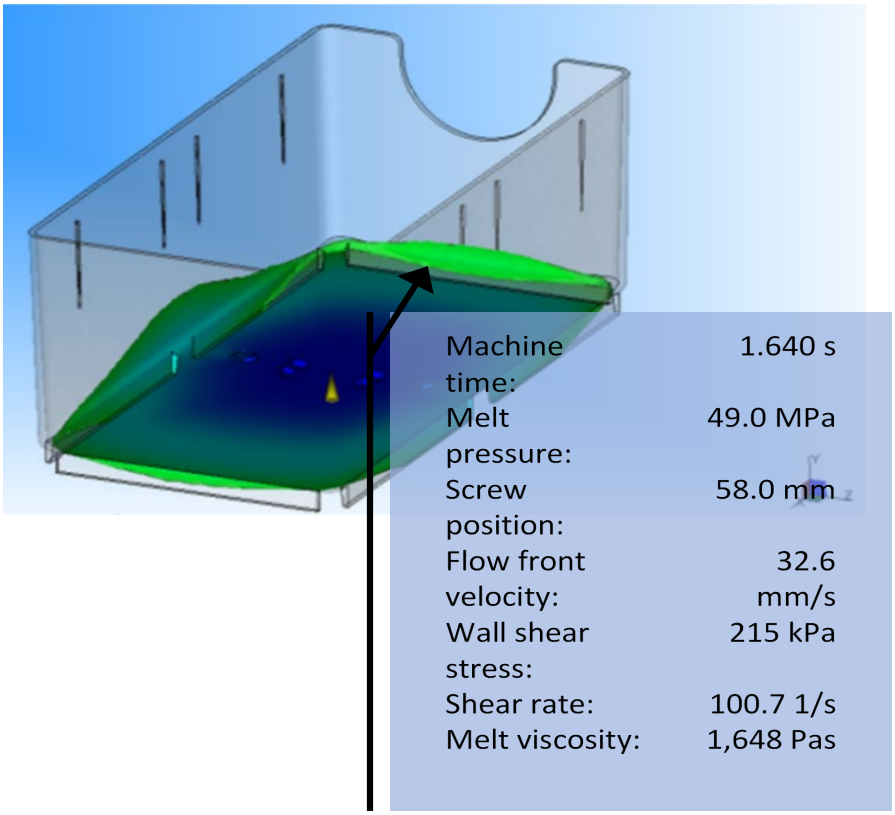

Fig. 6-11: Simulation result of the flow pattern of the stack box at event $E_{mach\,0}$

The next event along the flow path of the melt is at the arrival of the flow front at the recessed side (Fig. 6-12). According to theory, this is where an event point and, thus, a disproportional change in pressure loss are expected, because the recess can be perceived from the perspective of the melt front as a flow obstacle. However, compared with an event occurring at a location where the melt front is, for example, redirected at an angle of 90° or is passing through a sharp cross-sectional change, hitting a semi-circular flow obstacle at a constant flow channel height has a relatively small influence on pressure loss. It is remarkable that despite such a relatively small impact, both the virtual event, E_{sim1}, and the real event, E_{mach1}, can clearly be identified, matched, and assigned and that the relationship between the flow front location and the machine time at 2.56 s (with the screw stroke at 90.6 mm) can be determined.

At the last event, the flow front reaches the end of the flow channel first at the recessed side. As shown in Fig. 6-13, the screw is in position 109.3 mm at an injection time of 3.09 s.

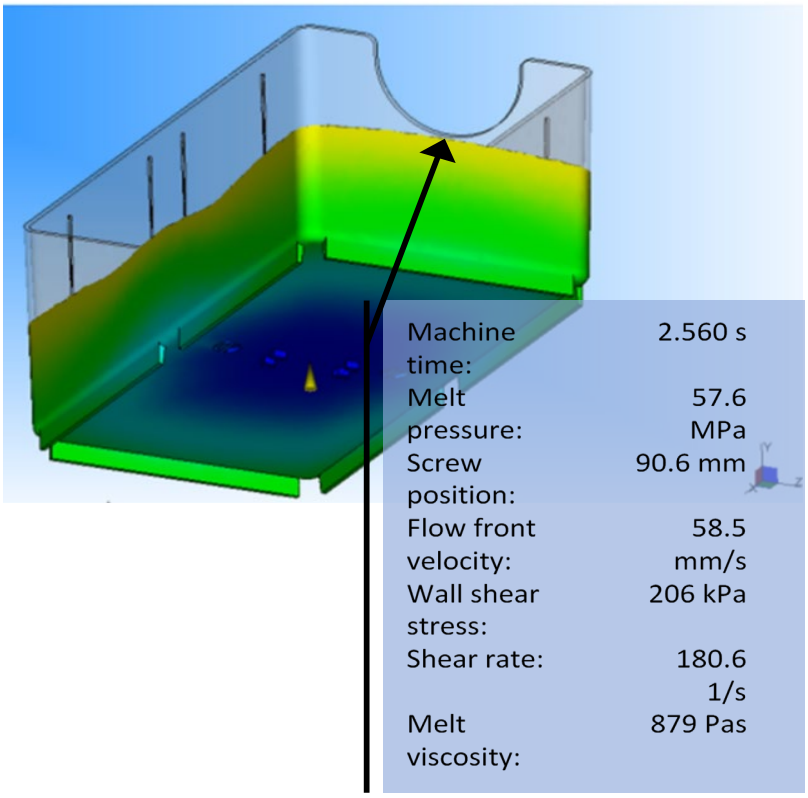

Fig. 6-12: Simulation result of the flow pattern of the stack box at event $E_{mach\ 1}$

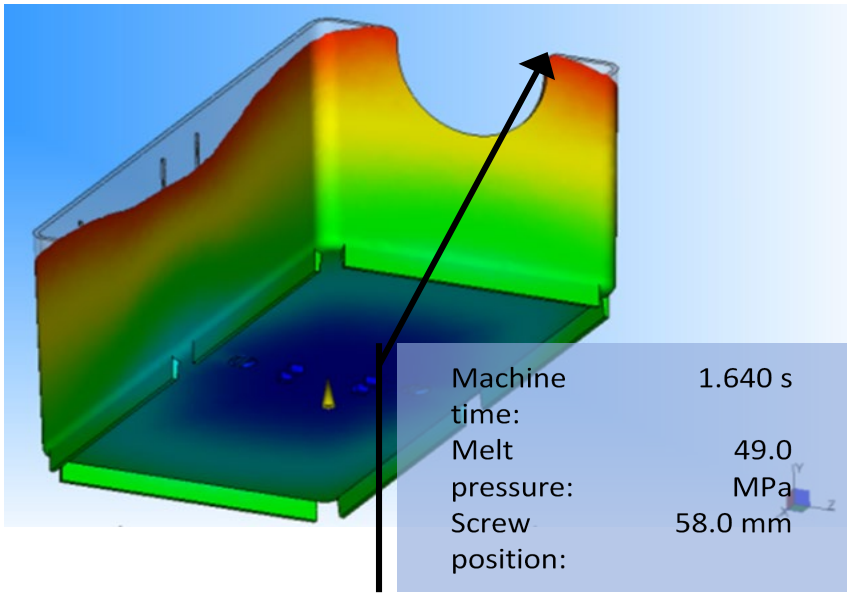

Fig. 6-13: Simulation result of the flow pattern of the stack box at event $E_{mach\ 2}$

Compared to the one-dimensional case, the general case of multidimensional filling is more complex for various reasons; on the one hand, the course of the flow front cannot be predicted as easily as in the one-dimension case. Due to the nonlinear dependencies of viscosity, shear rate, and other thermal and rheological conditions, the course of the flow front depends on location and time. Since the form part is symmetrical and frontally injected, the melt subsequently spreads multidimensionally after passing through the gate. In contrast to the one-dimensional form part model (step plate), which consists of three distinct sections with different wall thicknesses, the stack box has a uniform wall thickness distribution. As a result, potential event locations in the step box appear much less obvious than with the step plate. Furthermore, the simulated model is determined without a gating system. As a result, the pressure in the mould part-specific pressure curve starts to rise only when the simulated melt front passes the gate. In contrast, the measured pressure curve contains more information because it includes the pressure losses that occur when the melt has passed through the sprue bar. Thus, the results of the evaluation of the multidimensional case should be considered against this complexity.

The set of the filling pattern to the first event (Fig. 6-11) shows the arrival of the melt front at the base of the downward-pointing bottom rim, when the base plate of the stack box cavity has been filled through the central gate. The filling pattern then shows that the second event is identified at the arrival of the flow front at the recessed side (Fig. 6-12). Finally, when the flow pattern is set to the third event (Fig. 6-13), the flow front reaches the end of the flow channel at the recessed side of the stack box.

Assuming that the filling pattern is not known in advance, exactly these three events would be predicted by the theory on which the method is based when following the flow channel from the gate to the end from melt front perspective. The evidence that the superimposed events are successfully assigned is provided by the fact that at all three event sites, the filling patterns show situations that plausibly undergo a change in the pressure gradient due to changes in the

geometry of the flow channel. However, if events are successfully assigned, the relationship between screw position and flow front is also successfully established, and machine-independent parameters, such as flow front velocity, wall shear stress, shear rate, and melt viscosity, can be determined from the components of the virtual and real event vectors.

6.5 Chapter Summary

The results of the experimental validation of the multidimensional case show that the method proposed in Chapter 4 is effective for determining the flow front position and resulting flow front velocity of the melt for the entire flow path. It must be noted, that in these experimental studies, no specific measuring devices (sensors) were used within the cavity of the mould for locating the melt front position during the filling phase. The findings suggest that the new method is suitable for real practical applications in injection moulding and thus holds great potential for future machine control strategies based on machine-independent parameters.

In summary, the theoretical analysis and experimental validation of the multidimensional case have proven the following:

1. In both the real injection moulding process and the simulated models of the injection process, singular events exist. These events can be reliably identified by analysing the differentiated pressure graphs and applying the peak/flank analysis function in Origin Pro.

2. Singular events occur in the form of event groups. The sequence of all events from both the real injection moulding process and the simulated models of the injection process can be analysed to identify patterns. For the multidimensional case, the form part-specific event pattern comprises three virtual events, and the real event pattern comprises three real events.

3. The matching of the patterns and the assignment of the events ensues by means of a transformation as well as a displacement of the events. For the stack box, the algorithm determines the best matching of the patterns at a stretching factor of f_k = 0.90 and a displacement of j_{min} = 0.

4. Through matching the patterns, three virtual events can be assigned to three real events, which allows the real event vectors to be expanded by the components of the assigned virtual event vectors (i.e., the positions of all nodes along the melt front lines).

5. Thus, in the multidimensional case, in which the course of the flow front is dependent on location and time, the melt front position is consequently associated with injection time and screw position.

6. The relationship between melt front position and screw position is proven by visualising the filling pattern at the event sites, where simulated virtual events and measured events are superimposed. At these particular event sites, the filling patterns of the step plate show flow front locations where events can be expected.

7. Through knowledge of the relationships between the melt front locations, injection time and geometry of the form part, machine-independent parameters, such as melt front velocity, wall stress, shear rate, and melt viscosity, can be determined.

Since a primary requirement for the application of the proposed method is the matching of the event patterns using a new algorithm comprising functional methods for transforming and matching patterns and pattern fragments (Section 4.8), further investigation of the matching algorithm is conducted in Chapter 7.

7 ANALYSIS AND EVALUATION OF METHODS FOR PATTERN MATCHING

7.1 Introduction

Chapters 5 and 6 demonstrate that the new method proposed in Chapter 4 can be used to determine the flow front position of a melt as a function of the screw position over the entire length of the flow path using only one pressure sensor at the front of the screw. For validation, a relationship between simulated and measured pressure signals is established, events are assigned, and the relationship between assigned events is proven. The results of the experimental evaluations reveal that the method can be used to determine not only the flow front location at different event locations but also parameters such as flow front velocity, melt viscosity, shear rate, and wall shear stress; thus, the method offers potential for advanced process control strategies based on machine-independent parameters.

The previous chapters of this study have focused on designing and developing the new method; this chapter follows up on this by analysing and evaluating the methods for pattern matching. The matching of the form part-specific pattern to a real event pattern represents the actual mapping process and occurs with the aid of a matching algorithm. This chapter assesses matching methods and the question of which requirements the algorithm must meet so that the event locations of the simulated filling process can be reliably assigned to the event locations of the real injection moulding process. Furthermore, this chapter examines the conditions under which the mapping of the simulated injection moulding process to the real injection moulding process can be conducted with the aid of a ‘special’ matching algorithm with linear transformation, even with ‘large’ deviations between the boundary conditions of the simulation and the setting parameters of the machine. For this purpose, comparative real and simulated experiments are defined and conducted. To measure the effect of ‘large’ deviations between boundary conditions and settings, the variation of the independent variables is performed through the variation of boundary conditions such as melt temperature, mould temperature, and volumetric flow rate. The

analysis of the dependent variables either would or would not reveal an effect due to a particular cause on the smallest total deviation of the patterns after transformation.

7.2 Aims and Objectives for the Evaluation of Matching Methods

In Chapters 5 and 6, the patterns for both the one-dimensional and multidimensional cases are determined under conditions where the machine setting and the boundary conditions used in the simulation are identical. In other words, conditions are created where only ‘small’ deviations between the patterns obtained from the simulated and measured pressure curves can be expected. Such small deviations can occur, for example, due to the incorrect calibration of proportional valves or a broken injection unit check ring valve.

As the results from the experiments in Chapters 5 and 6 indicate, the chosen matching method for the validation, with its linear matching algorithm, can match the patterns. The required scale of the transformation for pattern alignment is relatively small, as expected.

This chapter presents further studies that analyse the conditions under which the matching of the patterns can be conducted, even with ‘large’ deviations between the boundary conditions of the simulation and the setting values of the machine. As such, the following questions are posed:

1. What functional requirements must the matching algorithm of the proposed new method meet so the event locations of the simulated filling process can be *reliably* assigned to the event locations of the real injection moulding process (robust matching)?

2. Under what conditions can a matching algorithm with a linear transformation be used to map the simulated injection moulding process to the real injection moulding process, even if there are ‘large’ deviations between the boundary conditions of the simulation and the injection machine settings?

3. What influence does a ‘large’ deviation between the boundary conditions of the simulation and the setting of the injection machine have on the matching of the pattern and the assignment of the event locations?

4. What knowledge can be drawn from this (e.g., for the generation of a matching method with a non-linear transformation)?

Based on theoretical considerations, a requirement profile for the matching method is developed. To measure the effect of ‘large’ deviations between boundary conditions and settings, the variation of the independent variables is performed through the variation of boundary conditions such as melt temperature, mould temperature, and volumetric flow rate. The analysis of the dependent variables using a suitable design of experiments (DoE) either would or would not reveal an effect due to a particular cause on the smallest total deviation S_{min} and the scaling factor f_k. Finally, the assumptions in Section 3.3 are tested. The experiments are conducted for the two different models already known from the experimental validation in Chapters 5 and 6; the step plate for the one-dimensional flow – the findings from this relatively simple case can be used for more complicated multidimensional cases for which the stack box is the model.

7.3 Discussion of the Full Functional Requirements of Pattern Matching Methods

This section describes the development of a requirement profile for a robust matching method as well as a matching algorithm suitable for the proposed new method. The requirement profile provides an answer to the question of why; in the first attempt to design the new method, a ‘special’ matching method with a linear transformation is used and also provides an initial assessment of the linear matching algorithm.

Generally speaking, the method for determining the flow front position is based on the idea of mapping a simulated filling process to a real injection moulding process. The mapping occurs at the event points, which can be isolated both from the simulated and measured pressure curves of the filling process. A number of

virtual singular events or real singular events form either the virtual form part-specific event pattern or the real event pattern, respectively. The matching of a pattern of the simulated filling process to one of the real filling processes represents the actual mapping process.

When developing a requirement profile for a matching method, the first question that arises concerns what makes the method basically suitable. It would be conceivable that *any* matching method that can match patterns is basically suitable. For example, with image recognition software, it is conceivable to plot both patterns on paper, scan them, and then use the software to match the patterns (or parts thereof). Since it cannot be assumed that the patterns look identical or have the same size, the method must have a function for transforming the patterns until they can be matched. To do this, both patterns must follow certain rules (e.g., plotting events over the machine time).

In terms of process, the matching of the patterns is not based on probability, since the total number of patterns is two. There is exactly one form part-specific event pattern and exactly one real event pattern for each matching process. In the matching process, both patterns are aligned by the transformation first and then matched. Even after transformation, a match with a deviation of $S_{min} = 0$ (identical pattern) cannot be expected. The simulated process, from which the form part-specific event pattern is obtained, will never exactly match the real injection process, from which the real event pattern is obtained. As a result, the patterns also differ from each another no matter how the transformation occurs, and the patterns are aligned. The only exception to this is if both patterns consist of exactly two events. In this special case, a match with a deviation of 0 can occur.

The matching algorithm must therefore have a function with a termination or optimisation criterion that considers, for example, terminating at the ‘smallest deviation of the patterns’ or ‘the smallest deviation of certain (weighted) events’.

7.3.1 Pattern Size, Number of Events, and Interference

The real event pattern is obtained using a pressure sensor from the measured pressure curve of the injection moulding (filling) process. The form part-specific event pattern is obtained by simulation from the calculated pressure curve of a simulated filling process. Depending on the location and placement of the pressure sensor (e.g., in front of the screw or along the flow path) and the scope of the simulation (e.g., a filling study with or without the gating system), both pressure curves 'might see' a different part or section of the total filling pressure and thus a different number of events.

In the real injection moulding process, the existence of 'interference' in the measured pressure curve is conceivable. Such interferences can have 'external causes', such as damage to the cavity along the flow path. In the worst case, interferences can generate events in the real pressure curve that have no equivalent in the simulated pressure curve.

Therefore, in practice, it can be assumed that both patterns have a different number of events (i.e., a different size). Matching in the sense of the new method does not necessarily mean the assignment of patterns that consist entirely of all identified real and virtual events. It is much more likely that a subset of events (parts or fragments of the patterns) is matched, and interferences are eliminated (i.e., filtered).

7.3.2 Defining Boundary Conditions

For solving the differential equations of injection moulding-related flow problems, the flow and filling analysis performed through simulation requires injection moulding-specific boundary conditions (Kennedy & Zheng, 2013). The boundary conditions must be described upon several surfaces: the surface through which the melt enters the cavity (gate surface); the top, bottom, and edge of the mould surfaces; the surfaces that define any inserts or pockets of the mould; and finally, the free surface that defines the melt front of the injected polymer. Except for the

free surface of the melt front, all surfaces are determined using the geometric data of the form part and its mould.

Flow analysis software usually employs specific flow rates in the filling phase; these are obtained by either dividing the volume to be filled by the user-specified filling time or, in advanced simulation software systems, by optimising the flow rate based on pressure losses and temperature changes. If constraints exist, for example, due to the maximum shear rate or any other material properties that should not be exceeded, further adjustments of the flow rate can be determined.

To conduct the simulation of the simulated melt pressure curve, at least the following data are required: part geometry, material parameter (material specifications), volume flow, melt temperature, and mould surface temperature. These are the 'boundary conditions' of the simulation. Since the form part-specific event pattern is obtained from the simulation, the pattern 'carries' these boundary conditions in itself.

7.3.3 Setting the Injection Machine

The setting of the injection moulding machine (the machine parameter setup) determines, among other things, the physical conditions that arise during the mould filling process and the subsequent holding pressure phase. The setup consists of numerous parameters (Osswald et al., 2008; Stitz & Keller, 2001) that have either direct, indirect, or no influence on (a) the volume flow, (b) the melt temperature, and (c) the mould surface temperature—i.e., the values that also serve as boundary conditions for the simulation.

For example, the machine operator can set the parameter of melt temperature directly on the machine control and thus influence the temperature of the molten resin directly. However, if they change the parameter of 'back pressure of the screw' in the machine setting, this operation also leads to a change in the melt temperature. In this case, the melt temperature is influenced indirectly.

Because the real event pattern is originated from the measured melt pressure curve in a real injection moulding process, the pattern ‘carries’ the setting of the injection moulding machine for the respective injection moulding process that was measured in itself.

If the boundary conditions of the simulation precisely match the conditions (setup) of the real injection moulding, the form part-specific event pattern should not deviate (in theory) from the real event pattern. Of course, it must be considered that the simulation can never achieve a 100% representation of the real event pattern.

7.3.4 Discussion of the Influence of Process Shifting

Factors such as the shot-to-shot repeatability of the machine can have a direct or indirect influence on physical values that are also considered as boundary conditions for the numerical calculation or simulation. This can result in deviations between the patterns.

Recurring injection moulding cycles are characterised in such a way that the physical conditions are shifting continuously during the filling process. This may occur, for example, because of an adjusted setting of the machine between cycles or an automatic control intervention by the closed-loop controller of the injection machine for disturbance variables. For the pattern matching, this circumstance must be considered. Therefore, the following two cases must be distinguished:

1. The changes in the conditions of two successive injection moulding cycles have no influence on the physical values that serve as boundary conditions for the simulation. In this case, no change in the deviation between the form part-specific pattern and the real event pattern is expected.

2. The change in the conditions of two successive injection moulding cycles leads directly or indirectly to changes in one or more physical parameters, which are also considered as boundary conditions for the numerical

calculation. In this case, the deviation between the form part-specific pattern and the real event pattern also changes.

7.3.5 Volume Flow

The form part-specific and real event patterns consist of a specific number of virtual or real events. Each event occurs at a specific time: a ‘virtual injection time’ in the case of the form part-specific event pattern or a ‘machine time’ in the case of the real event pattern. In practice, the virtual injection time and the machine time have no absolute time reference as both clocks can start and stop differently. The start time for the form part-specific event pattern, for example, can be defined as the time when the melt flow front enters the sprue channel or passes the gate of the cavity, depending on the scope of the simulation. The count of the machine time, for example, could start for each cycle with the start of the injection phase.

Accordingly, a form part-specific event pattern has an *absolute* deviation from the real event pattern, even if the machine setting and boundary conditions are identical. The matching algorithm must therefore have a function to calibrate the absolute time references.

In addition, any direct or indirect change in the parameter volume flow in the real injection moulding process leads to an immediate change in all *relative* time references of the event pattern. The matching algorithm must therefore have a function to transform the relative time references of the pattern (transformation of the pattern) to align the patterns.

7.3.6 Profile Requirements for the Matching Method

The matching method is based and depends on a suitable algorithm for matching form part-specific and real event patterns and assigning virtual and real events. In summary, a suitable algorithm must meet the following requirement profile:

1. Fragments of event patterns can be matched, and subsets of events can be assigned to each other;

2. An absolute time reference between the form part-specific and real event patterns or fragments thereof can be established;

3. Events caused by interferences can be filtered and/or eliminated;

4. Relative time relations between events of an event pattern can be transformed;

5. The algorithm has a function with a criterion for a (reproducible) termination; and

6. As long as the simulation or the generation of the form part-specific event pattern does not occur in real time in an injection moulding cycle, the method must be able to continuously assign form part-specific event patterns to constantly change real event patterns between cycles; the matching process must be 'robust', meaning that even if there are clear deviations between the real injection moulding process and the simulated filling process, events can be reliably assigned to each other.

7.3.7 Development and Validation of the Matching Method

To investigate how well real and virtual events correspond, event patterns must be matched. A prerequisite for this is the existence of a first (i.e., initial) matching procedure. Only after successfully matching the patterns and assigning events can the quality and performance of the matching algorithm be assessed. This approach is illustrated in Fig. 7-1.

Therefore, qualitative assessment is initially used. After matching the patterns and aligning the events, the filling pattern (obtained from the simulation) is successively set to the event points assigned to each other. If the filling pattern reveals a melt front at a significant event location where events could be expected

(e.g., at tapering, enlargement, edges, corners, and flow obstacles), then the matching has been successful.

In the quantitative assessment, however, certain parameters such as the transformation or stretching factor f_k or the smallest overall deviation of the pattern S_{min} can be analysed. The findings from this analysis can be used to improve the matching process in such a manner that, for example, the transformation of the pattern is optimised by an adapted algorithm or the patterns are 'better' matched (i.e., more robust or with less deviation) by means of a modified termination criterion.

A matching procedure would be generic if its transformation algorithm was able to consider the influence of changed boundary conditions or changed parameter settings. With the help of a generic matching method, a single form part-specific event pattern could be permanently assigned to a real event pattern, changing from injection cycle to injection cycle. This would occur regardless of how the physical injection moulding process is set or how much the boundary conditions used for the simulation deviate from the machine setting.

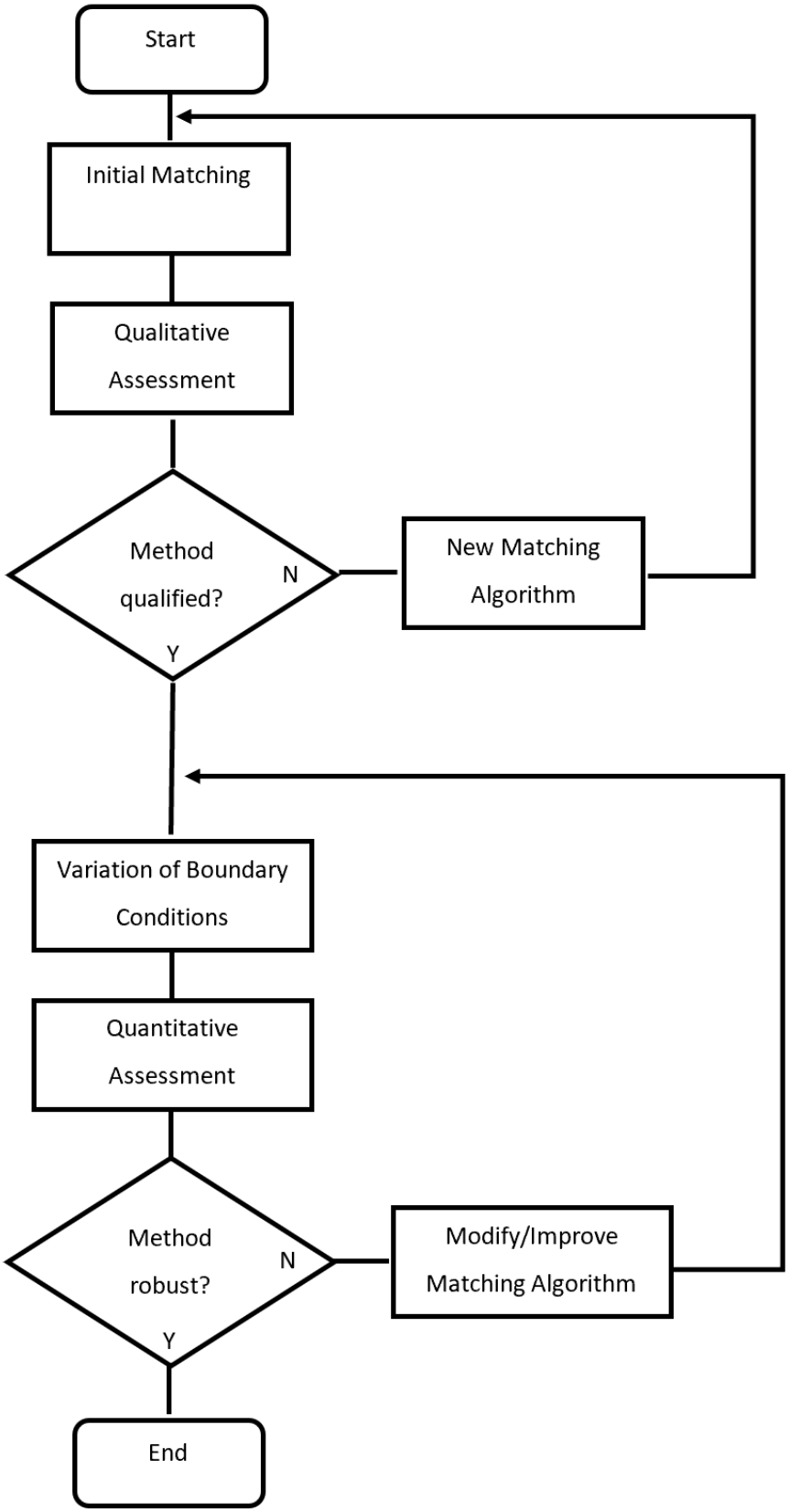

Fig. 7-1: Flowchart of the procedure for developing the matching method

7.3.8 Matching Method with Linear Transformation

The matching algorithm described in Section 4.8, with iteration loops and a linear transformation, is used in the matching method for the experiments in Chapters 5 and 6. In the inner loop of the algorithm, the form part-specific event pattern is transformed. The scaling factor f_k passes through a number of transformations. For each transformation k a new pattern is calculated from the form part-specific event pattern, and the attempt is made to align it with the real event pattern. The deviations are subsequently determined between the previous calculated time intervals in the scaled form part-specific event pattern and the real event pattern. For the absolute value of the sum of all individual deviations of the scaled pattern with the measured events, the total deviation for the respective scaling iteration is calculated. The smallest (pattern) deviation of all transformations is then searched for.

In case the number of events of the virtual event pattern is not equal to the number of events of the real event pattern, each virtual event is displaced in a further iteration loop, and then all transformations are performed to determine at which displacement the best matching is achieved. The smallest (pattern) deviation of all displacements S_{min} is sought.

7.3.9 Characteristics of the Linear Transformation

A linear transformation is ideal for the initial matching attempt. In compliance with the continuity equation for incompressible fluids, and on a one-dimensional flow path, the idea arises that the mould filling is only linearly influenced by the volume flow, not by the other boundary conditions (Section 3.2.2). For a first matching, patterns are determined under conditions where the machine setting and the boundary conditions used in the simulation are identical. As in theory, the matching of the patterns and the assignment of the events occurs with only extremely small transformations, and the linear matching algorithm is able to robustly match the patterns. The linear approach also offers a ‘first good start’

because it is programmable and therefore feasible (i.e., it takes a relatively short time) to implement into the method.

Typically, with complex geometries on multidimensional flow paths, the form part fills over three spatial directions, depending on location and time. The assumption is that the event times are non-linearly influenced by the variation in the boundary conditions (Section 3.2.3). However, such considerations are not relevant for the development of a first matching procedure due to the lack of knowledge of all dependent and independent variables. Only after an initial matching—and under the variation of boundary conditions—can a quantitative assessment lead to deeper understanding and provide further knowledge, which can be used to optimise the initial matching process or to develop a completely new one (Fig. 7-1).

7.4 Experimental Investigation of Pattern Matching Methods

The results from the experimental validation in Chapters 5 and 6 reveal that the method presented in Chapter 4 is effective at determining a relationship between the melt flow front location and the screw position of the injection moulding machine. For this purpose, the patterns for both one-dimensional and multidimensional cases are determined under conditions where the machine setting and the boundary conditions used in the simulation were identical. The results from the validation suggest that the chosen matching method, with its linear matching algorithm, can match the patterns. The required scale of the transformation for pattern alignment is relatively small, as expected.

However, it cannot be assumed in practical application that the conditions of the real injection moulding process exactly match the boundary conditions used in the simulation. As discussed in Section 7.3, this can result in event patterns differing in size, number of event locations, and event times.

In this section, for the analysis and evaluation of pattern matching methods, comparative real and simulated experiments are defined and conducted. To

measure the effect of ‘large’ deviation between boundary conditions and settings, the variation of the independent variables is performed by the variation of boundary conditions in the simulations, such as melt temperature, mould temperature, and volumetric flow rate. Thus, a number of event patterns are determined by simulation. These form part-specific event patterns are successively matched with the real event patterns obtained in injection moulding tests for the respective one-dimensional or multidimensional model. Matching is performed by using the matching method presented in Section 4.8 with its linear matching algorithm. The influences of the deviations of the event patterns on the matching process are investigated. The analysis of the dependent variables either would or would not reveal an effect due to a particular cause on the smallest total deviation S_{min} and the scaling factor f_k. According to the assumptions in Sections 3.2.2 and 3.2.3, the variations of the volume flow rate should have linear effects on the scaling factor f_k in the one-dimensional case, whereas they should cause nonlinear effects on the scaling factor in the multidimensional case. According to theory, the variation of melt and mould temperature should have no influence on the scaling factor in the one-dimensional case, but it should have an influence in the multidimensional case. The theory also predicts that the smallest total deviations S_{min} should increase with the strength of the deviation in the boundary conditions and the machine settings.

The tests are conducted for the two different models already known from the experimental validation in Chapters 5 and 6: the step plate for the one-dimensional flow and the stack box for the multidimensional flow.

7.4.1 Simulation under the Variation of Boundary Conditions

The two form part geometries with different characteristics in terms of flow path are used to validate different mapping methods, which are described in the following two subsections.

7.4.1.1 Application of One-Dimensional Filling

The step plate, as illustrated in Fig. 7-2 (duplicated from Section 5.2 for clarity when reading this section), comprises a sprue bar, lateral dove tail gate, and three-step varying wall thickness over the flow path; the injection occurs through a sprue bar, and the melt is distributed over a dovetail gate located on the largest cross section of the step plate (Fig. 5-4). Due to its rheologically balanced runner system, the flow front develops uniformly at the gate and runs almost perpendicularly to its main axis direction.

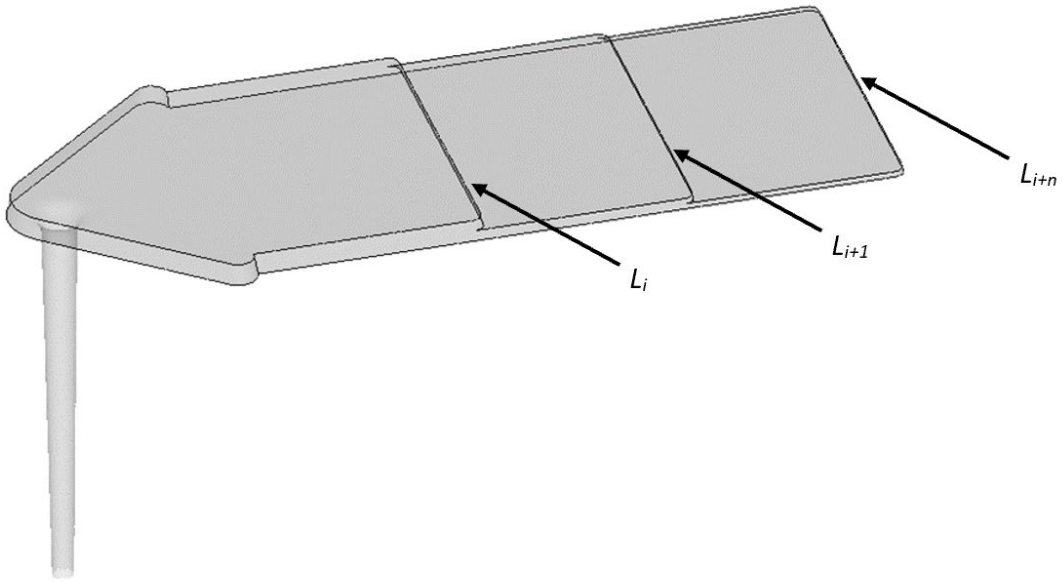

Fig. 7-2: Step plate

For the form part geometry, Moldflow 2016 was selected to perform the simulations for determining melt flow patterns as well as simulated pressure curves under the variation of the boundary conditions. The part geometry is imported as a step file into the simulation software. Thereafter, the mesh is generated as a solid 3D model. To obtain high-quality simulations, mesh elements with unsuitable aspect ratios were manually adjusted. For the step plate, the element size of 1 mm was chosen. This element size results in a total number of 677,859 elements (3D mesh with eight layers). The switchover from the filling

phase to the holding pressure phase is performed at 98% of the volumetric filling (default setting of the Moldflow solver). The selected resin for the simulations—an Acrylnitril Butadien Stryrol (ABS) polymer, type Terluran GP-22 from BASF—is identical to the resin used in the real injection moulding tests. The material specification is presented in Fig. 5-2. Viscosity dependence is expressed through the Williams-Landel-Ferry cross model (Agassant et al., 2017) in Equation (2-5), and the required resin properties are obtained using the simulation software's database. Further discussions of the form part geometry, simulation software, chosen element size, and resolution of the simulated pressure curves are provided in Sections 5.2 and 5.3.

The simulations for the step plate are performed under varied boundary conditions of volume flow $\dot{V}$, melt temperature T_m, and mould surface temperature T_{wz}. A 'screening' conducted in advance of the simulation helps to determine the interval limits of the boundary conditions. The aim is to determine by screening the matching process with the largest possible deviation between the setting parameters of the injection machine and the boundary conditions in the simulation. The limits are reached when the filling process is just still able to be conducted 'to a lowest/highest possible level' (simulative) or when the physical processing limits of the material specifications (e.g., maximum shear rate and maximum melt temperature) have been exceeded. The criterion for this is that, in the simulation, the switchover point to holding pressure at 98% of the volumetric mould filling can still be reached. It is not critical whether the chosen boundary conditions lead in the simulation to defective form parts—for example, form parts with surface defects and sink marks.

Table 7-1 presents variations of the boundary conditions for the step plate. Overall, 12 simulations are performed.

Table 7-1: Step plate variation of boundary conditions

$\dot{V}$ [cm³/s]	T_{wz} [°C]	T_m [°C]
10	33	248
15	**33**	**248**
20	33	248
25	33	248
30	33	248
40	33	248
50	33	248
75	33	248
15	10	248
15	70	248
15	33	210
15	33	300

At a volume flow rate of $\dot{V}$ = 15 cm³/s, a melt temperature of T_m = 248°C and a mould surface temperature of T_{wz} = 33°C, the boundary conditions are identical to the parameters of the injection moulding trial. They represent the standardised boundary conditions of the step plate and are presented in red type. In total, the volume flow rate varies in a range from 10 to 75 cm³/s in eight steps. This number of steps in the simulations ensures that effects can be investigated for non-linearity. The intervals of the volume flow are chosen to vary with small steps size around the standardised volume of $\dot{V}$ = 15 cm³/s (the flow rate with which the real injection moulding tests are performed). The mould temperatures range between 10° and 70°C, with the melt temperatures between 210°C and 300°C—both in three steps.

7.4.1.2 Application of Multidimensional Filling

The stack box is a symmetrical form part with one recessed side and an almost constant wall thickness over the flow path, as depicted in Fig. 7-3 (duplicated from Section 5.2 for clarity when reading this section). The base area of the stack box is

160 x 75 mm^2. The stack box represents the multidimensional flow course. After injecting the molten plastic from the machine nozzle into the sprue bar, the plastic melt front passes the centrally located gate and subsequently spreads towards its preferred direction.

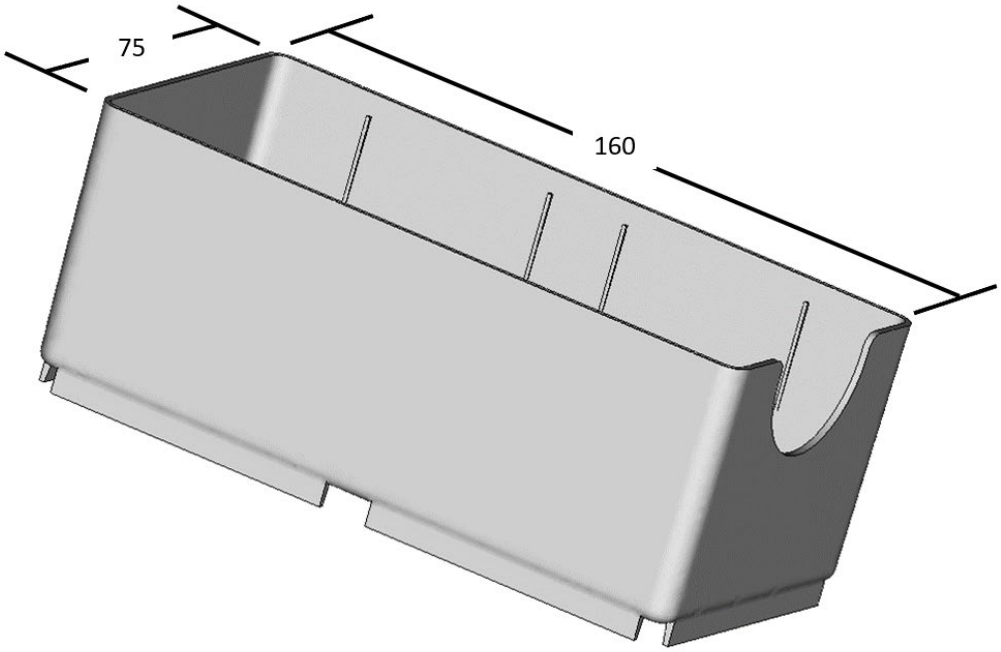

Fig. 7-3: Stack box

For the form part geometry, Moldflow 2016 was selected to perform the simulations to determine melt flow patterns as well as simulated pressure curves under the variation of boundary conditions. The part geometry is imported as a step file into the simulation software. Thereafter, the mesh is generated as a solid 3D model. To obtain high-quality simulations, mesh elements with unsuitable aspect ratios were manually adjusted. For the stack box the element size of 1.5 mm generates as a solid 3D model with four layers above the wall thickness (a total of 662,399 elements). The switchover from the filling phase to the holding pressure phase is performed at 98% of the volumetric filling, the default setting of the Moldflow solver. The selected resin for the simulations—an Acrylnitril Butadien Stryrol (ABS) polymer, type Terluran GP-22 from BASF—is identical to the resin used in real injection moulding tests. The material specification is presented

in Fig. 5-2. Viscosity dependence is expressed through the Williams-Landel-Ferry cross model (Agassant et al., 2017) in Equation (2-5), and the required resin properties are obtained using the simulation software's database. Further discussions of form part geometry, simulation software, chosen element size, and resolution of the simulated pressure curves are provided in Sections 6.2 and 6.3.

The simulations for the stack box are performed under varied boundary conditions of volume flow $\dot{V}$, melt temperature T_m, and mould surface temperature T_{wz}. As with the step plate, a screening conducted in advance of the simulation helps to determine the interval limits of the boundary conditions.

Table 7-2 presents the variants. The standardised boundary conditions with which the real injection moulding is conducted at a volume flow rate of $\dot{V}$= 25 cm^3/s, a melt temperature of T_m = 248°C, and a mould surface temperature of T_{wz} = 45°C are presented in red type.

Table 7-2: Stack box variation of boundary conditions

$\dot{V}$ [cm^3/s]	T_{wz} [°C]	T_m [°C]
10	45	248
15	45	248
25	**45**	**248**
30	45	248
40	45	248
50	45	248
75	45	248
25	10	248
25	70	248
25	45	210
25	45	300

The volume flow rate varies in seven steps in a range from 10 to 75 cm^3/s. This number of steps in the simulations ensures that effects can be investigated for non-linearity. The intervals of the volume flow rate are chosen to vary with a small

step size around the standardised volume flow of $\dot{V}$= 25 cm^3/s (the flow rate with which the real injection moulding tests are performed). The mould temperatures range between 10° and 70°C, and the melt temperatures range between 210°C and 300°C—both in two steps.

7.4.2 Experimental Setup

The real event patterns necessary for the examination of matching methods are analysed from the injection moulding tests conducted as part of the investigation of the new proposed method, as described in Sections 5.3.2 and 6.3.2. The injection moulding tests were conducted on a Battenfeld HM 800 machine with a 30 cm screw diameter. An ABS polymer (Terluran GP-22) was used as the material. The specifications can be found in Fig. 5-2.

Fig. 5-7 and Fig. 6-4 depict the injection moulded test parts of the step plate and the stack box, respectively. As Table 5-2 and Table 6-2 demonstrate, three distinct test cases for each form part were conducted and recorded. The number of 100 specimens per case ensures that the process parameters can be stabilised. In the case of the step plate, test case (1.2) was selected for further analysis. In this case, the volume flow is 15 cm^3/s, the melt temperature is 248°C, and the mould surface temperature is 33°C. For the stack box, test case (2.1) was selected for further analysis. In this case, the volume flow is 25 cm^3/s, the melt temperature is 248°C, and the mould surface temperature is 45°C. At these conditions, the parameter setting led to high quality moulded parts, free of surface defects. Compared with the other two test cases, the surface quality of the parts were rated as subjectively better.

The test setup and the mould of the step plate are presented in Fig. 5-8, Fig. 5-9, and Fig. 5-10. The set up consists of the injection moulding machine with the clamping unit and the injection unit together with the data acquisition unit. The acquisition of the data is conducted using a PC connected to both the machine control (MC) and a pressure sensor located in the machine nozzle (presented in red). The interface to the MC system is used to record process parameters that are

responsible for process stability. These parameters include melt and mould temperature, injection and holding pressure time, as well as the hydraulic pressure at the injection cylinder for each cycle. The actual measurement of the injection pressure curve is conducted using the pressure sensor fitted in the machine nozzle. The exact mounting location of the pressure sensor is presented in Fig. 5-11. A Dynisco MDT465FXL pressure sensor is placed in a mounting ring that is located between the machine nozzle and the injection unit. Thus, the melt pressure is acquired directly in front of the screw of the injection unit. The detailed technical specifications as well as a demonstration of the function of the pressure sensor can be found in Section 5.3.2.

The results of the injection moulding test are presented in the graphs in Fig. 5-14 and Fig. 6-5. The curves represent the measured pressure loss p_{mach} at the location of the machine nozzle during the filling phase of the moulding cycle for the step plate and the stack box, respectively. The resolution of the graph is 2 ms. As stated in Section 5.3.3, for further analysis of the measured pressure curve, only the yellow highlighted mould filling phase is examined. The pressure holding phase subsequent to mould filling is not relevant for the filling process and is thus not subject to observation.

7.4.3 Identification of Events and Determination of Patterns

7.4.3.1 Form Part-Specific Event Patterns

The analysis of the differentiated form part-specific pressure curves under different boundary conditions determines the form part-specific event patterns. To create the patterns, individual event locations are isolated from the differentiated pressure curves. For this purpose, the pressure graphs, obtained by simulation under different boundary conditions, are initially differentiated using Origin Pro. The differentiated graphs are then examined for significant sections where the pressure gradient changes from a relatively less steeply sloped section to a deeply sloped one. To obtain consistent results for validation, the

differentiated pressure graphs are examined using the standardised function peak/flank analysis tool in Origin Pro, as described in Section 5.3.3.

For the step plate, 12 simulations are performed overall for the 12 variations of the boundary conditions, as presented in Table 7-1. The upper section of Fig. 7-4 depicts the form part-specific pressure curve at the boundary condition $\dot{V}$ = 15 cm³/s in the range relevant for the analysis between the start of the injection time and the switchover to holding pressure. The lower section of the figure presents the differentiated graph, which consists of four virtual event vectors (presented in red).

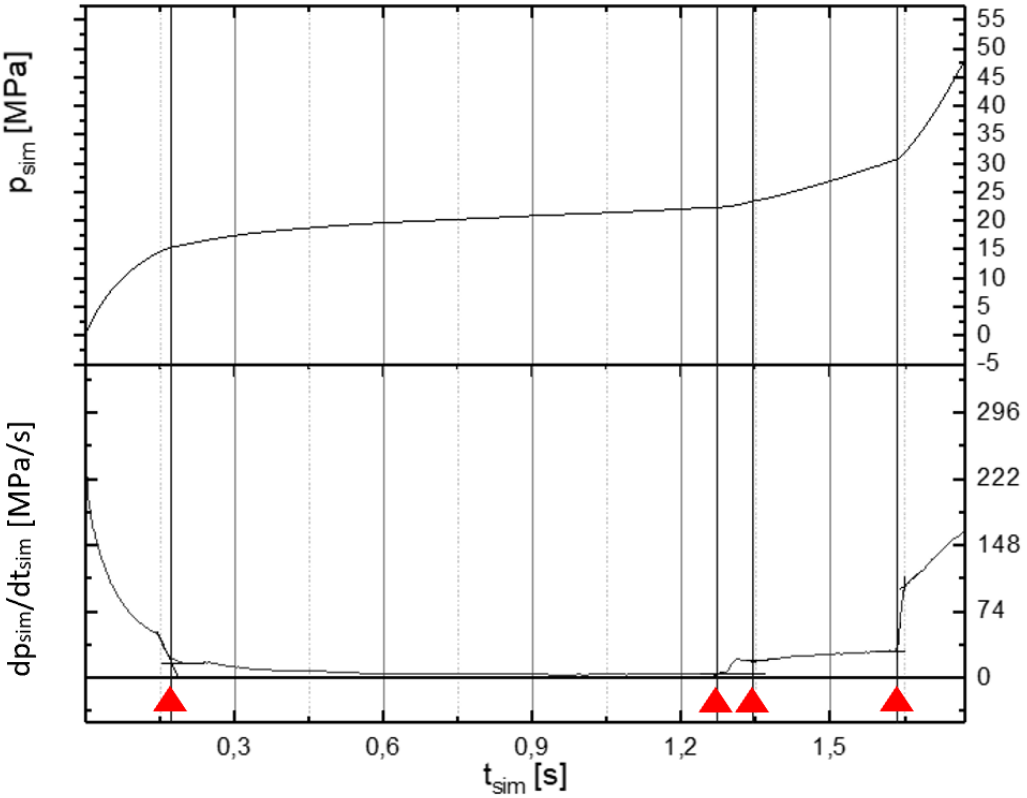

Fig. 7-4: Step plate determination of virtual events at $\dot{V}$ = 15 cm³/s

For the step plate, the analysis of the differentiated form part-specific pressure curves determined 12 different form part-specific event patterns M_s, comprising four virtual event vectors and their components: virtual event time t_{sim}, melt front position x_{sim}, and melt channel geometry h_{sim}.

Table 7-3 details all 12 form part-specific event patterns M_s, which are determined by varying the boundary conditions in ranges from 10 to 75 cm³/s for the volume flow rate, 10° to 70°C for the mould temperature, and 210°C to 300°C for the melt temperature. At a volume flow rate of $\dot{V}$ = 15 cm³/s, a melt temperature of T_m = 248°C, and a mould surface temperature of T_{wz} = 33°C, the boundary conditions are identical to the parameter of the injection moulding trial (standardised boundary conditions, as presented in red type).

Table 7-3: Step plate form part-specific event patterns

$\dot{V}$ [cm³/s]	T_{wz} [°C]	T_m [°C]	$E_{sim\,0}$ [s]	$E_{sim\,1}$ [s]	$E_{sim\,2}$ [s]	$E_{sim\,3}$ [s]
10	33	248	0.285	1.917	2.019	2.449
15	**33**	**248**	**0.193**	**1.274**	**1.346**	**1.631**
20	33	248	0.148	0.953	1.005	1.221
25	33	248	0.114	0.762	0.821	0.976
30	33	248	0.095	0.636	0.673	0.813
40	33	248	0.078	0.476	0.519	0.609
50	33	248	0.061	0.381	0.414	0.487
75	33	248	0.043	0.254	0.283	0.324
15	10	248	0.201	1.276	1.362	1.635
15	**33**	**248**	**0.193**	**1.274**	**1.346**	**1.631**
15	70	248	0.208	1.270	1.326	1.623
15	45	210	0.214	1.278	1.339	1.634
15	**33**	**248**	**0.193**	**1.274**	**1.346**	**1.631**
15	45	300	0.189	1.279	1.372	1.632

Fig. 7-5 illustrates how the patterns vary as an example of the variation in volume flow of the step plate (standardised boundary conditions, as presented in red). At the slowest injection speed of 10 cm³/s, virtual events occur in a time range from

0.3 to 2.5 s. At the simulative fastest injection speed of 75 cm^3/s, virtual events occur in a time range between 0.04 and 0.3 s. To investigate the influences of the deviations of the event patterns on the matching process, all 12 form part-specific event patterns are successively matched with the real event patterns obtained through injection moulding tests. Matching is performed using the matching method presented in Section 4.8 with its linear matching algorithm. The influences of the deviations of the event patterns on the matching process are investigated.

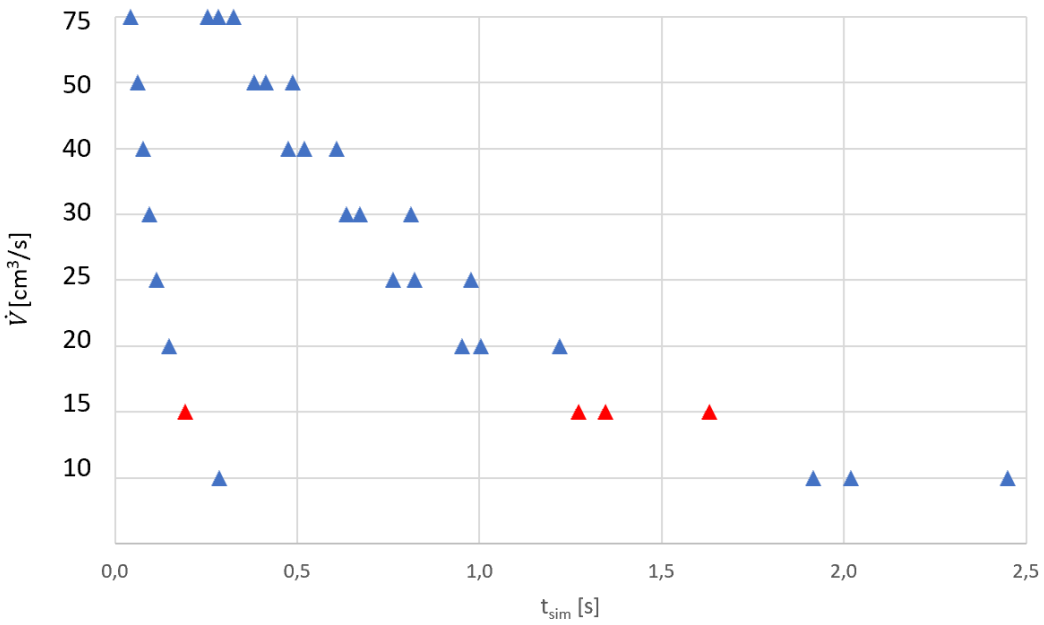

Fig. 7-5: Step plate form part-specific event patterns for volume flow in the range of 10 to 75 cm^3/s

The determination of the virtual patterns for the stack box is analogous to that of the step plate. Overall, 11 simulations are performed for the 11 variations of the boundary conditions, as presented in Table 7-2. The upper section of Fig. 7-6 depicts the form part-specific pressure curve of the stack box at the boundary condition $\dot{V}$ = 25 cm³/s in the range relevant for the analysis between the start of the injection time and the switchover to holding pressure. The lower section of the figure depicts the differentiated graph, which consists of three virtual event vectors (presented in red).

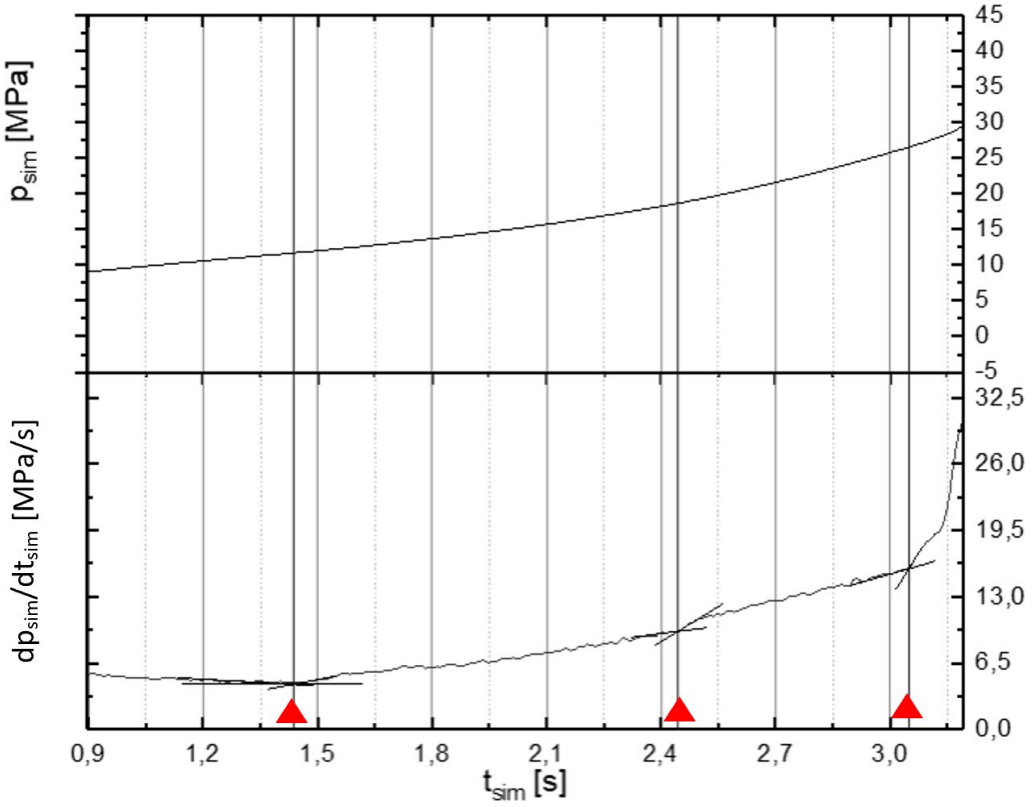

Fig. 7-6: Stack box determination of virtual events at $\dot{V}$ = 25 cm³/s

The analysis of the differentiated form part-specific pressure curves of the stack box determined 11 different form part-specific event patterns M_s, comprising three event vectors and their components: virtual event time t_{sim}, melt front position x_{sim}, and melt channel geometry h_{sim}. Table 7-4 shows all the form part-specific event patterns M_s, which are determined by varying the boundary

conditions in ranges from 10 to 75 cm^3/s for the volume flow rate, 10° to 70°C for the mould temperature and 210°C to 300°C for the melt temperature. At a volume flow rate of $\dot{V}$ = 15 cm^3/s, a melt temperature of T_m = 248°C, and a mould surface temperature of T_{wz} = 45°C, the boundary conditions are identical to the parameter of the injection moulding trial (standardised boundary conditions, as presented in red type).

Table 7-4: Stack box form part-specific event patterns

$\dot{V}$ $[cm^3/s]$	T_{wz} [°C]	T_m [°C]	$E_{sim\ 0}$ [s]	$E_{sim\ 1}$ [s]	$E_{sim\ 2}$ [s]
10	45	248	3.481	5.439	7.871
15	45	248	2.418	3.793	5.181
25	**45**	**248**	**1.474**	**2.444**	**3.063**
30	45	248	1.274	2.050	2.563
40	45	248	0.975	1.581	1.933
50	45	248	0.792	1.271	1.560
75	45	248	0.536	0.855	1.051
25	10	248	1.437	2.357	3.037
25	**45**	**248**	**1.474**	**2.444**	**3.063**
25	70	248	1.530	2.471	3.086
25	45	210	1.454	2.377	3.078
25	**45**	**248**	**1.474**	**2.444**	**3.063**
25	45	300	1.528	2.456	3.081

7.4.3.2 Real Event Patterns

To investigate the influences of the deviations of the event patterns on the matching process, the form part-specific event patterns determined under the variation of boundary conditions are successively matched with the real event patterns obtained by the injection moulding tests. As explained in Section 7.4.2, for this purpose, the results of the injection moulding tests (shown in the graphs in

Fig. 5-14 and Fig. 6-5) are used. The curves represent the measured pressure loss p_{mach} at the location of the machine nozzle during the filling phase of the moulding cycle for the step plate and the stack box, respectively. The analysis of the differentiated measured pressure signal is described in detail in Sections 5.3.3.2 and 6.3.3.2 and provides the real event patterns, which consist of six event vectors $E_{mach\,0}$ … $E_{mach\,5}$ for the step plate (Table 7-5) and three event vectors $E_{mach\,0}$ … $E_{mach\,2}$ for the stack box (Table 7-6). Each vector has the following components: machine time, melt pressure, and screw position.

Table 7-5: Step plate real event pattern

$\dot{V}$ [cm³/s]	T_{wz} [°C]	T_m [°C]	$E_{mach\,0}$ [s]	$E_{mach\,1}$ [s]	$E_{mach\,2}$ [s]	$E_{mach\,3}$ [s]	$E_{mach\,4}$ [s]	$E_{mach\,5}$ [s]
15	33	248	0.680	1.190	2.250	2.300	2.610	2.900

Table 7-6: Stack box real event pattern

$\dot{V}$ [cm³/s]	T_{wz} [°C]	T_m [°C]	$E_{mach\,0}$ [s]	$E_{mach\,1}$ [s]	$E_{mach\,2}$ [s]
25	45	248	1.640	2.560	3.090

7.4.4 Pattern Matching and Assignment of Events

Fig. 7-7, presents an example of the step plate in which both the real event pattern M_m (circle symbol) and the form part-specific event pattern M_s for the variation of the boundary conditions at $\dot{V}$ = 15 cm³/s (triangle symbol) are plotted against machine time t_m. Pattern matching and event assignment are performed using the matching algorithm described in Section 4.8, by means of linear transformation as well as the displacement of the events.

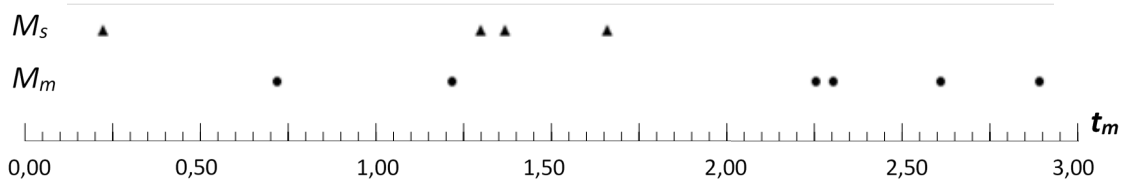

Fig. 7-7: Step plate real and form part-specific event patterns
at variation $\dot{V}$ = 15 cm³/s

For both the step plate and the stack box, the matching algorithm passes three levels of iterations with $j_{max} = m - n$ displacements and transformations with an interval of $f_{min} = 0.1$ to $f_{max} = 10$ for a scaling increment of $\Delta f = 0.01$. To assess the matching, the process is repeated for every variation of the boundary conditions. For each repetition, in addition to the assignment of the events at the smallest pattern deviation, the matching algorithm provides the raw data for further validation of the matching method: (a) the stretching factor f_k at the smallest total deviation of the pattern S_{min} and (b) the individual residues of the assigned events $S_{k,i}$. With its linear transformation function, the matching algorithm successfully matches 12 patterns for the step plate and 11 patterns for the stack box, which are determined under the variation of boundary conditions, for both form part geometries without any modification, and provides assignments of the events. The criteria for a 'successful match' are as follows:

a) A reliable matching of virtual patterns that have been determined under the variation of the boundary conditions, by reaching the termination criterion of the algorithm (i.e., 'termination with the smallest deviation of the patterns').
b) The same displacement $j = j_{min}$ that also occurs with form part-specific patterns, which is the same under standardised boundary conditions.

For the step plate, for all 12 variations of the boundary conditions (Table 7-1), the algorithm is used to determine the best matching of the patterns at a displacement j_{min} = 1. For the 11 variations of the stack box (Table 7-2), the best matching is obtained at a displacement of j_{min} = 0. The three virtual events are assigned to the three real events. As an example, Fig. 7-8 presents the assignment

of virtual and real events from the matched pattern of the step plate for the variation of the volume flow at 15 cm³/s. According to Equation (4-6) and with j_{min} = 1, four virtual events, $E_{sim\ I}$, can be assigned to four real events. $E_{mach\ i+j}$ ($E_{sim\ 0}$ to $E_{mach\ 1}$, $E_{sim\ 1}$ to $E_{mach\ 2}$, …). The two real events $E_{mach\ 0}$ and $E_{mach\ 5}$ have no correspondent virtual events and are thus excluded from further consideration.

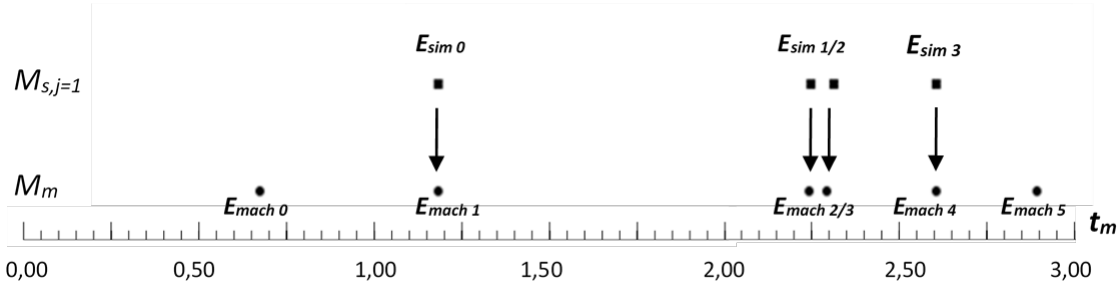

Fig. 7-8: Step plate assignment of virtual and real events at variation $\dot{V}$ = 15 cm³/s

As a result, for each individual matching with varying boundary conditions, the stretching factor f_k at the smallest total deviation of the pattern S_{min} and the individual residues of the assigned events $S_{k,I}$ are collected. These raw data are used to assess the matching and are discussed and evaluated in Section 7.5.

7.5 Discussion and Evaluation of the Pattern Matching Methods

7.5.1 One-Dimensional Case

The step plate represents an idealised one-dimensional flow front course (Fig. 7-2). The simulations of the filling process are conducted under the variation of the boundary conditions, such as volume flow, melt temperature, and mould surface temperature.

The patterns are matched, and the events are assigned using the algorithm with linear transformation function, as described in Sections 4.7.3 and 7.3.8. To assess the matching, the matching process is repeated for every variation of the boundary conditions. For each repetition, the matching algorithm provides the

stretching factor f_k at the smallest total deviation of the pattern S_{min} and the individual residues of the assigned events $S_{k,i}$.

Resulting from the assessment, Fig. 7-9 presents the dimensionless stretching factor at the smallest pattern deviation as a function of the volume flow. The linear dependency of the volume flow on the stretching factor is clearly visible.

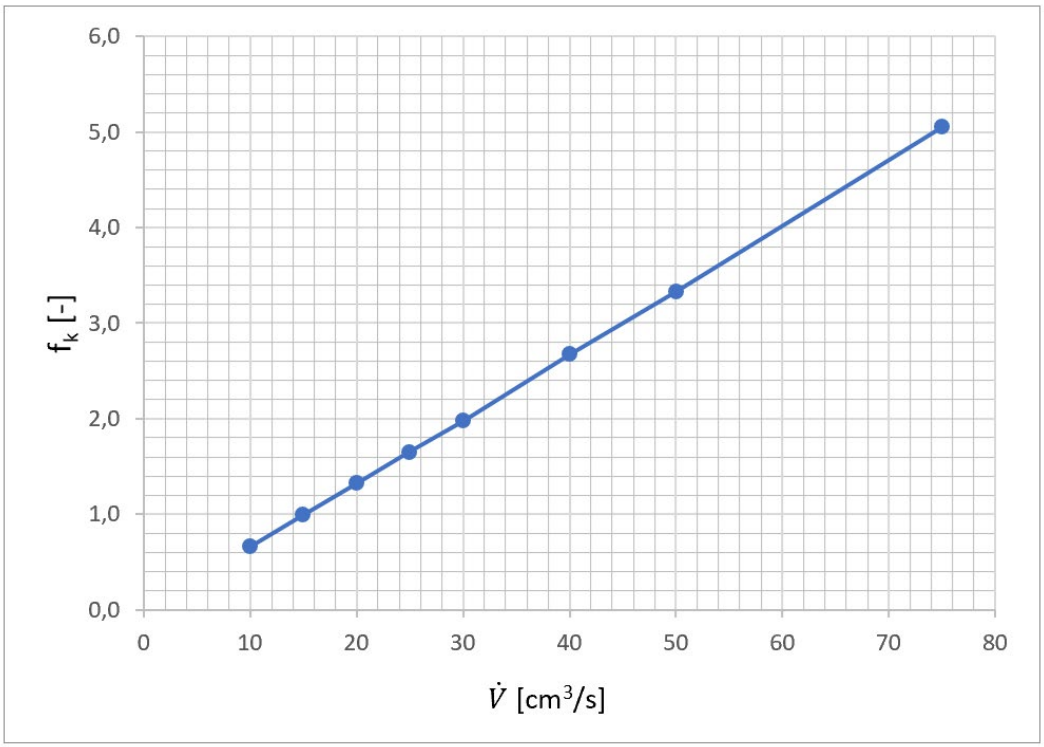

Fig. 7-9: Step plate stretching factor as a function of volume flow

The smallest total deviation of the patterns S_{min} is plotted in Fig. 7-10. The mean value of the pattern deviation is $-1.0 \cdot 10^{-3}$ s, and it has a standard deviation of $3.7 \cdot 10^{-3}$ s. The overall relatively small values (in the order of 10^{-3} s) of the pattern deviation imply the high consistency of the patterns due to transformation. In Section 7.8.4, the deviation of the patterns is further evaluated and discussed.

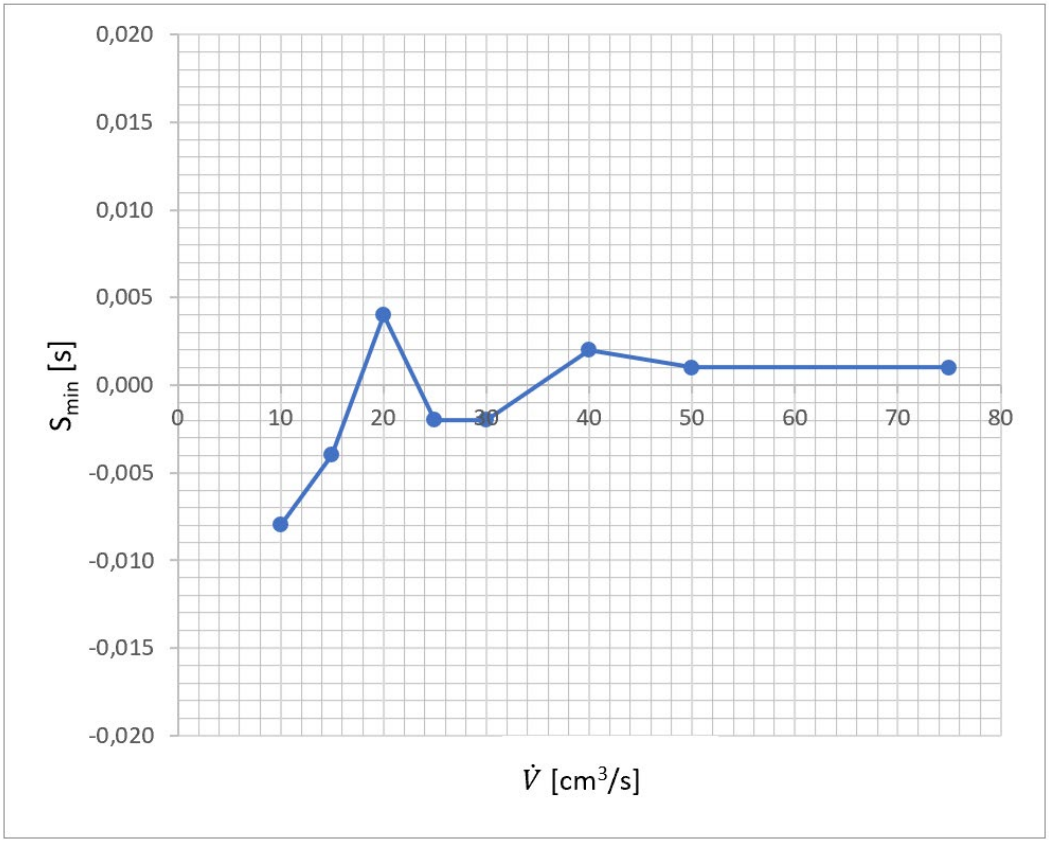

Fig. 7-10: Step plate deviation of the patterns as a function of volume flow

Fig. 7-11 and Fig. 7-12 present the stretching factor as a function of the melt and mould surface temperature; the graphs clearly indicate that the variation of the temperatures has no significant effect on the stretching factor.

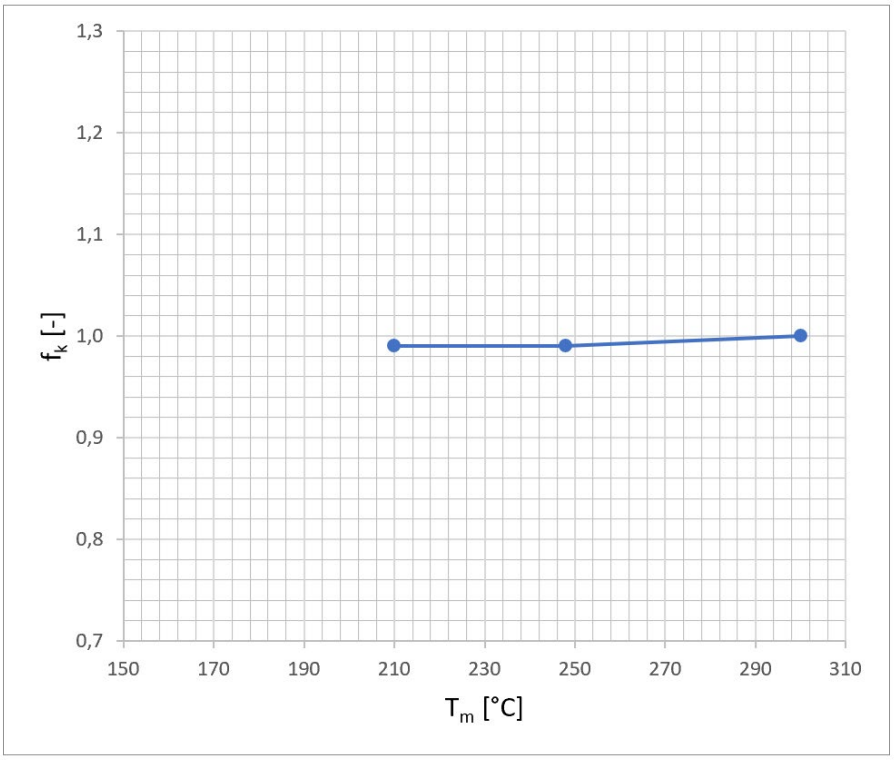

Fig. 7-11: Step plate stretching factor as a function of melt temperature

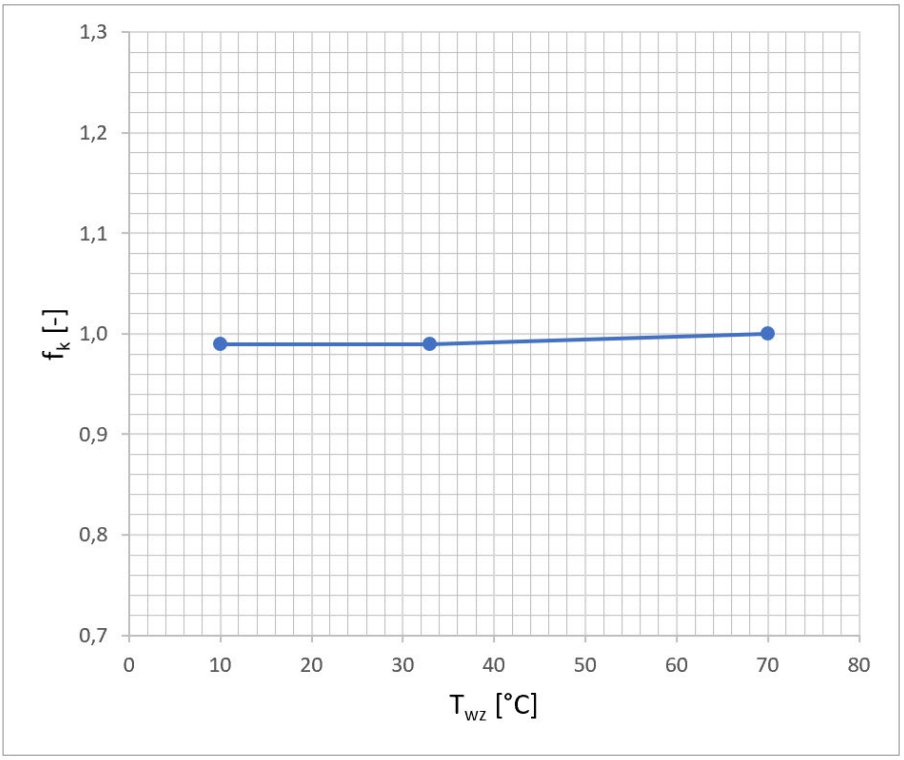

Fig. 7-12: Step plate stretching factor as a function of mould surface temperature

For a form part geometry with an almost one-dimensional flow front course, the

linear dependence of the stretching factor on the volume flow is an expected result (Section 3.2.2). The law of mass conservation requires that an event along a one-dimensional flow path occurs in inverse proportion to the volume flow (with incompressibility of the fluid as a prerequisite). The position of a flow front with a constant volume flow is proportional to the time and is independent of location. Boundary conditions, such as melt and mould surface temperature, do not influence the position of the flow front (as Fig. 7-11 and Fig. 7-12 clearly show) in a one-dimensional form part.

A first interim result can be derived from the evaluation above. For a form part with a geometry that closely resembles the idealised one-dimensional flow front path, a matching method with a linear matching algorithm is suitable. Assuming that, in addition to a linear transformation, the matching method fulfils the requirement profile from Section 7.3.6 and thus has functions for assigning event patterns (or fragments of those) and for eliminating disturbance events, a form part-specific event pattern for such a close to idealised one-dimensional part can be reliably assigned to a real event pattern. In this special case, it is completely irrelevant under which boundary conditions the form part-specific event pattern is determined or under which physical conditions (i.e., the setting) the moulded part is injected.

7.5.2 Multidimensional Case

The stack box is a symmetrical, front-centrally injected form part with one recessed side and an almost constant wall thickness over the flow path (Fig. 7-3). It represents the multidimensional flow front course. The numerical calculation of the filling process occurs under the variation of the boundary conditions of volume flow, melt temperature and mould surface temperature. The patterns are matched, and the events are assigned using an algorithm with a linear transformation function, as described in Sections 4.7.3 and 7.3.8. To assess the matching, the matching process is repeated for every variation of the boundary conditions. For each repetition, the matching algorithm provides the stretching

factor f_k at the smallest total deviation of the pattern S_{min} and the individual residues of the assigned events $S_{k,i}$.

Resulting from the assessment, Fig. 7-13 presents the dimensionless stretching factor at the smallest pattern deviation as a function of the volume flow. As with the step plate, a linear dependency of the volume flow on the stretching factor is clearly visible for the stack box.

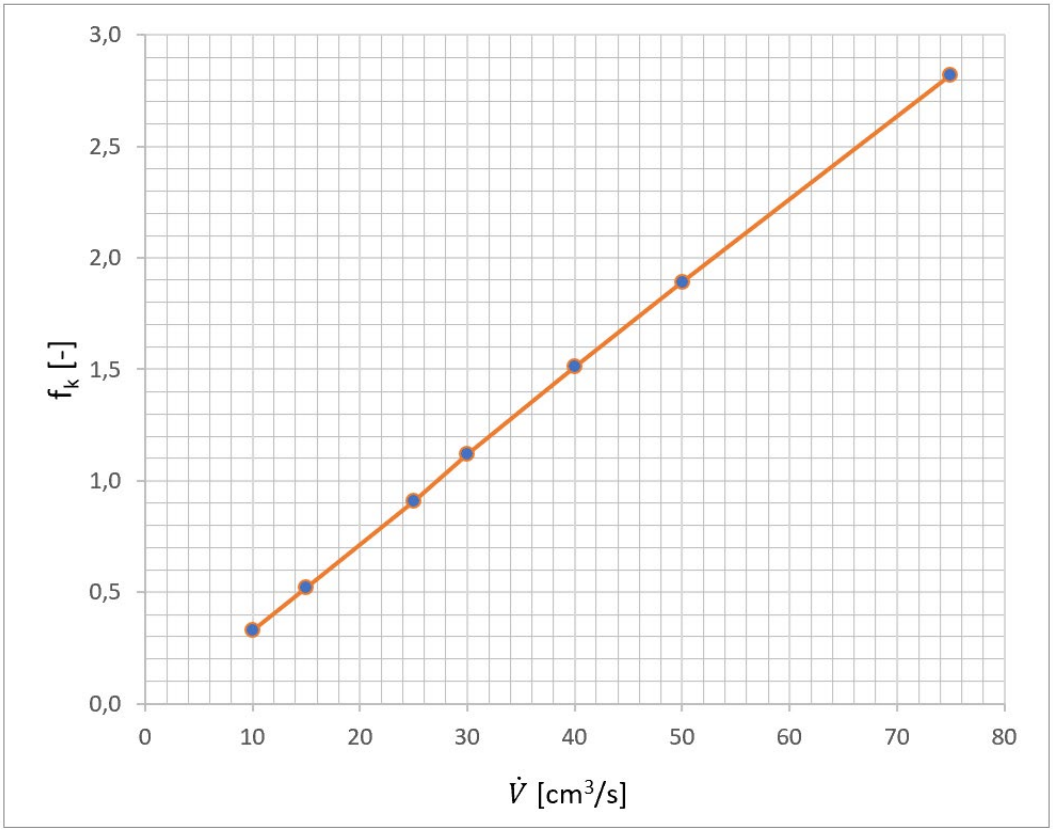

Fig. 7-13: Stack box stretching factor as a function of volume flow

The smallest total deviation of the patterns S_{min} as a function of the volume flow is presented in Fig. 7-14. The mean pattern deviation value is $3.0 \cdot 10^{-3}$ s and it has a standard deviation of $4.8 \cdot 10^{-3}$ s. As with the step plate, the overall relatively small values of the pattern deviation (in the order of 10^{-3} s) imply the high consistency of the patterns due to transformation and, thus, robust matching. In Section 7.8.4, the deviation of the patterns is further evaluated and discussed. Fig. 7-15 and Fig.

7-16 indicate no effect or a minimal effect of the temperature variants on the stretching factor.

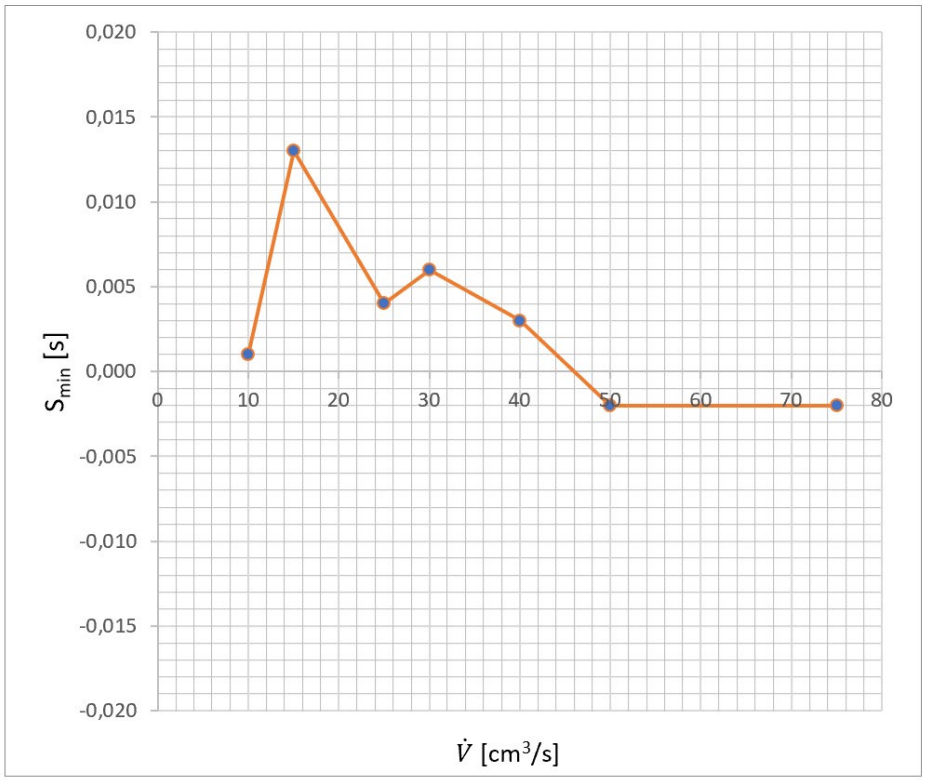

Fig. 7-14: Stack box deviation of the patterns as a function of volume flow

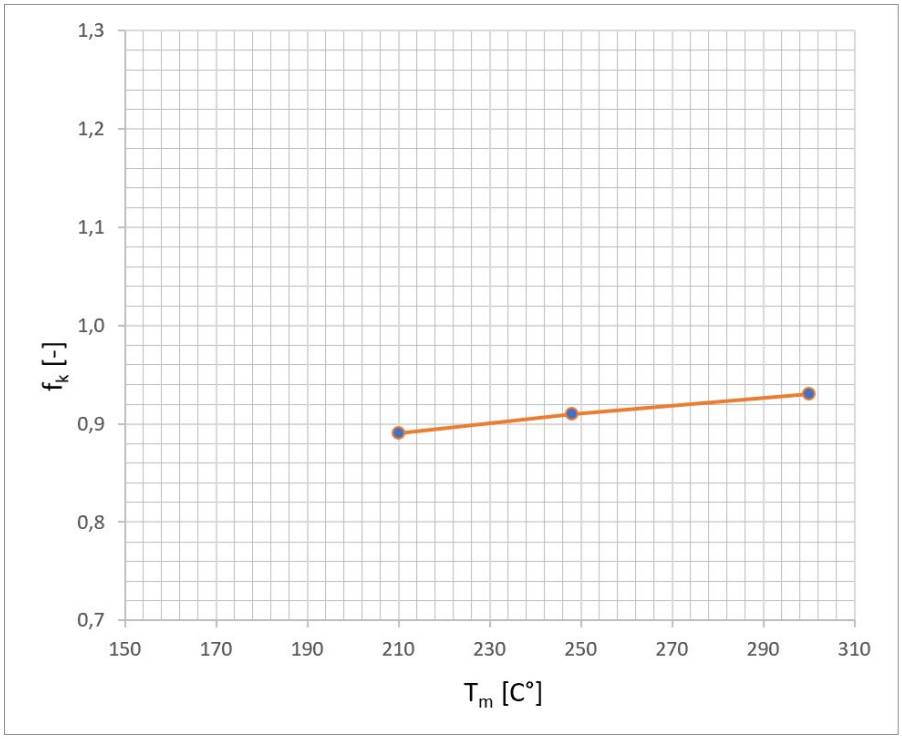

Fig. 7-15: Stack box stretching factor as a function of melt temperature

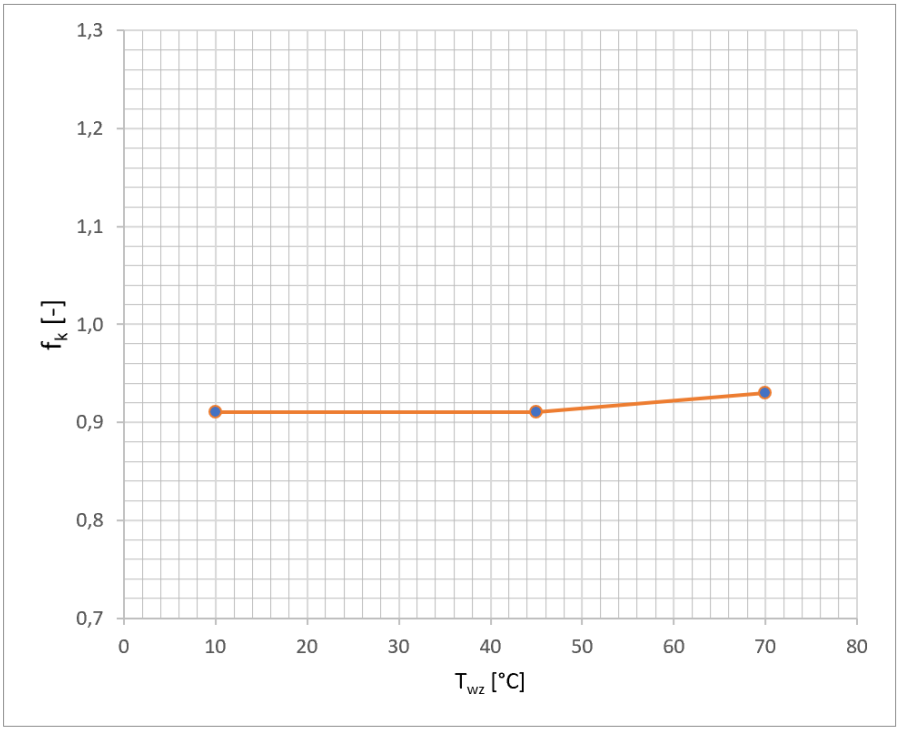

Fig. 7-16: Stack box stretching factor as a function of mould temperature

In contrast to the one-dimensional case, the result from the experimental investigation of the pattern matching of the stack box was unexpected when the

initial investigation was conducted. This is because the stack box fills multidimensionally. The preferred flow path of the melt and thus its volume flow depend on location and time. According to theory, the volume flow (as in the one-dimensional case) can be expected to have an effect on the stretching factor. However, it would be expected that events along the melt flow path would not occur in inverse proportion to the volume flow; consequently, linear dependence of the stretching factor on the volume flow would also not be expected (Section 3.2.3). Because the melt has the freedom to flow into different paths depending on location and time, the variants of the temperatures should have an effect on the time when the event occurs. Of course, a linear dependency of the volume flow or the absence of significant effects of melt and mould surface temperature on the stretching factor would be desirable in the sense of a simple matching. This would prove the suitability of a matching method based on linear transformation even in the general case of multidimensional filling. However, for the multidimensional case, the theoretical assumptions in Section 3.2.3 (i.e., linear dependence for volume flow, no influence of temperatures on the stretch factor) cannot be explained by the observed effects. This necessitates further considerations for the multidimensional case as described in Section 7.6.

7.6 Amendments to the Assumptions for the Multidimensional Case

The aforementioned results lead to the following lines of thinking:

1. From the law of mass conservation, it follows that the *total* filling time of *any* moulded form part is inversely proportional to volume flow (regardless of whether it is one-dimensionally or multidimensionally filled).

2. Assuming that a ‘thought’ form part only has one single event, this event is located in such a way that the melt front reaches it infinitesimally prior to the volumetric filling of the moulded part. The event time is infinitesimal before the filling time of the part (total injection time).

3. Although the thought form part fills multidimensionally, and the flow paths of the melt depends on location and time, the single event occurs infinitesimally prior to the time of volumetric filling (regardless of which flow path the melt has chosen on its way from the gate to the event location). From the time the event occurs to the total filling of the form part, the melt no longer has any degree of freedom to 'choose' its preferred direction in practice.

4. This implies that both the influence of volume flow and all other boundary conditions such as mould surface and melt temperatures in the multidimensional case depend on the event location. It is conceivable that with increasing strength, the event time inversely proportionally follows the volume flow the nearer the event occurs in relation to the time of volumetric filling.

5. Conversely, this would mean that the inversely proportional influence of the volume flow on the event time decreases the further the event site is located (or the sooner the event occurs) in relation to the volumetric filling. If the melt front hits an event site that is far from the volumetric filling, it has significantly more degrees of freedom to 'decide' which path to take from this event site.

6. For all other boundary conditions than the volume flow, it can be assumed that the nearer an event location is to the volumetric filling, the lower the effect of a change of the boundary conditions on the event time, and vice versa.

If the above 'thought experiment' is correct, then this would explain the linear dependency of volume flow and the lack of effects of melt and mould surface temperature on the stretching factor (results in Section 7.5.2) for the multidimensional case stack box.

Therefore, the assumptions made in Section 3.2.3 for the multidimensional case must be amended by the following distinguished cases:

In general, for the multidimensional case, the following relationship applies:

$$f_k, S_{min}, X = f(\dot{V})$$
$$f_k, S_{min}, X = f(\eta) \quad (7\text{-}1)$$

For a single event, the relationship can be distinguished into two cases:

1. The event location tends to be near the volumetric filling:

$$f_k = f(\dot{V}), \text{ linear dependence}$$
$$S_{min}, X \neq f(\dot{V})$$
$$f_k, S_{min}, X \neq f(\eta) \quad (7\text{-}2)$$

2. The event location tends to be far from the volumetric filling:

$$f_k, S_{min}, X = f(\dot{V}), \text{ non-linear dependence}$$
$$f_k, S_{min}, X = f(\eta), \text{ non-linear dependence} \quad (7\text{-}3)$$

These amendments to the assumptions for the multidimensional case could explain the results from Section 7.5.2. To validate the amended assumptions, further research is required. For this purpose, the investigation for the multidimensional model must be distinguished into cases where the event location tends to be near to and far from the volumetric filling, as discussed in Section 7.7.

7.7 Investigation of Far and Near Volumetric Filling

To prove the amended assumptions for the multidimensional case, an investigation of the multidimensional case with far and near volumetric filling is conducted.

7.7.1 Multidimensional Case – Investigation of Far and Near Volumetric Filling

As the analysis in Section 7.4.3 has demonstrated, the real event patterns of the stack box consist of $m = 3$ events ($E_{mach\,0} \ldots E_{mach\,2}$) and the form part-specific event

patterns consist of $n = 3$ events ($E_{sim\,0}$ … $E_{sim\,2}$). Because $m = n$, the following displacement factor applies:

$$j = j_{min} = 0 \tag{7-4}$$

With a linear transformation, the matching algorithm provides the assignment of events at the point of the smallest total pattern deviation S_{min}. As Fig. 7-17 demonstrates, exactly three virtual events are assigned to three real events.

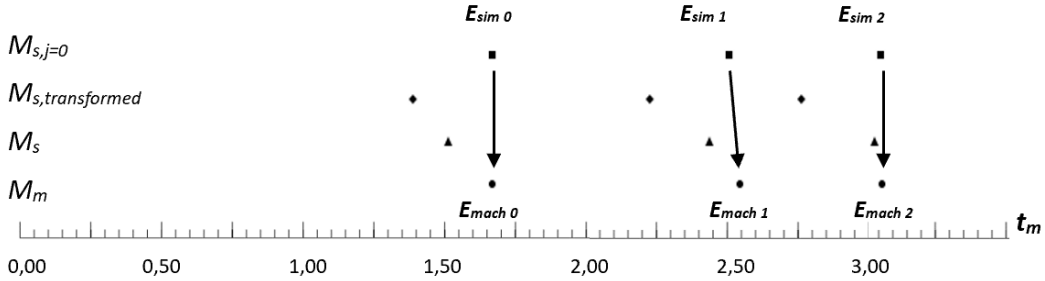

Fig. 7-17: Stack box assigning of transformed and displaced virtual events

Fig. 7-18 presents the visualisation of the melt front at a volume flow of 25 cm^3/s (standardised boundary condition, obtained from the CAE simulation software). The filling pattern is set to the superimposed event points $E_{sim\,1}$ -> $E_{mach\,1}$ and shows the melt front arrival at the recessed side. This event location, denoted as Investigation Point 1, is aimed at examining events that tend to be *far* from the volumetric *filling* of the moulded part.

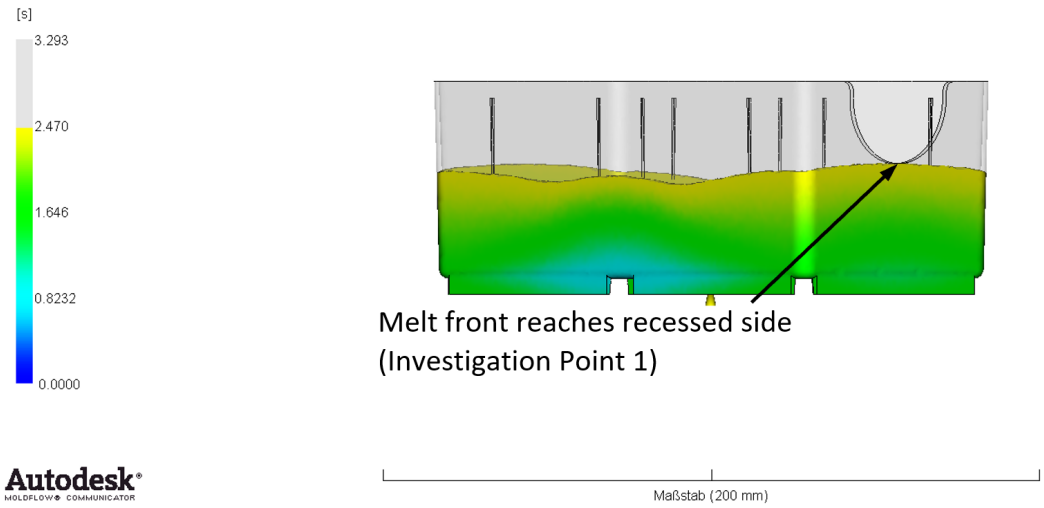

Fig. 7-18: Simulation result of the flow pattern of the stack box at event $E_{mach\ 1}$ (Investigation Point 1; volume flow of 25 cm^3/s)

As shown in Fig. 7-19, the filling pattern is set to the superimposed event points $E_{sim\ 2}$ -> $E_{mach\ 2}$. At this event location, denoted below as Investigation Point 2, the flow front reaches the end of the flow channel first at the recessed side. At Investigation Point 2, events are examined that tend to be *near* the volumetric *filling* of the moulded part.

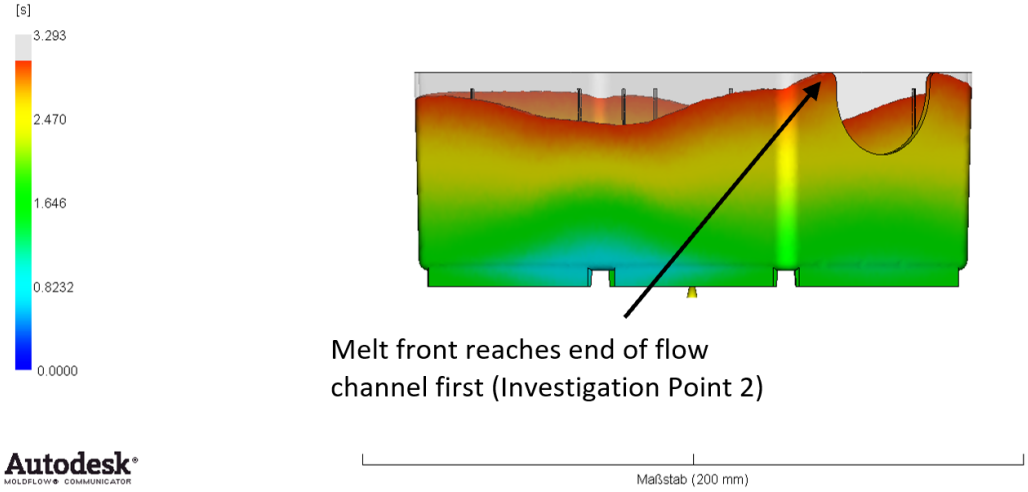

Fig. 7-19: Simulation result of the flow pattern of the stack box at event $E_{mach\ 2}$ (Investigation Point 2; volume flow of 25 cm^3/s)

For further investigations, all events that are *not* located at Investigation Points 1 (far) or 2 (near) are alternately removed from the event patterns. This procedure

is demonstrated in Fig. 7-20 and Fig. 7-21. Fig. 7-20 displays the examination of the pattern matching at Investigation Point 1 (far from volumetric filling). First, all events close to the volumetric filling are removed (symbolised by X). After removing the events, the patterns are matched, and the remaining events are assigned by linear transformation. The assessment is repeated for every variation of the boundary conditions. After removing all events close to the volumetric filling, each pattern consists of only two events; therefore, the matching is performed with the smallest total pattern deviation $S_{min} = 0$.

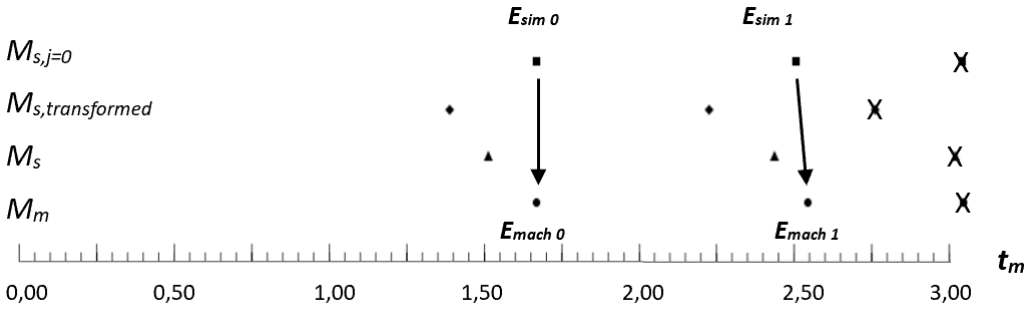

Fig. 7-20: Stack box events at Investigation Point 1

Similarly, the pattern matching is examined at Investigation Point 2 (near volumetric filling). As Fig. 7-21 demonstrates, all events far from the volumetric filling are removed (symbolised by X). After removing the events, the patterns are matched, and the remaining events are assigned by linear transformation. The assessment is repeated for every variation of the boundary conditions of volume flow, mould surface, and melt temperature. With this approach, for each investigation point—far from and near to the volumetric filling—the influence of the boundary conditions on the stretching factor can be examined individually.

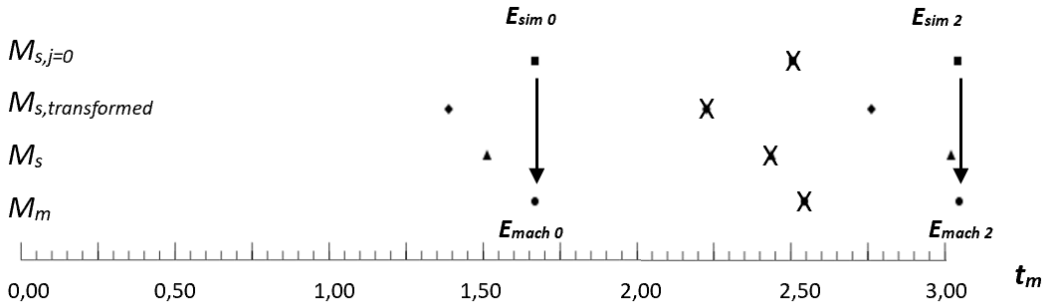

Fig. 7-21: Stack box events at Investigation Point 2

Resulting from the assessment, Fig. 7-22 indicates that the stretching factor at Investigation Point 2 is proportional to the volume flow, whereas the stretching factor at Investigation Point 1 is not proportional.

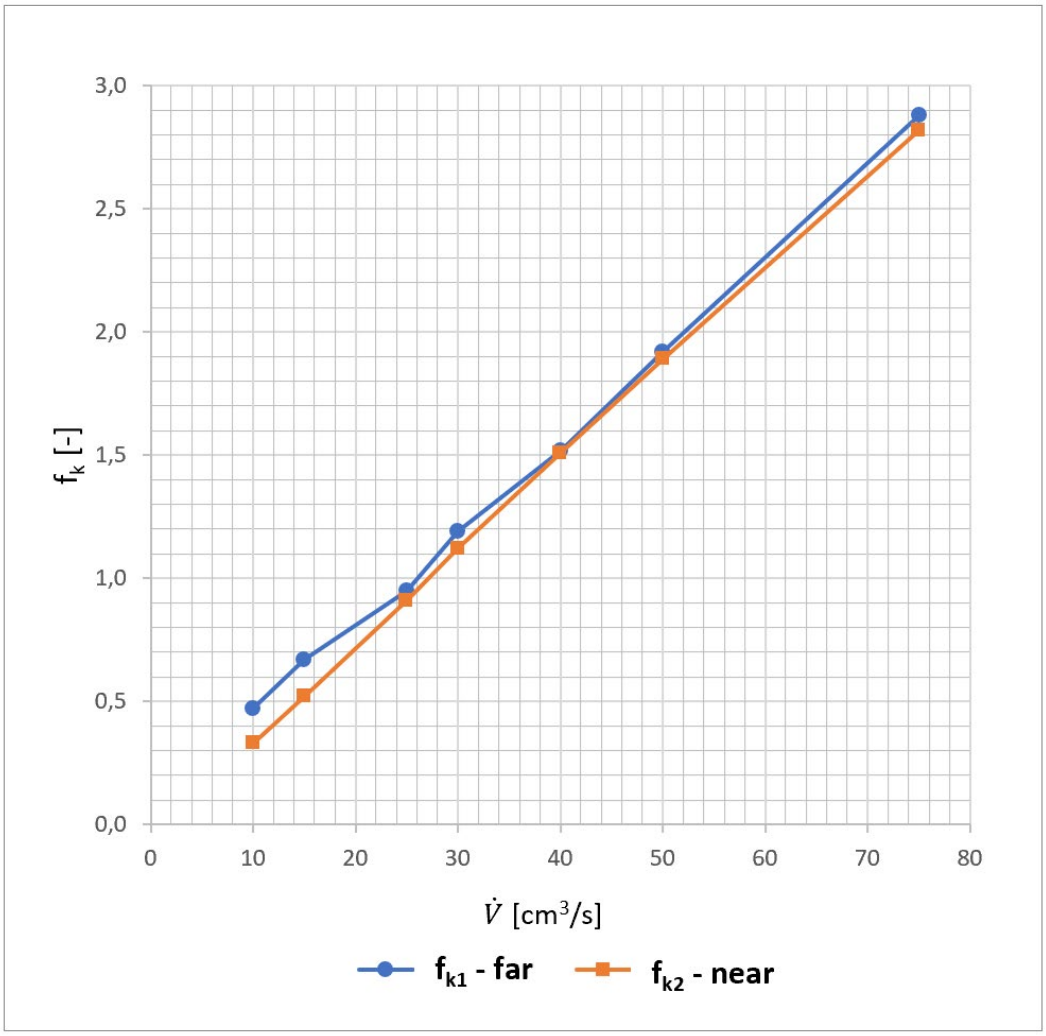

Fig. 7-22: Stack box stretching factor as function of volume flow at Investigation Points 1 and 2

If the partial mass volume V_i (partial amount of plastic that is already injected into the cavity at the time the event $E_{sim\,i}$ occurs) at an event $E_{sim\,i}$ for different volume flows is related to the partial mass volume $V_{0,i}$ at the event location for the standardised volume flow, the dimensionless figure $\frac{V_i}{V_{0,i}}$ can be established. With the help of this figure, the non-linearity of the 'far event location' at Investigation Point 1 can be revealed. As Fig. 7-23 demonstrates, the injected volume at Investigation Point 1 (Fig. 7-18) varies by up to 20% depending on the volume flow.

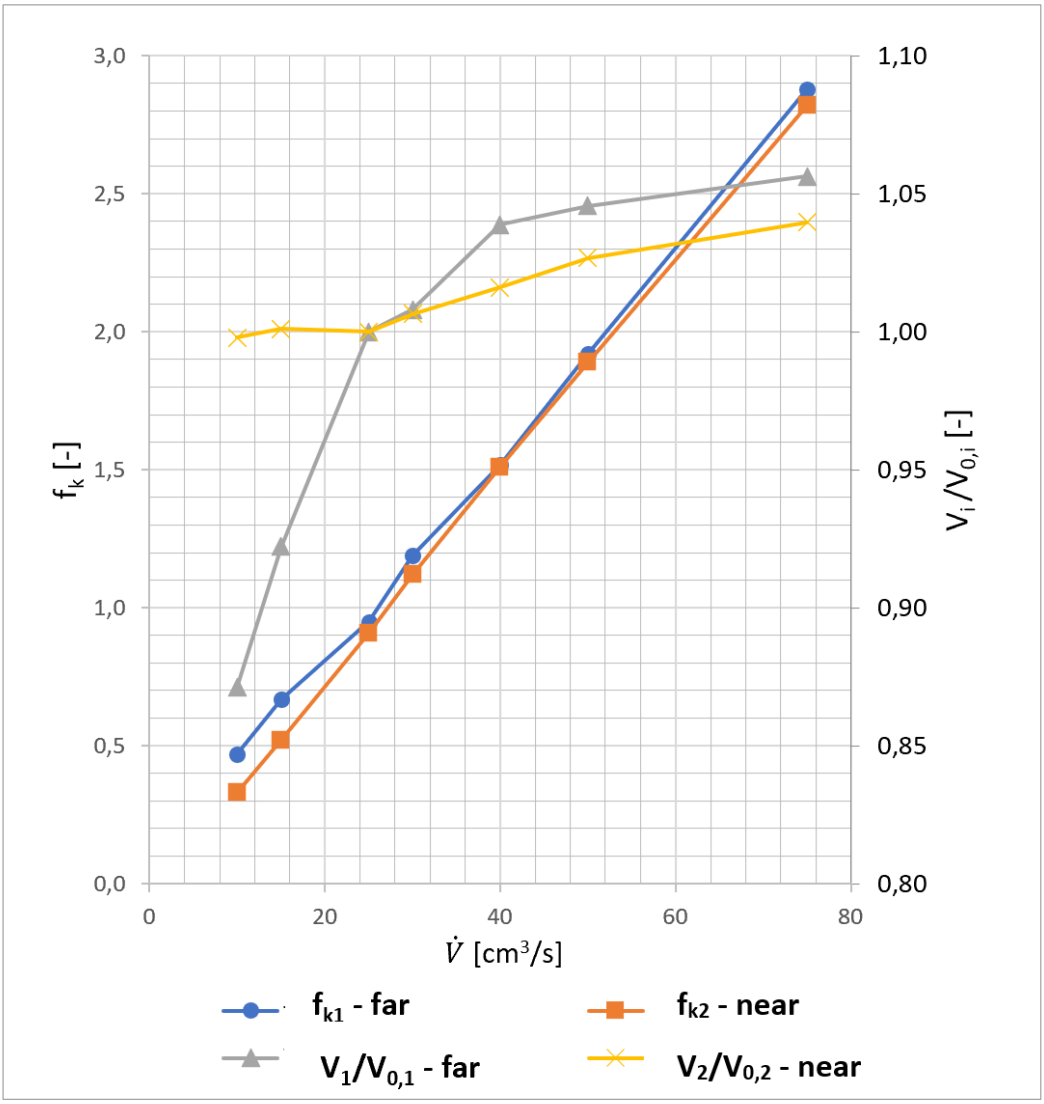

Fig. 7-23: Stack box stretching factor and partial volume as function of volume flow at Investigation Points 1 and 2

When the event $E_{sim\ 1}$ occurs at Investigation Point 1, the cavity of the stack box for small volume flows is significantly less filled with molten plastic (Fig. 7-24) than it is at a high-volume flow (Fig. 7-25). This proves that depending on the volume flow, the plastic melt travelling on its flow path between event locations $E_{sim\ 0}$ *and* $E_{sim\ 1}$ 'chooses' variant directions before reaching Investigation Point 1. In other words, depending on the volume flow, a *disproportionately* large amount of time elapses before Investigation Point 1 (far from volumetric filling) is reached.

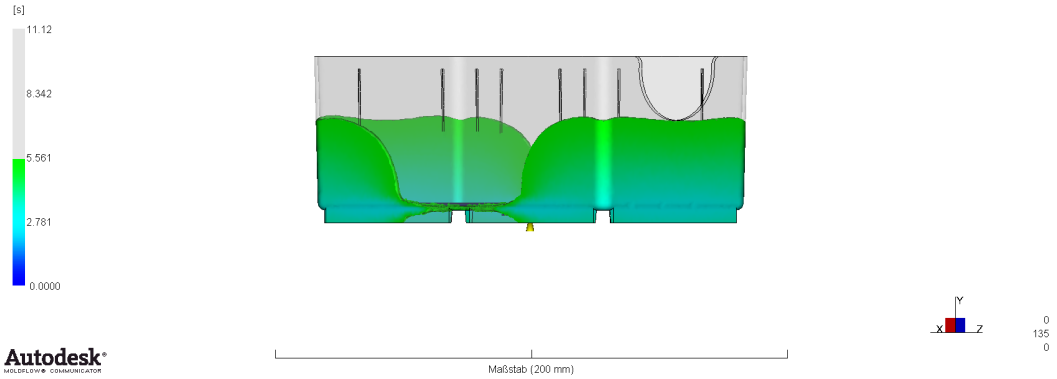

Fig. 7-24: Simulation result of the flow pattern
of the stack box at event $E_{mach\ 1}$ (Investigation Point 1) at $\dot{V}$= 10 cm³/s

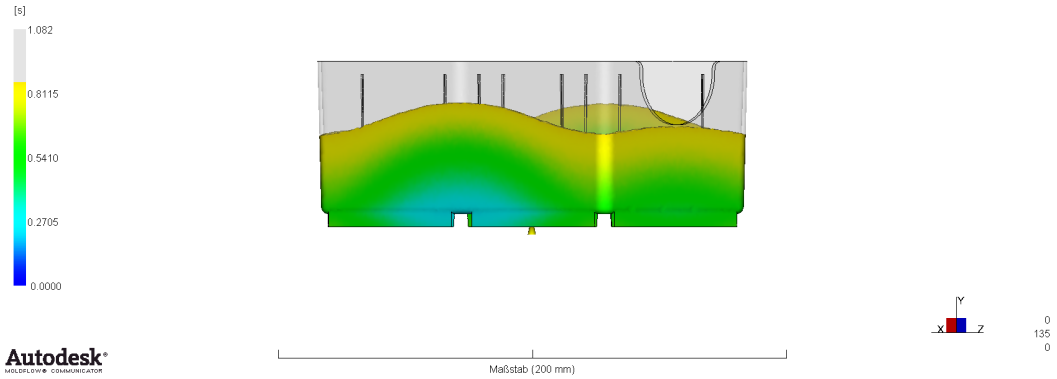

Fig. 7-25: Simulation result of the flow pattern
of the stack box at event $E_{mach\ 1}$ (Investigation Point 1) at $\dot{V}$= 75 cm³/s

By contrast, the flow path between event locations $E_{sim\ 1}$ and $E_{sim\ 2}$ is largely predetermined. When the melt reaches Investigation Point 2 (Fig. 7-19), the mass volume of the injected melt at different volume flows hardly fluctuates around the mass volume of the standardised volume flow. As Fig. 7-23 demonstrates, the injected volume at Investigation Point 2 varies by a maximum of 4% depending on the volume flow.

The aforementioned assessment also provides the effect of the melt and the mould surface temperature on the stretching factor for ‘near’ and ‘far’ events. The results in Fig. 7-26 and Fig. 7-27 prove that if an event occurs with an increasing distance from the volumetric filling, the effect of the mass or mould surface temperature on the stretching factor increases.

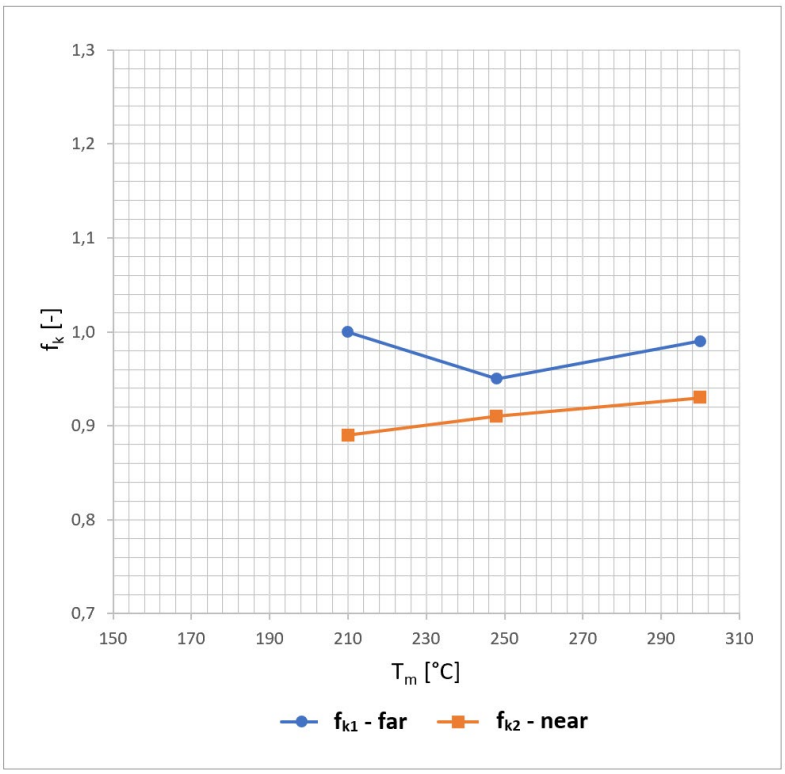

Fig. 7-26: Stack box stretching factor as a function of melt temperature at Investigation Points 1 and 2

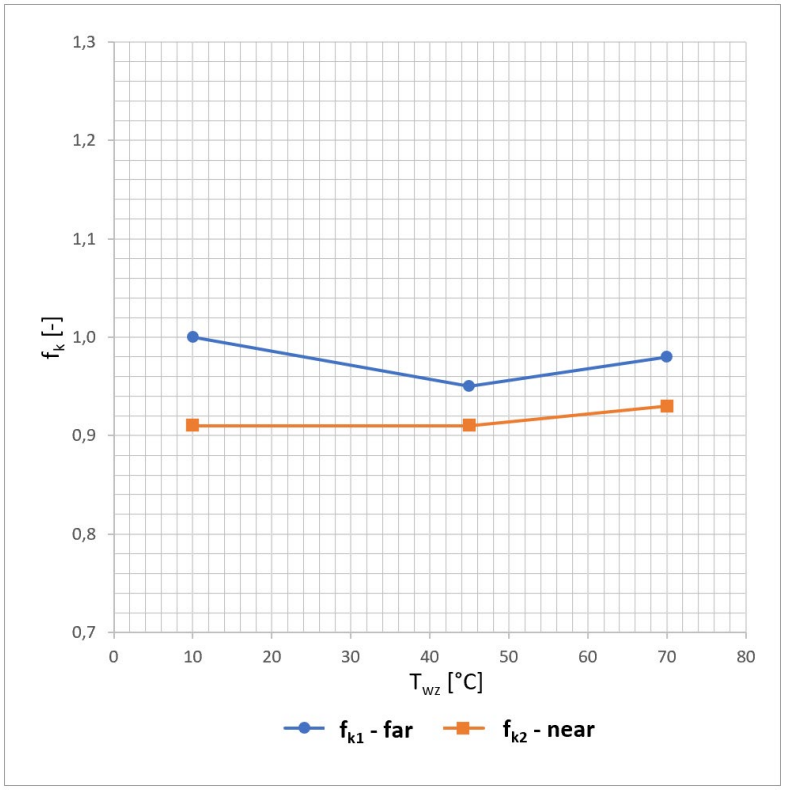

Fig. 7-27: Stack box stretching factor as a function of mould surface temperature at Investigation Points 1 and 2

The findings from the investigations of far and near volumetric filling for the multidimensional case prove the amendments to the assumptions made in Section 7.6. For further investigation, the step plate is examined at event locations far from and near to the volumetric filling. According to theory, for the one-dimensional case, the variation of the volume flow would only have linear dependency; the variation of the temperatures would have no effect on the stretching factors, regardless of how far or near the event occurs before volumetric filling.

7.7.2 One-Dimensional Case – Investigation of Far and Near Volumetric Filling

The step plate is examined at event locations far from and near the volumetric filling. If the aforementioned assumptions are correct, in contrast to the stack box, the variation of the volume flow would only have linear dependency; the variation of the temperatures would have no effect on the stretching factors, regardless of how far or near the event occurs before volumetric filling.

As the analysis in Section 7.4.3 has demonstrated, the real event patterns of the step plate consist of $m = 6$ events ($E_{mach\ 0}$ … $E_{mach\ 5}$), and the form part-specific event patterns consist of $n = 4$ events ($E_{sim\ 0}$ … $E_{sim\ 3}$). The matching algorithm provides the best matching for the patterns of the step plate at a displacement of $j_{min} = 1$. As Fig. 7-28 demonstrates, in total, four virtual events $E_{sim\ i}$ can be assigned to four real events, $E_{mach\ i+j}$ ($E_{sim\ 0}$ to $E_{mach\ 1}$, $E_{sim\ 1}$ to $E_{mach\ 2}$, …). The two real events, $E_{mach\ 0}$ and $E_{mach\ 6}$, have no corresponding virtual events.

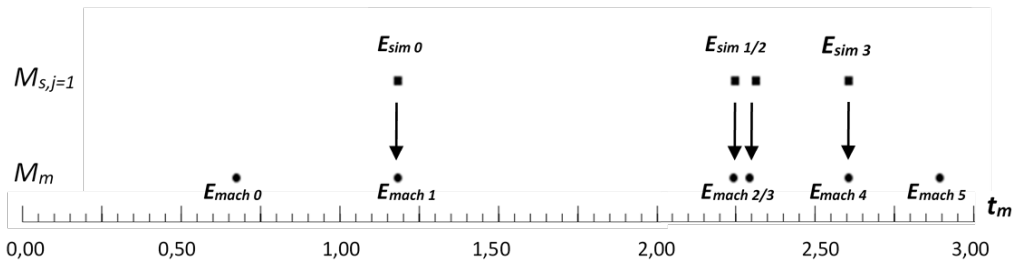

Fig. 7-28: Step plate assigning of transformed and displaced virtual events

Fig. 7-29 presents a visualisation of the melt front at a volume flow of 15 cm^3/s (standardised boundary condition, obtained from the CAE simulation software). The filling pattern is set to the superimposed event points $E_{sim\ 0}$ -> $E_{mach\ 1}$ and shows the melt front hitting the upper front plate of the cavity after it passed through the sprue bar. This event location, denoted as Investigation Point 1, is aimed at examining events that tend to be *far* from the volumetric *filling* of the step plate.

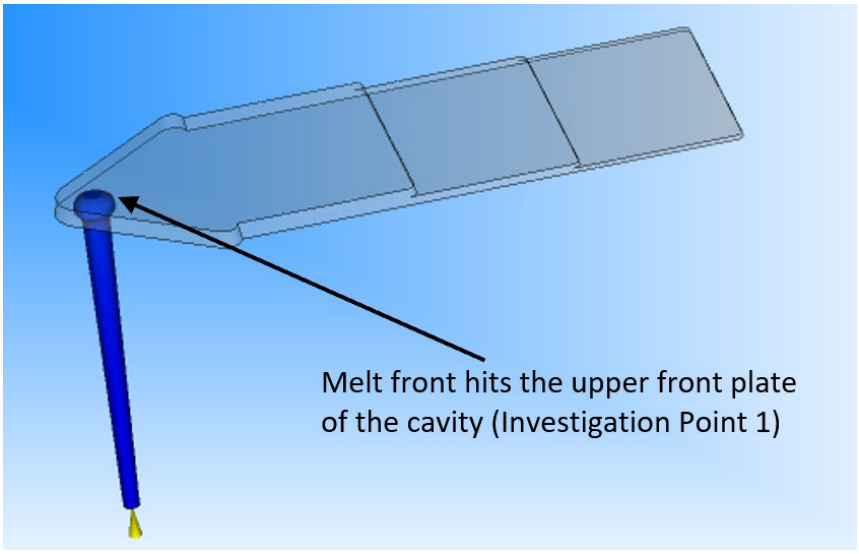

Fig. 7-29: Simulation result of the flow pattern of the stack box at event $E_{mach\ 1}$ (Investigation Point 1; volume flow of 15 cm^3/s)

As Fig. 7-30 shows, the filling pattern is set to the superimposed event points $E_{sim\ 3}$ -> $E_{mach\ 4}$. At this event location, denoted below as Investigation Point 2, the melt front passes the second change in the cross section towards the flow direction. At Investigation Point 2, events are examined that tend to be *near* the volumetric *filling* of the moulded part.

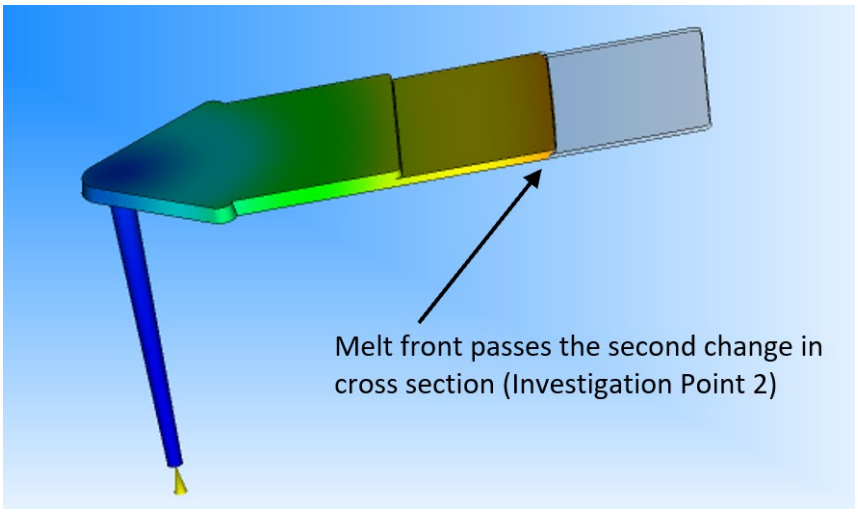

Fig. 7-30: Simulation result of the flow pattern of the stack box at event $E_{mach\ 4}$ (Investigation Point 2; volume flow of 15 cm^3/s)

As with the stack box, all events that are *not* located at Investigation Points 1 (far) or 2 (near) are alternately removed from the event patterns. This procedure is demonstrated in Fig. 7-31 and Fig. 7-32. Fig. 7-31 shows an examination of the pattern matching at Investigation Point 1 (far from volumetric filling). First, all events close to the volumetric filling are removed (symbolised by X). After removing the events, the patterns are matched, and the remaining events are assigned by linear transformation. The assessment is repeated for every variation of the boundary conditions. After removing all events close to the volumetric filling, each pattern consists of only two events; therefore, the matching is performed with the smallest total pattern deviation $S_{min} = 0$.

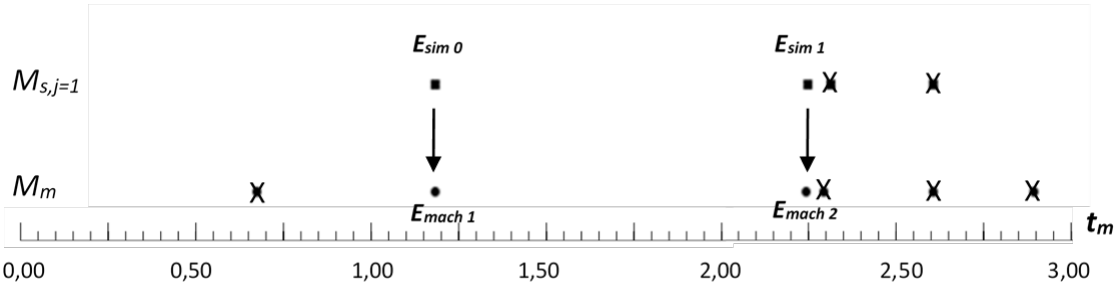

Fig. 7-31: Step plate events at Investigation Point 1

Similarly, the pattern matching is examined at Investigation Point 2 (near volumetric filling). As Fig. 7-32 demonstrates, all events far from the volumetric filling are removed (symbolised by X). After removing the events, the patterns are matched, and the remaining events are assigned by linear transformation. The assessment is repeated for every variation of the boundary conditions of volume flow, mould surface, and melt temperature. With this approach, for each investigation point—far from and near to the volumetric filling—the influence of the boundary conditions on the stretching factor can be examined individually.

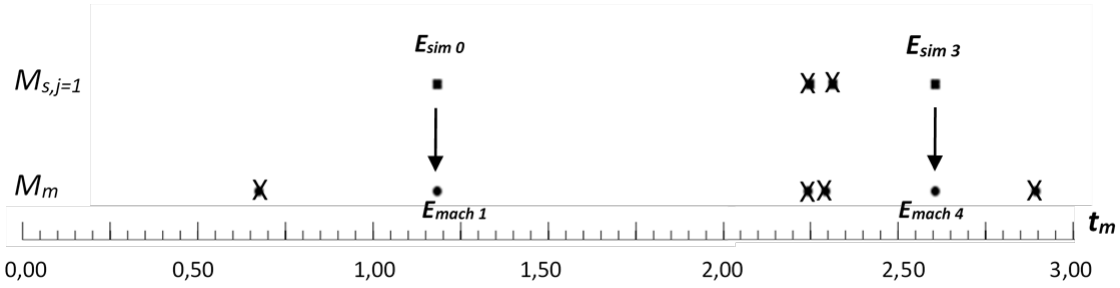

Fig. 7-32: Step plate events at Investigation Point 2

Resulting from the assessment, Fig. 7-33 demonstrates that, in contrast to the stack box, the variations of the volume flow only have linear dependency regardless of how far or near the event occurs before volumetric filling. Regardless of how far or near the investigation point is in relation to the volumetric filling, at the time the events occur, the injected volume is constant and independent of the boundary conditions. The results in Fig. 7-34 and Fig. 7-35 reveal that the variations of the temperatures have no effect on the stretching factors regardless of how far or near the event occurs before volumetric filling.

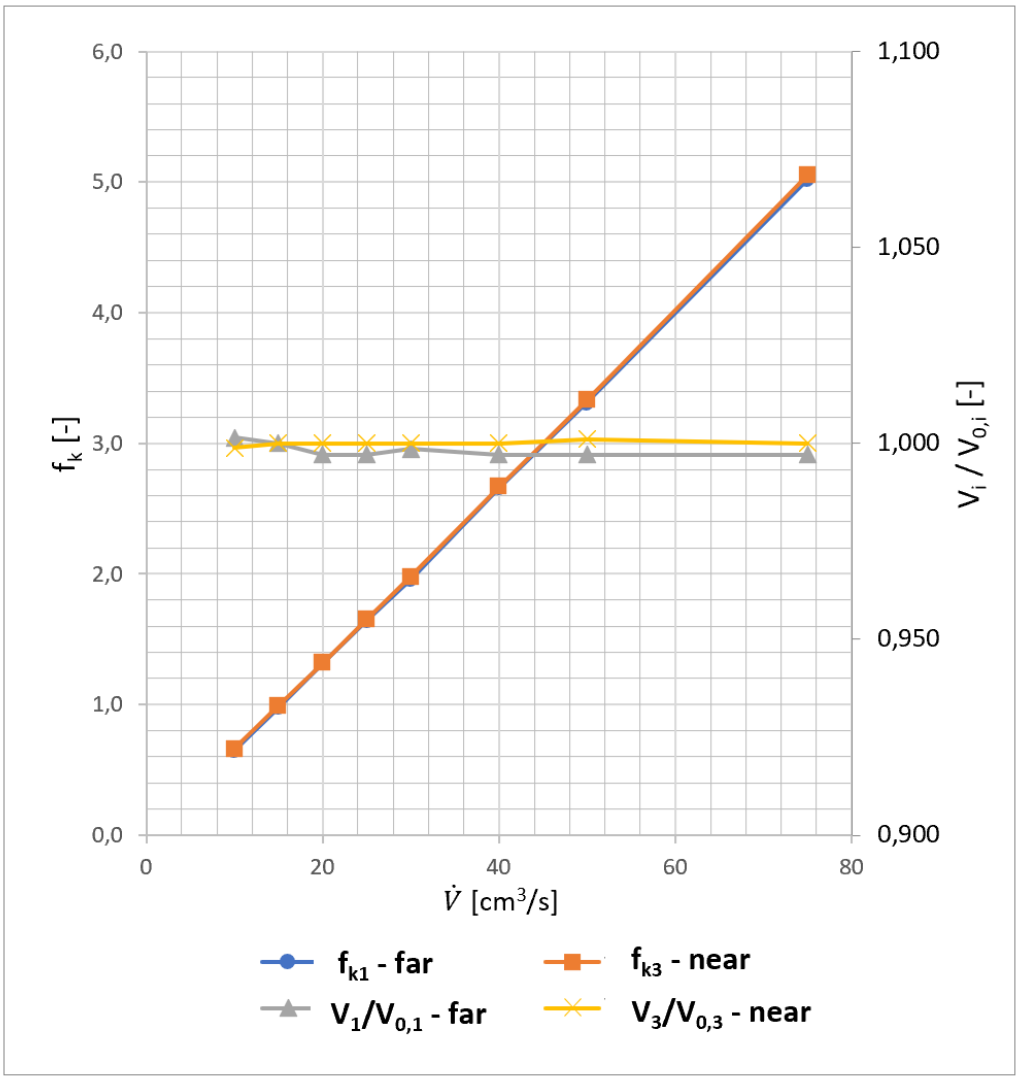

Fig. 7-33: Step plate stretching factor and partial volume as a function of volume flow at Investigation Points 1 and 2

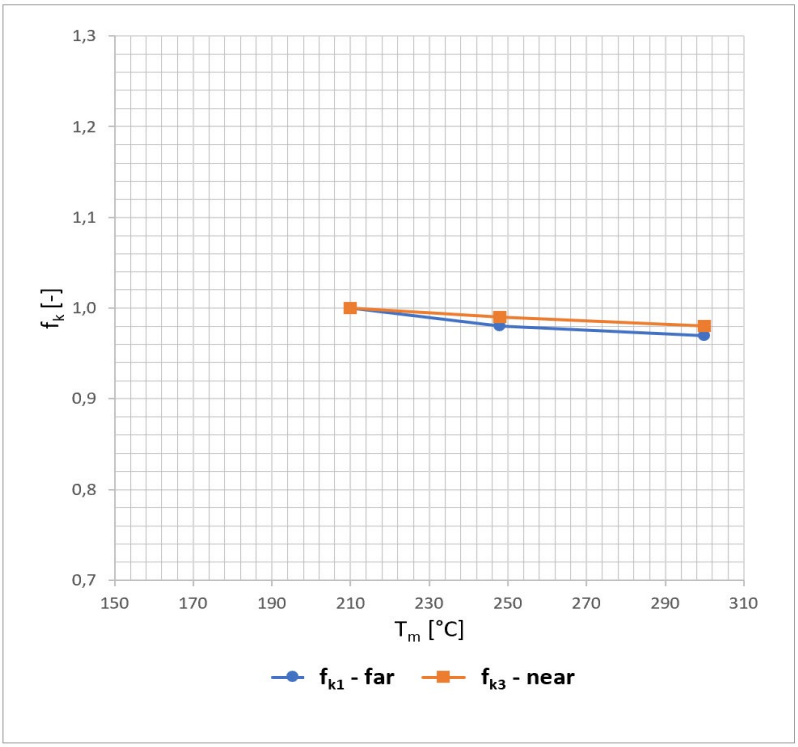

Fig. 7-34: Step plate stretching factor as a function of melt temperature at Investigation Points 1 and 2

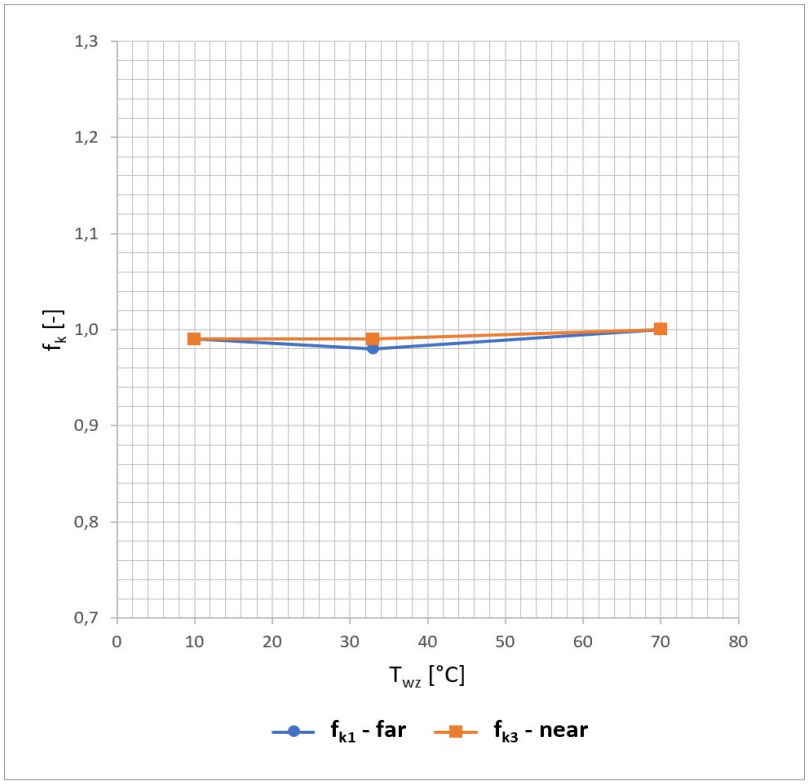

Fig. 7-35: Step plate stretching factor as a function of mould temperature at Investigation Points 1 and 2

7.7.3 Discussion of Far and Near Volumetric Filling

The results of the investigation of far and near volumetric filling for the multidimensional case indicate the following:

- The stretching factor at event sites near the volumetric filling has proportional dependency on the volume flow, whereas the stretching factor at event sites far from the volumetric filling is not proportional to the volume flow.
- If an event occurs with increasing distance from the volumetric filling, the effect of the melt or mould surface temperature on the stretching factor increases.

The findings from the investigations of far and near volumetric filling for the one-dimensional case suggest the following:

- The variations of the volume flow have a linear dependency on the stretching factor regardless of how far or near the event occurs before volumetric filling.
- The variations of the mould surface and melt temperatures have no effect on the stretching factors, regardless of how far or near the event occurs before volumetric filling.

The results prove the amendments to the assumptions made in Section 7.6 and lead to the following conclusion: The matching method robustly matches form part-specific and real event patterns and assigns virtual and real events using a matching algorithm with linear transformation, as in the cases below.

1. Case: The moulded part has a geometry or is injected in a way the mould filling approximates the idealised one-dimensional flow; or

2. Case: The moulded part fills multidimensionally, and the injection occurs under conditions where the setting parameters of the injection moulding machine are similar or identical to the boundary conditions of the simulation; or

3. Case: The moulded part fills multidimensionally and has a number of event locations and events that occur a short distance and time before the volumetric filling of the cavity.

In practice, it can be assumed that injection moulding operations have relatively ‘small process windows’. In other words, in real operations, it is not likely that the setting parameters of the injection moulding machine will deviate significantly from the boundary conditions used for the simulation (Case 2). However, for the unusual case that the setting of the injection machine largely differs from the boundary conditions with which the simulation was performed, the respective form part may only require one event location near the volumetric filling for robust matching with a linear transformation (Case 3). This demonstrates that matching with linear transformation covers nearly the entire range of practical applications. It can be concluded that the matching algorithm proposed in Section 4.8 with a linear transformation is a suitable method for mapping a simulated and a real injection process.

7.8 Proposition of a Generic Method for Non-Linear Pattern Matching

The previous part of this chapter demonstrates that matching with linear transformation covers a wide range of potential practical applications. For robust matching, a moulded part that fills multidimensionally may only need one significant event that occurs a short time before the volumetric filling. In this case, and with linear matching, the reliable assignment of real and virtual events is guaranteed, even with large deviations in the parameter settings and boundary conditions of the simulated model. The analysis and evaluation suggest that a matching method with other than linear transformation method is only necessary for applications with large deviations between machine settings and boundary conditions, which simultaneously have only event locations far from the volumetric filling. Such a situation, however, could be avoided using real time simulation (from cycle to cycle) of the injection moulding process with constant

adaptation of the boundary conditions to the changing setting parameters of the injection moulding machine.

A matching procedure would be generic if its transformation algorithm could consider the influence of changed boundary conditions or changed parameter settings. Such a generic matching method would only be used if (a) the moulded part fills multidimensionally, (b) the boundary conditions of the simulation deviate strongly from the setting parameters of the injection moulding machine, and (c) the part only has significant events that occur long before the volumetric filling (based on total filling time). With the help of a generic matching method, a single form part-specific event pattern could be permanently assigned to a real event pattern that changes from injection cycle to injection cycle. This would occur regardless of how the physical injection moulding process is set or how much the boundary conditions used for the simulation deviate from the machine setting. A generic matching method would use an algorithm for the transformation of the pattern that considers both (a) the non-linear dependency of the volume flow and (b) the effect of other boundary conditions such as melt and mould surface temperature.

Assuming that there will be no real-time simulation (simulation from cycle to cycle) of the injection moulding process in the foreseeable future for avoiding large deviations between machine settings and boundary conditions, a generic matching procedure—in the sense of the complete coverage of all possible practical cases—would be desirable. This chapter addresses such a requirement by proposing and developing a generic matching method. The proposed matching method contains a non-linear matching algorithm and is calibrated and tested for the case of ‘multidimensional filling under the variation of the volume flow’. If the modified method results in residuals (deviations of the patterns) that are significantly reduced compared with the linear transformation method, then this would indicate that the robustness of the proposed generic matching process and the reliable assignment of events are even better than those of the linear model.

7.8.1 Proposition of the Generic Method from the Linear Model

In the matching method with linear transformation proposed in Section 4.8, the events in the form part-specific event pattern M_s are transformed. For each transformation, a new pattern M_k is calculated from the pattern M_s, and the alignment of the calculated new pattern with the real event pattern M_m is attempted. For this purpose, virtual events of the form part-specific event pattern are multiplied by the scaling factor f_k in Equation (7-5), and the differences in time for the scaled virtual events are then calculated. This process is repeated k times with an incremented stretching factor f_k until the algorithm has determined the smallest (pattern) deviation of all transformations $S_{min,k}$ and recorded it at the iteration k_{min}.

$$E_{k,i} = f_k \cdot E_{sim\,i} \tag{7-5}$$

Through the transformation, the linear influence of the volume flow on the event times can be compensated. All other effects on the event times, such as the influence of the mould surface and melt temperature, are not considered.

7.8.1.1 Analysis of Non-Linear Volume Flow

The results from the investigation of far and near volumetric filling in Section 7.7 have revealed that for single events located far from the volumetric filling, a non-linear dependency of the volume flow can occur. A generic matching method can consider these non-linear influences. For this purpose, the stretching factor f_k is divided into a linear component

$$f_{k\dot{V}\,lin} \tag{7-6}$$

and a non-linear component:

$$f_{k\dot{V}\,nlin}(\mathcal{F}_{\dot{V}}) \tag{7-7}$$

The non-linear component $f_{k\dot{V}\,nlin}$ is defined as a function of $\mathcal{F}_{\dot{V}}$, which is used to express the magnitude of the relative deviation of the volume flow $\mathcal{R}_{\dot{V}}$ to the standardised volume flow $\mathcal{R}_{\dot{V}0}$, as in Equation (7-8).

$$\mathcal{F}_{\dot{V}} = \frac{|\mathcal{R}_{\dot{V}0} - \mathcal{R}_{\dot{V}}|}{\mathcal{R}_{\dot{V}0}} \tag{7-8}$$

The results in Section 7.7.1 support the assumption that at standardised boundary conditions (those identical to the setting of the injection moulder), a non-linear influence of the volume flow on the stretching factor—and thus the non-linear component of the stretching factor—does not exist. This implies that the stronger the relative deviation of the volume flow between the real and virtual cases, the stronger the non-linear influence of the volume flow on the event times. This results in a first generic (non-linear) transformation for the volume flow:

$$E_{k,i} = f_{k\dot{V}\,nlin}(\mathcal{F}_{\dot{V}}) \cdot f_{k\dot{V}\,lin} \cdot E_{sim\,i} \tag{7-9}$$

7.8.1.2 Analysis of Melt and Mould Surface Temperature

As discussed in Section 7.7.1, for events located far from the volumetric filling point, effects of melt and mould surface temperature on the stretching factor can appear. The results in Section 7.7.1 suggest that the stronger the relative deviation of the melt and mould surface temperature between the real and simulated cases, the stronger the effect of the temperatures on the event times. Similar to the volume flow, the effect of temperature increases with the strength of the relative deviation between the virtual and real event patterns. This results in a first generic (non-linear) transformation for the mould surface and melt temperature.

As with volume flow, a non-linear component of the stretching factor is defined for each condition, namely melt and mould surface temperature, in Equations (7-10) and (7-11).

$$f_{km\,nlin}(\mathcal{F}_m) \tag{7-10}$$

$$f_{kwz\ nlin}(\mathcal{F}_{wz}) \tag{7-11}$$

The non-linear components are functions of $\mathcal{F}_{\mathrm{m}}$ in Equation (7-12) and $\mathcal{F}_{\mathrm{wz}}$ in Equation (7-13), namely, the relative size of the deviation of the real and virtual mould surface and melt temperatures, respectively.

$$\mathcal{F}_m = \frac{|\mathcal{R}_{m0} - \mathcal{R}_m|}{\mathcal{R}_{m0}} \tag{7-12}$$

$$\mathcal{F}_{wz} = \frac{|\mathcal{R}_{wz0} - \mathcal{R}_{wz}|}{\mathcal{R}_{wz0}} \tag{7-13}$$

7.8.1.3 Discussion of the Generic Transformation Method

The generic transformation for the volume flow expressed in Equation (7-9) extended by the non-linear components for the melt, as in Equation (7-10), and mould surface temperature, as in Equation (7-11), results in the general form of the generic transformation:

$$E_{k,i} = f_{k\dot{V}\ nlin}(\mathcal{F}_{\dot{V}}) \cdot f_{k\dot{V}\ lin} \cdot f_{km\ nlin}(\mathcal{F}_m) \cdot f_{kwz\ nlin}(\mathcal{F}_{wz}) \cdot E_{sim\ i} \tag{7-14}$$

In contrast to the linear transformation in Equation (7-5), the generic transformation comprises the non-linear components for each condition such as volume flow, mould surface, and melt temperature (presented in red type). These components are functions of the relative size of the deviation of the real and virtual conditions.

To apply the generic transformation method, the non-linear components must be determined individually for the respective form part. The non-linear components are determined to calibrate the general form of the generic transformation method, as expressed in Equation (7-14), to the application of a specific form part. The calibration is conducted using the method for events at locations assigned individually, and the stretching factors are analysed when the non-linearity of the volume flow or the effects of the temperature boundary conditions are expected, as proposed in Section 7.7.1. The procedure for the calibration is developed in

Section 7.8.2. In Section 7.8.3, for the application of the stack box, the non-linear matching is calibrated and tested for the case of multidimensional filling under the variation of the volume flow.

7.8.2 Calibration of the Generic Transformation Method

Before generic matching can be performed, the transformation algorithm must be calibrated. This means that all the non-linear components of the stretching factor from Equation (7-14) must be determined for a specific form part, and the matching algorithm is modified by the determined components. The calibration is applied to all event locations of the specific form part where non-linear effects are expected. The method developed in Section 7.7 is used for the calibration, where events at locations are assigned individually and the stretching factors are analysed when non-linearity of the volume flow or effects of the temperature boundary conditions are expected.

The procedure for calibrating a generic matching algorithm to a specific form part application is illustrated in Fig. 7-36 and described in the individual steps below:

1. The simulation of the form part and analysis of the form part-specific pattern with standardised boundary conditions (same or similar to the expected setting of the injection moulding machine).

2. The performing of a single injection moulding process with setting parameters identical (or similar) to the boundary conditions of the simulation, and analysis of the real event pattern.

3. The first initial matching of the patterns and the assignment of the events.

4. The evaluation of the event locations and assessment for non-linearity.

5. The simulation and analysis of form part-specific event patterns under the variation of the boundary conditions.

6. The events at locations are assigned individually and the stretching factors are analysed when non-linearity of the volume flow or effects of the temperature boundary conditions are expected.

7. For the volume flow: dividing of the stretching factors into linear and non-linear components.

8. The determination of the non-linear components of the stretching factor for the respective boundary conditions by non-linear regression and calibration of the matching algorithm through insertion of the function parameters.

The underlying concept of developing a new non-linear matching procedure (as described in Section 7.3.7) clearly results in the necessity of a ‘first initial’ (linear) model as a basic requirement for the development and calibration of the new one (Step 3). Only after the initial matching and the qualitative and quantitative assessment of the event locations for non-linearity can the determination of the non-linear components of the stretching factor in Equation (7-14)—and thus the calibration of the generic method to a specific form part application—be conducted.

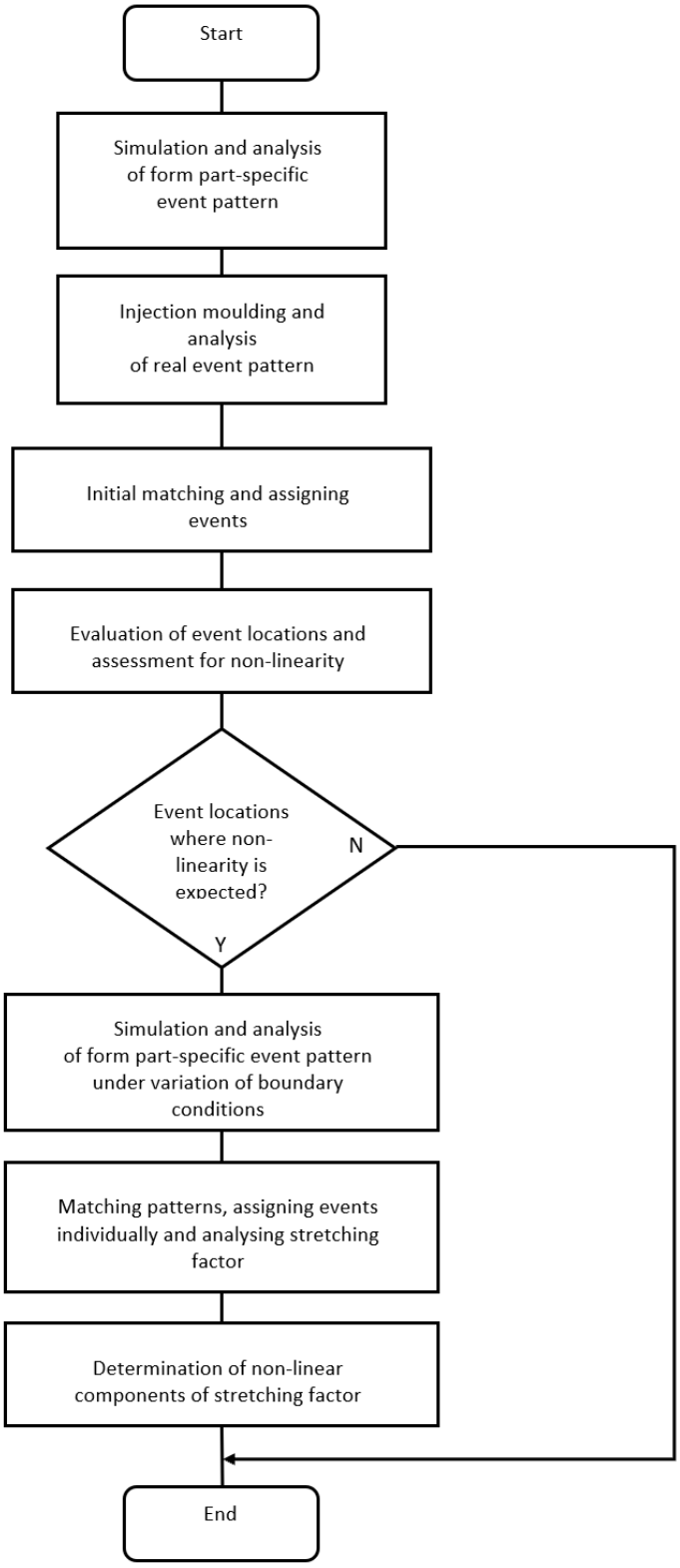

Fig. 7-36: Procedure for calibrating a generic matching algorithm to a specific form part

7.8.3 Application of the Proposed Method for Non-Linear Pattern Matching

With the data obtained from the investigation in Section 7.7.1 for the application of the stack box, the non-linear matching is calibrated and tested for the case of multidimensional filling under the variation of volume flow.

As illustrated in Fig. 7-23, event $E_{sim\ 1}$ (Investigation Point 1) is a candidate for a non-linear transformation due to its remote location (far from volumetric filling). In Section 7.7.1, Investigation Point 1 has been assessed and the stretching factor has been analysed for every variation of the boundary conditions. Table 7-7 presents the stretching factor f_{k1} determined in Section 7.7.1 for Investigation Point 1 as a function of the volume flow.

Table 7-7: Stack box stretching factor as function of volume flow at $E_{sim\ 1}$

$\dot{V}$ [cm³/s]	f_{k1} [-]
10	0.47
15	0.67
25	0.95
30	1.19
40	1.52
50	1.92
75	2.88

To calibrate the matching algorithm for the volume flow, f_{k1} is divided according to Equation (7-9) into a linear component $f_{k1\ lin}$ and a non-linear component $f_{k1\ nlin}$. From Equations (7-5) and (7-9), it follows that:

$$f_{k1\ nlin} = \frac{f_{k1}}{f_{k1\ lin}} \tag{7-15}$$

The non-linear component $f_{k1\ nlin}$ can be determined if the linear component $f_{k1\ lin}$ is known. The results from the investigation in Section 7.7.1 support the

assumption that at standardised boundary conditions (those identical to the setting of the injection moulder), the volume flow has a solely linear effect on the stretching factor. Based on this assumption, for a volume flow of 25 cm^3/s (the standardised boundary condition of the stack box) the linear part of the stretching factor is set to $f_{k1\ lin} = 1$ (Table 7-8, presented in red type). According to the theory, a linear stretching factor $f_{k1\ lin}$ of 1 means that the event patterns are determined under the same simulated boundary conditions as the real process, that the simulated patterns and the real patterns are identical, and matching without transformation (i.e., without stretching or shrinking the pattern) is possible. For all others than the standardised volume flow, the linear components are set to their proportional share in relation to the standardised volume flow. For example, with a simulated flow rate of 50 cm^3/s (presented in green type), the injection speed in the simulation is twice as high as in the real injection moulding test and thus twice as high as the standardised boundary condition. Assuming that the volume flow has a solely linear influence on the stretching factor, all simulated events occur in half the time compared with the real events. To match the pattern, the form part-specific pattern must be transformed by a stretching factor of 2. As a result, the linear component of the stretching factor is set to $f_{k1\ lin} = 2$ for a volume flow of 50 cm^3/s. According to Equation (7-15), with both the stretching factor f_{k1} (determined in Section 7.7.1) and the linear component $f_{k1\ lin}$, the non-linear component of the stretching factor $f_{k1\ nlin}$ can be determined.

Table 7-8 lists the entire linear part $f_{k1\ lin}$ of the stretching factor set to its proportional share in relation to the standardised volume and also presents the non-linear components of the stretching factor of the stack box at Investigation Point 1.

Table 7-8: Stack box linear and non-linear components of the stretching factor as a function of volume flow at $E_{sim\ 1}$

$\dot{V}$ [cm³/s]	f_{k1} [-]	$f_{k1\ lin}$ [-]	$f_{k1\ nlin}$ [-]
10	0.47	0.40	1.18
15	0.67	0.60	1.12
25	0.95	1.00	0.95
30	1.19	1.20	0.99
40	1.52	1.60	0.95
50	1.92	2.00	0.96
75	2.88	3.00	0.96

Through the analysis of the non-linear part, the generic matching algorithm for the volume flow can be fully calibrated to the application of the stack box. For this purpose, the non-linear components $f_{k1\ nlin}$ from Table 7-8 are plotted as a function of the volume flow and approximated by means of non-linear regression. Fig. 7-37 presents the plot of the non-linear components of the stretching factor as a function of the volume flow (red symbols) for the stack box.

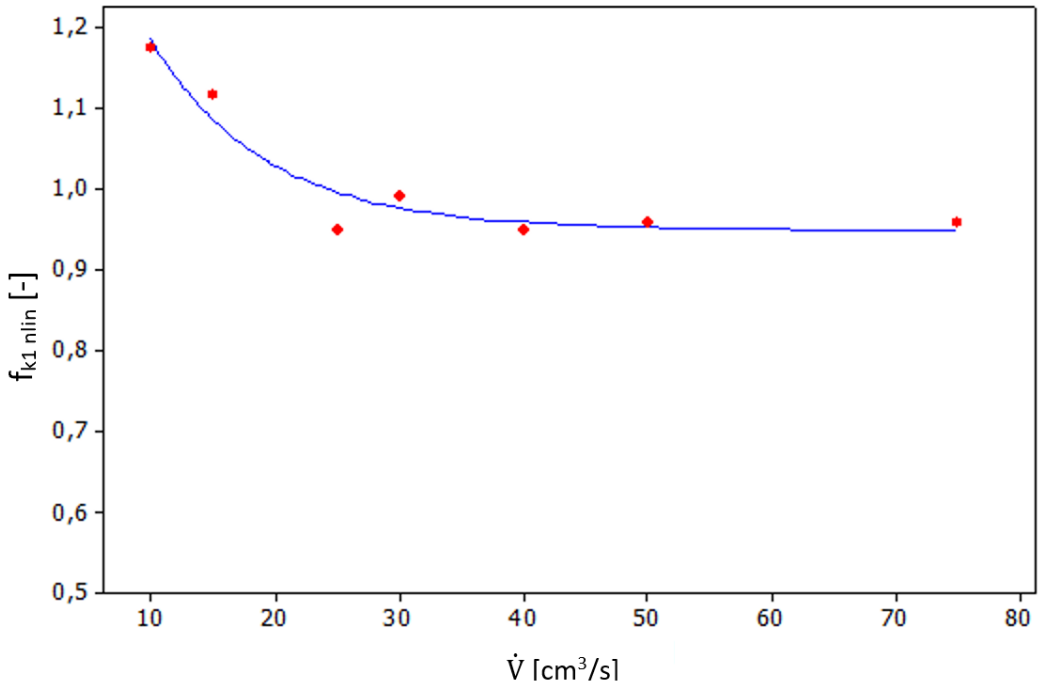

Fig. 7-37: Stack box non-linear component of the stretching factor at event E_{sim1}

To approximate the non-linear part of the stretching factor as a function of volume flow, a non-linear regression is conducted using a model of the type 'A * EXP (B * X') + C' in the program MINITAB 16. This yields the following non-linear relationship:

$$f_{k1\dot{V}\,nlin} = 0.7 \cdot e^{-0.11\dot{V}} + 0.95 \tag{7-16}$$

This relationship is plotted as a blue graph in Fig. 7-37.

With the Equations (7-9) and (7-16), the non-linear transformation for the application stack box can be expressed as follows:

$$E_{k,1} = (0.7 \cdot e^{-0.11\,\dot{V}} + 0.95) \cdot f_{k\dot{V}\_lin} \cdot E_{sim\,1} \tag{7-17}$$

Thus, for the case study stack box, the algorithm for the generic (non-linear) transformation is fully determined. To validate the non-linear transformation, the matching algorithm proposed in Section 4.8 is modified and calibrated by the non-

linear relationship expressed in Equation (7-17) and then tested.

7.8.4 Discussion and Evaluation of the Non-Linear Pattern Matching

Fig. 7-38 is already known from the discussion in Section 7.5.2. The figure presents the results of the evaluation of pattern matching with linear transformation for the multidimensional case. The smallest total deviation of the pattern S_{min} is plotted as a function of the volume flow. The mean value of the graph is $3.2 \cdot 10^{-3}$ s and has a standard deviation of $4.8 \cdot 10^{-3}$ s. As discussed in Section 7.5.2, the overall relatively small values of the pattern deviation (in the order of 10^{-3} s) imply the high consistency of the patterns due to linear transformation and thus robust matching.

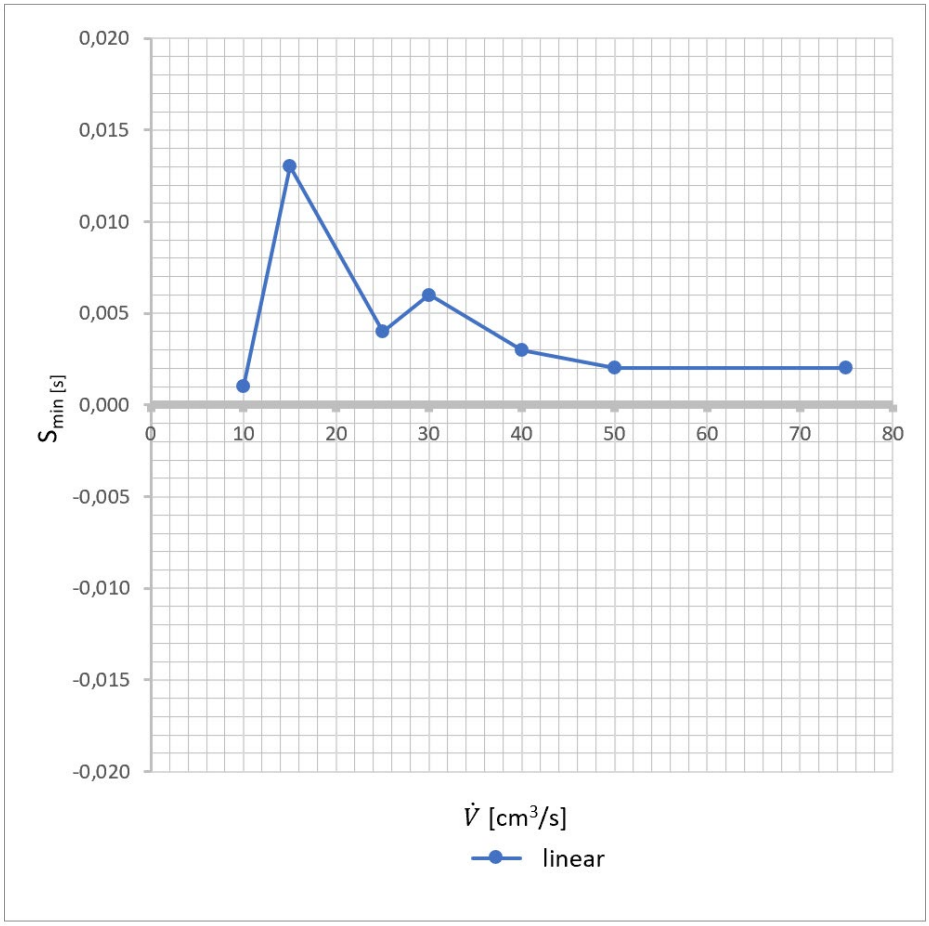

Fig. 7-38: Linear matching algorithm: Stack box deviation of the patterns as a function of volume flow

To validate the non-linear transformation, all patterns are matched, and virtual and real events are assigned using the non-linear modified version of the matching algorithm (determined in Section 7.8.3). For an evaluation of the results, the pattern deviation of the non-linear matching is compared with the pattern deviation of the linear matching. Fig. 7-39 presents the total deviation of the event patterns as a function of the volume flow for both the linear and non-linear matching. The mean value of the non-linear pattern deviation is $2.7 \cdot 10^{-3}$ s and has a standard deviation of $2.5 \cdot 10^{-3}$ s. The non-linear method yields residues and standard deviation is reduced by half compared with the linear matching. This comparison suggests that in certain cases the robustness of the generic matching method with non-linear transformation is even more robust than that of the linear model. In particular, this is the case if large deviations occur between the setting parameters of the injection moulding machine and the boundary conditions required for the simulation, and if the form part only has significant events that take place long before the volumetric filling (based on total filling time).

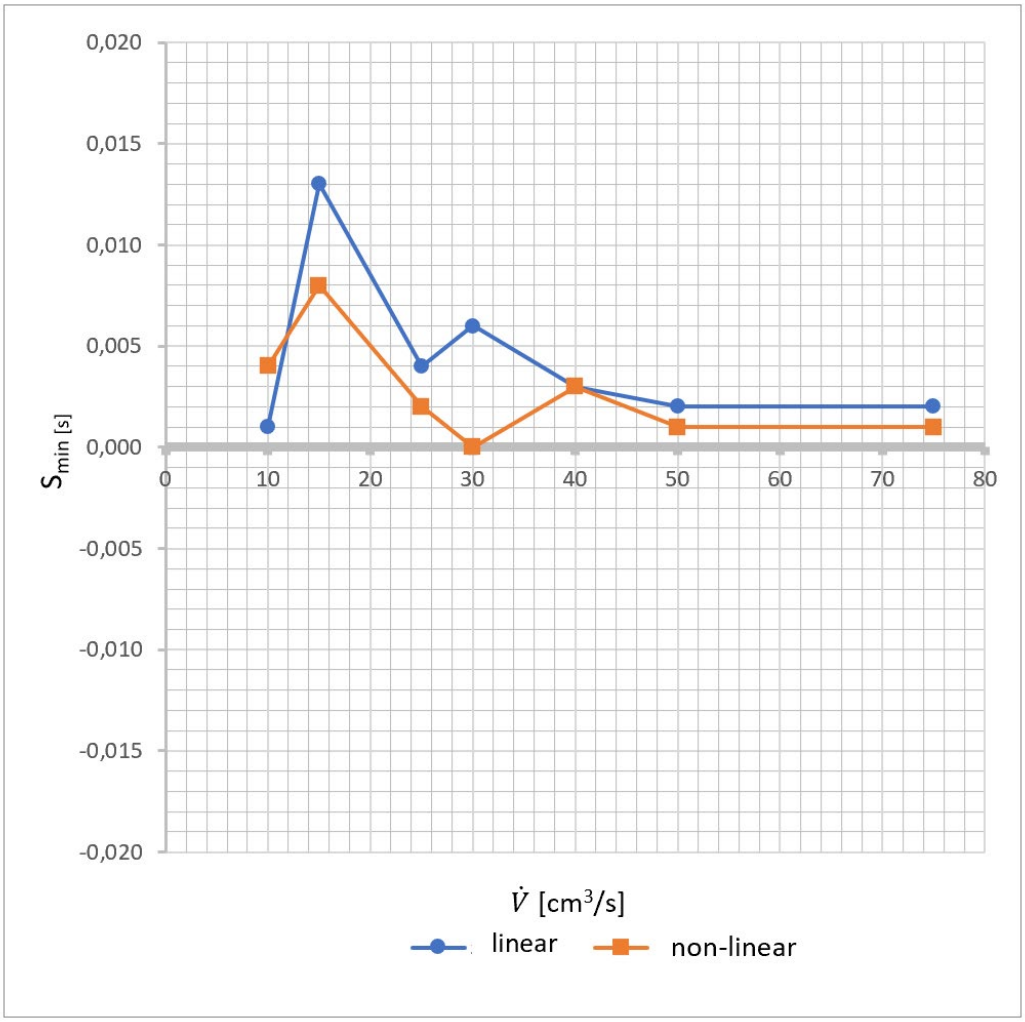

Fig. 7-39: Comparison between linear and non-linear matching algorithm: Stack box deviation of the patterns as a function of volume flow

7.9 Chapter Summary

This chapter has assessed the functional requirements of matching methods for the robust matching of event patterns and reliable assignment of events as well as investigated pattern matching methods. For this purpose, comparative real and simulated experiments have been conducted under the variation of boundary conditions such as volume flow, mould surface, and melt temperature.

The results of the experimental investigations have demonstrated that the matching algorithm with a linear transformation proposed in Section 4.8 is a suitable method for mapping a simulated and a real injection process. In addition

to the simplicity of the proposed matching algorithm with linear transformation, ‘a large part’ of all possible practical applications can be covered by linear matching. A robust pattern matching of a form part that fills multidimensionally may only require one significant event location that occurs a short distance from the volumetric filling. In this case, the assignment of real and virtual events is still guaranteed if the injection moulding process and simulated model differ.

In summary, the assessment of the functional requirements of matching methods and the experimental investigation of pattern matching methods have demonstrated the following:

1. A basic requirement for the matching algorithm is that it applies functional methods to match pattern fragments, assign subsets of events, and eliminate events caused by interference.

2. The matching algorithm must be able to continuously match and assign form part-specific event patterns to (between the cycles constantly altering) real event patterns.

3. The new matching algorithm proposed in Section 4.8 with linear transformation is a suitable candidate for the mapping of simulated and real injection processes.

4. A moulded form part that fills multidimensionally for robust mapping often requires only one significant event location, occurring a short distance from the volumetric filling.

5. The reliable assignment of real and virtual events is guaranteed even if the injection moulding process and simulated model differ greatly, for example, due to different parameter settings.

6. A large portion of all possible practical applications is covered by the matching algorithm with linear transformation.

A matching procedure would be *generic* if its transformation algorithm could

consider the influence of changed boundary conditions in the simulation or changed parameter settings of the injection moulding machine. With the help of a generic matching method, a single form part-specific event pattern could be permanently assigned to a real event pattern that changes from injection cycle to injection cycle. This would occur regardless of how the physical injection moulding process is set or how much the boundary conditions used for the simulation deviate from the machine setting.

The results presented in this chapter suggest that a generic matching method is only necessary for moulded parts with a large deviation between machine settings and boundary conditions, which simultaneously have only event locations far from the volumetric filling. However, to fully cover all possible practical cases, such a generic method is proposed and developed. The new matching method is tested for the case of 'multidimensional filling under the variation of the volume flow'. For non-linear pattern matching, the matching algorithm proposed in Section 4.8 is modified and calibrated for the application of the stack box using the non-linear components of the stretching factor for the volume flow. All patterns are matched, and virtual and real events are assigned using the non-linear modified version of the matching algorithm. For the evaluation, the pattern deviations of the non-linear matching are compared with the pattern deviations of the linear matching method. The results from the evaluation suggest the following:

1. In certain cases, the generic matching method matches event patterns and assigns events more robustly (with a smaller total deviation) than its linear counterpart.

2. In particular, this can be expected if large deviations occur between the setting parameters of the injection moulding machine and the boundary conditions required for the simulation and analysis of the form part-specific event pattern.

3. For the multidimensional application of the stack box, the developed non-linear method yields residues and standard deviation reduced by half compared with the linear matching.

4. The ‘qualification’ or ‘suitability criteria’ of the proposed generic (non-linear) matching method is based on its consideration of both the non-linearity of the volume flow and the effects of other boundary conditions in all conceivable practice-relevant applications.

5. The non-linear method is complex and requires calibration through numerous simulations at different boundary conditions.

6. Moreover, the underlying concept of developing a new non-linear matching procedure (as described in Section 7.3.7) clearly implies the need for the existence of a ‘first initial’ (linear) model as a basic requirement for the development and calibration of the new one.

8 CONCLUSIONS AND FURTHER WORK

8.1 Primary Achievements

For any given injection moulding process, it is not possible to reasonably determine the flow front position or velocity of the melt in relation to the screw position of the injection moulding machine. To solve this problem, the overall aim of this project is to propose, design, and develop an innovative and generic method for an advanced process control strategy based on the idea of mapping a simulated filling process to a real injection moulding process using only a single pressure sensor. This aim has been achieved. Two case studies have provided the necessary evidence that the new method is effective at determining the flow front position and resulting flow front velocity of the melt on the entire flow path.

Following the initially formulated research objectives (RO), the main achievements of this thesis are as follows:

The literature review has revealed that:

1. For the direct determination of the melt front, several approaches for developing methods to measure the flow front velocity have been made.
2. These direct measurement methods comprise techniques for directly obtaining the flow front position through capacitive sensors or combinations of pressure and temperature sensors inside the mould.
3. With this controller nearly all conceivable advanced control strategies, such as constant flow front velocity or constant melt viscosity, can be achieved.
4. Despite the good performance of the controller, the injection moulding industry is hesitant to switch to advanced control strategies based on machine-independent parameters.
5. The limitations lie not in the concept of the controller itself but rather in its input.
6. The most significant problem associated with the direct measurement method is that flow front position and all derived parameters, such as flow

front velocity and melt viscosity, can only be determined in the limited spaces between the two successive sensor positions; continuous measurement over the entire flow path is nearly impossible.

7. Other problems are associated with system design and form part quality: it is often too complicated to place more sensors in the limited space along the flow path, and the installation of the sensors significantly reduces the stiffness of the mould and the ability of the part surface to cool uniformly.
8. Equipping and retrofitting the mould is time consuming and expensive, so the direct measurement method is suitable to only limited practical applications.

The results from the experimental validation of the one-dimensional case and the multidimensional case have proven that:

1. In both the real injection moulding process and the simulated model of the injection process, singular events exist.
2. These events can reliably be identified by analysing the differentiated pressure graphs and applying the peak/flank analysis.
3. Singular events occur in the form of event groups.
4. The sequence of all events from both the real injection moulding process and the simulated model of the injection process can be analysed to identify patterns.
5. Through matching the patterns, virtual events can be assigned to real events. The assignment of the events allows the real event vectors to be expanded by components of the assigned virtual event vectors.
6. Through the assignment of the events, the relationship between the flow front position of the melt and the screw position of the injection moulding machine can be established.
7. Machine-independent parameters for advanced machine control—such as melt front velocity, wall stress, shear rate, and melt viscosity—can be determined.

The results from the analysis and evaluation of methods for pattern matching suggest that:

1. A basic requirement for the matching algorithm is that it applies functional methods to match pattern fragments, assign subsets of events, and eliminate events caused by interference.
2. The algorithm must be able to continuously match and assign form part-specific event patterns to real event patterns, which are constantly altering between the cycles.
3. The proposed new matching algorithm with linear transformation is a suitable candidate for the mapping of simulated and real injection moulding processes.
4. A large portion of all possible practical applications is covered by linear transformation.
5. A moulded form part that fills multidimensionally for robust mapping often only requires one significant event location, occurring a short distance from the volumetric filling.
6. The reliable assignment of the real and virtual events is guaranteed even if the injection moulding process and simulated model differ greatly, for example, due to different parameter settings.

The evaluation of the multidimensional application has provided evidence that:

1. A generic matching method for some exceedingly rare cases, where large deviations occur between the setting parameters of the injection moulding machine and the boundary conditions required for the simulation, can be proposed and designed.
2. The ‘qualification’ or ‘suitability criteria’ of the proposed generic (non-linear) matching method is based on its consideration of both the non-linearity of the volume flow and the effects of other boundary conditions in all conceivable practice-relevant applications.

3. The proposed generic matching method can match event patterns even more robustly, with a smaller total deviation, and thus align events even more reliably than its linear counterpart.

The results of the simulation analysis and experimental evaluation demonstrate that:

1. The proposed method is effective at determining the flow front position and resulting flow front velocity of the melt on the entire flow path.
2. No specific measuring devices (sensors) were used within the mould cavity to locate the melt front position during the filling phase in any of the experimental studies.
3. Only one single pressure sensor, located outside the mould, was required to determine the flow front velocity of the melt.
4. The new method offers great potential for rule-based setting of the injection moulding machine and advanced process control strategies based on machine-independent parameters, such as constant melt flow velocity or constant melt viscosity during the filling phase.
5. Because the method dispenses with any sensor technology within the mould, it can be used for any existing application without complex and expensive retrofits of existing moulds.
6. With the obtained parameters, the new method can be an essential component in the quest for autonomous injection moulding.

8.2 Contributions to New Knowledge Generation

From a theoretical perspective, the thesis has made the following contributions to new knowledge generation:

1. The thesis has critically reviewed current research activities and identified the research gaps in the areas of measurement and control of the melt front velocity and has investigated existing methods for directly

determining the melt front in injection moulding for advanced control strategies.

2. The thesis has analysed and evaluated real injection moulding processes and simulated models of the injection processes for identifying, determining, and isolating singular events from a measured or simulated pressure curve and describing them mathematically.

3. The thesis has proven that a number of virtual events can be assigned to a number of real events, and the relationship between the flow front position and the screw position can be established.

4. The thesis has proven that if the melt front position is known in relation to the injection time, then the relationship between flow front velocity and screw position can be established; thus, other machine-independent parameters—such as viscosity, shear rate, and wall shear stress—can be derived either at the event locations or continuously over the entire part geometry.

5. The thesis has examined matching methods and identified and analysed which functional requirements the matching algorithm must meet such that the event locations of the simulated filling process can be reliably assigned to the event locations of the real injection moulding process.

6. The thesis has analysed and evaluated the particular conditions under which the mapping of the simulated injection moulding process to the real injection moulding process can be conducted with the aid of a matching algorithm proposed in this thesis with linear transformation, even with ‘large’ deviations between the boundary conditions of the simulation and the setting parameters of the machine.

7. A new method for determining the flow front position and velocity of a plastic melt with only a single sensor and a generic (non-linear) matching method for the robust matching of moulded parts with a large deviation

between machine settings and boundary conditions have advanced the theoretical study in injection moulding.

The thesis has made the following contributions towards practical applications:

1. A new method for determining the flow front position and velocity of a plastic melt with only a single sensor can be applied to design practical injection moulding control strategies in industry.

2. A generic (non-linear) matching method can be utilised for the robust matching of moulded parts with a large deviation between machine settings and boundary conditions.

3. The proposed new method can be used to identify, analyse, and optimise machine-independent parameters for advanced process monitoring and advanced control strategy design and implementation.

4. The software and hardware developed can be used to determine process parameters for the purpose of an injection velocity profiling strategy through visualisation and an algorithm-based, advanced control strategy for injection velocity profiling and closed-loop control of the filling process on machine-independent parameters.

8.3 Limitations

Despite the contributions that this thesis has made to new knowledge generation, there are some limitations and areas where further research is required, which must be addressed. The limitations are due to the researcher's time and resource constraints and are discussed below:

The investigations in Sections 5.3.1.1 and 6.3.1.1 have revealed that with the solver used for the simulation of the pressure curve, a maximum resolution of 1,050 data points cannot be exceeded. Although this maximum resolution has not caused any limitations in the analysis of the pressure curve for the respective form part, such an upper limit leads to a fixed dependency of

resolution of the computed pressure curve and injection time. For larger form parts with long injection times in particular, this could be a limiting factor in the application of the new method and must be investigated. This would require an experimental design (DoE) in which the resolution of the pressure curve is investigated as an influencing factor on the analysability of the pressure curve with regard to the existence of events.

8.4 Further Work

Although the development and use of generative manufacturing processes has accelerated over proportionately in recent years, injection moulding is expected to remain the dominant process for the mass production of plastic parts for the foreseeable future. As in the entire industry, this manufacturing process is subject to the trend of ever higher requirements on form parts in relation to quality, tolerance, and manufacturing cost. Despite the fact that state-of-the-art injection moulding machines can be used to produce a high level of repeatability from shot to shot and offer users a variety of quality monitoring options, the situation in the past—which is still applicable today—has been characterised by constant form part quality being largely derived from the machine setup.

This setting of the injection velocity has been studied thoroughly, and many approaches have been adopted by researchers to monitor and dynamically control the quality and stability of the injection moulding process. Only recently—and with the development of new methods for determining the flow front velocity of the melt in a flow channel—has the recognition prevailed that quality defining parameters are independent of the machine.

With the new method proposed, an advanced control strategy based on machine independent parameters is conceivable. In an intelligent way, the mould—and not the machine—could control the injection moulding process. In such future control strategies, machine-independent parameters, such as the flow front velocity and melt viscosity at specific flow path sections, will act as control variables. Machine-

setting parameters will become dependent variables. In this regard, the machine used becomes immaterial to the mould, provided that the required parameters can be achieved. A prerequisite for this and for the practical implementation of the proposed method would be the practical and theoretical continuation of research in the following areas:

- Further scientific investigations should focus on the influence of different polymer types (amorphous or semi-crystalline) on the mapping process as well as on the robustness of matching.
- The suitability of the method for multi-cavity moulds should be investigated.
- The applicability of the method for special processes in injection moulding, such as cascade injection moulding, should be evaluated.
- With a view to the future use of the proposed method, the development of hardware and software for a process parameter detection unit resulting in a prototype would be desirable to prove the practical suitability of the method.

It remains to be seen whether direct measurement methods with multiple in-mould sensors will become the state-of-the-art method for determining machine-independent parameters in the future, or whether indirect methods such as the one proposed and developed will prevail. However, the advantages of a method which does not require complex sensor technology and can be adapted to almost any existing mould or form part are apparent. Decisive use criteria include the ease of implementation of the method as well as the robustness and reliability of the process upon which the method is based.

References

Agassant, J.-F., Avenas, P., Carreau, P., Vergnes, B., & Vincent, M. (2017). *Polymer Processing* (2nd ed.). Munich: Carl Hanser.

Bader, C. (2013, June 14). Switch-Mold erkennt Schmelzestrom und Werkzeugposition [Switch-module detects flow-stream and mould position]. *K Zeitung*.

Bader, C., König, E., & Schmidt, C. (2013, June 19). Qualität aus der Tiefe des Werkzeuges [Quality from the depth of the mold]. *Kunststoffe International, 2013*(6), 64–69.

Bader, C., & Zeller, S. C. (2010, June 16). Sensortechnik: Die Entdeckung der Schmelzefront [Sensor technology: The discovery of the melt front]. *Kunststoffe, 2011*(6), 27–31.

Bader, C., & Zeller, S. C. (2011, June 20). Process control: Hitting the nail on the head. *Kunststoffe International, 2011*(6), 6–11.

Badische Anilin- und Soda Fabrik (BASF). (2007). *Terluran GP-22 (ABS).* Retrieved from https://www.rolec-usa.com/en/technocase/datenblatt_technocase_abs_terluran-gp22_en.pdf

Becker, C., & Schümmer, P. (2000). Regions of vortices in an axisymmetric contraction, examined at the example of a second-order fluid (SOF). *Rheologica Acta, 39*(5), 503–515. doi: 10.1007/s003970000101

Belofsky, H. (1995). *Plastics: Product design and process engineering.* Munich: Carl Hanser.

Bernstein, B., Kearsley, E., & Zapas, L. (1963). A study of stress relaxations with finite strain. *Transactions of The Society of Rheology, 7*(1), 391–410.

Böhme, G. (1981). *Strömungsmechanik nicht-newtonscher Fluide* [Fluid mechanics of non-Newtonian fluids]. Stuttgart: Teubner.

Boldizar, A., Kubát, J., & Rigdahl, M. (1990). Influence of mold filling rate and gate geometry on the modulus of high-pressure injection molded polyethylene. *Journal of Applied Polymer Science, 39*(1), 63–71. doi: 10.1002/app.1990.070390106

Bress, T., & Dowling, D. (1998). Visualization of injection molding. *Journal of Reinforced Plastics and Compostits, 17*(15), 1374–1384. doi:10.1177%2F073168449801701505

Brinkmann, T. (2010). *Handbuch Produktentwicklung mit Kunststoffen* [Product development with polymers]. Munich: Carl Hanser.

Camacho, E., & Bordons, C. (1995). *Model Predictive Control in the Process Industry.* London: Springer.

Cha, J., Kim, M., & Park D. (2019). Experimental determination of the viscoelastic parameters of K-BKZ model and the influence of temperature field on the thickness distribution of ABS thermoforming. *International Journal of*

Advanced Manufacturing Technology, 103, 985–995. doi: 10.1007/s00170-019-03408-8

Chen, X. (2002). *A study on profile setting on injection molding* (Doctoral dissertation, Hong Kong University of Science & Technology: Hong Kong). Retrieved from http://hdl.handle.net/1783.1/2858

Chen, X., Chen, G., & Gao, F. (2004). Capacitive transducer for in-mold monitoring of injection molding. *Polymer Engineering and Science, 44*(8), 1571–1578. doi: 10.1002/pen.20154

Chen, X., & Gao, F. (2000). An on-line measurement scheme of melt-front-area during injection filling via a soft-sensor implementation. In Society of Plastic Engineers (ed.), *Conference proceedings (vol. 2: Materials*, pp. 633–637). CRC Press.

Chen, X., Zhang, L., Kong, X., Lu, J., & Gao, F. (2010). Automatic velocity profile determination for uniform filling in injection molding. *Polymer Engineering and Science, 50*(7), 1358–1371. doi: 10.1002/pen.21674

Chiu, C.-P., Shih, M.-C., & Wei, J.-H. (1991). Dynamic modeling of the mold filling process in an injection molding machine. *Polymer Engineering and Science, 31*(19), 1417–1425. doi: 10.1002/pen.760311908

Clark, D. W., Mohtadi, C., & Tuffs, P. S. (1987). Generalized predictive control—Part I. The basic algorithm. *Automatica, 23*(2), 137–148. doi: 10.1016/0005-1098(87)90087-2

Crochet, M. J., Davies, A. R., & Walter, K. (1984). *Numerical simulation of non-Newtonian flow.* Amsterdam: Elsevier.

Dassault Systems. (2021). Solidworks plastics help - Mesh detailed report. Retrieved from http://help.solidworks.com/2021/english/swplastics/r_mesh_details_report.htm

Domininghaus, H. (1992). *Kunststoffe und ihre Eigenschaften* [Plastics and their properties]. Düsseldorf: VDI.

Dupont, S., Marchal, J. M., & Crochet, M. J. (1985). Finite element simulation of viscoelastic fluids of the integral type. *Journal of non-Newtonian Fluid Mechnics, 17*(2), 157–183. doi: 10.1016/0377-0257(85)80013-6

Dynisco. (2021). *Dynisco polymer evaluation.* Retrieved from https://www.dynisco.com/userfiles/files/mdt_series_manual.pdf

Engels, T. A. P. (2008). *Predicting performance of glassy polymers: Evolution of the thermodynamic state during processing and service life.* Technische Universiteit Eindhoven.

Fernandes, C., Pontes, A. J., Viana, J. C., & Gaspar-Cunha, A. (2016). Modeling and optimization of the injection-molding process: A review. *Advances in Polymer Technology, 37*(2), Art. 21683. doi: 10.1002/adv.21683

Ferry, J. D. (1980). *Viscoelastic properties of polymers* (3rd ed.). New York: Wiley.

Flow Science. (2021). Flow 3D - Implicit vs. Explicit Numerical Methods. Retrieved from https://www.flow3d.com/resources/cfd-101/numerical-issues/implicit-versus-explicit-numerical-methods/

Flügge, S. (1960). *Encyclopedia of physics vol. 9: Fluid dynamics III.* Berlin-Göttingen-Heidelberg: Springer.

Franchetti, M., & Kress, C. (2017). An economic analysis comparing the cost feasibility of replacing injection molding processes with emerging additive manufacturing techniques. *The International Journal of Advanced Manufacturing Technology, 88*(9-12), 2573–2578. doi: 10.1007/s00170-016-8968-7

Gao, F., Patterson, W. I., & Kamal, M. R. (1994). Self-tuning cavity pressure control of injection molding filling. *Advances in Polymer Technology, 13*(2), 111–120. doi: 10.1002/adv.1994.060130202

Gao, H., Zhang, Y., Zhou, X., & Li, D. (2018). Intelligent methods for the process parameter determination of plastic injection molding. *Frontiers of Mechanical Engineering, 13*(1), 85–95. doi: 10.1007/s11465-018-0491-0

Gordon, G., Kazmer, D., Fischer, M., Gao, R. X., Fan, Z., & Asadiznajani, N. (2013). Melt flow simulation of an injection molding cavity for validation of a multivariate sensor. In Society of Plastic Engineers (ed.), *ANTEC 2013: Conference proceedings* (vol. 2, pp. 1116–1121). Society of Plastic Engineers.

Govaert, L. E., Engels, T. A. P., Klompen, E. T. J., Peters, G. W. M. & Meijer, H. E. H. (2005). Processing-induced properties in glassy polymers: Development of the yield stress in PC. *International Polymer Processing, 20*(2), 170–177. doi: 10.3139/217.1870

Heinrich, J. C., & Vionnet, C. A. (1995). The penalty method for the Navier-Stokes equations. *Archives of Computational Methods in Engineering, 2*(2), 51–65. doi: 10.1007/BF02904995

Hieber, C. A., & Chiang, H. H. (1992). Shear-rate-dependence modeling of polymer melt viscosity. *Polymer Engineering & Science, 32*(14), 931–938. doi: 10.1002/pen.760321404

Hohmann, M. (August 10, 2021). Statistiken zur Kunststoffindustrie in Deutschland [Statistics on the plastics industry in Germany]. *Statista*. Retrieved from https://de.statista.com/themen/3094/kunststoffindustrie-in-deutschland/#dossierSummary__chapter2

Hunkar, D. (1975). The interdependence of part parameters on process control adjustable function in injection molding of thermoplastics. *SPE ANTEC Tech. Paper, 21*, 161–164.

Johannaber, F., & Michaeli, W. (2004). *Handbuch Spritzgießen.* Munich: Carl Hanser.

Karbasi, H., & Reiser, H. (2006). *Smart mold: Real-time in-cavity data acquisition*. Paper presented at the First Annual Technical Showcase & Third Annual Workshop. Ottawa, ON, Canada. Retrieved from

https://citeseerx.ist.psu.edu/viewdoc/download?doi=10.1.1.487.6357&rep=rep1&type=pdf

Kaye, A. (1962). *Non-Newtonian flow in incompressible fluids.* College of Aeronautics Cranfield.

Kennedy, P. K., & Zheng, R. (2013). *Flow analysis of injection molds* (2nd ed.). Munich: Carl Hanser.

Khalili Garakani, A., Mostoufi, N., Sadeghi, F., Hosseinzadeh, M., Fatourechi, H., Sarrafzadeh, M., & Mehrnia, M. (2011). Comparison between different models for rheological characterization of activated sludge. *Iranian Journal of Enviromental Health Science & Engineering, 8*(3), 255–264.

Kulkarni, S. (2010). *Robust process development and scientific molding* (1st ed.). Munich: Carl Hanser.

Kutsch, O. (2021). *Cerensana Market Research*. Retrieved 04 09, 2021, from https://www.ceresana.com/en/market-studies/industry/plastic-injection/

Menges, G., Haberstroh, E., Michaeli, W., & Schmachtenberg, E. (2011). *Werkstoffe der Kunststoffe* [Menges materials science plastics]. Munich: Carl Hanser.

Menges, G., Michaeli, W., & Mohren, P. (1999). *How to make injection molds* (1st ed.). Munich: Carl Hanser.

Mensler, H., Zhang, S., & Win, T. (2019). A method for determining the flow front velocity of a plastic melt in an injection molding process. *Polymer Engineering and Science, 59*(6), 1132–1145. doi: 10.1002/pen.25092

Michaeli, W., & Schreiber, A. (2009). Online control of the injection molding process based on process variable. *Advances in Polymer Technology, 28*(2), 65–76. doi: 10.1002/adv.20153

Mks Instruments (MKS). (2012). The optimization of injection molding processes using design of experiments – Application note. Retrieved from https://www.mksinst.com/mam/celum/celum_assets/resources/SenselinkQMDOE-AppNote.pdf

Oldroyd, J. G. (1958). Non-Newtonian effects in steady motion of some idealized elastic co-viscous liquids. *Proceedings of the Royal Society, 245*(1241), 278–297. doi: 10.1098/rspa.1958.0083

OriginLab. (n.d.). The rise time gadget (pro only). Retrieved April 11, 2017 from http://www.originlab.com/doc/Origin-Help/Gadget-RiseTime

Osswald, T. A. (2011). *Understanding polymer processing: Processes and governing equations* (1st ed.). Munich: Carl Hanser.

Osswald, T. A., Turng, L.-S., & Gramann, P. (eds.). (2008). *Injection molding handbook* (2nd ed.). Munich: Carl Hanser.

Ouyang, G., Li, X., Guan, X., Zhang, Z., Zhang X., & Du, R. (2004). Ram velocity control in plastic injection molding machines with neural network learning

control. In F. Yin, J. Wang & C. Guo (Eds.) *Advances in neural networks – ISNN 2004 proceedings part II* (pp. 169–174). Berlin: Springer.

Plastverarbeiter. (2016). Kunststoff-Institut Lüdenscheid - Projekt "Einstieg in die Medizintechnik". Retrieved May 05, 2020, from https://www.plastverarbeiter.de/9376/kunststoff-institut-luedenscheid-projekt-einstieg-in-die-medizintechnik/

Quartapelle, L. (1993). *Numerical solution of the incompressible Navier-Stokes equations.* Basel: Birkhäuser.

Rannacher, R. (2000). Finite element methods for incompressible Navier-Stokes Equations. In G. Galdi, J. Heywood, & R. Rannacher, *Fundamental directions in mathematical fluid mechanics* (pp. 191–293). Basel: Birkhäuser. doi: 10.1007/978-3-0348-8424-2_6

Reference for Business. (n.d.). Moldflow corporation. Retrieved May 01, 2021, from https://www.referenceforbusiness.com/history/Mi-Nu/Moldflow-Corporation.html

Rheinisch-Westfälische Technische Hochschule Aachen [RWTH Aachen University]. (January 18, 2017). Selbstoptimierender Spritzgießprozess [Self-optimizing injection molding]. Retrieved from: https://www.iop.rwth-aachen.de/cms/Produktionstechnik/Forschung/Demonstratoren/~hoxn/Selbstoptimierender-Spritzgiessprozess/

Schröder, T. (2018). *Rheologie der kunststoffe: Theorie und praxis [Rheology of plastics: Theory and practice].* Munich: Carl Hanser.

Shi, J., & Gao, F. (2007). Higher-order generalized 2D predictive learning control schemes. *IFAC Proceedings Volumes. 40*(5), 243–248. doi: 10.3182/20070606-3-mx-2915.00088

Shi, J., Gao, F., & Wu, T.-J. (2005). Robust design of integrated feedback and iterative learning control of a batch process based on a 2D Roesser system. *Journal of Process Control, 15*(8), 907–924. doi: 10.1016/j.jprocont.2005.02.005

Shi, J., Gao, F., & Wu, T.-J. (2006). 2D model predictive iterative learning control scheme for batch processes. *IFAC Proceedings Volumes, 39*(2), 215–220. doi: 10.3182/20060402-4-BR-2902.00215

Stitz, S., & Keller, W. (2001). *Spritzgießtechnik: Verarbeitung, Maschinen, Peripherie* [Injection moulding technology: processing, machines, peripherals]. Munich: Hanser.

Tan, K. K., & Tang J. C. (2002). Learning enhanced PI control of ram velocity in injection molding machines. *Engineering Applications of Artificial Intelligence, 15*(1), 65–72. doi: 10.1016/S0952-1976(02)00032-5

Tanner, R. I. (2000). *Engineering rheology* (2nd ed.). London: Oxford University Press.

Tsoi, H.-P., & Gao, F. (1999). Control of injection velocity using a fuzzy logic rule-base controller for thermoplastic injection molding. *Polymer Engineering and Science, 39*(1), 3–17. doi: 10.1002/pen.11392

van Krevelen, D. W., & te Nijenhuis, K. (2009). *Properties of polymers: Their correlation with chemical structure; Their numerical estimation and prediction from additive group contributions* (4th ed.). Amsterdam: Elsevier.

Vijayakumar, S. R., & Gajendran, S. (2014). Improvement of overall equipment effectiveness (OEE) in injection moulding process industry. *Journal of Mechanical and Civil Engineering*, 47–60.

Wang, H. Y., Fung, K. T., & Gao, F. (2008). Development of a transducer for in-line and through cycle monitoring of key process and quality variables in injection molding. *Sensors and Actuators A: Physical, 141*(2), 712–722. doi: 10.1016/j.sna.2007.10.038

Wang, S.-M., Liaw, W.-L., & Chen, S.-C. (2006). Effective fast-response pressure control for thin-wall gas-assisted injection molding. *The International Journal of Advanced Manufacturing Technology, 28*(9-10), 890–898. doi: 10.1007/s00170-005-2542-z

Wang, Y., Zhou, D., & Gao, F. (2008). Iterative learning model predictive control for multi-phase batch processes. *Journal of Process Control, 18*(6), 543–557. doi: 10.1016/j.jprocont.2007.10.014

Yang, Y. (2004). *Injection molding machine control: From process to quality* (Doctoral dissertation, Hong Kong University of Science & Technology: Hong Kong). Retrieved from http://hdl.handle.net/1783.1/1912

Yang, Y., & Gao, F. (1999). Cycle-to-cycle and within-cycle adaptive control of nozzle pressure during packing-holding for thermoplastic injection molding. *Polymer Engineering and Science, 39*(10), 2042–2063. doi: 10.1002/PEN.11597

Yang, Y., & Gao, F. (1999). Injection velocity control using a self-tuning adaptive controller for thermoplastic injection molding. *International Polymer Processing, 14*(2), 196–204. doi: 10.3139/217.1537

Yang, Y., & Gao, F. (2000). Adaptive control of the filling velocity of thermoplastics injection molding. *Control Engineering Practice, 8*(11), 1285–1296. doi: 10.1016/S0967-0661(00)00060-5

Yang, Y., Chen, X., Ningyun, L., & Furong, G. (2016). *Injection molding process control, monitoring, and optimization.* Munich: Carl Hanser.

Yokoi, H., & Inagaki, Y. (1992). Dynamic visualization of cavity filling process. In Society of Plastic Engineers (ed.), *ANTEC 92: Conference proceedings* (pp. 457–461). Society of Plastic Engineers.

Yokoi, H., Hayashi, T., Tado, K., & Morikita, N. (1988). Direct observation of jetting phenomena under high injection pressure using a prismatic glass inserted mold. In Society of Plastic Engineers (ed.), *ANTEC 88: Conference proceedings* (pp. 329–333). Society of Plastic Engineers.

Zhao, P., Zhang, J., Dong, Z., Huang, J., Zhou, H., Fu, J., & Turng, L.-S. (2020). Intelligent injection molding on sensing, optimization, and control.

Advances in Polymer Technology, 2020, Art. 7023616. doi: 10.1155/2020/7023616

Zhou, F., Yao, K., Chen, X., & Gao, F. (2009). In-mold melt front rate control using a capacitive transducer in injection molding. *International Polymer Processing, 24*(3), 253–260. doi: 10.3139/217.2242

Zhou, H. (ed.). (2013). *Computer modelling for injection molding.* Singapore: Wiley.

Zoller, P., Bolli, P., Pahud, V., & Ackermann, H. (1976). Apparatus for measuring pressure-volume-temperature relationships of polymers to 350°C and 2200 kg/sqcm. *Review of Scientific Instruments, 47*(8), 948–952. doi: 10.1063/1.1134779